1-1-2007

Thermochronological constraints on Mesozoic tectonism in southwest US and New Zealand; and argon-argon age spectra from artificially mixed micas

Joseph Kula
University of Nevada, Las Vegas

THERMOCHRONOLOGICAL CONSTRAINTS ON MESOZOIC TECTONISM IN SOUTHWEST U.S. AND NEW ZEALAND; AND $^{40}Ar/^{39}Ar$ AGE SPECTRA FROM ARTIFICIALLY MIXED MICAS

by

Joseph Kula

Bachelor of Science, Geoscience
Montclair State University
2000

Masters of Science, Geoscience
University of Nevada, Las Vegas
2002

A dissertation submitted in partial fulfillment
of the requirements for the

Doctor of Philosophy Degree in Geoscience
Department of Geoscience
College of Sciences

Graduate College
University of Nevada, Las Vegas
December 2007

UNLV
UNIVERSITY OF NEVADA LAS VEGAS

Dissertation Approval

The Graduate College
University of Nevada, Las Vegas

DECEMBER, 2007

The Dissertation prepared by

JOSEPH KULA

Entitled

THERMOCHRONOLOGICAL CONSTRAINTS ON MESOZOIC TECTONISM IN SOUTHWEST U.S. AND NEW ZEALAND; AND 40AR/39AR AGE SPECTRA FROM ARTIFICIALLY MIXED MICAS

is approved in partial fulfillment of the requirements for the degree of

DOCTOR OF PHILOSOPHY IN GEOSCIENCE

Terry L. Spell

Examination Committee Chair

Dean of the Graduate College

Examination Committee Member

Examination Committee Member

Graduate College Faculty Representative

PR/1017-52/1-00

ABSTRACT

Thermochronological constraints on Mesozoic tectonism in southwest U.S. and New Zealand; and $^{40}Ar/^{39}Ar$ age spectra from artificially mixed micas

by

Joseph Kula

Dr. Terry Spell, Examination Committee Chair
Associate Professor of Geoscience
University of Nevada, Las Vegas

Dr. Michael Wells, Examination Committee Co-Chair
Professor of Geoscience
University of Nevada, Las Vegas

The four chapters in this dissertation consist of projects that utilized $^{40}Ar/^{39}Ar$ thermochronometry. Chapters 1 and 2 are from a study of the Sisters shear zone on Stewart Island, New Zealand. In these studies, thermal histories obtained using $^{40}Ar/^{39}Ar$ thermochronometry were combined with field and microstructural observations collected from deformed rocks. These data indicate extensional deformation along the Sisters shear zone was the youngest event related to the breakup of the paleo-Gondwana margin. The Sisters shear zone is related to formation of the Great South Basin and thinning of the Campbell Plateau. The shear zone is also spatially and kinematically linked to the Pacific-Antarctic spreading ridge indicating the shear zone was involved in the separation of New Zealand from West Antarctica. Comparison of timing constraints from Stewart Island with those from other studies and locations indicates the breakup of the Gondwana margin was likely the result of two distinct extensional events.

Chapter 3 consists of a $^{40}Ar/^{39}Ar$ laboratory experiment dealing with the biotite and muscovite micas. Artificial samples of mixed mica populations were analyzed using the vacuum furnace step-heating method. These samples were prepared and analyzed to test the possibility of recovering original ages of individual mica populations from natural samples consisting of multiple generations. The results indicate this is not likely in the vacuum furnace. Additionally, the results indicate that the compositional controls on argon retentivity in nature may also be active during furnace heating in the laboratory.

Chapter 4 shows the results of a $^{40}Ar/^{39}Ar$ study of plutonic rocks that have cross cutting relationships with structures of the Clark Mountains thrust complex in southern California. These data indicate the earliest episode of crustal shortening occurred pre-155 Ma. The Pachalka thrust at ~144 Ma was previously considered the oldest deformation episode in the region. Diorite-granodioritic magmatism at ~155 Ma was followed closely by felsic magmatism of the Ivanpah granite (>149 Ma). The ductile Morning Star Mine thrust, which likely correlates to the Keaney-Mollusk Mine thrust cuts the Ivanpah granite.

TABLE OF CONTENTS

LIST OF FIGURES

ACKNOWLEDGMENTS

There was a lot of outside contribution that helped create this dissertation, and so those people who provided are mentioned here. Much like those stupid award shows, this could get long. Ok, here it goes.

Teespell. I notice a lot of people call you that these days. I can only hope it has caught on to the point where your family does it as well in the privacy of your home. Only then will my mission be complete. Anyways, I don't even know what to say to you. Thanks. A lot. I didn't even know what argon dating was when I arrived at UNLV. You showed me it and in doing so, introduced me to my favorite part of geology. You also never discouraged me from trying something. Rather, you typically said something like "go for it, and tell me what you end up with". I really appreciate that. You even helped me with stuff that wasn't directly related to this dissertation. Like pining through my argon calculator spreadsheet. You have been a great advisor and friend to me. Now, if you could just maybe grow one more beard again, say for my defense, that would mean the world to me...

Hey Michael. We had a lot of fun these past few years haven't we? I know there have been several times where we both wanted to give one another nothing more than a swift kick in the taint, but I'm glad we're ok. Thanks for pushing me. You always challenged me and that forced me to really dive into both geology and science in general. Thanks for always providing fast turnaround edits and comments on papers. Thanks for letting us come over and camp out in your house. We got a front load washer too now, and it is awesome. Oh, and thanks for teaching me Harlan Coben and telling me to read stuff that isn't geology every now and then. I think most of all, thanks for sticking with me and not kicking my teeth in during those times when I surely deserved it.

KZ. Kathleen. We had times both good and bad, but I truly see you as a friend and plan on keeping you as one. You have taught me so much just by allowing me into the lab all the time. Maybe I give Teespell too much credit for teaching me argon dating. (just kidding Teespell, unless you didn't read this far...) Thank you for everything, and just wait for this muscovite experiment. It's gonna be awesome! Let's go get some pints, or maybe go wine tasting. Ciao!

Andy Tulloch from GNS in Dunedin has been like a third advisor for me. He has worked tirelessly on keeping me up to date with New Zealand geology, trading back and forth comments on papers and abstracts, and securing funding for fieldwork. Thanks Andy, you madman.

I had a lot of help from other people too. These include grad students and faculty. The Geo-Anthro-Physics drinking team. Without this lot I most surely would have driven myself psychotic and spiraled into grad student dementia. I had help in the field from Melissa Hicks, Darren Burgett, Matt McKelvey, Teespell, and Michael Wells. Amy Brock let me move in with her for my last year in Las Vegas. Thank you Amy, we'll see you in Colorado in February! Dan, Jason, and Brian from Physics were almost always willing to party and help relieve stress. Thanks Brett and Sue for being great friends, party companions, counselors, field partners, and hosting Pirate New Years. Thanks to Andrew Hanson, who always had time to hear a complaint or offer insight when things didn't seem to be going right. I'm lucky to have 'lived' across the hall from Debbie

Soukup for a year because she was a great lunch buddy and gave me some great insights into science in general. Not once in the seven years I was at UNLV did Clay Crow ever make me wait or refuse to help me with something. Even when it was something as dumb as needing my bicycle tires filled. Thanks Clay!

My core group of friends over the years that consisted of: Melissa, Amy, Brett, Sue, Kathy, AnthroRob, Nathan, Jim, Chris, Jeffy, Amber, Kasey, Tiffany, Dan, Jason, Brian, Tania, Matt, Darren and Rosa, Colin, Aaron, and I'm sure I'm forgetting someone, made being a graduate student extra fun.

Of course, my family was always supportive to me and I thank them. They said "stay in school" but we probably should have talked about 'how long'.

I want to especially mention Melissa. All the crap that comes along with graduate school is worth it because it brought me to you. Thanks UNLV for that. No matter what, Melissa has had my back from the start and never judged me but rather encouraged me to satisfy my curiosities whether they be in the fields of geology, idealogy, or whatever. I'm so sorry to have kept you waiting so long, you and Amelia are my family and I couldn't imagine a happier home life. I love you more than burritos and Gandhi's combined.

Funding from the Geoscience Department Scholarships, Graduate and Professional Student Association, AEG Tilford Field Scholarship, and Geological Society of America Graduate Research Grants also was superhelpful in getting this work done. The next four paragraphs are the specific acknowledgments for the four chapters.

We thank Uwe Ring, Nick Mortimer, Andrew Allibone, and James Scott for discussions and earlier reviews that improved the manuscript. We thank Andrew Allibone and Ian Turnbull for initial collection of some key samples. Tim Little and an anonymous reviewer provided detailed and helpful reviews. Kathy Zanetti's assistance with argon analysis is greatly appreciated. Boat-based fieldwork in southern Stewart Island was funded by GNS Science. Colin and Margaret Hopkins fed us like kings on the *Aurora Australis*. JLK's travel was funded by Geological Society of America (GSA) graduate student grants 8027-05 and 7720-04.

We are grateful for reviews on earlier versions of the paper by James Scott, Wanda Taylor, and Rod Metcalf. GNS Science provided funding for boat-based fieldwork in southern Stewart Island. Colin and Margaret Hopkins were generous hosts aboard the *Aurora Australis*. JK's travel was funded by Geological Society of America (GSA) graduate student grants 8027-05 and 7720-04.

We thank Mengesha Beyene and Michael Wells for providing NY25 muscovite. Michael Wells, Wanda Taylor, and Rod Metcalf provided reviews of earlier versions of the paper. Robert Fairhurst and Adam Simon assisted in obtaining electron microprobe chemical analyses. JK is grateful to Tom Hoisch for discussions on mica chemistry and Clay Crow for assistance with sample preparation procedures.

We are grateful to Rod Metcalf and Wanda Taylor for discussions, fieldtrips, and reviews of this paper. JK thanks Melissa Hicks, Darren Burgett, and Matt McKelvey for coming out in the field, not complaining during death marches, and helping carry heavy rock samples. JK also acknowledges patience and assistance in the argon lab from Kathy Zanetti. The UNLV Geoscience Department, and AEG Tilford Field Studies Scholarship provided funding for this project.

CHAPTER 1

TWO-STAGE RIFTING OF ZEALANDIA – AUSTRALIA – ANTARCTICA: EVIDENCE FROM $^{40}Ar/^{39}Ar$ THERMOCHRONOMETRY OF THE SISTERS SHEAR ZONE, STEWART ISLAND, NEW ZEALAND

Abstract

The Sisters shear zone is a newly discovered Late Cretaceous detachment fault system exposed for 40 km along the southeast coast of Stewart Island, southernmost New Zealand. Footwall rocks consist of variably deformed ~310 and 105 Ma granites ranging from undeformed to protomylonite, mylonite, and ultramylonite. The hanging wall includes non-marine conglomerate and brittlely deformed granite. K-feldspar thermochronometry of the footwall indicates moderately rapid cooling (20–30C°/Ma) due to tectonic denudation over the interval ~89–82 Ma. Return to slow cooling at 82 Ma coincides with the age of oldest seafloor adjacent to the Campbell Plateau, reflecting the mechanical transition from continental extension to lithospheric rupture and formation of the Pacific-Antarctic Ridge. Our findings support a two-stage rift model for continental breakup of this part of the Gondwana margin. Stage one (~101–88 Ma) is the northward propagation of continental extension and the Tasman Ridge as recorded in mylonite dredged from the Ross Sea and the Paparoa core complex. Stage two (~89–82 Ma) is

extension between the Campbell Plateau and West Antarctica leading to formation of the Pacific-Antarctic Ridge.

Introduction

Plate reconstructions of Mesozoic Gondwana place Zealandia (New Zealand and surrounding continental shelf, e.g. Mortimer, 2004) at the Pacific margin, adjacent to southeast Australia and West Antarctica (e.g., Sutherland, 1999; Eagles et al., 2004). Much attention has been directed toward extension between western Zealandia and eastern Australia leading to opening of the Tasman Sea (Tulloch and Kimbrough, 1989; Etheridge et al., 1989; Spell et al., 2000) and rift related deformation in Marie Byrd Land, West Antarctica and the adjacent Ross Sea (e.g., Luyendyk et al., 2003; Siddoway et al., 2005). These studies have outlined the timing and style of extension and breakup between Australia and Zealandia, and of extension between East and West Antarctica. This paper focuses on the outstanding problem of the nature and timing of extension in eastern Zealandia leading to Pacific-Antarctic Ridge formation and separation of the Campbell Plateau from West Antarctica.

Field observations and $^{40}Ar/^{39}Ar$ data from the Sisters Shear Zone on Stewart Island, southernmost New Zealand, are presented here as evidence for a Late Cretaceous detachment fault system that accommodated continental extension, thinning of the Campbell Plateau, and was kinematically linked to formation of the Pacific-Antarctic Ridge. The timing of extension and the transition from continental rifting to seafloor spreading is documented using $^{40}Ar/^{39}Ar$ thermochronometry, which indicates this event is 5-10 Ma younger than extension documented in the Ross Sea and western New

Zealand. Our new results and observations, combined with published thermochronology data from western New Zealand and West Antarctica, reveal a sequence of extensional tectonism that can be best explained by a two-stage model for breakup of the Pacific margin of Gondwana.

Sisters shear zone, Stewart Island

Stewart Island is part of the Median Batholith and Western Province of New Zealand (Fig. 1). The Median Batholith represents the magmatic arc developed above a paleo-subduction zone along the Gondwana Pacific margin (Tulloch and Kimbrough, 2003). Major structures on Stewart Island include the northwest-striking Freshwater Fault Zone, Escarpment Fault, and Gutter Shear Zone. These structures are related to pre-breakup convergent margin tectonism and are described by Allibone and Tulloch (1997, 2004). In contrast, the Sisters shear zone, located along the southeast coast and oriented obliquely to these structures, is here interpreted to represent an extensional detachment fault system.

The Sisters shear zone is exposed along the southeast coastline of Stewart Island for ~40 km (Fig. 1). At some localities it is as wide as 5 km (map view), however the boundaries are not well constrained due to relatively poor exposure. The shear zone is developed within Carboniferous and Early Cretaceous granitic rocks exhibiting varying degrees of deformation from essentially undeformed to protomylonite, mylonite, and ultramylonite, with widespread but generally minor brittle deformation overprints. Shear bands, oblique-grain shape fabrics, sigma- and delta-type feldspar porphyroclasts and mica fish indicate shear sense.

The Sisters shear zone is divided into two segments based on the nature of ductile fabrics, predominant kinematics, and along-strike offset of the western boundary of ductile fabric (Fig. 1). The northern segment of the shear zone typically consists of granite mylonite and protomylonite with foliations dipping 20–30° SSE and top-to-southeast shear sense. Footwall rocks here are locally overprinted by southeast-dipping brittle normal faults, commonly subparallel to the ~060° strike of the foliation. In the southern segment, foliations are generally less well developed than in the north, and deformation tends to be localized into 5-50m thick high-strain zones including ultramylonite. Ductile kinematic indicators in the southern portion exhibit both top-to-northwest and top-to-southeast down-dip shear sense, but brittle normal faults are consistently top-to-southeast. Stretching lineations throughout the shear zone consistently trend 330/150° ± 15°. Because of apparent along-strike offset of the western boundary of ductile fabric and differences in kinematics and foliation attitudes, we infer the north and south segments of the shear zone are separated by a transfer fault (e.g. Lister et al., 1986) (Fig. 1).

Microstructures in the deformed granites indicate greenschist facies metamorphic conditions followed by decreasing temperatures during shearing. In thin section quartz exhibits features of plastic deformation including oblique grain-shape fabrics in dynamically recrystallized grains (regime 2 of Hirth and Tullis, 1992) and ribbons with patchy to undulose extinction, whereas feldspars exhibit dominantly brittle deformation. The lack of post-deformational growth in ~30 μm grains of recrystallized quartz, preservation of unrecovered quartz ribbons with undulose extinction, and cataclastic 'crush zone' overprinting collectively indicate cooling during deformation.

A brittle detachment surface oriented 061/27S is exposed in a small bay in the northern segment opposite the Sisters Islets (Fig. 2). A 10cm-thick black flinty ultracataclasite underlies the fault surface, and separates mylonite of the footwall from chloritic hydrothermally altered and brecciated granitic rocks of the hanging wall. Slickenlines measured on the detachment surface are of the same trend as stretching lineations throughout the shear zone. The detachment fault/surface appears to be entirely offshore in the southern segment of the shear zone (Fig. 1).

The Sisters Islets, a pair of ~200 × 400 m islets ~1 km offshore (Fig. 2) are composed of essentially undeformed conglomerate (Fleming and Watters, 1974) and represent the hanging wall of the Sisters shear zone. Conglomerate beds on the Sisters strike ~070, dip 20–25° NNW, and consist of rounded, with lesser subangular, dominantly granitic clasts enclosed in an arkosic sandstone matrix. Many clasts exhibit ductile fabric, however a provenance from the footwall rocks has not yet been confirmed.

$^{40}Ar/^{39}Ar$ thermochronometry

Samples were collected from granitic outcrops at locations shown in Figure 1 and detailed in the PETLAB database (http://data.gns.cri.nz/pet/). $^{40}Ar/^{39}Ar$ analyses were conducted at the Nevada Isotope Geochronology Laboratory at UNLV; data tables and descriptions of analytical methods are given in appendices DR1 and DR2.

Footwall mica ages

Muscovite and biotite were collected from footwall rocks from the Knob Pluton in the northern segment ~50–100m below the detachment surface (P76106, Fig. 1). Muscovite yielded a relatively flat age spectrum with a plateau age of 93.8 ± 0.4 Ma (uncertainties 2σ), incorporating 96% of the gas released (Fig. 3A). Biotite yielded a plateau age of 90.0 ± 0.8 Ma over 59% of the gas released and an isochron age of 90.6 ± 1.2 Ma with a $^{40}Ar/^{36}Ar$ intercept of 294.5 ± 2.2, indicating no excess ^{40}Ar in the sample.

Footwall and hanging-wall K-feldspar

Three K-feldspar separates were analyzed using detailed furnace step-heating, including isothermal duplicates, to determine argon diffusion kinetics for application of multiple diffusion domain (MDD) thermal modeling (Lovera et al., 1989; 1991). Two samples were collected from footwall rocks: P76106, (discussed above); and P67866 from the western side of the southern segment of the shear zone (Fig. 1). The footwall samples yield maximum ages of 89–90 Ma with sample P76106 exhibiting a prominent age gradient over the initial gas release that is absent in sample P67866 (Fig. 3A). The third sample (P62424) was collected from hanging-wall granite of North Traps (~120 Ma, U-Pb zircon, Allibone and Tulloch, 2004), 35 km southeast of the coast (Fig. 1). This sample yields maximum ages ~25 Ma older than the footwall samples. Following an initial age gradient over the first 10% of the gas release, the age spectrum flattens at 115–116 Ma, close to the granite crystallization age.

Thermal history of the Sisters shear zone

The muscovite (93 Ma) and biotite (90 Ma) footwall ages and 'nominal' closure temperatures of 400 and 350 °C (cf. McDougall and Harrison, 1999), respectively, yield a crude cooling rate estimate of ~17 °C/Ma. The two footwall K-feldspars (P76106 and P67866) (Fig. 3) yield similar MDD modeling results (Fig. 3B). Both show moderately rapid cooling (20–30°/Ma) beginning at ~89 Ma followed by a transition to very slow cooling at ~82–78 Ma (Fig. 3).

Hanging-wall sample P62424 yields a distinctly different thermal history from those of the footwall samples. Rapid cooling from 116 to 105 Ma following emplacement at ~120 Ma likely reflects conductive thermal re-equilibration with the surrounding shallow crust. At 105 Ma a decrease to very slow cooling (nearly isothermal) (Fig. 3b) indicates prolonged residence in the upper crust for over 40 Ma following cessation of Median Batholith arc magmatism.

Discussion

The above field observations indicate the Sisters shear zone contains all the elements of a continental extensional detachment fault system with a footwall of variably mylonitic granitoids with localized brittle overprint, and a brittlely-deformed hanging wall of unfoliated granite and conglomerate (Fig. 2B). Brittle overprinting of ductile fabrics is consistent with exhumation of the footwall during deformation. Juxtaposition of mid-crustal plutonic (lower plate) rocks against tilted sedimentary (upper plate) rocks is typical of large-magnitude detachment faults such as those of the Basin and Range of the western United States. (Wernicke, 1992).

An extensional setting for the shear zone is further supported by contrasting thermal histories from footwall and hanging-wall samples. $^{40}Ar/^{39}Ar$ mica ages from footwall rocks indicate slow cooling from ~93–89 Ma. This interval is followed by a period of moderately rapid cooling (20–30 °C/Ma) from ~89–82 Ma, as determined from K-feldspar thermal modeling (Fig. 3B), and is attributed to extensional exhumation along the detachment fault. At ~82 Ma the cooling rate decreased substantially to nearly isothermal conditions and thermal equilibrium with the hanging wall (Fig. 3B). The hanging-wall K-feldspar indicates thermal equilibration with the surrounding upper crust ~25 Ma earlier. From Figure 3B the currently exposed footwall rocks were ~200 °C hotter than the hanging-wall rocks at 89 Ma. Assuming a pre-extensional geothermal gradient of 20–30 °C/km (Rothstein and Manning, 2003), the thermal histories reflect 7–10 km of crustal excision along the Sisters shear zone. Using these constraints and the dip angle of the ultracataclasite described above (27°, assuming no rotation), a range of 15–22 km of slip is estimated along the detachment fault.

The transition to slow cooling observed in footwall K-feldspar at ~82 Ma corresponds with the age of oldest seafloor (chron 33r, 83.0–79.1 Ma) along the southeast margin of the Campbell Plateau (Larter et al., 2002) and is consistent with the tectonic model of Sutherland and Hollis (2001). Therefore, the decrease in cooling rate may reflect the timing of transition from continental extension to lithosphere rupture and formation of the Pacific-Antarctic spreading ridge between the Campbell Plateau and West Antarctica.

The discovery of the Sisters shear zone has at least three important implications for Southwest Pacific Cretaceous tectonics. Firstly, the Sisters shear zone lies along strike from the fault-bounded northwest margin of the Great South Basin (Cook et al., 1999). Lineations in footwall rocks are coincident with the extension direction inferred for the basin based on dip directions of seismically identified normal faults, indicating a major role for the Sisters Shear Zone in the formation of this large hydrocarbon-prospective basin. Secondly, the Sisters shear zone cuts across the trend of thickened arc crust of the Median Batholith (Tulloch and Kimbrough, 2003) indicating it is unlikely that gravitational collapse was the driving mechanism for Sisters Shear Zone extension (cf.

Dewey, 1988; Rey et al., 2001). Thirdly, $^{40}Ar/^{39}Ar$ thermochronometry data from the Sisters shear zone supports a two-stage rifting model for the Gondwana Pacific margin (discussed below).

Two-stage Zealandia rifting model

The timing of cooling recorded by K-feldspar of the Sisters shear zone (~89–82 Ma) is younger than that in both the Ross Sea (~100–92 Ma; Siddoway et al., 2004) and the Paparoa metamorphic core complex (~92–88 Ma; Spell et al. 2000) (Fig. 4A). This discrepancy may be explained by a two-stage rift model that incorporates the model of detachment fault control on the formation of asymmetric continental margins of Lister et al. (1986). In this model, stage 1 (101–88 Ma) is asymmetric extension between a lower plate of Zealandia/West Antarctica and an upper plate of Australia/East Antarctica, resulting in formation of the Tasman Ridge (Tulloch and Kimbrough, 1989; Spell et al., 2000). Thermal histories determined for mylonite dredged from the Ross Sea (Siddoway et al., 2004) and the Paparoa footwall (Spell et al., 2000) would thus record the northward propagation of the Tasman rift zone (Fig. 4). Stage 2 (89–82 Ma) is extension between a lower plate of Zealandia and an upper plate of West Antarctica, producing the Pacific-Antarctic Ridge; the thermal history of the Sisters shear zone footwall records this event and lineations here are subparallel to Pacific-Antarctic Ridge spreading supporting a kinematic relationship. A second, short-lived interval of rapid cooling at ~80 Ma from West Antarctica (Fig. 4) may reflect a second stage of exhumation by rift flank uplift of the upper plate in proximity to the newly formed spreading ridge (see Sutherland and Hollis, 2001). This interpretation is consistent with rapid exhumation of a mid-crustal shear zone in the Fosdick Mountains that was subsequently tilted and cut by Late Cretaceous normal faults (Richard et al., 1994). In this two stage rifting model, Zealandia represents the lower plate to two asymmetric rift systems, Australia and East Antarctica both represent the upper plates to an asymmetric rift, and West Antarctica changes from the lower plate of the Tasman rift to the upper plate of the Pacific-Antarctic rift. This model and the thermochronometry data presented herein are consistent with and support previous assertions that the separation of New Zealand from West Antarctica was the final stage of Gondwana breakup (Larter et al., 2002; Siddoway et al., 2004).

Figure captions

Figure 1. Generalized geologic map of southern Stewart Island (Modified from Allibone and Tulloch, 2004) showing the dominantly plutonic nature (Median Batholith- black in inset). Note distribution of ductile fabric, stretching lineation orientation, and inferred transfer fault (see text). Sample locations are labeled with P-numbers (PETLAB database (http://data.gns.cri.nz/pet/). North Traps are a set of low-lying rock and reefs consisting of undeformed granite. Box indicates area of Figure 2. PP—Port Pegasus.

Figure 2. A. Stewart Island coast opposite the Sisters Islets showing outcrop relationships of ductile fabrics, chloritic breccia, and conglomerate of the Sisters Islets. X-X' line marks section line for figure 2B. B. Schematic cross section depicting upper-lower plate relationship between Sisters Islets, North Traps, and Stewart Island coast.

Figure 3. A. Age spectra from samples P76106, P67866 (footwall), and P62424 (hanging wall) (Fig. 1) (uncertainties 1σ). B. Comparison of thermal histories from footwall and hanging wall samples (see text). Outer envelope of curves indicates 90% confidence interval for the distribution of obtained thermal histories, inner envelope indicates 90% confidence interval for the median.

Figure 4. Two-stage rift model for breakup of Gondwana margin. A. Comparison with regional thermochronometry data from Western Province, New Zealand (Spell et al., 2000) and Marie Byrd Land, West Antarctica (Siddoway et al., 2004). Onset of footwall cooling occurs ~15 Ma after final phase of Median Batholith HiSY magmatism indicating tectonic origin rather than conductive cooling. B. Rigid plate reconstruction (~95 Ma) of the Gondwana margin – fragments of New Zealand represent the arc/forearc region (from Mortimer et al. 2005). Thermal histories in A correspond to numbered arrows in B representing two distinct stages of margin rifting: thick gray line: stage 1- northward propagation of Tasman Ridge; thick black line: stage 2- Sisters Shear Zone extension leading to opening of the Pacific-Antarctic Ridge (see discussion). (Camp—Campbell Plateau; CR—Chatham Rise; HP—Hikurangi Plateau; W—Wishbone Ridge; Chall—Challenger Plateau; SLHR—South Lord Howe Rise; STR—South Tasman Rise; ET—East Tasman Rise; SNR—South Norfolk Ridge; IB—Iselin Bank)

Figures

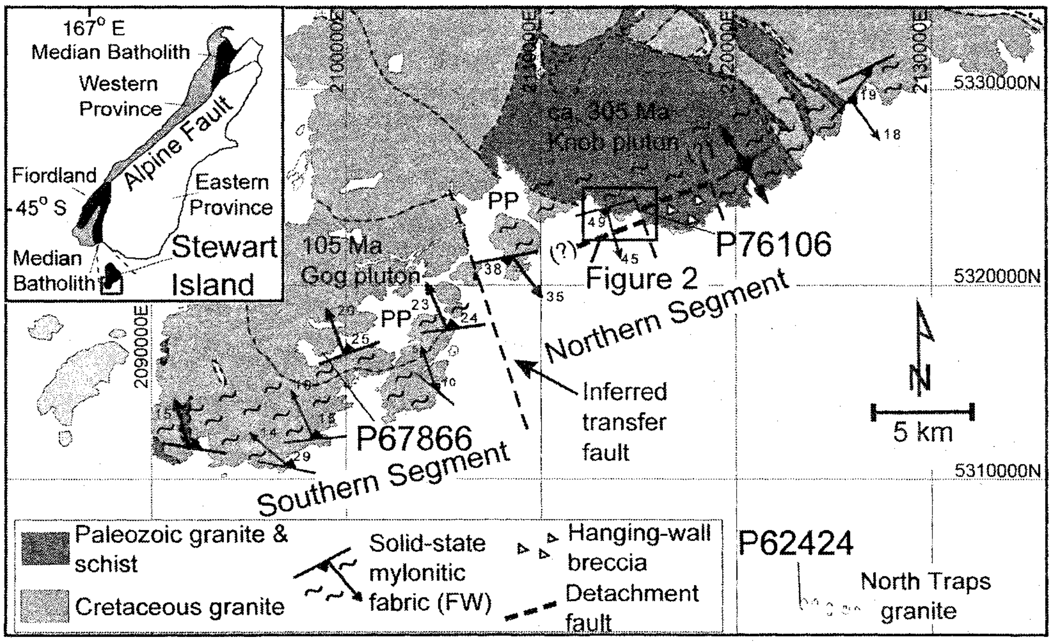

Figure 1

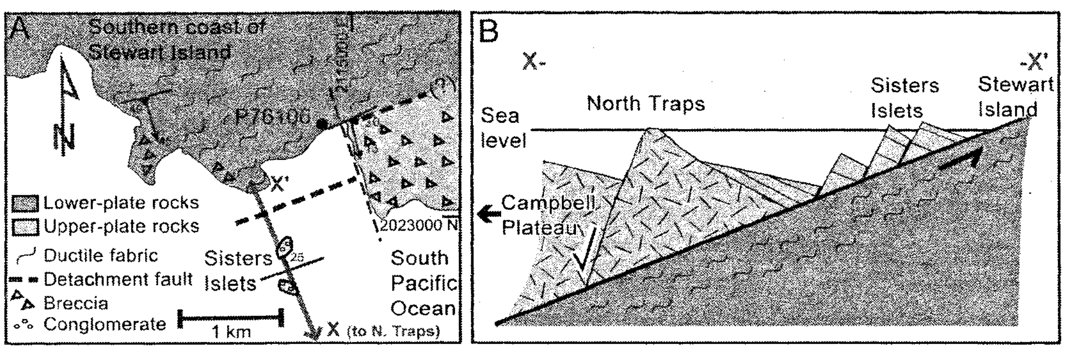

Figure 2

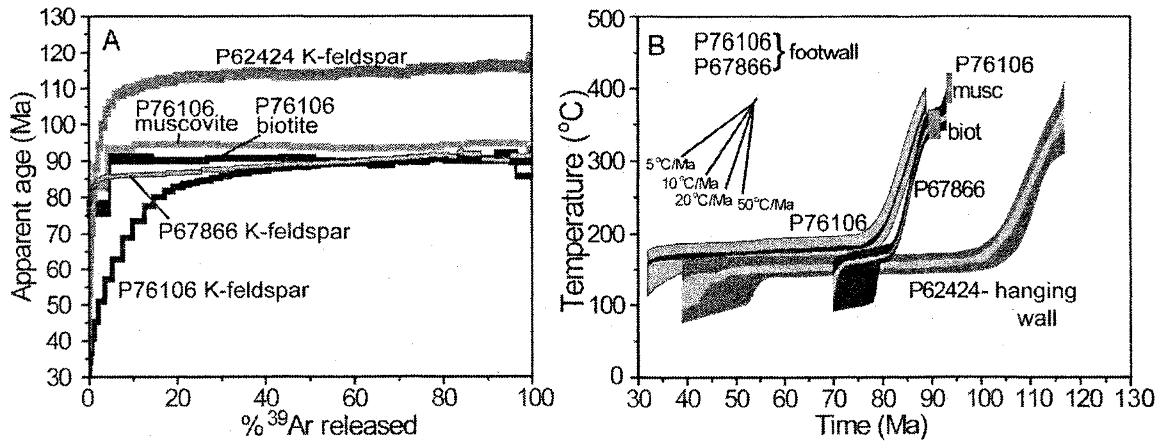

Figure 3

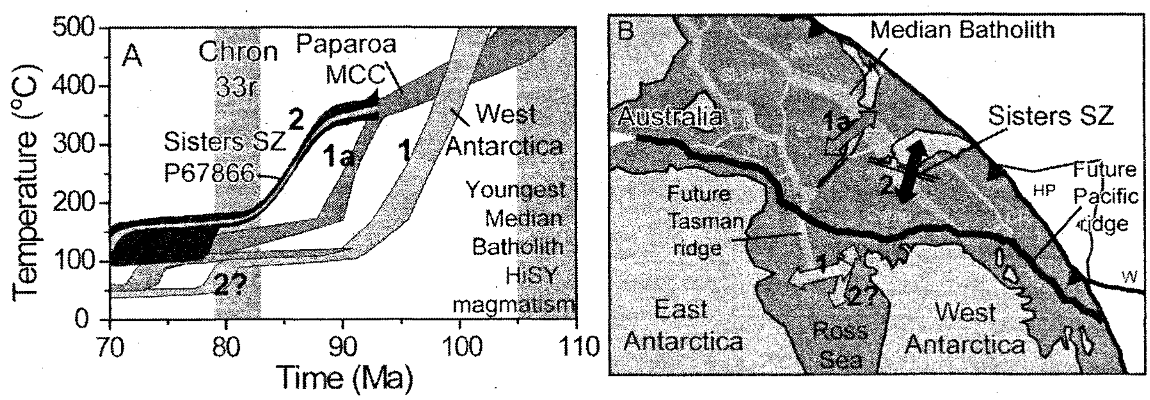

Figure 4

References

Allibone, A.H., and Tulloch, A.J., 2004, Geology of the plutonic basement rocks of Stewart Island, New Zealand: New Zealand Journal of Geology and Geophysics, v. 47, p. 233–256.

Allibone, A.H., and Tulloch, A.J., 1997, Metasedimentary, granitoid and gabbroic rocks central Stewart Island, New Zealand: New Zealand Journal of Geology and Geophysics, v. 40, p. 53–68.

Cook, R.A., Sutherland, R., Zhu, H., et al., 1999, Cretaceous-Cenozoic geology and petroleum systems of the Great South Basin, New Zealand, Institute of Geological and Nuclear Sciences monograph 20, 188pp.

Dewey, J.F., 1988, Extensional Collapse of Orogens: Tectonics, v. 7, p. 1123–1139.

Eagles, G., Gohl, K., and Larter, R.D., 2004, High-resolution animated tectonic reconstruction of the south Pacific and West Antarctic margin: Geochemistry, Geophysics, Geosystems, v. 5, no. 7, p. Q07002, doi: 10.1029/2003GC000657.

Etheridge, M.A., Symonds, P.A., and Lister, G.S., 1989, Application of the detachment model to reconstruction of conjugate passive margins, in Tankard, A.J., and Balkwill, H.R., eds., Extensional Tectonics and stratigraphy of the North Atlantic margins, American Association of Petroleum Geologists Memoir 45, p., 23–40.

Fleming, C.A., and Watters, W.A., 1974, Geology and petrography of a conglomerate in southern Stewart Island: New Zealand Journal of Geology and Geophysics, v. 17, p. 225–231.

Hirth, G., and Tullis, J., 1992, Dislocation creep regimes in quartz aggregates: Journal of Structural Geology, v. 14, p. 145-159.

Larter, R.D., Cunningham, A.P., Barker, P.F., Gohl, K., and Nitsche, F.O., 2002, Tectonic evolution of the Pacific margin of Antarctica. 1. Late Cretaceous tectonic reconstructions: Journal of Geophysical Research, v. 107, ser. B12, DOI 10.1029/2000JB000052.

Lister, G.S., Etheridge, M.A., and Symonds, P.A., 1986, Detachment faulting and the evolution of passive continental margins, v. 14, p. 246–250.

Lovera, O.M., Richter, F.M., and Harrison, T.M., 1989, The $^{40}Ar/^{39}Ar$ Thermochronometry for Slowly Cooled Samples Having a Distribution of Diffusion Domain Sizes: Journal of Geophysical Research, v. 94, p. 17,917–17,935.

Lovera, O.M., Richter, F.M., and Harrison, T.M., 1991, Diffusion domains determined by ^{39}Ar released during step heating: Journal of Geophysical Research, v. 96, p. 2057–2069.

Luyendyk, B.P., Wilson, D.S., and Siddoway, C.S., 2003, Eastern margin of the Ross Sea rift in western Marie Byrd Land, Antarctica: Crustal structure and tectonic development: Geochemistry, Geophysics, Geosystems, v. 4, G3, p. 1090, doi: 10.1029/2002GC000462.

McDougall, I., and Harrison, T.M., 1999, Geochronology and Thermochronology by the $^{40}Ar/^{39}Ar$ Method, 2nd edition, Oxford University Press, New York, NY, 269 p.

Mortimer, N., 2004, New Zealand's geological foundations: Gondwana Research, v. 7., p. 261-272.

Mortimer, N., Graham, I., Adams, C., Tulloch, A., and Campbell, H., 2005, Relationships between New Zealand, Australian and New Caledonian mineralised terranes: a regional geological framework: New Zealand Minerals Conference, p 151-159: http://www.crownminerals.govt.nz/minerals/conference/papers/151_Papers_42.pdf.

Rey, P., Vanderhaeghe, O., and Teyssier, C., 2001, Gravitational collapse of the continental crust: definition, regimes and modes: Tectonophysics, v. 342, p. 435-449.

Richard, S.M., Smith, C.H., Kimbrough, D.L., Fitzgerald, P.G., Luyendyk, B.P., and McWilliams, M.O., 1994, Cooling history of the northern Ford Ranges, Marie Byrd Land: West Antarctica: Tectonics, v. 13, p. 837–857, doi: 10.1029/93TC03322.

Siddoway, C.S., Sass, L.C., III, and Esser, R.P., 2005, Kinematic history of western Marie Byrd Land, West Antarctica: direct evidence from Cretaceous mafic dykes, *in* Vaughan, A.P.M., Leat, P.T., and Pankhurst, R.J., (eds.), Terrane processes at the margins of Gondwana, Geological Society, London, Special Publications, 246, p. 417–438.

Siddoway, C.S., Baldwin, S.L., Fitzgerald, P.G., Fanning, C.M., and Luyendyk, B.P., 2004, Ross Sea mylonites and the timing of intracontinental extension within the West Antarctic rift system: Geology, v. 32, p. 57–60, doi: 10.1130/G20005.1.

Spell, T.L., McDougall, I., and Tulloch, A.J., 2000, Thermochronologic constraints on the breakup of the Pacific Gondwana margin: the Paparoa metamorphic core complex, South Island, New Zealand: Tectonics, v. 19, p. 433–451, doi: 10.1029/1999TC900046.

Sutherland, R., 1999, Basement geology and tectonic development of the greater New Zealand region: an interpretation from regional magnetic data: Tectonophysics, v. 308, p. 341–362, doi: 10.1016/S0040-1951(99)00108-0.

Sutherland, R., and Hollis, C., 2001, Cretaceous demise of the Moa plate and strike-slip motion at the Gondwana margin: Geology, v. 29, p. 279-282.

Tulloch, A.J., and Kimbrough, D.L., 1989, The Paparoa metamorphic core complex, New Zealand: Cretaceous extension associated with fragmentation of the Pacific Margin of Gondwana: Tectonics, v. 8, p. 1217–1234.

Tulloch, A.J., and Kimbrough, D.L., 2003, Paired plutonic belts in convergent margins and the development of high Sr/Y magmatism: Peninsular Ranges batholith of Baja-California and Median Batholith of New Zealand, *in* Johnson, S.E., Paterson, S.R., Fletcher, J.M., Girty, G.H., Kimbrough, D.L., and Martin-Barajas, A., eds., Tectonic evolution of northwestern Mexico and the southwestern USA: Boulder, Colorado, Geological Society of America special paper 374, p. 275–295.

Wernicke, B., 1992, Cenozoic extensional tectonics of the U.S. Cordillera, *in* Burchfiel, B.C., Lipman, P.W., and Zoback, M.L., eds., The Cordilleran Orogen: Conterminous U.S., The Geology of North America: Boulder, Colorado, Geological Society of America, p. 553-582.

CHAPTER 2

THERMAL EVOLUTION OF THE SISTERS SHEAR ZONE, SOUTHERN NEW ZEALAND; FORMATION OF THE GREAT SOUTH BASIN AND DRIVING MECHANISMS FOR CONTINENTAL BREAKUP

Abstract

The separation of Zealandia from West Antarctica was the final stage in the Cretaceous breakup of the Gondwana Pacific margin. Continental extension resulting in formation of the Great South Basin and thinning of the Campbell Plateau leading to development of the Pacific-Antarctic spreading ridge was partially accommodated along the Sisters shear zone. This east-northeast striking ductile structure exposed along the southeast coast of Stewart Island, NZ is a greenschist facies extensional shear zone that separates a hanging wall of chloritic breccia and undeformed conglomeratic sediments from a footwall of mylonitic Carboniferous and Early Cretaceous granites. It is a complex structure that exhibits bivergent kinematics and can be subdivided into a northern and southern segment. $^{40}Ar/^{39}Ar$ thermochronology indicates cooling of the shear zone footwall beginning at ~94 Ma with the most rapid cooling occurring over the interval ~89-82 Ma. Structural and thermochronological data indicate a spatial and temporal link with initial sedimentation within the offshore Great South Basin, extension of the Campbell Plateau, and initiation of the Pacific-Antarctic spreading ridge. Based on

thermochronological constraints and the observation that the Sisters shear zone cuts across Zealandia basement terrane trends, it is evident that extension along the Sisters shear zone began 5-10 Ma later than extension in western Zealandia related to the opening of the Tasman Sea and was likely caused by interactions along the continental-oceanic plate boundary (i.e. slab capture).

Introduction

The isolation of Zealandia in the South Pacific was a result of continental extension leading to formation of the Tasman Ridge and the Pacific-Antarctic Ridge oceanic spreading systems (Figure 1). Development of the Tasman Ridge and separation of western Zealandia from eastern Australia due to Early Cretaceous metamorphic core complex-forming continental extension is well documented [*Tulloch and Kimbrough,* 1989; *Etheridge et al.,* 1989; *Lister et al.,* 1991; *Spell et al.,* 2000]. In contrast, details of continental extension leading to formation of the Pacific-Antarctic Ridge and separation of eastern Zealandia from West Antarctica are more cryptic. Increased understanding of this latter phase of tectonism holds important implications for the development of Zealandia as a continent because several offshore continental features (e.g. the Great South Basin and the Campbell Plateau) formed contemporaneously with this event.

Kula et al. [2007] proposed the isolation of Zealandia resulted from two distinct rifting events with separation from West Antarctica partially accommodated along the Sisters shear zone located on the southeast coast of Stewart Island in southern New Zealand. This tectonic model was based on comparison of $^{40}Ar/^{39}Ar$ K-feldspar thermochronometry from the Sisters shear zone with that of other Early Cretaceous shear zones in New Zealand and Antarctica. Here, a detailed field, kinematic, and thermochronometry study of the Sisters shear zone is presented. These data are used to constrain the shear zone architecture, determine the deformation mechanisms active (and thus temperature conditions) during extensional shearing of the footwall, and demonstrate the Sisters shear zone played a significant role in the Cretaceous extensional tectonics resulting in formation of the Great South Basin, thinning of the Campbell Plateau, and development of the Pacific-Antarctic Ridge. Additionally, observations from the Sisters shear zone indicate the driving mechanism for this episode of extension leading to separation Zealandia from West Antarctica was likely plate boundary forces (i.e. slab capture).

Stewart Island geology

Stewart Island is located just south of South Island and represents the southeastern continuation of the Median Batholith and Western Province of New Zealand [*Allibone and Tulloch,* 1997; 2004] (Figure 2). Mapping by *Allibone and Tulloch* [1997, 2004] shows the basement rocks making up Stewart Island are dominantly plutonic and of various granitoid compositions. Intrusions range from late Paleozoic through Mesozoic marking pulses of magmatism during the Carboniferous (345-290 Ma), Early-Middle Jurassic (170-165 Ma), latest Jurassic to earliest Cretaceous (151-128 Ma), and Early Cretaceous (128-100 Ma) [*Allibone and Tulloch,* 2004]. The spatial distribution and age constraints of pluton exposures on Stewart Island indicates that in the Early Cretaceous, magmatism migrated southwards (paleo-continentward) into the Western Province contemporaneous with episodes of crustal shortening [*Allibone and Tulloch,* 2004;

Klepeis et al., 2004]. Additionally, the distribution and chemical signatures of plutons exposed on Stewart Island supports the paired-plutonic belt interpretation of *Tulloch and Kimbrough* [2003] where the southern portion of the island represents the continuation of the thick HiSY belt and the north represents the thin LoSY belt with the Escarpment Fault roughly marking the boundary between the two [*Tulloch et al.,* 2006].

Structures present on the island include the Freshwater fault zone, the Escarpment Fault, and the Gutter shear zone which are all northwest-southeast striking reverse faults that, when restoring oroclinal bending through the Alpine Fault, are consistent with accommodating arc-normal shortening [*Allibone and Tulloch,* 2004], and may correlate to Early Cretaceous structures in the Fiordland region [*Klepeis et al.,* 2004].

The Sisters shear zone

The Sisters shear zone strikes northeast along the southeast coast of Stewart Island and consists of variably deformed granitoids that include breccia, protomylonite, mylonite, and ultramylonite [*Kula et al.,* 2007]. Recognition of the shear zone as a significant structure is based on outcrop sites visited along ~40 km of the southeast coast of Stewart Island (Figures 2, 3, 4). Descriptions of the outcrop locations visited and microstructural observations made from oriented samples collected at these sites are presented here to develop the shear zone architecture and to assess the conditions of deformation.

Kula et al. [2007] initially described the Sisters shear zone as consisting of two segments, North and South, based on deformation fabrics, kinematics, and apparent left lateral offset of the northern boundary of deformation (Figure 2). Figure 3 shows the site locations studied in the southern segment and figure 4 shows the locations of sites studied in the northern segment.

Field and microstructural observations – southern segment

In the southern segment, deformation fabrics are recorded in two granitic units; the 105 Ma Gog and Kaninihi plutons of *Allibone and Tulloch,* [2004]. Outcrop exposures tend to show high-strain zones on the order of tens of meters thick separated by intervals exhibiting very weak fabric to virtually undeformed textures. The following are descriptions of field and thin section data collected from key locations (shown in fig. 3) visited within the Sisters shear zone along the southeast coast of Stewart Island. The northern boundary of deformation in the southern segment is estimated to occur in the vicinity of South Arm (Figures 2, 3) based on a lack of deformation fabric in exposures to the north of this inlet.

At site 1 near the southern tip of Stewart Island (Figure 3) exposures of fine-to-medium grained biotite-K-feldspar-plagioclase-quartz granodiorite of the Kaninihi pluton exhibit a north-dipping foliation (282°/24° N) and a poorly developed lineation oriented at 314°/14°. The foliation is well defined by the grain-shape orientation of elongate 3-5 mm feldspar crystals. This ductile fabric is cut by a northwest-dipping high angle normal fault. In thin section quartz occurs between larger feldspar and biotite crystals as polycrystalline bands consisting of southwest dipping <50 μm grains with lobate margins (Figure 5a).

Site 2 also consists of outcrops of medium grained Kaninihi granodiorite. The mineralogy is the same as site 1 with the addition of minor muscovite growth within biotite clusters and along some grain boundaries. In outcrop there is a very weak foliation (085°/15° N) in the rock with a strong lineation (332°/12°) defined by elongate plagioclase (4x1 mm) crystals. In thin section feldspar and biotite crystals are mostly flat lying however, many are also oriented at high angles to the weak foliation plane. Polycrystalline quartz bands occur between the larger feldspar grains (Figure 5b).

Site 3 is located within the 105 Ma Gog pluton (Allibone and Tulloch, 2004). Ourcrops consist of north-dipping slabs of ultramylonite with a prominent foliation (099°/22° N) and lineation (354°/22°). The matrix is very fine grained with a banded appearance supporting highly rounded feldspar clasts (Figure 5c). Kinematic indicators include σ- and δ-shaped feldspar porphyroclasts and overturned microfolds (Figure 5c).

Site 4 is an outcrop of quartz-biotite-K-feldspar-plagioclase granite of the Gog pluton. Feldspars are as large as ~1-3 mm across and thin section shows minor muscovite growth within bands of biotite. Foliation (314°/38° N) and lineation (322°/ °) are both well developed in the outcrop. C'-type shear bands cm-scale ultramylonite zones with winged porphyroclasts are visible in hand sample, quartz grain-shape fabric is present in thin section (Figure 5d). Thin section analysis also shows cleavage fractures in feldspar crystals.

Site 5 is an exposure of the Kaninihi pluton consisting of intermixed intervals of dark and light granitic material. Both intervals consist of biotite-feldspar-quartz granite with the more mafic intervals having an increased abundance of biotite. Feldspar crystals range from ~0.5-3 mm across and sphene, zircon and epidote are relatively abundant. The mixed intervals of granite are subparallel to the prominent foliation (310°/10° N) which contains a lineation oriented 342°/5°. Thin sections show a well-preserved quartz grain-shape fabric (Figure 5e, f). Quartz is also present as ribbons and biotite shows mica-fish morphology. Feldspars are brittley deformed showing kink bands, dense fractures, and rotation along microfaults (Figure 5e, f).

Site 6 consists of exposures of quartz-K-feldspar-plagioclase-biotite granite of the Kaninihi pluton. Rock outcrops consists of northeast-dipping slabs with a well-developed foliation (130°/80° N) and lineation (125°/8°). Several south-dipping normal faults are present that cut the ductile fabric. In thin section quartz appears as ribbons and also exhibits a poor grain-shape orientation (Figure 5g). Feldspar crystals are highly fractured and microfaulted (Figure 5g).

Site 7 consists of medium-to-coarse grained K-feldspar-plagioclase-quartz-biotite Kaninihi granite. Foliation (044°/ 17° S) and lineation (160°/17°) are well developed in the outcrops with K-feldspar dominating the mineralogy and oriented in a framework defining the ductile fabric. In thin section quartz occurs as polycrystalline bands and biotite as mica-fish along the grain boundaries of larger feldspar crystals (Figure 5h). Fracture and kink-banding occurs in microcline crystals.

Site 8 consists of the same Kaninihi granite described for site 7. Ductile fabric in the outcrops is defined by foliation (025°/24° S) and lineation (155°/13°), which is cut by steep south-dipping normal faults. In thin section quartz is in polycrystalline ribbons and feldspar clasts show asymmetric wing-development as well as fracture and kink-banding (Figure 5i). White mica growth occurs along fractures and the foliation.

Site 9 is exposures of coarse feldspar-quartz-biotite Kaninihi granite. The outcrops appear weakly deformed with poorly developed foliation (265°/20° N) and lineation (330°/14°). In thin section quartz appears as ribbons and feldspars exhibit strong undulatory extinction. Feldspar crystals are also fractured and rotated along microfaults.

As stated above, some examples of the microstructures observed at these sites in the southern segment are shown in Figure 5. To summarize observations, several locations consist of ultramylonite (sites 3, 4, 5) either as a dominant component of the outcrop (site 3) or as intervals within coarser mylonitic or lesser deformed rocks (sites 4, 5). Common to all observed ultramylonites is the presence of highly rounded and winged feldspar porphyroclasts within a dark, banded very-fine-grained matrix (Figure 5). Feldspar deformation is dominated by fracturing, microfaulting, and kink-banding. Quartz is dominantely observed as ribbons and polycrystalline bands exhibiting grain-shape fabric, that occur between the larger feldspar crystals oriented subparallel to the foliation.

Field and microstructural observations – northern segment

Several sites studied in the northern segment of the Sisters shear zone are depicted in Figure 4. Ductile fabrics include protomylonite, mylonite, and ultramylonite and are present in three different plutons as mapped by *Allibone and Tulloch* [2004]— the Knob (305 Ma), Blakies (115 Ma), and Easy (130 Ma) plutons. Figure 6 shows a summary of the deformation fabrics observed in the northern segment and descriptions of these data as obtained from field observations, field measurements, and thin section analyses, follows.

Site 10 is within the Easy pluton on the western side of Pearl Island (Figure 4). The outcrop is generally a granodiorite consisting of intervals dominated by an assemblage of biotite-muscovite-quartz. The granodiorite exhibits a relatively weak south-dipping ductile fabric while the mica-rich intervals show a strong mylonitic fabric with S-C texture. The foliation is south-dipping with a strong lineation plunging toward 150° (Figure 4). In thin section mica fish, polycrystalline quartz ribbons, and quartz grain-shape fabric are all present (Figure 6a).

Site 11 is to the north-northeast of Pearl Island and also within the Easy Pluton (Figure 4). Here outcrops consist of medium grained biotite-K-feldspar-plagioclase-quartz granodiorite with rare hornblende. The exposures are undeformed and thus constrain the northern boundary of the shear zone at this location (Figure 4).

Site 12 is within the medium grained two-mica Knob granite. The general mineralogy consists of biotite-muscovite-K-feldspar-plagioclase-quartz with biotite more abundant than muscovite. There is a well-developed ductile fabric with foliation (075°/49° S) and lineation (164°/45°) that is cut locally by several south-dipping normal faults (Figure 4, 6f). Thin section shows preservation of a strong quartz grain-shape fabric, sigma shaped clasts, and shear bands (Figure 6b). Plagioclase exhibits kink-banding and deformation lamellae.

Site 13 is the Sisters Islets for which the Sisters shear zone is named (Figures 4, 6d). The islets consist of boulder conglomerate (Figure 6d) and were originally described by *Fleming and Watters* [1974]. The conglomerate beds consist dominantly of clasts of deformed granitoids within an arkosic sand matrix. Beds dip north at approximately 25° and show some chloritization and/or hydrothermal alteration. Fleming and Watters (1974) report zeolitization of feldspars.

Site 14 marks the only location where a fault surface has been observed and measured (Figures 4, 6c). The surface is marked by a black ultra-cataclastic ledge that separates brittley-overprinted granite mylonite below (north) from hydrothermally altered chloritic brecciated granite above (south) (Figures 4, 6c). The fault surface strikes northeast at 061°, dips south at 27° and has slickenlines oriented 153°/27°. The black ultracataclasite exhibits extreme grain size reduction and the overlying chlorite breccia is highly fractured consisting mostly of feldspar fragments with minor interstitial sericite and calcite growth. In thin section feldspar fragments show undulose extinction with crush zones at the grain boundaries.

Site 15 consists of deformed two-mica Knob granite with muscovite more abundant than biotite in the finer grained intervals and biotite more abundant in the coarser intervals. Strong foliation (040°/19° S), lineation (145°/18°), C'-type shear bands, asymmetric clasts, and cm-scale intervals of ultramylonite are observable in hand sample (Figure 6g). Thin section shows well-preserved mica fish, winged σ- and δ-shaped clasts, polycrystalline quartz bands, and quartz grain-shape fabric (Figure 6e).

To summarize observations from the northern segment; all deformation fabrics (foliation/lineation) measured are south-dipping as are all faults that cut these fabrics. Quartz is preserved in deformed rocks as polycrystalline ribbons and exhibits a strong grain-shape fabric. Feldspars exhibit some undulatory extinction in thin section and show deformation by fracture and microfaulting. Heavily fractured granitic chlorite-breccia sits above a fault surface and offshore conglomerate is oriented coaxially but oppositely dipping to coastal mylonitic fabrics.

$^{40}Ar/^{39}Ar$ procedures

Sample locations are shown in Figures 2, 3, and 4. Biotite, muscovite, and K-feldspar were separated from hand samples by crushing, sieving, heavy liquid density separation, and hand-picking to >99% purity. Samples P77057 biotite and muscovite and P77056 biotite were irradiated for 7 hours at the McMaster Nuclear Reactor at McMaster University, Ontario, Canada. Samples P75092 biotite and muscovite, P75084 biotite and K-feldspar, P75079 biotite, and P75086 biotite and K-feldspar were irradiated for 7 hours at the Oregon State University Radiation Center in the In-Core Irradiation Tube (ICIT) of the 1 MW TRIGA type reactor at Oregon State University. Sample P75092 K-feldspar was irradiated for 14 hours at the Nuclear Science Center at Texas A&M University on the core edge (fuel rods on three sides, moderator on the fourth side) of the 1MW TRIGA type reactor in a dry tube device, shielded against thermal neutrons by a 5 mm thick jacket of B_4C powder. Synthetic K-glass and optical grade CaF_2 were included in the irradiation packages to monitor neutron induced argon interferences from K and Ca, and Fish Canyon Tuff sanidine (27.9 Ma; *Steven et al.,* [1967]; *Cebula et al.,* [1986]) was included in the irradiation to determine J-factors. These data are listed with the respective samples in Table 3.

Following irradiation, samples were analyzed at the Nevada Isotope Geochronology Laboratory at the University of Nevada, Las Vegas using the furnace step heating method with a double vacuum resistance furnace similar to the *Staudacher et al.* [1978] design. Reactive gases were removed by three GP-50 SAES getters prior to being admitted to a MAP 215-50 mass spectrometer by expansion. Peak intensities were measured using a Balzers electron multiplier by peak hopping through 7 cycles; initial peak heights were determined by linear regression to the time of gas admission. Mass spectrometer discrimination and sensitivity was monitored by repeated analysis of atmospheric argon aliquots from an on-line pipette system. The discrimination used in calculating ages for each sample is also listed in Table 3.

K-feldspar samples P75086 and P75084 were interpreted using the multiple diffusion domain (MDD) modeling approach of *Lovera et al.* [1989, 1991]. Activation energy (E) was determined using a least squares linear regression of data from low-temperature steps of the experiment plotted on an Arrhenius diagram [*Lovera et al.*, 1989]. The frequency factor (D_o) for each diffusion domain was determined using the calculated activation energy and modeling the form of the Arrhenius plot [*Lovera,* 1992]. Ten E-D_o pairs were then randomly selected from a Gaussian distribution around the values and their uncertainties obtained from the Arrhenius diagram. For each pair, a single activation energy was assumed to be representative of all domains used in the modeling. The number of domains along with their size and volume fraction was modeled using a variational iterative technique to determine the best fit between the experimental and modeled results on a domain size distribution plot [log (r/r_o) vs. $\%^{39}Ar$ released] [*Richter et al.*, 1991]. Cooling histories were then determined for each E-D_o pair by fitting modeled age spectra to the experimental age spectrum using these parameters and domain distributions. The cooling histories obtained were then used to calculate 90% confidence intervals for the total distribution and the median of the distribution [*Lovera et al.*, 1997].

$^{40}Ar/^{39}Ar$ results

Age spectra obtained for muscovite, biotite, and K-feldspar are summarized in Figure 7 with corresponding data tables presented in Appendix A. All ages cited in text and figures are at the 2σ level of uncertainty. Plateau ages are defined as three or more consecutive steps totaling greater than 50% of the gas release that overlap at the 2σ level of uncertainty. In Figure 7 an asterisk denotes the age interpreted as representative for each sample. Below are descriptions of the age spectra and isotopic behavior.

P75086 biotite and K-feldspar (Site 1)

Biotite yielded a total gas age of 92.9 ± 0.8 Ma. A flat age spectrum was obtained with 95% (14 of 15 steps) of the gas release corresponding to a plateau age of 93.1 ± 0.8 Ma. Isochron regression of all 15 steps (MSWD = 0.19) results in an age of 93.7 ± 0.7 Ma corresponding to an initial $^{40}Ar/^{36}Ar$ ratio of 250.8 ± 7.4. The plateau age is the preferred age for the sample.

K-feldspar yielded an age spectrum showing a progressive increase in age from 80-90 Ma (Figure 7). The first four steps of the analysis yield higher ages indicative of excessive argon, however these only account for 0.3% of the total gas release. Arrhenius data calculated from the ^{39}Ar release pattern for MDD thermal modeling are E = 45.99 ± 0.95 kcal/mol and D_o/r^2 = 4.35 ± 0.23 sec^{-1} (Figure 8).

P75079 biotite (NW of Pearl Island)

The age spectrum for P75079 biotite shows an initial increase in age to a plateau-like crest, a subsequent decrease in age to a trough, and a final staircase shaped increase in ages. The total gas age for the sample is 91.2 ± 0.6 Ma, however omission of the first step (youngest age in spectrum) yields a preferred age of 94.6 ± 0.6 Ma. The 'plateau' (steps 3-5) and 'trough' (steps 8-11) yield weighted mean ages of 96.1 ± 0.8 Ma and 91.1 ± 0.7 Ma, respectively. These two segments of the age spectrum can be expanded by inclusion of adjacent steps to yield statistically acceptable (MSWD criteria) isochron regressions. Steps 2-5 yield an isochron age of 97.0 ± 2.4 Ma with a $^{40}Ar/^{36}Ar$ intercept of 122 ± 350 and an MSWD of 2.7. Steps 8-13 yield an isochron age of 93.5 ± 1.3 Ma with a $^{40}Ar/^{36}Ar$ intercept of 160 ± 84 and an MSWD of 2.3. Neither of these regressions include 50% or more of the total gas released during the analysis and all regressions yield initial $^{40}Ar/^{36}Ar$ ratios significantly less than atmosphere (295.5).

P77056 biotite (Site 10)

Biotite yielded a discordant age spectrum with ages ranging from ~50 to 90 Ma. The total gas age for the sample is 82.2 ± 0.9 Ma; omitting the first two steps (youngest of spectrum) yields a preferred age of 86.6 ± 0.9 Ma. Two segments of the age spectrum can be identified that include contiguous steps with ages that are indistinguishable at 2σ. Steps 4-9 (36.6% of the gas release) yield an age of 86.4 ± 1.2 Ma and steps 7-12 (27.3 % of the gas release) yield an age of 85.7 ± 1.2 Ma. Statistically valid isochrons were obtained from regressions using steps 1-6 and 7-13 corresponding to ages (and $^{40}Ar/^{36}Ar$ intercepts) of 92.5 ± 1.2 Ma (283.1 ± 2.9) and 93.1 ± 3.1 Ma (266 ± 17).

P75084 biotite and K-feldspar (Site 11)

The total gas age for the biotite sample is 90.3 ± 0.7 Ma, however when the first step is excluded (minimal age of spectrum) the remaining steps yield a preferred age of 93.3 ± 0.7 Ma. The age spectrum is discordant with apparent ages range from ~75 to ~95 Ma in a spectrum consisting of a hill-trough-rise shape. These three identifiable segments of the age spectrum yield ages of 94.4 ± 1.0 Ma (steps 3-6), 90.3 ± 1.0 Ma (steps 8-11), and 92.3 ± 1.0 Ma (steps 12-15), respectively. These same increments of gas release yield statistically acceptable (MSWD criteria of *Wendt and Carl* [1991]) isochron regressions with ages and $^{40}Ar/^{36}Ar$ intercepts of 95.6 ± 1.4 Ma, 52 ± 270; 90.3 ± 1.5 Ma, 308 ± 88; and 93.0 ± 1.0 Ma, 195 ± 170, respectively. Steps 3 through 6 account for 45.6% of the gas release, whereas steps 8-11 and 12-15 account for 11.3 and 12.0 %, respectively.

K-feldspar produced an age spectrum with an increase in ages over the analysis from 80 to 89 Ma. Minor effects of excess argon are evident over the first ~9% of the gas release based on age decreases for the second of isothermal duplicate steps. Arrhenius parameters calculated from the ^{39}Ar release are E= 42.77 ± 1.06 kcal/mol and D_o/r^2 = 0.74 ± 0.28 sec^{-1}.

<u>P77057 biotite and muscovite (Site 12)</u>

The age spectrum from muscovite shows an initial increase in ages followed by a plateau and a final high temperature increase in ages. The plateau segment consists of 76.8% (steps 3-13) of the gas release with an age of 93.2 ± 0.4 Ma. This is the preferred age for the sample. The total gas age for the sample is 92.7 ± 0.3 Ma. Isochron regressions reveal two thermally distinct trapped $^{40}Ar/^{36}Ar$ components [e.g. *Heizler and Harrison,* 1988]. Steps 1-13 (MSWD = 1.6) result in an age of 93.6 ± 0.6 Ma with a $^{40}Ar/^{36}Ar$ intercept of 271.9 ± 6.2. Steps 14-16 (MSWD = 3.1) yield an age of 94.3 ± 13 Ma and a $^{40}Ar/^{36}Ar$ intercept of 448 ± 900. Although all of these ages are indistinguishable at the 2σ level, the plateau age is considered the accepted age for the muscovite because the isochron ages and intercepts are more poorly constrained due to the high radiogenic yields.

Biotite yielded an age spectrum with a plateau over the final 64% (steps 4-13) of the gas release following an initial stepwise increase in ages. The plateau age for this volume of gas is 89.1 ± 0.5 Ma, which is the preferred age for the sample. The same steps define an isochron (MSWD = 1.6) corresponding to an age of 89.6 ± 1.7 Ma and a $^{40}Ar/^{36}Ar$ intercept of 300 ± 17. The total gas age for the sample is 84.37 ± 0.5 Ma.

P75092 muscovite, biotite, and K-feldspar (Site 15)

Muscovite produced a flat age spectrum with 95.4% of the gas release (steps 2-16) yielding a plateau age of 92.9 ± 0.7 Ma (preferred age), which is indistinguishable from the total gas age of 92.7 ± 0.7 Ma. Steps 2-16 also define an isochron (MSWD = 0.94) with an age of 92.8 ± 1.4 Ma and a $^{40}Ar/^{36}Ar$ intercept of 328 ± 27, indicating a minor component of excess ^{40}Ar.

Biotite yielded a 'plateau-trough-plateau' shaped age spectrum corresponding to a total gas age of 88.3 ± 0.7 Ma. When omitting step 1 from the calculation, a preferred total gas age of 89.5 ± 0.7 Ma is obtained. Steps defining the two 'plateaus' (3-6; 40.1% of gas release, and 12-14; 20.0% of gas release) yield weighted mean ages of 90.1 ± 0.8 Ma and 90.0 ± 0.8 Ma, respectively. Therefore, 60% of the gas release yielded an age of 90 Ma. Statistically valid isochron regressions yield ages around 90-91 Ma, however the $^{40}Ar/^{36}Ar$ intercepts are significantly less than atmospheric (~190).

K-feldspar yielded a discordant age spectrum. Initially, ages progressively increased as expected for samples fit for MDD thermal modeling, however dramatic increases and decreases in ages resulting in a 'hump-shaped' spectrum indicate the presence of excess argon in the middle-to-larger domains resulting in data unsuitable for thermal history modeling.

Discussion

Conditions of deformation within the Sisters shear zone

From the field and microstructural data described above and depicted in figures 3-6, estimates can be made on the crustal conditions of deformation within the Sisters shear zone. Additionally, these data provide evidence to support interpretation of the shear zone as an extensional structure representing a detachment fault system. Interpretations of the conditions of crustal deformation within the Sisters shear zone and the case for an extensional tectonic regime is presented here.

Southern segment of the Sisters shear zone

The southern segment of the Sisters shear zone includes ductile mylonitic fabrics preserved in the Kaninihi and Gog plutons (Figure 3). At several locations within the Kaninihi pluton (sites 1, 2, 7) thin sections show coarse feldspar crystals creating a framework that appears to control the geometric plasticity of quartz. These thin sections show smaller recrystallized quartz grains that are interconnected between the larger feldspar grain boundaries and are sometimes isolated as lenses between the larger grains (Figure 5a, b, h). Feldspar crystals at all southern segment sites show evidence of brittle deformation including fracturing, microfaulting, and cataclasis. However, kink-banding of feldspar crystals is also observed in several thin sections indicating deformation temperatures in excess of ~350°C [*Pryer,* 1993]. Temperatures in this range are consistent with ribbon development and subgrain rotation recrystallization of quartz [*Hirth and Tullis,* 1992; *Stipp et al.,* 2002], which are microtextures present at several locations (Figure 5). The preservation of fine-grained oblique-grain-shape fabric and a lack of annealing of recrystallized grains indicates cooling during deformation. Although brecciation has not been observed to overprint the ductile fabrics to further support progressive cooling during shearing, outcrop scale brittle faults that cut the foliation have been observed in the vicinity of sites 7 and 8.

Northern segment of the Sisters shear zone

Photomicrographs in Figure 6 indicate the dominant deformation mechanisms in the northern segment of the Sisters shear zone were subgrain rotation recrystallization of quartz and some fracturing and kink band development of feldspar grains. These features indicate similar deformation temperatures (450 - 350°C) as the southern segment of the shear zone. Evidence for cooling during shearing in the northern segment includes cataclasis and brecciation overprinting the ductile fabrics as seen at site 14 (Figure 6c). Also, high-angle, south-dipping, brittle normal faults cut mylonitic fabric in the vicinity of Seal Point (Figures 4, 6f) indicating deformation under cooler conditions.

Progressive cooling during deformation is consistent with an extensional regime, however the best evidence for the extensional nature of the shear zone and its representing a detachment fault system is based on two key locations (sites 13 and 14). Site 14 exposes critical structural relationships including a south-dipping fault surface separating a mylonite zone below (footwall) from brecciated and chloritically altered granitoids above (hanging wall) (Figure 5c). The orientation of slicken lines on the fault surface is consistent with lineation orientations measured from mylonites throughout the shear zone, implying kinematic compatibility of the detachment fault and footwall mylonite [e.g. *Davis,* 1980].

Site 13 is the conglomerate beds of the offshore Sisters Islets. Bedding in the conglomerate has a strike similar to the coastal mylonitic fabric (~070°), but dips oppositely to the north-northwest at 20-25°. This orientation indicates the Sisters Islets are a remnant of rotated sedimentary hanging-wall rocks sitting above the mylonitic footwall rocks exposed along the coast to the north (Figure 4). This relationship requires the presence of an intervening detachment fault [e.g. *Davis,* 1980], evidence of which has been recorded at site 14. Combined observations at sites 13 and 14 indicate a footwall of ductile mylonites that are brittley overprinted in fault contact with a hanging wall consisting of brecciated granite and tilted sedimentary rocks. These are the major components of detachment fault systems as recognized in the Basin and Range Province of the western U.S. [*Wernicke,* 1992].

Kinematics of the Sisters shear zone

Kinematic indicators in the southern segment of the Sisters shear zone include σ- and δ-type winged porphyroclasts, quartz grain-shape fabrics, and rotation of crystals along microfaults (Figure 5). There is some variation in foliation attitudes in the southern segment, however lineations are consistently oriented 330-150° throughout the shear zone (Figure 3). The southern segment is dominated by top-to-the-north ductile shear with the exceptions of site 6, which exhibits top-to-the-south kinematics and site 7, which exhibits both top-north and top-south shear (Figures 3, 5). Shear sense at site 7 is evident from quartz shear bands and mica fish developed between rigid feldspar crystals (Figure 5h). These small deformation zones show both top-to-north and top-to-south kinematics-possibly reflecting dominant pure shear deformation at this location. This interpretation requires the bivergent shear bands to have deformed simultaneously. A lack of cross-cutting relationships between these zones may support this assertion.

Thin section analysis from a sample collected from site 8 indicates subgrain rotation recrystallization in quartz (Figure 5i). The quartz grain-shape fabric indicates top-to-north kinematics although the foliation and lineation dip and plunge south. This site is the only location visited where kinematics appear updip; possibly reflecting roll-over of foliation surface. Downdip top-to-north kinematics are recorded from all other sites with the exception of site 6, which shows top-to-south shear sense.

All fabrics observed in the northern segment exhibit top-to-the-south shear sense based on C'-type shear bands (site 15), asymmetric wing growth on feldspar porphyroclasts (site 15), well-developed mica fish (site 10), oblique grain shape fabrics (site 12), and winged porphyroclasts (site 12) (Figure 6). In addition to these microstructural kinematic indicators, sites 13 and 14 show evidence for top-to-the-south extensional deformation.

From the field and microstructural observations presented, it is evident the Sisters shear zone consists of a top-to-the-north southern segment and a top-to-the-south northern segment. The structural data also show that the north and south segments contain consistently oriented lineations regardless of kinematics, microstructures indicating similar deformation conditions including cooling during shearing, and yield similar $^{40}Ar/^{39}Ar$ data (discussed below). These consistencies indicate the two segments likely represent a single fault system, however the architecture is complex. In map view there is an apparent left-lateral offset in the shear zone boundary between the north and south segments (Figure 2), which led *Kula et al.* [2007] to postulate the presence of a yet-unidentified transfer fault. This interpretation is consistent with the presence of several transform faults in the northern segment that juxtapose mylonitic footwall rocks and breccia outcrops across bays and inlets. This possible interpretation will be further developed later when the Sisters shear zone is placed into the regional tectonic framework.

Interpretation of mica ages

The approach taken in interpreting the discordant age spectra obtained for biotites in this study is to use the total-gas age (K/Ar equivalent) calculated when excluding the initial young step(s) (Figure 7). This interpretation applies to samples that did not yield valid plateau or isochron ages. Paragraphs below describe some details of the biotite analyses that led to this interpretation of ages.

Common to four biotites analyzed in this study (P75079, P77056, P75084, P75092) is an age spectrum with a 'rise-plateau-trough-rise' shape (Figure 7). *Lo and Onstott* [1989] found this shape to be representative of ^{39}Ar recoil during irradiation from high K-bearing sites (biotite) into low-K sites (typically chlorite). This interpretation may be supported by an inverse correlation between age and ^{37}Ar released for each furnace step indicating chlorite interlayers outgas lower $^{40}Ar^*/^{39}Ar_K$ due to recoil implanted ^{39}Ar from neighboring biotite during the irradiation. In this scenario it would be expected that the resulting biotite ages (indicated by low ^{37}Ar signals) calculated would be overestimates of the 'actual' age due to recoil induced increased $^{40}Ar^*/^{39}Ar_K$ values. *Roberts et al.* [2001] looked at argon isotopes ^{36}Ar, ^{37}Ar, and ^{38}Ar as ratios over ^{39}Ar and compared them with the ages calculated for each gas volume extracted from laser spot analyses. Inverse correlation of $^{36}Ar/^{39}Ar$ with age indicated that younger ages were a reflection of alteration in biotite however, a lack of elevated $^{37}Ar/^{39}Ar$ and

$^{38}Ar/^{39}Ar$ values with decrease in age indicated the alteration was not introducing calcium or chlorine into the mineral.

The biotites in this study yield different trends from those noted in these previous studies. Aside from the gas released from the first furnace step, the release patterns for isotopes ^{40}Ar and ^{39}Ar are basically uniform across the analyses indicating recoil may only be a factor in producing the initial low ages but not the entire discordant age spectra. In the case of ^{39}Ar recoil from biotite layers into chlorite layers, the ^{39}Ar and $^{40}Ar^*$ release patterns would be expected to be antithetic over the sample gas derived dominantly from chlorite. Inverse correlations between $^{36}Ar/^{39}Ar$, $^{38}Ar/^{39}Ar$ and age may support arguments for degree of alteration as a factor controlling biotite ages [*Roberts,* 2001]. $^{40}Ar^*$, ^{39}Ar, and ^{38}Ar all show similar release patterns for all biotite age spectra, however ^{36}Ar shows an antithetic release pattern to these isotopes. Dominant ^{36}Ar release occurs at two points during the step heat: the first step- 650°C and over the temperature interval ~800-950°C. This is consistent with the temperature constraints of *Lo and Onstott* [1989] for outgassing of chlorite interlayers. No appreciable ^{37}Ar was measured during the $^{40}Ar/^{39}Ar$ analyses resulting in low Ca/K values with only small fluctuations over the analyses. The lack of correlation of Ca/K values with age indicates that if in fact chlorite interlayering played a role in ^{39}Ar recoil, then it likely accounts for only a small volume in the mica. This is consistent with petrographic evidence indicating only subtle chloritization of the biotites, and the pristine appearance of the biotites observed during mineral separation under a binocular microscope.

Nearly all isochron regressions for the mica samples in this study yield $^{40}Ar/^{36}Ar$ intercepts less than atmosphere. While these values are typically deemed as impossible, they may reflect an artifact of ^{39}Ar recoil from more retentive high-K (biotite) sites into less retentive low-K (chlorite?) interlayers. The effect of this would be reductions in the ^{39}Ar/^{40}Ar values for the gas released from biotite (drive points left on isochron diagram) and increases in the ^{39}Ar/^{40}Ar values for the chlorite (drive points to the right) resulting in a steeper slope for the linear array and thus a higher ^{36}Ar/^{40}Ar intercept.

Thermochronological constraints on the Sisters shear zone

Two samples yielded both muscovite and biotite ages (P77057 and P75092) and in both cases the muscovite ages (~93 Ma) are 3-4 Ma older than the biotite ages (~89 Ma) (Figure 7). This is consistent with the results of *Kula et al.* [2007] indicating the northern segment underwent relatively slow cooling (~17°C/Ma) during this time interval. The remaining biotites yield ages ranging from 94.6 Ma to 86.6 Ma (Figure 7). Samples P75079, P75084, and P77056 crudely define a systematic decrease in ages from north-to-south consistent with progressive north-directed exhumation along a top-to-the-south detachment fault, however the uncertainty in the placement of the putative transfer fault separating the north and south segments as well as the likely presence of other transfer faults in the area (Figure 4) makes it difficult to attempt to quantify an exhumation rate between these samples with any certainty.

K-feldspar from samples P75084 (northern segment) and P75086 (southern segment) yielded very similar ages, however thermal modeling indicates some subtle differences in the thermal histories recorded in these samples (Figures 8, 9). The thermal history for P75084 K-feldspar is concave upward indicating a progressive decrease in cooling rate from initially 25-30°C/Ma at 87-89 Ma to near 10°C/Ma at 80 Ma (Figure 8d). In contrast, the thermal history for P75086 K-feldspar appears slightly convex upward beginning at 89 Ma followed by a transition to concave upward at ~84 Ma (Figure 9d).

Cooling during progressive northward exhumation is apparent from comparison of the thermal history of P75084 K-feldspar to that from the northern segment reported in *Kula et al.* [2007]. Both samples yield very similar shaped cooling curves, however the thermal history for P75084 is ~75°C cooler than P76106 at any given time indicating the sample reached cooler temperatures (or shallower crustal levels) earlier (Figure 10). As sample P75084 was collected north of P76106, it is expected that the sample should record a slightly earlier cooling if exhumation had occurred along a south-dipping detachment fault. Because the microstructures developed during shearing indicate cooling from deformation temperatures as high as ~350-400°C, the mica ages likely reflect slow cooling during the earliest stages of shearing, and the subsequent increase in cooling rate determined from K-feldspar MDD modeling reflects the beginning of significant exhumation along the detachment fault at 89 Ma. Therefore, in the northern segment, shearing may have initiated as early as ~93 Ma (muscovite ages) with significant exhumation and cooling of footwall rocks taking place over the interval ~89-80 Ma. Interpretation of cooling as a result of exhumation and not post-intrusion thermal relaxation is supported by the ~10 Ma time lag between mica cooling ages and the age of the youngest plutons cut by the Sisters shear zone (~105 Ma- Gog/Kaninihi, Table 1).

Comparison of P75086 K-feldspar with sample P67866 of *Kula et al.* [2007] indicates these samples record virtually identical thermal histories (Figure 10). The inflection to rapid cooling at 89 Ma as reported by *Kula et al.* [2007] (Figure 10) is reproduced when the P75086 biotite age and a nominal closure temperature of 350° ±

25°C is plotted along with the K-feldspar cooling paths. A complexity that arises in interpreting these data is that sample P75086 is in the footwall and P67866 is in the hanging wall of a top-to-the-north sense shear zone, however they record the same thermal history. This can be explained by considering the southern segment of the Sisters shear zone within the footwall of the top-to-the-south northern segment, representing an overall bivergent geometry.

Microstructures indicate deformation occurred at temperatures as high as 350-400°C, therefore the 93 Ma biotite age from sample P75086 and the slow cooling rate inferred for ~93-89 Ma may indicate cooling during initial top-to-the-north shearing, which therefore did not accommodate much exhumation. A structurally higher top-to-the-south detachment fault related to that in the northern segment (Figure 11) could have initiated by ~89 Ma, and accommodated the cooling recorded in the K-feldspars. If correct, then the lack of top-to-the-south overprinting fabric, brecciation, and cataclasis (as seen in the northern segment) can be explained by the southern segment representing a deeper portion of crust than that exposed in the northern segment.

Bivergent shear zones have been documented in the Paparoa metamorphic core complex [*Tulloch and Kimbrough,* 1989] and the Otago Schist [*Deckert et al.,* 2002], which may lend further credibility to this hypothesis under the pretense that New Zealand arc-crust and/or the dynamics of Cretaceous rifting was amenable to development of bivergent geometries. An alternative explanation for the thermal histories and spatial relationships of the southern segment is a structurally higher top-to-the-north detachment fault exists north of South Arm. If so, hanging-wall sediments (perhaps similar to those of the Sisters Islets in the northern segment) would be expected to have been deposited north of South Arm, however no evidence of this has been reported.

The Sisters shear zone, the Great South Basin, and the Campbell Plateau

Southeast of Stewart Island, the physiography of Zealandia fragments consists of the broad Campbell Plateau and its internal sub-basins; specifically the Great South Basin (Figure 1A). The Great South Basin (GSB) represents one of several Cretaceous basins related to the final stages of separation of Zealandia from the dispersing Gondwana supercontinent [e.g. *Cook et al.,* 1999]. The northwest boundary of the GSB is denoted by a prominent southeast dipping bathymetric scarp representing a basin-bounding normal fault. The northeast strike of the Sisters shear zone can be extended offshore to meet with this feature (Figure 12). The shape of the main depocenter (Central Sub-basin) and related subbasins of the GSB may have implications for interpreting the Sisters shear zone, especially the relationship between the northern and southern segments.

The western edge of the deepest part of the GSB, the Central Sub-basin, sits near the intersection of the arc-belt trend and the Sisters shear zone [*Tulloch et al.,* 2006]. More specifically in the arc-belt, near the boundary between LoSY and HiSY belts, which represent thin, low-lying and thick, high-standing arc crust, respectively [*Tulloch and Kimbrough,* 2003; *Tulloch et al.,* 2006]. Formation of the GSB was synchronous with deposition of Hoiho Group sediments, which are terrestrial sediments that unconformably overlie basement rocks [*Cook et al.,* 1999]. The onset of rapid cooling in Sisters shear zone footwall-rocks at ~89 Ma from K-feldspar thermochronometry is consistent with the inferred age for the base of the Hoiho Group sediments [*Cook et al.,* 1999]. Additionally, dip directions on normal faults that were active during Hoiho Group deposition are oriented subparallel to the lineation orientations measured throughout the Sisters shear zone [*Cook et al.,* 1999].

Sedimentation within the GSB may also reflect crustal deformation along the Sisters shear zone fault system. Provenance directions for the Hoiho Group sediments are from the southwest (the adjacent HiSY belt) and from the northwest (Sisters shear zone footwall) (Figure 12) [*Cook et al.,* 1999]. The implications of these sources are 1) the HiSY belt was a topographic high shedding sediment onto the low-lying LoSY belt supporting assertions that the HiSY belt represents a once high-standing arc-plateau [*Tulloch et al.,* 2006], and 2) footwall exhumation along the Sisters shear zone provided terrestrial detritus into the Central Sub-basin. Therefore at the time of extension along the Sisters shear zone, the HiSY belt was being both extended (thinned) and erosionally exhumed. The lack of volcanic and sedimentary units in this belt is typically explained by widespread denudation due to the once high-standing topography of this belt of thick crust [*Tulloch et al.,* 2006]. Significant erosion and thinning of a high-standing arc-plateau would likely required more isostatic adjustment than the adjacent thin LoSY belt which may explain why Sisters shear zone exposures terminate to the northeast at the paired belt boundary and the structure is inferred to likely continue submerged as represented by the prominent scarp bounding the northwest edge of the Great South Basin (Figure 12).

By assuming the interpretation of the role of the Sisters shear zone in formation of the GSB is correct, features of the GSB may be used to help constrain the architecture of the fault system. The location of the transfer fault between the northern and southern segments of the Sisters shear zone is aligned with what may be left-lateral offset of the main bounding fault scarp defining the northwest margin of the GSB. If the northwest margin of the Rakiura Trough correlates to the northwest margin of the Central Sub-basin, then left-lateral offset within the GSB is apparent. This supports the hypothesis of a structurally higher top-to-the-south normal fault system in the southern segment, that if exposed would be expected to be farther to the south. This is also consistent with inferences of a transfer fault separating the northern and southern segments of the Sisters shear zone [*Kula et al.,* 2007] in that the location of offset, though poorly constrained, in both features is aligned (Figure 12). Additionally, the postulated transfer fault may be supported by seismic data interpreted by *Davey* [2005] to represent the Triassic suture between the Brook Street island arc terrane and the Gondwana margin. An alternative interpretation is that the seismic reflection data imaged the transfer fault separating the north and south segments of the Sisters shear zone. This alternative view doesn't require the interpretation of *Davey* [2005] to be incorrect, as the suture could simply have been reactivated as a transfer fault during Sisters shear zone extension.

The Campbell Plateau is a broad submerged feature consisting of sedimentary basins (including the GSB discussed above) formed during mid-Cretaceous time [*Cook et al.,* 1999] (Figure 1). The plateau was separated from West Antarctica by initiation of the Pacific-Antarctic spreading ridge during chron 33r (83-79 Ma; *Sutherland,* [1999]). The timing of chron 33r corresponds with the timing of transition to slow cooling recorded in K-feldspar from the Sisters shear zone (this paper; *Kula et al.,* [2007]) indicating a temporal link between continental extension along the Sisters shear zone and incipient seafloor spreading. Additionally, the ~300°/150° trend of lineations is consistent with the spreading directions for the Pacific-Antarctic ridge, thus supporting a kinematic link between the two [*Kula et al.,* 2007]. Furthermore, the main tectonic features of the Campbell Plateau, which include the Bounty Trough [*Davey,* 1993], the Bollons Seamount [*Davey,* 2006], and the continental slope marking the southeastern boundary of the plateau are all the result of continental extension and the resulting formation of the Pacific-Antarctic Ridge [*Cook et al.,* 1999]. The connection between the Sisters shear zone and the spreading ridge based on lineation orientations and thermochronometry indicates the deformation within the shear zone and the formation of the Campbell Plateau were likely synchronous.

Based on this synthesis of data, it is proposed that the Sisters shear zone represents a portion of a major extensional detachment fault system upon which the Great South Basin was constructed and along which the Campbell Plateau as a whole may have been extended and thinned prior to the final stage of Gondwana breakup and formation of the Pacific-Antarctic spreading ridge.

Breakup of the Gondwana margin

The Sisters shear zone is the youngest extensional structure yet recognized related to Gondwana breakup, accommodating footwall exhumation from ~89-80 Ma. Additionally, it is the only structure we are aware of that demonstrates continental extension continued until the timing of formation of oceanic spreading ridges. Elsewhere in Zealandia, the record of continental extension and ocean ridge formation includes a lag time of 5-10 Ma between cessation of the former and initiation of the latter [e.g. *Spell et al.,* 2000].

Recognition of continued extension from 89-80 Ma along the Sisters shear zone has implications for the evolution of the Gondwana margin rift zone. The Sisters shear zone is kinematically linked to the Pacific-Antarctic Ridge, which rendered comparison with the Paparoa MCC-Tasman Ridge, which is constrained by the same type of thermochronometry data [*Kula et al.,* 2005, 2007]. Extension in the Paparoa MCC began up to 20 m.y. prior to that along the Sisters shear zone, and it is likely the Tasman and Pacific-Antarctic Ridges represent the final products of two distinct stages in Gondwana margin breakup [*Kula et al.,* 2007].

Several different mechanisms have been proposed for initiating extension and breakup of the Zealandia-Australia-Antarctica portion of Gondwana. These include cessation of subduction due to introduction of or nearing of a buoyant spreading ridge [*Bradshaw,* 1989; *Luyendyk,* 1995], gravitational collapse of overthickened arc crust [*Waight et al.,* 1998], mantle plume activity coupled with ridge subduction [*Weaver et al.,* 1994], and one or more of these mechanisms ensuing following dextral-oblique slab-rollback conditions [*Forster and Lister,* 2004; *Gray and Foster,* 2006]. Each of these mechanisms appears to be plausible based on certain lines of evidence. However, the new data from the Sisters shear zone afford the opportunity to put constraints on the likely driving mechanisms for extension leading to separation of Zealandia and West Antarctica.

Figure 12 illustrates the relationship of the Sisters shear zone to the GSB as well as the trends of Zealandia terrane boundaries, which are constrained by geophysics and bore hole data [*Cook et al.,* 1999; *Tulloch et al.,* 2006]. The Sisters shear zone cuts across the trend of the paired plutonic belts of the Median Batholith, and (when including the northwest margin of the Central Sub-basin) the forearc, and Otago Schist terranes. The HiSY belt of the Median Batholith represents a once high-standing arc-plateau that was constructed along the Gondwana margin [*Tulloch and Kimbrough,* 2003; *Tulloch et al.,* 2006]. Plateau collapse due to gravitational instability would be expected to occur in the direction of the steepest gradient of gravitational potential energy [e.g. *Rey et al.,* 2001]. The steepest gradient would have been between the thick HiSY belt and the thin LoSY belt and thus extension would have been perpendicular to the Gondwana margin. However, as the Sisters shear zone cuts across the trace of the plateau, it is unlikely that this extension was caused by collapse of overthickened crust [e.g. *Waight et al.,* 1998].

Another interesting characteristic of the Sisters shear zone is the lack of syn- and post-tectonic magmatism. The youngest pluton deformed by the shear zone is ~105 Ma [*Allibone and Tulloch,* 2004], which is 10 m.y. older than the oldest $^{40}Ar/^{39}Ar$ muscovite cooling age yet obtained. The lag time between magmatism and deformation and the lack of dikes or sills either cross cutting shear zone fabrics or being rotated into the fabric may indicate that extension along the Sisters shear zone was not directly triggered by anorogenic magmatism or mantle plume activity [e.g. *Weaver et al.,* 1994].

A growing body of marine geophysical data has been aimed at deciphering the tectonic evolution of the dispersed Gondwana continental fragments as recorded in ocean floor features [e.g. *Sutherland and Hollis,* 2001; *Eagles et al.,* 2004; *Davey,* 2006; *Worthington et al.,* 2006]. Based in part on this data, we propose plate boundary forces as the driving mechanism for Sisters shear zone extension. Subduction along the Chatham Rise portion of the Gondwana margin is considered to have stopped due to collision of the buoyant Hikurangi Plateau (Figure 1). The timing of this event is not well constrained, however, 97 Ma A-type granite and basalt from the eastern edge of the Chatham Rise indicate subduction had ceased prior to this time [*Mortimer et al.,* 2006].

Additionally, extension along the Sisters shear zone from 89-80 Ma is incompatible with models calling for Hikurangi Plateau- Chatham Rise collision at ~85 Ma [e.g. *Worthington et al.,* 2006], because if this were the case, the buoyant plateau would likely have acted as a backstop to impede extension. Therefore, it is likely that by ~100 Ma, the Hikurangi Plateau and adjacent oceanic lithosphere (Phoenix/Pacific Plates) to the northwest had stopped subducting and became coupled to the Zealandia portion of the Gondwana margin. Subduction continued south and east of the Hikurangi Plateau and Chatham Rise beneath West Antarctica [*Bradshaw et al.,* 1997; *McCarron and Larter,* 1998]. *Engebretson et al.* [1985] proposed a shift in Pacific Plate motion by ~85 Ma to a northwest direction (in a hotspot reference frame). These data are compatible with a tectonic model in which the post-subduction coupling of Zealandia and Pacific lithosphere results in pulling Zealandia northward away from West Antarctica as lithospheric failure and Tasman Ridge formation initiated to the west in the Tasman Sea at ~89 Ma [see *Spell et al.,* 2000]. Extension along the Sisters shear zone continued resulting in thinning of the Campbell Plateau and by ~83 Ma, ridge formation began that would eventually rift Zealandia away from West Antarctica [*Davey,* 2006]. Initiation of seafloor spreading resulted in cessation of spreading of the Osbourn Trough at this time, leading to reactivation of the West Wishbone Ridge as an extensional feature as the new Pacific-Antarctic spreading ridge plate boundary was established between the southeast Campbell Plateau margin and Marie Byrd Land, Antarctica [e.g. *Davey,* 2004; *Mortimer et al.,* 2006; *Worthington et al.,* 2006].

Conclusions

The Sisters shear zone represents a Cretaceous extensional detachment fault system that accommodated footwall denudation from ~93-82 Ma. The shear zone consists of two segments showing opposite kinematics that are likely separated by a left-lateral transfer fault. Although the Sisters shear zone is only exposed along 40km of Stewart Island coast, it can be inferred to project along the northwest boundary of the Central Sub-basin of the GSB based on orientation, kinematics, timing of Hoiho Group deposition, and the geophysically deduced structure of the GSB based on seafloor bathymetry and seismic profiles [*Cook et al.,* 1999]. $^{40}Ar/^{39}Ar$ mica and K-feldspar thermochronometry indicate the Sisters shear zone is the youngest detachment structure related to Gondwana breakup yet identified, with the main phase of extensional exhumation occurring from ~89-82 Ma. The timing and orientation of the Sisters shear zone supports tectonic models for slab capture of Zealandia lithosphere due to the cessation of subduction along the Gondwana margin. Extension and crustal thinning along the shear zone contributed in the formation of the GSB and may have lead to separation of the Campbell Plateau from West Antarctica marking the final step in the isolation of Zealandia from the dispersing Gondwana supercontinent.

Figure captions

Figure 1. A. Present day configuration of New Zealand and related environs (Zealandia) in the South Pacific [from *Sutherland,* 1999]. Box around southern South Island refers to the inset map in Figure 2. B. Rigid plate reconstruction of the Gondwana margin prior to seafloor spreading along the Tasman and Pacific-Antarctic Ridges. Restored orientation

of the SSZ is shown. Dark gray regions indicates continental crust submerged beneath less than 2000m of water depth [from *Mortimer et al.,* 2005; *Kula et al.,* 2007]. (Camp—Campbell Plateau; CR—Chatham Rise; HP—Hikurangi Plateau; W—Wishbone Ridge; Chall—Challenger Plateau; SLHR—South Lord Howe Rise; STR—South Tasman Rise; ET—East Tasman Rise; SNR—South Norfolk Ridge; IB—Iselin Bank).

Figure 2. Simplified geologic map of the SSZ along the southeast coast of southern Stewart Island [from *Allibone and Tulloch,* 2004; *Kula et al.,* 2007]. 'P' numbers refer to thermochronology samples (see Figure 7) referenced to the PETLAB database (http://data.gns.cri.nz/pet/); sample numbers in italics from *Kula et al.* [2007]. Boxes indicate the areas shown in Figures 3 and 4.

Figure 3. Map depicting site locations in the southern segment of the SSZ. White arrows denote motion of upper plate and site numbers refer to the adjacent foliation orientation symbols. Sites also correspond to descriptions in Table 1. Equal area stereographic projections in lower right corner show lineation orientations measured throughout the SSZ indicating consistent NW-SE transport direction regardless of shear sense and foliation attitude. Kamb contours at 2.0 contour interval and 3.0 σ significance. Plots were created using the program StereoWin [*Allmendinger,* 2002].

Figure 4. Map showing site locations in the northern segment of the SSZ. All sites show top-to-the-south shear sense. Site numbers correspond to descriptions in Table 2, and photomicrographs and field photos in Figure 6. Triangles indicate presence of chlorite

breccia outcrops. Small offset south-dipping brittle normal faults cut breccia and mylonitic outcrops at several locations along the coast.

Figure 5. Photomicrographs of microstructures in rocks of the southern segment of the SSZ. Numbers in the top right correspond to the site locations in Figure 3 and Table 1. A. Recrystallization of quartz occurs along boundaries of large feldspar grains. Zoom shows quartz grain-shape fabric. B. recrystallized quartz bands in spaces between mostly flat-lying feldspar grains, C. slab of ultramylonite showing rounded feldspar porphyroclasts and kinematic indicators, D. ultramylonite interval with abundant white mica growth, E & F. ultramylonite (E) and mylonite (F) intervals at site 5 demonstrating heterogeneous strain, G. brittley deformed microfaulted feldspar grain, H. both top-to-the-south and top-to-the-north shear sense indicators at site 7— top-to-the-north wing development around feldspar grains and a top-to-the-south oriented biotite mica-fish, I. Quartz grain shape fabric and kink-banding in K-feldspar is seen at site 8.

Figure 6. Photomicrographs and field photos from the northern segment of the SSZ showing microstructures and field relations supporting interpretation of the SSZ as an extensional detachment fault system. A. Strong mica-fish development (biotite and muscovite) and S-C fabric observed at site 10. B. Strong quartz grain-shape fabric preserved at site 12. C. Exposure of a detachment fault surface separating hanging-wall chloritic breccia from mylonitic granite is at site 14. D. Site 13 is the north-dipping conglomerate of the Sisters Islets. E & G. Site 15 consists of ultramylonite intervals with rigid rounded feldspar porphyroclasts and strong quartz grain-shape fabric and coarse

biotite and muscovite rich C'-type shear bands. F. brittle normal faults cutting ductile fabric near Seal Point.

Figure 7. Summary of $^{40}Ar/^{39}Ar$ results from muscovite, biotite, and K-feldspar. Asterick denotes the preferred age for samples with complex age spectra (see text).

Figure 8. MDD thermal modeling results for K-feldspar sample P75084. A. Arrhenius data. B. Domain distribution plot. C. Modeled age spectra compared with sample spectrum. D. Confidence intervals for thermal histories corresponding to age spectra in C.

Figure 9. MDD thermal modeling results of K-feldspar sample P75086. A. Arrhenius data. B. Domain distribution plot. C. Modeled age spectra compared with sample spectrum. D. Confidence intervals for thermal histories corresponding to age spectra in C.

Figure 10. Comparison of K-feldspar MDD thermal histories in this study with those of *Kula et al.* [2007] for the southern and northern segments of the SSZ.

Figure 11. Schematic cross-sections for the northern and southern segments of the SSZ (see text for discussion). Northern segment section is from *Kula et al.* [2007]. Southern segment schematic depicts hypothesis of structurally higher-detachment fault system (now offshore- see text) cutting the top-to-the-north fabric as evidenced by brittle normal faults observed in the field.

Figure 12. Map of Stewart Island, SSZ, and the Great South Basin showing spatial relationship between the SSZ (thick gray dashes), the Central Sub-basin, and the Rakiura Trough (see text). Medium gray encloses area of 2000 m sediment isopach of the GSB. Dark gray of Central Sub-basin and Rakiura Trough denotes 5-6000 m isopach. Thick black features mark prominent bathymetric structures/scarps. Dotted lines mark the trace of terrane boundaries labeled on the right hand side. Note the location of the deepest part of the Central Sub-basin (dark gray) occurs on the low-lying LoSY belt and forearc terranes with the HiSY-LoSY boundary marking the western boundary [from *Tulloch et al.*, 2006].

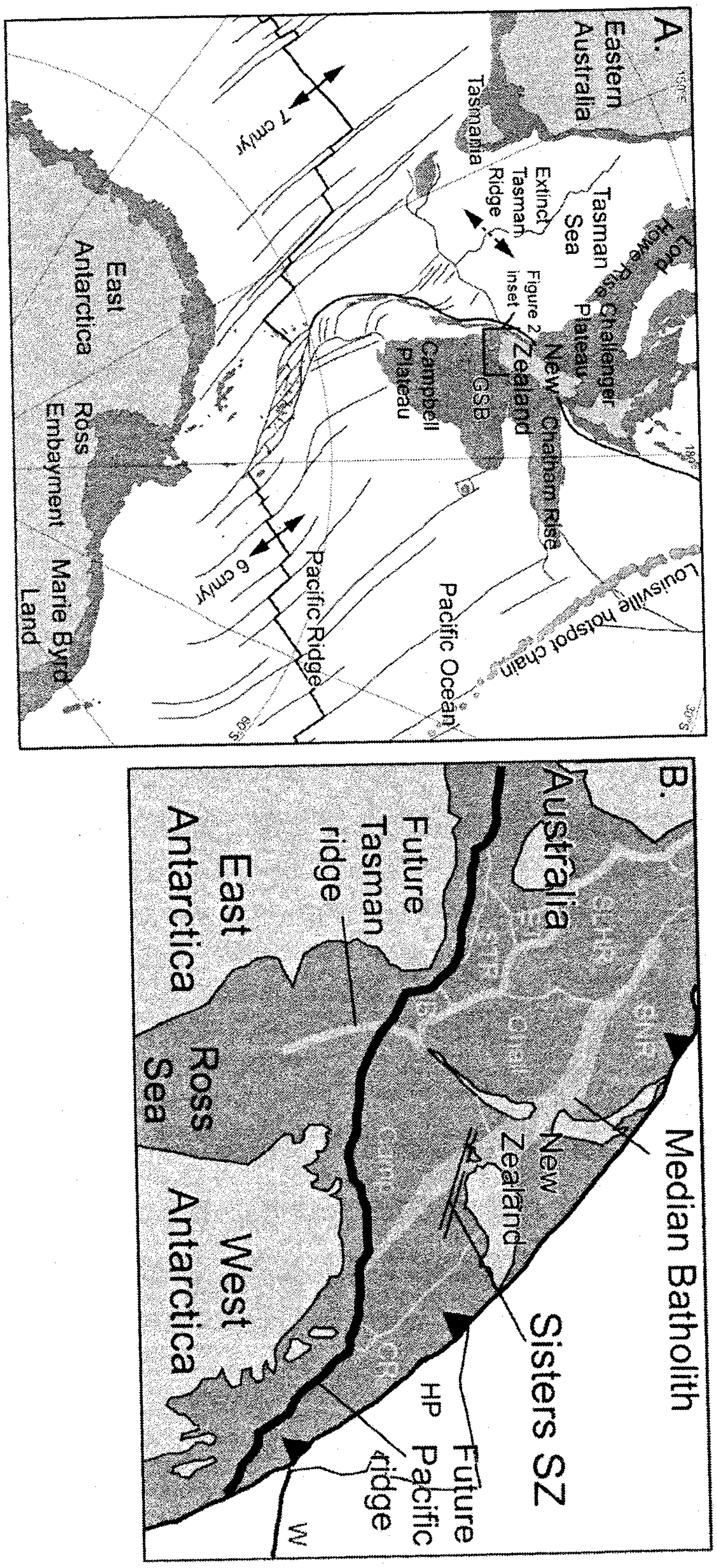
A.
Eastern Australia
Tasmania
Extinct Tasman Ridge
Tasman Sea
Lord Howe Rise
Challenger Plateau
New Zealand
Figure 2 inset
GSB
Campbell Plateau
Chatham Rise
Louisville hotspot chain
Pacific Ocean
Pacific Ridge
7 cm/yr
6 cm/yr
East Antarctica
Ross Embayment
Marie Byrd Land
B.
Australia
Future Tasman ridge
East Antarctica
Ross Sea
West Antarctica
New Zealand
Median Batholith
Sisters SZ
Future Pacific ridge
HP
W

Figure 1

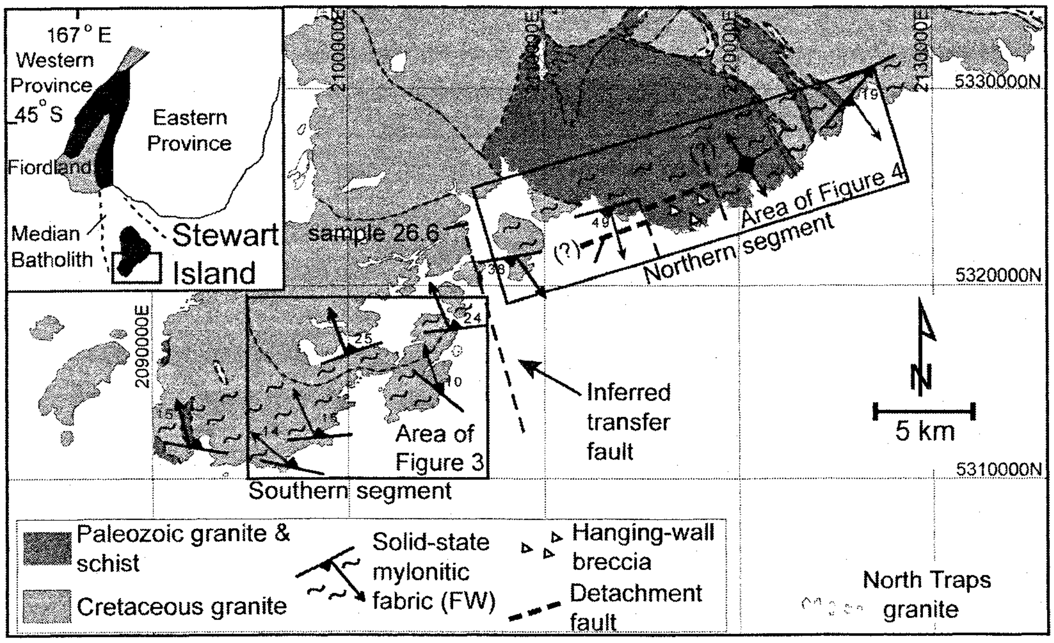

Figure 2

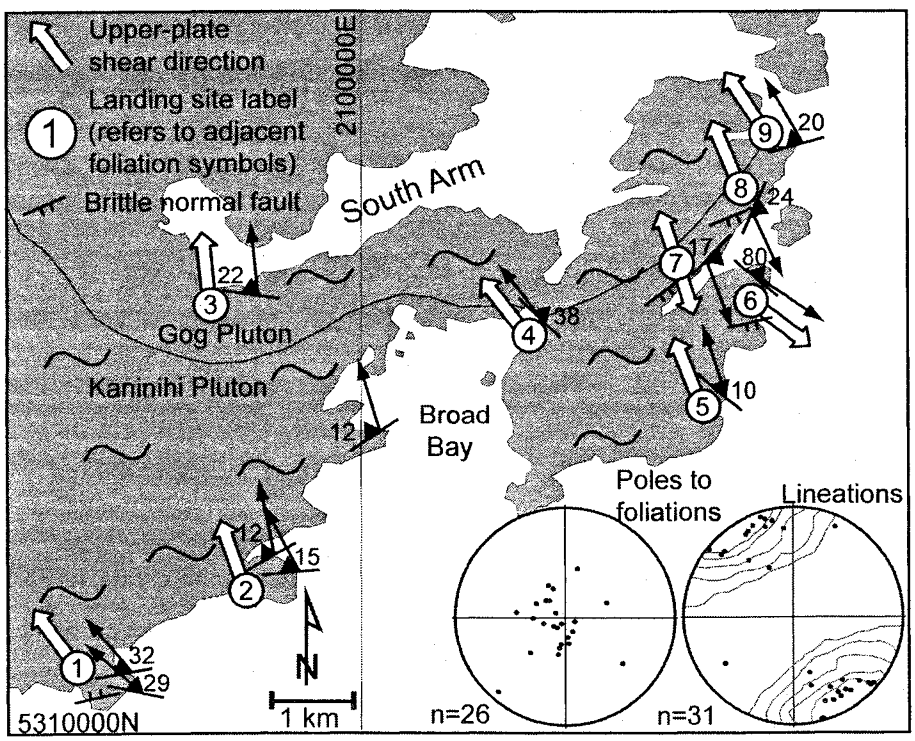

Figure 3

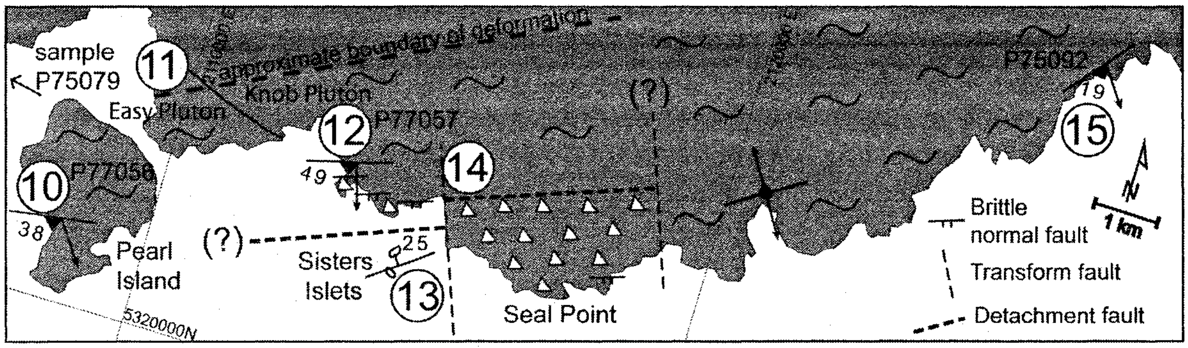
sample
P75079
11
approximate boundary of deformation
Knob Pluton
Easy Pluton
12
P77057
49
10
P77056
38
14
(?)
(?)
Pearl
Island
Sisters
Islets
25
13
Seal Point
P75092
79
15
Brittle
normal fault
Transform fault
Detachment fault
1 km
N
5320000N

Figure 4

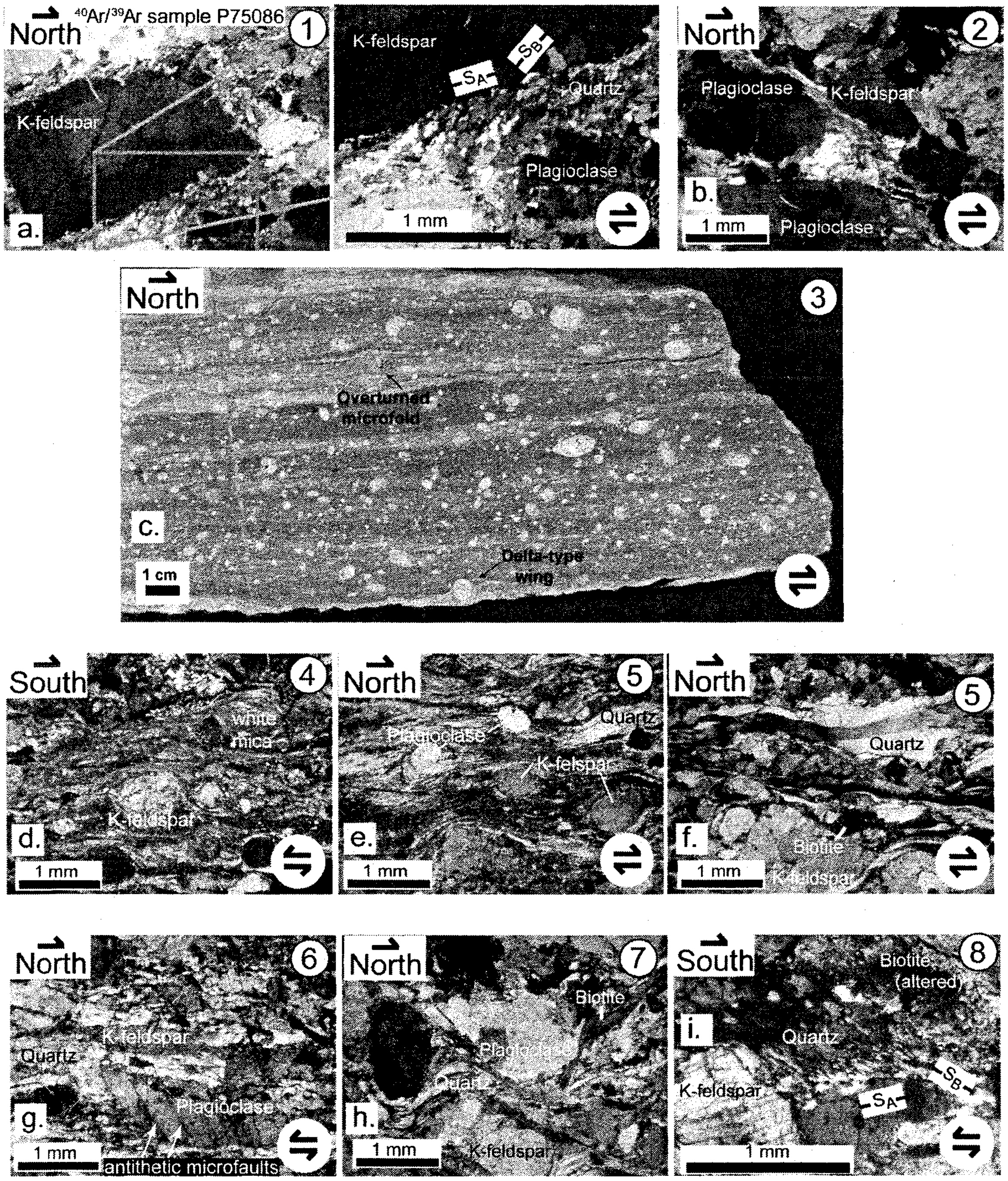
North
$^{40}Ar/^{39}Ar$ sample P75086
1
K-feldspar
a.
K-feldspar
S_A
S_B
Quartz
Plagioclase
1 mm
North
2
Plagioclase
K-feldspar
b.
1 mm
Plagioclase
North
3
Overturned microfold
c.
1 cm
Delta-type wing
South
4
white mica
K-feldspar
d.
1 mm
North
5
Plagioclase
Quartz
K-felspar
e.
1 mm
North
5
Quartz
f.
1 mm
Biotite
K-feldspar
North
6
K-feldspar
Quartz
Plagioclase
g.
1 mm
antithetic microfaults
North
7
Biotite
Plagioclase
h.
1 mm
K-feldspar
South
8
Biotite (altered)
i.
Quartz
K-feldspar
S_A
S_B
1 mm

Figure 5

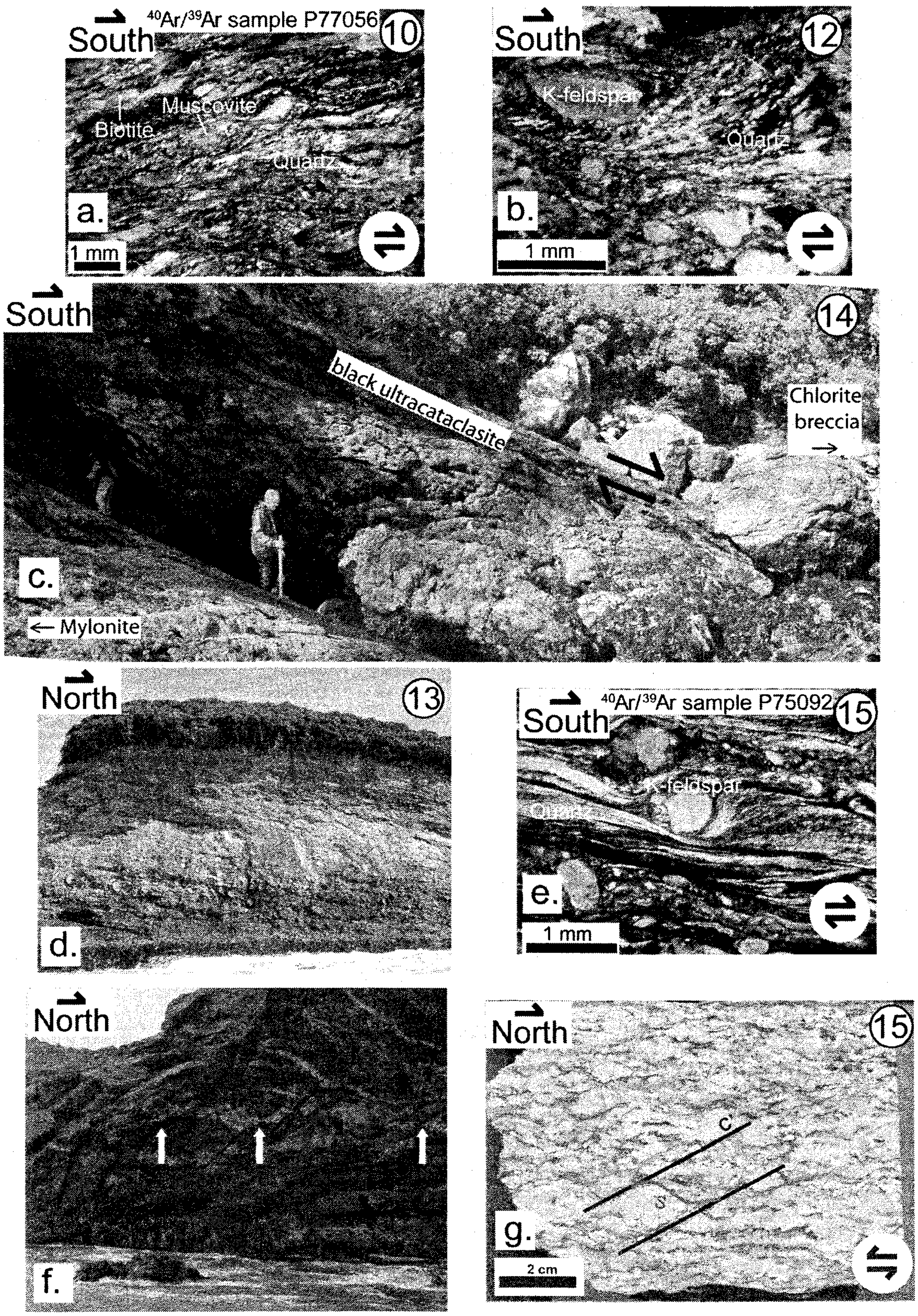

South
40Ar/39Ar sample P77056
10
Biotite
Muscovite
Quartz
a.
1 mm
South
12
K-feldspar
Quartz
b.
1 mm
South
14
black ultracataclasite
Chlorite breccia →
c.
← Mylonite
North
13
d.
South
40Ar/39Ar sample P75092
15
K-feldspar
e.
1 mm
North
f.
North
15
C
S
g.
2 cm

Figure 6

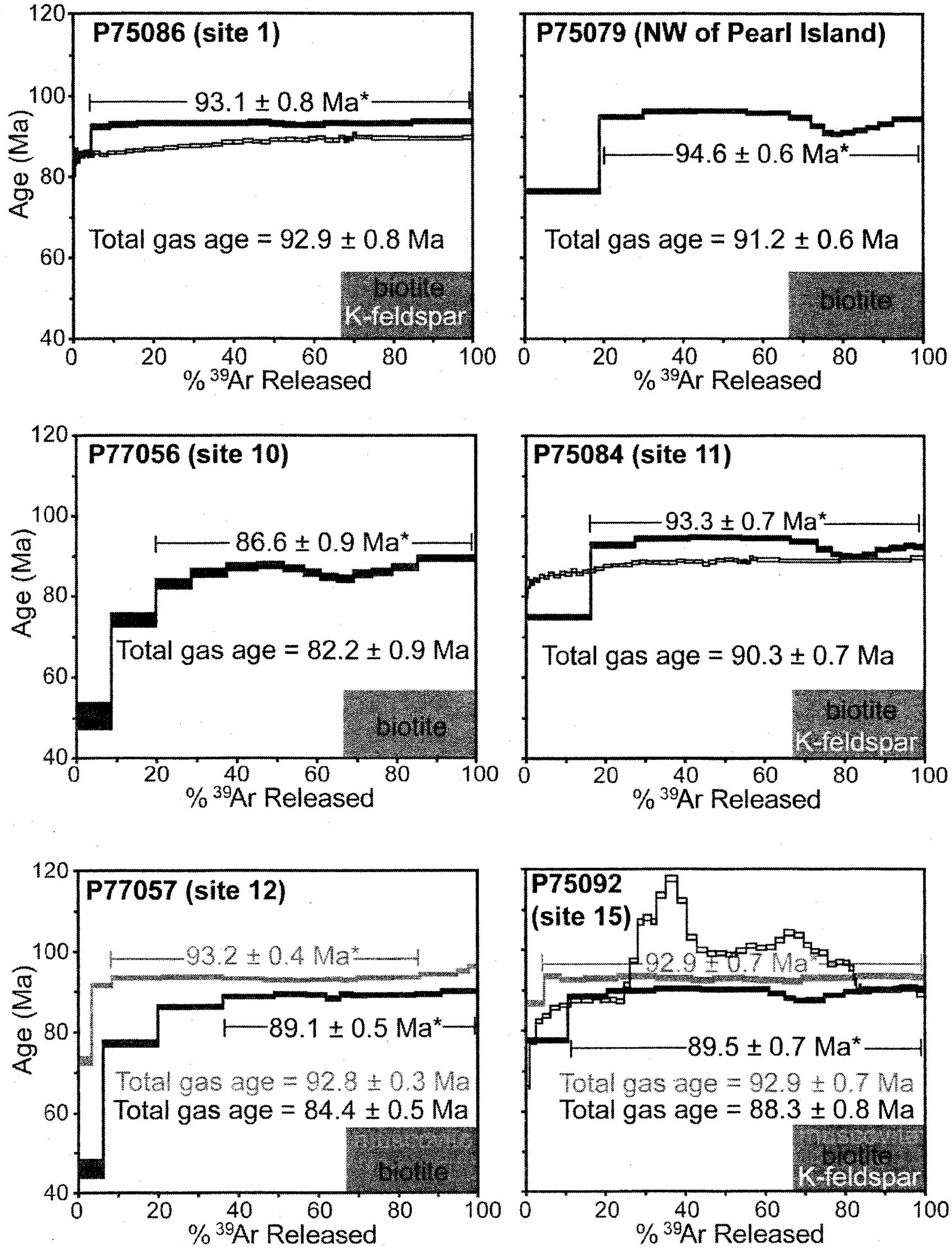
P75086 (site 1)
93.1 ± 0.8 Ma*
Total gas age = 92.9 ± 0.8 Ma
biotite
K-feldspar
P75079 (NW of Pearl Island)
94.6 ± 0.6 Ma*
Total gas age = 91.2 ± 0.6 Ma
biotite
P77056 (site 10)
86.6 ± 0.9 Ma*
Total gas age = 82.2 ± 0.9 Ma
biotite
P75084 (site 11)
93.3 ± 0.7 Ma*
Total gas age = 90.3 ± 0.7 Ma
biotite
K-feldspar
P77057 (site 12)
93.2 ± 0.4 Ma*
89.1 ± 0.5 Ma*
Total gas age = 92.8 ± 0.3 Ma
Total gas age = 84.4 ± 0.5 Ma
biotite
P75092 (site 15)
92.9 ± 0.7 Ma*
89.5 ± 0.7 Ma*
Total gas age = 92.9 ± 0.7 Ma
Total gas age = 88.3 ± 0.8 Ma
biotite
K-feldspar
Age (Ma)
% 39Ar Released

Figure 7

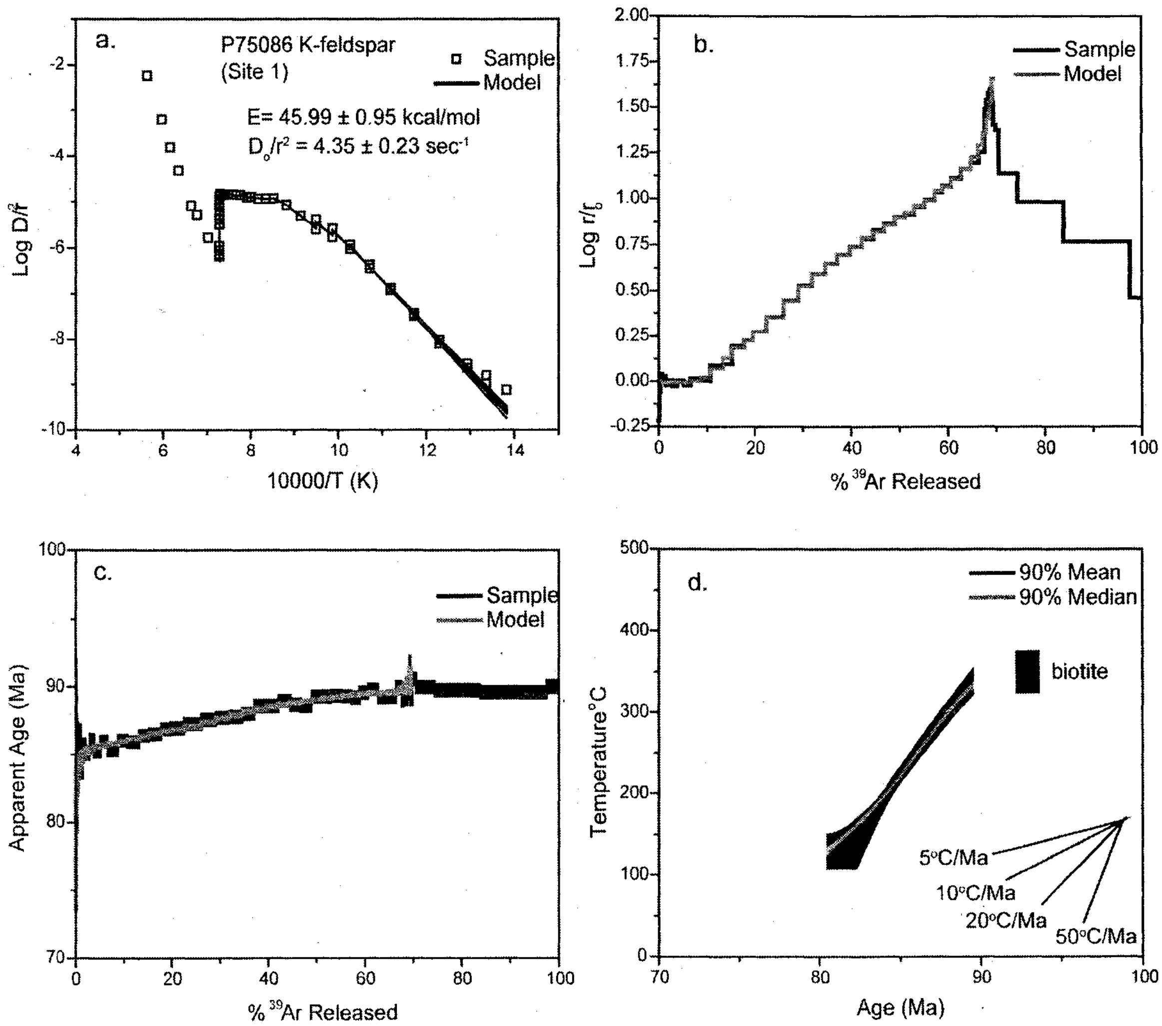
a.
P75086 K-feldspar
(Site 1)
Sample
Model
E= 45.99 ± 0.95 kcal/mol
D₀/r² = 4.35 ± 0.23 sec⁻¹
Log D/r²
10000/T (K)
b.
Sample
Model
Log r/r₀
% ³⁹Ar Released
c.
Sample
Model
Apparent Age (Ma)
% ³⁹Ar Released
d.
90% Mean
90% Median
biotite
5°C/Ma
10°C/Ma
20°C/Ma
50°C/Ma
Temperature°C
Age (Ma)

Figure 8

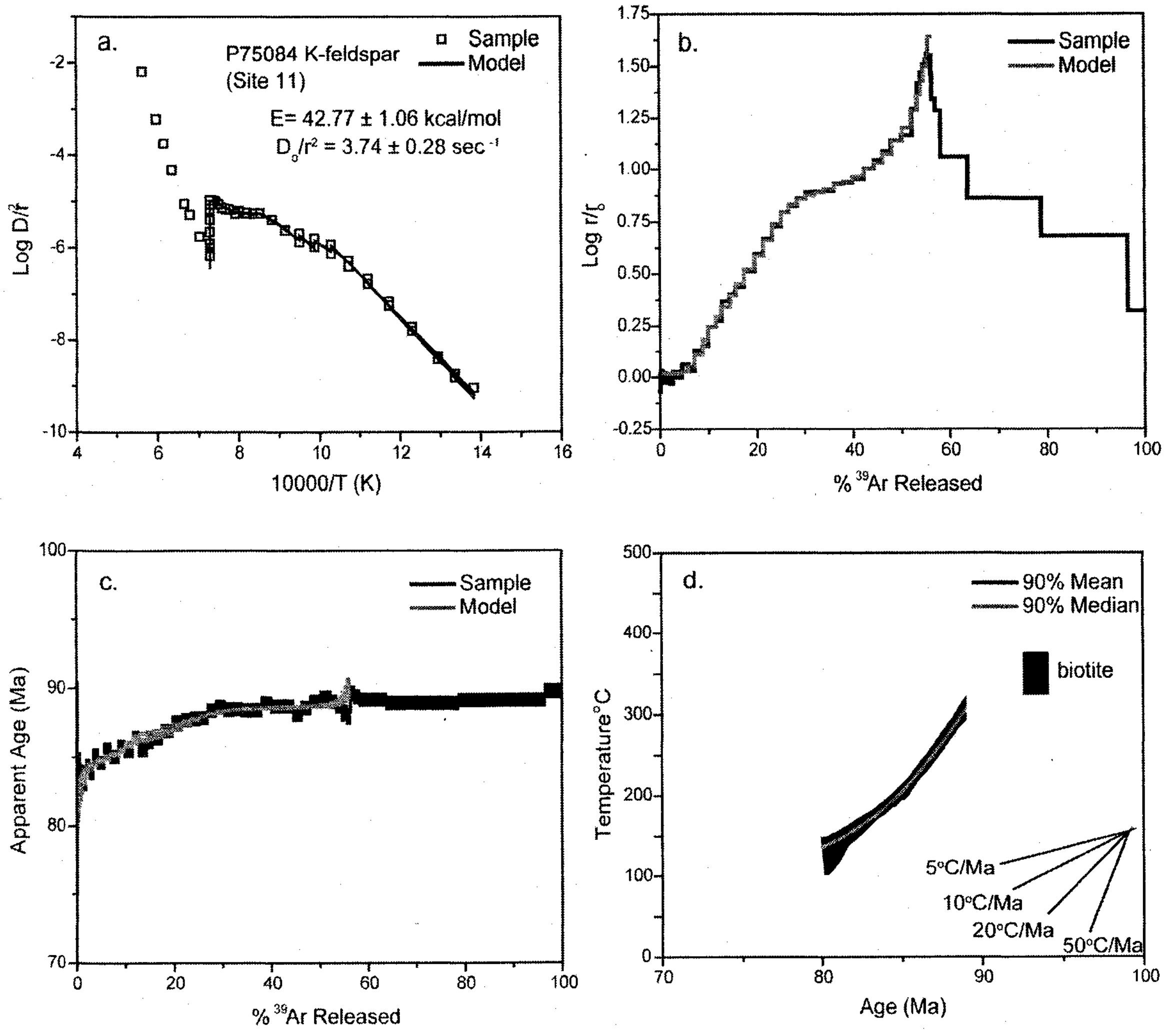

a.
P75084 K-feldspar
(Site 11)
Sample
Model
E= 42.77 ± 1.06 kcal/mol
D$_0$/r^2 = 3.74 ± 0.28 sec^{-1}
Log D/r^2
10000/T (K)
b.
Sample
Model
Log r/r$_0$
% ^{39}Ar Released
c.
Sample
Model
Apparent Age (Ma)
% ^{39}Ar Released
d.
90% Mean
90% Median
biotite
5°C/Ma
10°C/Ma
20°C/Ma
50°C/Ma
Temperature°C
Age (Ma)

Figure 9

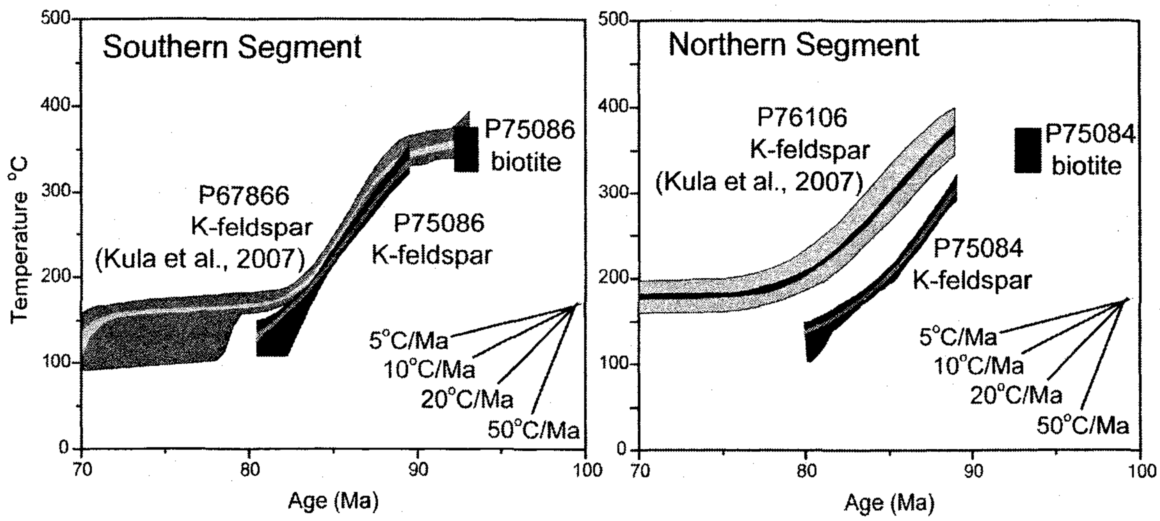
Southern Segment
Northern Segment
Temperature °C
Age (Ma)
P75086
biotite
P67866
K-feldspar
(Kula et al., 2007)
P75086
K-feldspar
P76106
K-feldspar
(Kula et al., 2007)
P75084
biotite
P75084
K-feldspar
5°C/Ma
10°C/Ma
20°C/Ma
50°C/Ma

Figure 10

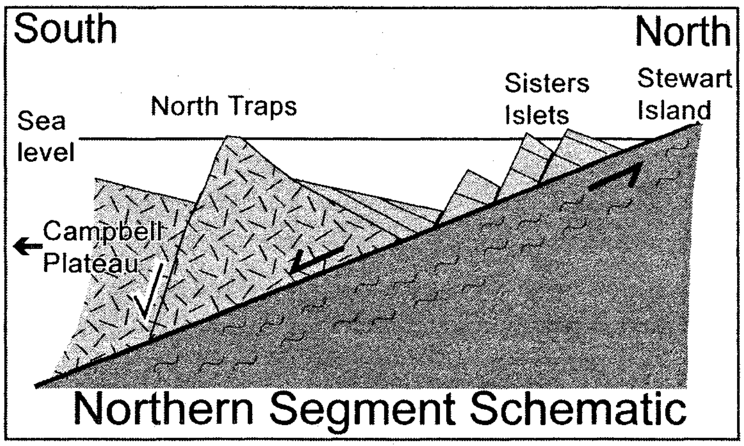
South
North
Sea
level
North Traps
Sisters
Islets
Stewart
Island
Campbell
Plateau
Northern Segment Schematic

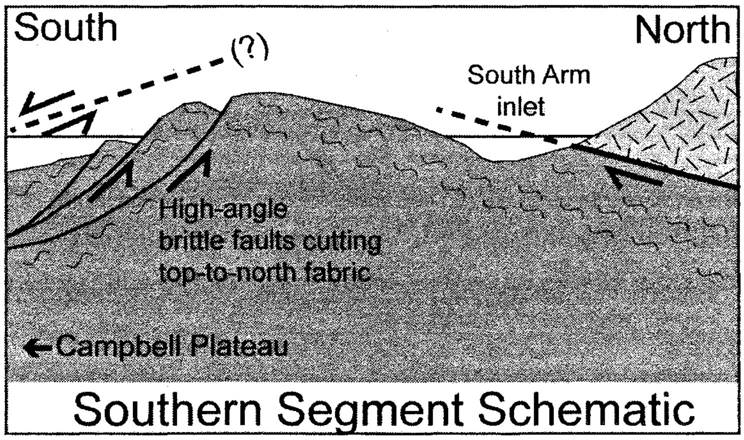
South
(?)
North
South Arm
inlet
High-angle
brittle faults cutting
top-to-north fabric
Campbell Plateau
Southern Segment Schematic

Figure 11

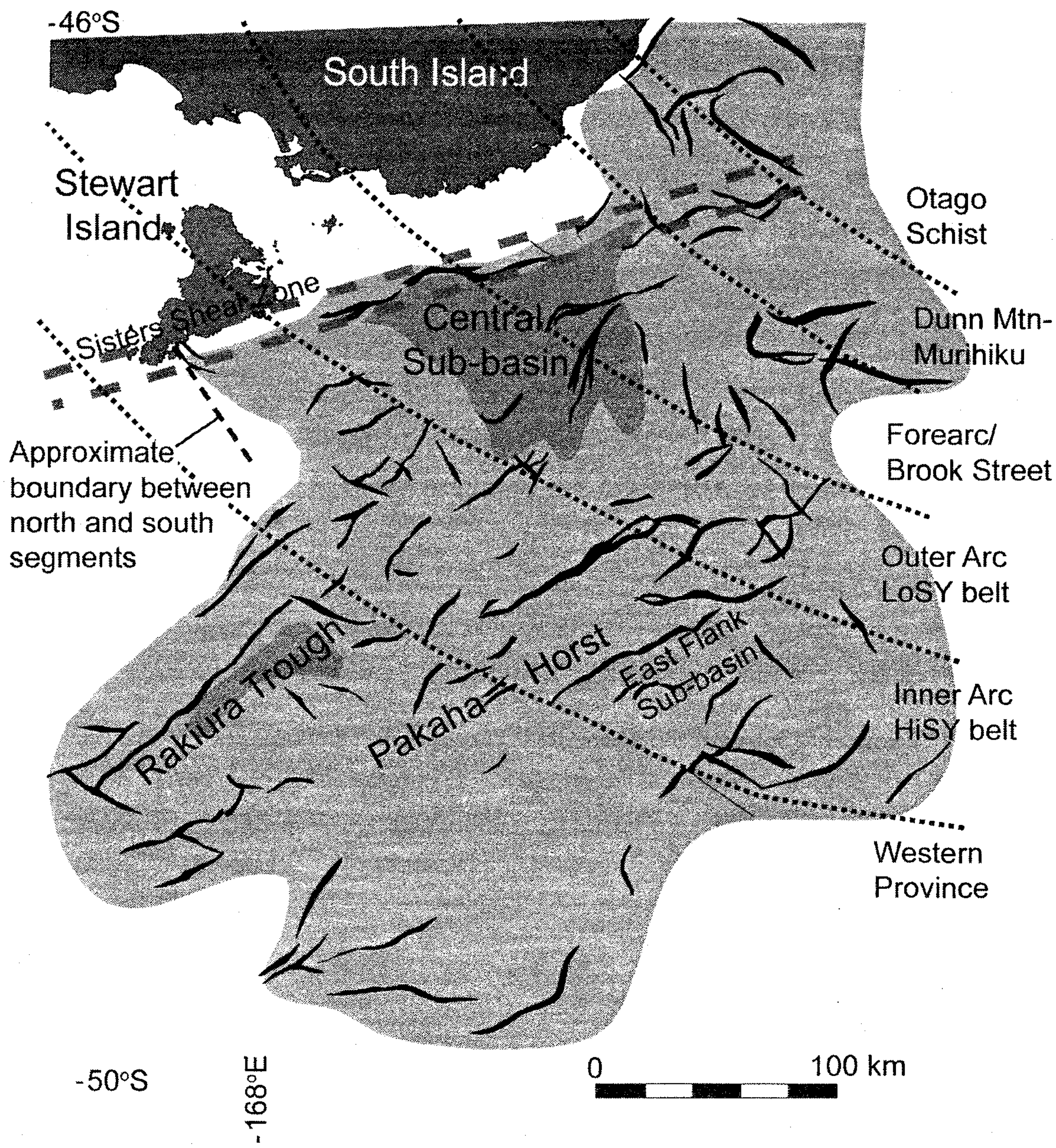
-46°S
South Island
Stewart Island
Sisters Shear Zone
Central Sub-basin
Otago Schist
Dunn Mtn-Murihiku
Forearc/ Brook Street
Approximate boundary between north and south segments
Outer Arc LoSY belt
East Flank Sub-basin
Pakaha Horst
Rakiura Trough
Inner Arc HiSY belt
Western Province
-50°S
-168°E
0
100 km

Figure 12

References

Allibone, A.H., and Tulloch, A.J. (1997), Metasedimentary, granitoid and gabbroic rocks from central Stewart Island, New Zealand, *New Zealand Journal of Geology and Geophysics, 40,* 53-68.

Allibone, A.H., and Tulloch, A.J. (2004), Geology of the plutonic basement rocks of Stewart Island, New Zealand, *New Zealand Journal of Geology and Geophysics, 47,* 233-256.

Allmendinger, R.W. (2002), StereoWin for Windows available at ftp://www.geo.cornell.edu/pub/rwa.

Bradshaw, J.D. (1989), Cretaceous geotectonic patterns in the New Zealand region, *Tectonics, 8,* 803-820.

Bradshaw, J.D., Pankhurst, R.J., Weaver, S.D., Storey, B.C., Muir, R.J., and Ireland, T.R. (1997), New Zealand superterranes recognized in Marie Byrd Land and Thurston Island, in *The Antarctic region: geological evolution and processes*, edited by C.A. Ricci, pp. 429-436, Terra Antartica Publ., Siena, Italy.

Cebula, G.T., M.J. Kunk, H.H. Mehnert, C.W. Naeser, J.D. Obradovich, and J.F. Sutter, (1986), The Fish Canyon Tuff, a potential standard for the ^{40}Ar-^{39}Ar and fission-track dating methods, *Terra Cognita, 6th Int. Conf. on Geochronology, Cosmochronology and Isotope Geology, 6*, 139.

Cook, R.A., Sutherland, R., Zhu, H. and others (Eds.) (1999), *Cretaceous-Cenozoic geology and petroleum systems of the Great South Basin, New Zealand*, 188 pp., Institute of Geological and Nuclear Sciences monograph 20.

Davey, F.J. (2005), A Mesozoic crustal suture on the Gondwana margin in the New

Zealand region, *Tectonics, 24*, doi:10.1029/2004TC001719.

Davey, B.W. (1993), The Bounty Trough: Basement structure influences on sedimentary basin evolution, in *Sedimentary Basins of the World,* Vol. 2 South Pacific Sedimentary Basins, Edited by P.F. Balance, P.F., pp. 69-92, Elsevier, New York.

Davey, B. (2006), Bollons Seamount and early New Zealand-Antarctic seafloor spreading, *Geochemistry, Geophysics, Geosystems, 7*, Q06021, doi: 10.1029/2005GC001191.

Davis, G.H. (1980), Structural characteristics of metamorphic core complexes, southern Arizona, in *Cordilleran metamorphic core complexes*, Geological Society of America Memoir, 153, Edited by M.D. Crittenden, P.J., Coney, and G.H., Davis, pp. 35-77.

Deckert, H., Ring, U., and Mortimer, N. (2002), Tectonic significance of Cretceous bivergent extensional shear zones in the Torlesse accretionary wedge, central Otago Schist, New Zealand, *New Zealand Journal of Geology and Geophysics, 45*, 537-547.

Eagles, G., Gohl, K., and Larter, R.D. (2004), High-resolution animated tectonic reconstruction of the south Pacific and West Antarctic margin, *Geochemistry, Geophysics, Geosystems, 5(7)*, Q07002, doi:10.1029/2003GC000657.

Engebretson, D.C., Cox, A., and Gordon, R.G. (1985), Relative motions between oceanic and continental plates in the Pacific basin, Geological Society of America Special Paper 206.

Etheridge, M.A., Symonds, P.A., and Lister, G.S, (1989), Application of the detachment model to reconstruction of conjugate passive margins, in *Extensional Tectonics and stratigraphy of the North Atlantic margins*, American Association of Petroleum Geologists Memoir 45, Edited by A.J. Tankard, and H.R. Balkwill, pp. 23-40.

Fleming, C.A., and Watters, W.A. (1974), Geology and petrography of a conglomerate in southern Stewart Island, *New Zealand Journal of Geology and Geophysics, 17*, 225-231.

Forster, M.A., and Lister, G.S. (2003), Cretaceous metamorphic core complexes in the Otago Schist, New Zealand, *Australian Journal of Earth Sciences, 50*, 181-198.

Gray, D.R., and Foster, D.A. (2004), $^{40}Ar/^{39}Ar$ thermochronologic constraints on deformation, metamorphism and cooling/exhumation of a Mesozoic accretionary wedge, Otago Schist, New Zealand, *Tectonophysics, 385,* 181-210.

Heizler, M.T., and Harrison, T.M. (1988), Multiple trapped argon isotope components revealed by $^{40}Ar/^{39}Ar$ isochron analysis, *Geochimica et Cosmochimica Acta, 52*, 1295-1303.

Hirth, G., and Tullis, J. (1992), Dislocation creep regimes in quartz aggregates, *Journal of Structural Geology, 14*, 145-159.

Klepeis, K.A., Clarke, G.L., Gehrels, G., and Vervoort, J. (2004), Processes controlling vertical coupling and decoupling between the upper and lower crust of orogens: results from Fiordland, New Zealand, *Journal of Structural Geology, 26,* 765-791.

Kula, J.L., Tulloch, A.J., Spell, T.L., and Wells, M.L. (2005), Timing of continental extension leading to separation of eastern New Zealand from west Antarctica; $^{40}Ar/^{39}Ar$ thermochronometry from Stewart Island, NZ, *Geological Society of America Abstracts with Programs, 37*, 73.

Kula, J., Tulloch, A., Spell, T.L., Wells, M.L. (2007), Two-stage rifting of Zealandia-Australia- Antarctica: evidence from $^{40}Ar/^{39}Ar$ thermochronometry of the Sisters Shear Zone; Stewart Island, New Zealand, *Geology, 35,* 411-414.

Lister, G.S., Etheridge, M.A., and Symonds, P.A. (1991), Detachment models for the formation of passive continental margins, *Tectonics, 10,* 1038-1064.

Lo, C.H., Onstott, T.C. (1989), ^{39}Ar recoil artifacts in chloritized biotite, *Geochimica et Cosmochimica Acta, 53*, 2697 – 2711.

Lovera, O.M., Richter, F.M., and Harrison, T.M. (1989), The $^{40}Ar/^{39}Ar$ Thermochronometry for slowly cooled samples having a distribution of diffusion domain sizes, *Journal of Geophysical Research, 94*, 7,917-17,935.

Lovera, O.M., Richter, F.M., and Harrison, T.M. (1991), Diffusion domains determined by ^{39}Ar released during step heating, *Journal of Geophysical Research, 96*, 2057-2069.

Lovera, O.M. (1992), Computer Programs to Model $^{40}Ar/^{39}Ar$ diffusion data from multidomain Samples, *Computers and Geosciences, 18*, 789-813.

Lovera, O.M., Grove, M., Harrison, T.M., and Mahon, K.I. (1997), Systematic analysis of K-feldspar $^{40}Ar/^{39}Ar$ step heating results: I. Significance of activation energy determinations, *Geochimica et Cosmochimica Acta, 61*, 3171-3192.

Luyendyk, B.P. (1995), Hypothesis for Cretaceous rifting of east Gondwana caused by subducted slab capture, *Geology, 23*, 373-376.

McCarron, J.J. and Larter, R.D. (1998), Late Cretaceous to early Tertiary subduction history of the Antarctic Peninsula, *Journal of the Geological Society of London, 155*, 255-268.

Mortimer, N., Hoernle, K., Hauff, F., Palin, J.M., Dunlap, W.J., Werner, R., Faure, K. (2006), New constraints on the age and evolution of the Wishbone Ridge, southwest Pacific Cretaceous microplates, and Zealandia-West Antarctica breakup, *Geology, 34*, 185-188.

Mortimer, N., Graham, I., Adams, C., Tulloch, A., and Campbell, H. (2005), Relationships between New Zealand, Australian and New Caledonian mineralised terranes: a regional geological framework, paper presented at the New Zealand Minerals Conference, pp. 151-159.

Pryer, L.L. (1993), Microstructures in feldspars from a major crustal thrust zone: the Grenville Front, Ontario, Canada, *Journal of Structural Geology, 15*, 21-36.

Richter, F.M., Lovera, O.M., Harrison, T.M., and Copeland, P. (1991), Tibetan tectonics from $^{40}Ar/^{39}Ar$ analysis of a single K-feldspar sample, *Earth and Planetary Science Letters, 105*, 266-278.

Roberts, H.J., Kelley, S.P., and Dahl, P.S. (2001), Obtaining geologically meaningful $^{40}Ar/^{39}Ar$ ages from altered biotite, *Chemical Geology, 172*, 277-290.

Spell, T.L., McDougall, I., and Tulloch, A.J. (2000), Thermochronologic constraints on the breakup of the Pacific Gondwana margin: the Paparoa metamorphic core complex, South Island, New Zealand, *Tectonics, 19*, 433-451.

Staudacher, T., Jessberger, E.K., Dorflinger, D., and Kiko, J. (1978), A refined ultrahigh

-vacuum furnace for rare gas analysis, *Journal of Physical Engineering: Scientific Instrumentation, 11*, 781-784.

Steven, T.A., H.H. Mehnert, and J.D. Obradovich, (1967), Age of volcanic activity in the San Juan Mountains, Colorado, *U.S. Geol. Surv. Prof. Pap., 575-D*, 47-55.

Stipp, M., Stunitz, H., Heilbronner, R., and Schmid, S.M. (2002), The eastern Tonale fault zone: a 'natural laboratory' for crystal plastic deformation of quartz over a temperature range from 250 to 700 °C, *Journal of Structural Geology, 24*, 1861-1884.

Sutherland, R. (1999), Basement geology and tectonic development of the greater New Zealand region: an interpretation from regional magnetic data, *Tectonophysics, 308*, 341-362.

Sutherland, R., and Hollis, C. (2001), Cretaceous demise of the Moa plate and strike-slip motion at the Gondwana margin, *Geology, 29*, 279-282.

Tulloch, A.J., Beggs, M., Kula, J.L., Spell, T.L., Mortimer, N. (2006), Cordillera Zealandia, the Sisters Shear Zone and their influence on the early development of the Great South Basin, paper presented at the New Zealand Petroleum Conference Proceedings.

Tulloch, A.J., and Kimbrough, D.L. (2003), Paired plutonic belts in convergent margins and the development of high Sr/Y magmatism: Peninsular Ranges batholith of Baja-California and Median batholith of New Zealand, in *Tectonic evolution of northwestern Mexico and the southwestern USA,* Geological Society of America special paper 374, Edited by S.E., Johnson, S.R. Paterson, J.M. Fletcher, G.H. Girty, D.L. Kimbrough, and A. Martin-Barajas, Boulder, Colorado, pp. 275-295.

Tulloch, A.J. and Kimbrough, D.L. (1989), The Paparoa metamorphic core complex, New Zealand: Cretaceous extension associated with fragmentation of the Pacific Margin of Gondwana, *Tectonics, 8*, 1217-1234.

Weaver, S.D., Storey, B.C., Pankhurst, R.J., Mukasa, S.B., DiVenere, V.J., and Bradshaw, J.D. (1994), Antarctica-New Zealand rifting and Marie Byrd Land lithospheric magmatism linked to ridge subduction and mantle plume activity, *Geology, 22*, 811-814.

Waight, T.E., Weaver, S.D., Muir, R.J., Maas, R., Eby, G.N. (1998), The Hohonu Batholith of North Westland, New Zealand: granitoid compositions controlled by source H_20 contents and generated during tectonic transition, *Contributions to Mineralogy and Petrology, 130*, 225-239.

Wernicke, B.P. (1992), Cenozoic extensional tectonics of the US Cordillera, in *The Cordilleran Orogen: Conterminous US,* Edited by B.C. Burchfiel, P.W. Lipman, and M.L. Zoback, Boulder, CO, pp. 553-581.

Worthington, T.J., Hekinian, R., Stoffers, P., Kuhn, T., and Hauff, F., (2006), Osbourn Trough: Structure, geochemistry and implications of a mid-Cretaceous paleospreading ridge in the South Pacific, *Earth and Planetary Science Letters, 245*, 685-701.

CHAPTER 3

$^{40}Ar/^{39}Ar$ AGE SPECTRA FROM ARTIFICIALLY MIXED MICAS

Abstract

Artificial mixtures of two age populations of muscovite and of biotite were prepared at relative weight percents of 3:1, 1:1, and 1:3 and analyzed by the $^{40}Ar/^{39}Ar$ vacuum furnace step-heating method. The starting materials consisted of Late Jurassic and Late Cretaceous mica that yield flat age spectra with plateau ages defined by 97-100% of the gas release and no evidence for excess argon. The age spectra from mica mixtures yield patterns that systematically decrease with decreasing Jurassic mica content and increasing Cretaceous component. The mixed muscovite spectra are relatively flat, consistent with the two original samples showing similar degassing patterns during their original analyses. The mixed biotite spectra are highly discordant with an overall decrease in age over the entire step-heating run. This is consistent with the degassing patterns of the end member starting materials that indicate the Jurassic biotite (high Fe/Mg) outgases at lower temperatures and the Cretaceous biotite (low Fe/Mg) remains retentive until the higher temperature steps (~1100 °C). The individual degassing patterns and compositions show consistencies with known compositional controls on argon diffusivity indicating micas maintain argon retention characteristics rooted in crystal chemistry during vacuum furnace heating. All but one of the mixed samples

failed to yield ages reflecting the age of the starting materials. This result indicates complex age spectra obtained for multiply-deformed rocks may yield geologically meaningless ages as a result of simultaneous degassing (ie. mixing of sample reservoirs) during heating. Based on the results of this study it is evident that compositional controls on argon retention in mica are likely preserved during vacuum furnace step-heating, and complex age spectra obtained from polymetamorphosed rocks consist of ages with no geological significance. Comparison of laboratory degassing rates and crystal chemistry indicates micas may degas/retain argon in a predictable manner, therefore supporting assertions that recovery of fossil age gradients in slowly cooled samples may be possible using furnace step-heating.

Introduction

Biotite and muscovite are two of the most commonly used minerals in $^{40}Ar/^{39}Ar$ chronometry (McDougall and Harrison, 1999) due to their ubiquitous presence in common igneous and metamorphic rocks and their relatively high K content. However, the validity of interpreting mica step-heating data from a thermochronometry standpoint falls into question largely because of concerns regarding the physical behavior of hydrous phases during vacuum heating (e.g., Hodges et al, 1994; Sletten and Onstott, 1998; Lo et al., 2000). Structural (i.e. delamination) and compositional (i.e. dehydroxylation) breakdown of micas during vacuum heating has been implicated as compromising the extraction of internal $^{40}Ar^*$ concentration gradients, resulting in erroneously shaped flat age spectra (e.g., de Jong, 1992; Hodges et al., 1994). This has led some to believe the shape of mica age spectra does not correspond to the thermal history of the sample (Dunlap, 1998).

Relating the shape of the age spectrum to the thermal history (i.e. cooling rate) of a sample requires degassing of the sample during vacuum heating to occur in the same way as that during natural cooling of the sample (i.e. solid-state volume diffusion) (Lovera et al., 1989; Richter et al., 1991; Lovera et al., 2002). Reproduction of natural argon diffusion mechanisms in hydrous phases using the vacuum furnace has been deemed impossible due to the structural instability of these minerals during vacuum heating (e.g., Sletten and Onstott, 1998; Lee et al., 1991). However, staircase age spectra from metamorphic micas have been successfully reproduced using numerical diffusion models (Baldwin and Lister, 1996; Lister and Raouzaios, 1996; Wells et al., 2000) indicating the degassing behavior of micas during furnace step-heating may in some cases reflect natural geologic cooling. Therefore, it may be possible that the same controls that define the argon diffusion kinetics in nature may also be active during laboratory step-heating, where they dictate the sample degassing behavior.

In addition to uncertainties surrounding reproduction of natural argon diffusion mechanisms in the laboratory, complications regarding the interpretation of mica $^{40}Ar/^{39}Ar$ data may also occur when samples having undergone complex geologic histories are analyzed. Samples falling into this category would include metamorphic tectonites that may have undergone multiple deformation and/or neo-recrystallization events resulting in the presence of several age populations of mica (e.g., Lanphere and Albee, 1974; Chopin and Maluski, 1980; Wijbrans and McDougall, 1986; Hames and Cheney, 1997). Further complexity in these samples may be derived from the presence of internal age gradients reflecting ancient residence in the partial retention zone and/or heterogeneous thermal overprinting of a mixture of coarse older crystals and fine neocrystallized crystals. For many mica-bearing rocks with more complex thermal histories than rapid monotonic cooling, $^{40}Ar/^{39}Ar$ dating using laser spot gas extraction has been successfully applied (Wijbrans et al., 1990; Scailliet et al., 1990, 1992; Hames and Hodges, 1993; Kramer et al., 2001; Putlitz et al., 2005). However, extraction of meaningful information from multiply deformed rocks using the vacuum furnace may be problematic, especially for samples yielding complex age spectra for which a 'plateau age' (see McDougall and Harrison, 1999) is not obtainable.

Recently, Forster and Lister (2004) proposed a method to evaluate complex age spectra obtained from mixed mica populations coexisting in multiply-deformed rocks such as the Otago Schist of New Zealand. Their method consists of recognizing asymptotes and limits within complex age spectra and statistical analysis of frequently measured ages from samples within the same geologic region to assess the thermotectonic significance. Although this method boasts independence from "...knowledge of the underlying system behavior" (Forster and Lister, 2004), Wijbrans and McDougall (1986) had previously demonstrated a complication in interpreting age spectra from mixed mica populations in deformed rocks when they recovered intermediate ages by artificially mixing muscovite and phengite.

The study presented here builds upon the mixing experiment of Wijbrans and McDougall (1986) to test if geologically meaningful ages can be obtained by the vacuum furnace step-heating of mixed populations of micas. The results show complex age spectra with an inability to recover original end member ages. This is due to contemporaneous degassing of each mica population during each heating step. Additionally, the degree of sample homogenization for each increment of gas released can be predicted using the degassing rates of the original mica analyses. These rates are found to correlate with the mica chemistry and have implications for preservation of the compositional controls on argon retentivity in the vacuum furnace.

Experiment design and methods

The purpose of this experiment was to evaluate the effects of mixing two distinct age populations of micas on $^{40}Ar/^{39}Ar$ age spectra derived by vacuum furnace step-heating in order to gain insight into the validity of ages obtained for samples containing multiple generations of the same mineral. To understand the effects of mixing two mineral populations on $^{40}Ar/^{39}Ar$ age spectra we chose to use samples with good age constraints and simple thermal histories (i.e. rapid monotonic cooling) to minimize complexities in the degassing behavior and interpretation of ages due to heterogeneous internal $^{40}Ar^*$ distributions. In this experiment artificial mixtures of biotite and muscovite were prepared and analyzed by the $^{40}Ar/^{39}Ar$ furnace step heating method. Igneous biotite and muscovite were used from four samples (two for each mica) that were previously dated in other geologic studies. Selection of these micas was based on previous $^{40}Ar/^{39}Ar$ dating (discussed below) indicating 1) flat (plateau) age spectra, 2) simple thermal histories, and 3) they yielded distinct ages- Late Jurassic and Late Cretaceous. Based on these properties, it is assumed each mica has a uniform internal $^{40}Ar^*$ distribution and is free of excess ^{40}Ar, therefore affording direct comparison of 'actual' end-member ages and 'artifact' mixed ages. Although previous $^{40}Ar/^{39}Ar$ dating studies of mixed micas are typically of metamorphic rocks (especially polymetamorphosed terranes, e.g. Wijbrans and McDougal, 1986) the use of igneous materials in this study allowed the simplest system in which to interpret age spectrum complexities that arise solely as an effect of mixed sample volumes of gas. The effects of partial resetting and neo/recrystallization including internal age gradients and chemical heterogeneity were avoided.

Three aliquots of 2.5, 5.0, and 7.5 mg were handpicked from the 177-250 μm size fraction for each muscovite and biotite sample. The muscovite and biotite aliquots were then combined to produce six ~10 mg samples (3 biotite and 3 muscovite) consisting of weight ratios between Late Jurassic and Late Cretaceous aged crystals of 3:1, 1:1, and 1:3.

The six mixed samples were irradiated for 7 hours at the Oregon State University Radiation Center along with 92-176 Fish Canyon Tuff sanidine, synthetic K-glass, and optical grade CaF_2 to monitor neutron dosage (J-factor) and interfering neutron reactions on K and Ca. Repeated analysis of K-glass and CaF fragments resulted in a measured $(^{40}Ar/^{39}Ar)_K$ value of 5.1 (± 63.0%) x 10^{-3} and Ca correction factors of $(^{36}Ar/^{37}Ar)_{Ca}$ = 2.7178 (± 4.66%) x 10^{-4} and $(^{39}Ar/^{37}Ar)_{Ca}$ = 6.7376 (± 0.922%) x 10^{-4}. J factors were determined by fusion of 4-8 individual crystals of Fish Canyon sanidine using a 20 W CO_2 laser and are listed with each sample in Appendix C.

During analysis of the six mixed samples in this study, measured $^{40}Ar/^{36}Ar$ ratios determined by repeated analysis of atmospheric aliquots from an on-line pipette system were 285.67 ± 0.26% yielding a mass discrimination correction of 1.03441 (4 AMU) for measured isotopes. Samples were step heated in a double vacuum resistance furnace similar to the Staudacher et al. (1978) design. Reactive gases were removed by three GP-50 SAES getters prior to admittance to an MAP 215-50 mass spectrometer by expansion. Peak intensities for argon isotopes 36-40 were measured using a Balzers electron multiplier by peak hopping through 7 cycles for linear regression to the time of gas admittance. All data are presented at the 1σ uncertainty level.

Description of starting materials

Descriptions of the sample backgrounds and the results of $^{40}Ar/^{39}Ar$ dating are presented in this section. The four mica samples used in this study were previously dated by the $^{40}Ar/^{39}Ar$ furnace step-heating method at the Nevada Isotope Geochronology Laboratory at UNLV. Analytical and irradiation procedures for NY25 muscovite are presented in Wells et al. (2005). Samples IV14 muscovite and IV8 biotite were irradiated at the Nuclear Science Center at Texas A&M University for 14 hours. Sample PM1 biotite was irradiated for 7 hours in the McMaster Nuclear Reactor at McMaster University. Correction and J-factors are presented in the data tables in Appendix A. The chemical composition of these biotites and muscovites are summarized in Table 1. Analytical procedures for electron microprobe chemistry determinations are presented in Appendix B.

NY25 muscovite

Muscovite from sample NY25 was originally dated by the $^{40}Ar/^{39}Ar$ method as part of a thermochronometry study of the Pinto shear zone in the New York Mountains of southern California (Wells et al., 2005). The muscovite was separated from a quartz vein within the shear zone and yielded a flat age spectrum with 99% of the gas release defining a plateau age of 71.85 ± 0.39 Ma (1σ uncertainty) (Fig. 1). This age is indistinguishable from the total gas age (71.86 ± 0.47 Ma) and isochron age (72.18 ± 0.89 Ma), and is the accepted age of the sample as the isochron regression indicates a poorly constrained initial $^{40}Ar/^{36}Ar$ value (282 ± 15 Ma).

<u>IV14 muscovite</u>

Sample IV14 was collected from the eastern margin of the Ivanpah granite in the New Trail Canyon region of the Ivanpah Mountains in southern California as part of an ongoing regional thermochronometry study of the eastern Mojave Desert (see Chapter 4). This phase of the Ivanpah pluton is coarse two-mica granite with characteristic pink K-feldspar and smoky quartz. This sample yielded a flat age spectrum with a plateau age of 148.83 ± 0.79 Ma including all steps (100% of gas release) (Fig. 1). This age is within uncertainty of the U/Pb zircon crystallization age of 147 ± 7 Ma (Walker et al., 1995) and is consistent with rapid cooling of the pluton margins during intrusion.

<u>PM1 biotite</u>

Sample PM1 was collected from a stock of fine-grained Late Cretaceous granite in the southern Providence Mountains of southern California as part of a geo-/thermochronometry study of Late Cretaceous magmatism and extension (Kula et al., 2002; Wells et al., 2005). Biotite yielded a flat age spectrum with indistinguishable total gas (75.28 ± 0.40 Ma), plateau (75.31 ± 0.40 Ma), and isochron (75.71 ± 0.71 Ma) ages (Fig. 2). The plateau and isochron ages both include 100% of the gas release in their calculations, but the plateau age is considered the 'accepted' age for the biotite because the $^{40}Ar/^{36}Ar$ intercept of the isochron is poorly constrained indicating a value less than atmospheric (279 ±15).

IV8 biotite

Sample IV8 was collected from the eastern margin of the Ivanpah pluton approximately 1 km south of sample IV14 as part of the same study mentioned above. Indistinguishable total gas and plateau ages of 146.10 ± 0.81 and 146.13 ± 0.82 Ma, respectively were obtained. The plateau age includes 97.9% of the gas release and is considered the accepted age for the biotite (Fig. 2). A statistically valid isochron was not obtained, however regressions consistently yield $^{40}Ar/^{36}Ar$ intercept values of 295 indicating the sample is free of excess ^{40}Ar.

$^{40}Ar/^{39}Ar$ results from mixed samples

Results in this section are from the six mixed samples (3- biotite, 3-muscovite) created using the Jurassic and Cretaceous samples described above. Data tables corresponding to the age spectra in Figures 1 and 2 are in Appendix C.

Muscovite

The three age spectra obtained from the mixed muscovite samples are shown in Figure 1. The shape of these spectra are very similar to one another with moderately discordant ages over the initial ~25% of the gas release, followed by a relatively flat to gently increasing age gradient over the next ~55% of the gas release and a final dramatic decrease in ages over the last ~20% of the gas release. The ages making up each spectrum systematically decrease with decrease in Jurassic muscovite component (IV14) and increase in Cretaceous muscovite component (NY25) (Fig. 1). Total gas ages for each spectrum are 130.5 ± 0.5 Ma for 3:1(IV14:NY25), 110.5 ± 0.4 Ma for 1:1(IV14:NY25), and 91.9 ± 0.4 Ma for 1:3(IV14:NY25). The 25% IV14 (Jurassic) mixture yielded a pseudo plateau age of 94.7 ± 0.5 Ma over steps 5-8 consisting of 49.1% of the gas release.

Biotite

Age spectra obtained from the three mixed biotite samples are shown in Figure 2. All three age spectra are discordant with similar shapes showing a peak-valley-peak pattern over the first ~60-70% of the gas release and then a progressive decrease in ages over the final ~30% of the release. As with the muscovite spectra, each mixture yielded an age spectra consisting overall of decreasing ages with decrease in the older biotite component (IV8) and increase in the younger (PM1) component. There are no contiguous segments of the same age consisting of greater than 25% of the gas release in any of the three age spectra. The total gas ages for these mixed samples are 127.9 ± 0.5 Ma for 3:1(IV8:PM1), 110.2 ± 0.5 Ma for 1:1(IV8:PM1), and 92.7 ± 0.4 Ma for 1:3(IV8:PM1).

Discussion

Comparison of original mica spectra with mixed spectra

A striking observation from Figures 1 and 2 is that nearly all steps from the mixed samples yield ages that do not correspond to those of the original micas. This implies that, as expected, both populations of mica in the mixed biotite and muscovite samples were concurrently outgassing during each step and thus an 'intermediate' age was obtained (e.g. Wijbrans and McDougall, 1986). Mixed biotite sample 1:3(IV8:PM1) was the only sample that yielded any steps with ages reflecting an individual component of the mixture (Fig 2; Appendix C). This occurred over the final two steps of the analyses

(23% of the gas release) and indicates that at this point in the analysis IV8 biotite (25 wt% of this mixture) had completely outgassed. It seems the only way that 'real' ages may be obtained from a mixed sample is if at any point during a step-heat analysis (1) one population has completely outgassed earlier than the other, or (2) at any given temperature during the step-heat, one population fails to release any gas. This result is at odds with studies of metamorphic micas that yield staircase shaped spectra interpreted as representing the duration of deformation (Kirschner et al., 1996). For the case of staircase shaped spectra, there is an underlying assumption that the younger ages obtained early in the step-heat reflect the later stages of progressive deformation. For this assumption to be satisfactory, it would then be required that either (1) the crystals being analyzed have identical internal age gradients and all true crystal shapes are preserved and closely approximate a cylindrical diffusion geometry (e.g. Hames and Bowring, 1996), (2) the youngest ages are recorded in the smallest crystals and each increase in furnace temperature progressively 'taps' a larger, older crystal population, or (3) there is a natural correlation between age and retentivity during furnace heating that may or may not be independent of composition. The mixed spectra results here indicate that, for samples of uniform grain size, there is no reason to expect young crystals to outgas earlier than older crystals during furnace step-heating.

Figures 1 and 2 also indicate that the mixed biotite samples yielded age spectra with higher degrees of discordance than the muscovite. The general flatness of the mixed muscovite age spectra compared to the biotite may indicate samples NY25 and IV14 have more similar degassing behaviors during vacuum step-heating than biotite samples IV8 and PM1. All samples were prepared from the same 177-250 μm size fraction and there is no apparent systematic progression in the age spectra patterns (e.g. staircase shape). Consequently, it appears the degree of discordance in the age spectra is a function of the difference in the degassing behaviors between the mixed populations at each temperature step during an analysis.

^{39}Ar release patterns and shape of the age spectra

From Figure 1 it is apparent that the components of NY25 and IV14 muscovite were degassing at very similar rates over the first 60-70% of the gas release, as fluctuations in age are small. This is consistent with the gas release patterns from the original ^{40}Ar/^{39}Ar analyses of these samples (Fig. 3). The cumulative %^{39}Ar release patterns and stepwise %^{39}Ar release patterns in Figure 3 indicate two 'degassing peaks' at 850-900°C and ~1100°C for NY25 muscovite. A similar lower temperature degassing peak exists for IV14, however this sample appears to have a less variable stepwise release overall than NY25. The degassing rates in Figure 3 also indicate NY25 muscovite retains more gas into the higher temperature steps than IV14, which is consistent with the decrease in ages approaching the 'actual' age for NY25 seen in the mixed age spectra (Fig. 1). Slightly higher retentivity of NY25 muscovite is consistent with this sample showing less Fe replacement in the octahedral site (Table 1) than IV14 and a greater amount of F; two properties attributed to lowering diffusivities in white micas (Wijbrans and McDougall, 1986; Scaillet et al., 1992; Dahl, 1996).

In contrast to the muscovites that exhibit somewhat similar degassing patterns (Fig. 3) and relatively flat age spectra (Fig. 1), the degassing patterns for biotites IV8 and PM1 are quite different (Fig. 4) and the mixed age spectra are highly disturbed (Fig. 2). The degassing patterns in Figure 4 indicate biotite IV8 releases ~60% of the gas by the

860°C step. Conversely, biotite PM1 shows a more consistent gas release through the step-heat until ~1100°C where there is a larger pulse outgassing (Fig. 4). These degassing patterns indicate that when mixed, biotite IV8 should dominate the early release, and biotite PM1 should dominate the later high-temperature release. This is consistent with the age spectra from the mixed biotite samples (Fig. 2). Although the spectra show a two-peak morphology, they also exhibit an overall trend indicating a gradual decrease in age over the entire step-heat, as the final steps approach the age of biotite PM1.

If earlier outgassing of biotite IV8 during the step-heat reflects a higher diffusivity than biotite PM1, this is consistent with the higher Fe content in the IV8 versus PM1 (Table 1) (Harrison et al., 1985; Dahl, 1996; Grove and Harrison, 1996; Lo et al., 2000). Biotite IV8 also shows a higher degree of Al^{VI} incorporated into the octahedral site than PM1 (Table 1), which would also be expected to lower the diffusivity of IV8. This fails to balance the elevated Fe-Mg exchange effect (Dahl, 1996), indicating perhaps the greater octahedral deficiency (i.e. vacancies) in IV8 may contribute to enhanced degassing during lower temperatures.

Consistent relationships between degassing patterns and mixed age spectra indicate that both muscovite and biotite retain properties that control degassing rates during vacuum step-heating. This conclusion is at odds with several studies concluding that structural and chemical breakdown during vacuum step-heating compromise the shape of the age spectra due to intracrystalline $^{40}Ar^*$ homogenization (e.g. Lo et al., 2000). The mixed mica age spectra indicate the shape of the age spectra obtained for mixed populations of micas is directly related to the degassing patterns (rates) of the individual populations and the relative abundance of each population in the bulk sample being analyzed. Therefore, if the age and degassing behavior of two micas are known, the shape of the resulting age spectrum of a mixture can be predicted by the equation:

$$t_p = [B_1/(B_1+B_2)*t_1] + [B_2/(B_1+B_2)*t_2], \qquad \text{Eq. 1}$$

where t_p = predicted age, B_1 = $\%^{39}Ar$ release from one mica at a given temperature step, B_2 = $\%^{39}Ar$ release from the second mica at a given temperature step, t_1 = the accepted age of the mica corresponding to B_1, and t_2 = the accepted age of the mica corresponding to B_2. This is based on the assumption that degassing patterns during vacuum furnace step heating are constants specific to each individual sample. This assumption can be tested by attempting to reproduce the mixed age spectra by prediction based on the degassing patterns determined from the original samples.

Inherent to the accuracy of the age predictions is that the two initial samples should be analyzed using the same heating schedule. The data presented here do not conform to this requirement because previous analyses were used for the study, however interpolation between temperature steps may provide insight into the consistency of degassing patterns during vacuum furnace heating.

Figure 5 shows examples from two prediction models using biotites IV8 and PM1. These models assume equal volumes of each sample and thus correspond to the 1:1 biotite mixture (1:1(IV8:PM1). Figures 5a and 5b show the results of interpolating the $\%^{39}Ar$ released from the original step-heating analyses to correspond to the step-heating schedule used for the mixed samples. The cumulative $\%^{39}Ar$ release pattern was fit using the MATLAB curve fitting toolbox. From this model curve, the stepwise $\%^{39}Ar$ release for each temperature step from the mixed mica heating schedule was obtained (Fig. 5b.) The mismatch in the low temperature degassing pattern (Fig. 5a) demonstrates the degassing pattern is influenced by the heating schedule, as interpolating between temperature steps does not take into account the fixed volume of gas in the system which requires the volume released at each step to be limited by the amount released by the previous steps. The resulting predicted ages show a poor fit to the measured ages up until 845 °C where the model ages roughly mimic the measured ages over the remaining steps (Fig. 5b).

Figures 5c and 5d show the results of fitting the stepwise $\%^{39}Ar$ release pattern with a nearest neighbor line fit from the MATLAB curve fitting toolbox. The nearest neighbor line fit assigns values (y-axis; $\%^{39}Ar$ released) along the model curve using the closest (x-axis distance; temperature) point along the sample curve. The resulting age vs. temperature plot (Fig. 5d) roughly mimics the measured pattern from the mixed sample although there is some discordance. While the discordance is likely a result of inconsistency between the heating schedules used for the original samples and that used for the mixed samples, the somewhat close prediction of ages indicates the micas degas during vacuum furnace step-heating according to their individual retention characteristics that are likely rooted in their composition (Dahl, 1996).

Total gas ages of age spectra

Total gas ages were calculated by summation of the ages for each step weighted by the $\%^{39}Ar$ released for each step. Therefore, the total gas age should represent a conventional K/Ar age reflecting the total parent-daughter ratio of the bulk sample. As such, the ages of the original starting materials could be scaled by weight % in the mixed samples and combined to calculate an expected total gas age for the mixed samples. Complexities to this theoretical framework can arise if the samples consist of different abundances of K. However, the chemical analyses indicate the K-content of both biotites and both muscovites are nearly identical (Table 1) and therefore the mixed samples should approximate the theoretical basis.

Using the ages obtained for the original muscovite samples IV14 and NY25, total gas ages based on mixture ratios of 3:1, 1:1, and 1:3 are 129.7 Ma, 110.5 Ma, and 91.1 Ma, respectively. For the biotite samples of the same ratios, calculated total gas ages are 128.4 Ma, 110.8 Ma, and 93.0 Ma. These ages are all within uncertainty to those obtained from the furnace step-heating analyses discussed above. So, even though all but the last two steps of the 1:3 (1:3(IV8:NY25)) muscovite mixture, yield meaningless ages with respect to the starting materials, the full step-heat analyses correctly indicate the bulk $^{40}Ar/^{39}Ar$ (i.e. K/Ar age) of the mixed samples. This is an expected result for samples free of excess argon, which is indicated by the similarity between plateau and total gas ages for the original micas.

These results may also have implications for interpreting discordant age spectra obtained from single mica populations. Discordant age spectra are commonly obtained from biotites that have been affected by ^{39}Ar recoil during irradiation. Depending on the degree of alteration/chloritization, the magnitude of discordance in the age spectrum can vary, however, typically the ability to obtain a plateau is compromised. The success of the total gas ages reflecting the bulk age of the mixed samples in this study indicates that for samples yielding disturbed age spectra due to recoil and not excess argon, where the recoil redistributes parent or daughter atoms within the crystals and not out of them (e.g. Lo and Onstott, 1989), the total gas age should represent the actual age of the sample. The validity of this hypothesis may be tested by correlating isotopes indicative of alteration/decrepitation with age for each step (e.g., Roberts et al., 2001) and comparison of results from other chronometers within the same geologic region (e.g. Reiners et al., 2004).

Recognition of meaningless ages as a result of mixing two samples of known age indicates caution must be taken when interpreting complex age spectra from metamorphic micas. Introduction of variables not dealt with in this study such as chemical heterogeneity (Smith et al., 2005), fossil age gradients (Hames and Bowring, 1994; Hodges and Bowring, 1995), neo-/recrystallization at multiple grain-sizes (Goodwin and Renne, 1991, Markley et al., 2002), and deformation induced structural changes (Kramar et al., 2001) likely results in increasingly complex age spectra consisting of mixed ages that have no geologic significance when vacuum furnace step-heated.

Implications for multiple populations in natural samples

An important result of this study is the inability to reproduce the original mica ages in any heating steps in all but one mixed sample (1:3(IV8:PM1) biotite). This is consistent with the results of Wijbrans and McDougall (1986) where a 3:1 phengite:muscovite mixture was compared with pure phengite and muscovite spectra. Therefore, when excess argon is not an issue, maximum ages from a mixed age spectra should be treated as minimum ages for the oldest fossil isotopic signature in the samples and vice versa (e.g., Forster and Lister, 2004). Additionally, this result appears to invalidate the method of asymptotes and limits to interpreting complex age spectra produced from rocks containing multiple generations of mica (Forster and Lister, 2004).

Typically, mixed populations of micas are obtained from metamorphic rocks (Wijbrans and McDougall, 1986; Kirschner et al., 1996) and therefore complications exist that were avoided in the study presented here. The use of homogeneous, rapidly cooled igneous micas from a specific size fraction afforded the opportunity to avoid the effects of fossil age gradients, and complex grain size distributions due to neo- or recrystallization (e.g. Scaillet et al., 1992, Kirschner et al., 1996). However, the results herein indicate that for staircase spectra derived from deformed micas, initial young steps should not be assumed to represent degassing of solely the youngest and finest neocrystallized materials and therefore the youngest ages likely represent an overestimate of the timing of final isotopic closure for the sample. The mixed spectra presented here only approach an original mica age in the final steps of the analyses. Therefore, preserved, unmixed ages should only be expected to be obtained when one population (for a mix of two populations) has been shown to have completely outgassed already (i.e., the final portion of the age spectra). For the case of staircase shaped spectra, meaningful initial young ages may only be obtainable if it can be demonstrated that at the lower initial temperatures sample gas was extracted from one population and not the other due to differences in their argon retention characteristics- most notably the grain size (i.e., diffusion radius).

Implications for mica stability during vacuum step-heating

The relationship between the shape of the mixed age spectra and the original degassing patterns along with correlation between mica chemistry and the degassing patterns (discussed above) indicates micas maintain argon retention characteristics during vacuum furnace step-heating. Therefore, sample degassing behavior in the laboratory is controlled by the same crystal-chemical basis that governs argon retentivity during geologic cooling (e.g. Dahl., 1996; Grove and Harrison, 1996). It then follows that some stability with respect to argon diffusion mechanisms must be maintained during vacuum furnace heating and therefore it may be possible to link the shape of mica-derived age spectra to the thermal history of the sample.

This conclusion implies the possibility for recovery of fossil age gradients in slowly cooled samples. Based on argon diffusion being approximated by a cylindrical geometry (Hames and Bowring, 1994) it is likely that if age gradients are to be recovered in the vacuum furnace, the original grain boundaries of the micas would need to be preserved during sample preparation. For the case of neocrystallized subgrains with dimensions significantly smaller than the original mica crystals, recovery of diffusion-radius controlled age gradients may be possible especially if the pre-existing mica is more retentive at higher temperatures (e.g. Wijbrans and Mc Dougall, 1986).

Figure captions

Figure 1. Age spectra from the end member (IV14, NY25) and mixed muscovite samples. Note overall age of mixed spectra systematically decreases with decrease in Jurassic (IV14) component and increase in Cretaceous (NY25) component. None of the gas increments in the three mixed samples yield original ages.

Figure 2. Age spectra from end member (IV8, PM1) and mixed biotite samples. The mixed spectra are highly discordant but show an overall decrease in age with decrease in Jurassic (IV8) component and increase in Cretaceous (PM1) component. Only the final two gas increments from 1:3(IV8:PM1) yield ages corresponding with one of the original ages (PM1).

Figure 3. Degassing patterns for muscovites NY25 and IV14. Plot includes incremental $\%^{39}Ar$ released and cumulative $\%^{39}Ar$ released patterns. Note similar shape between incremental outgassing patterns, although NY25 has more pronounced pulses at the 850-900˚C and 1100 ˚C steps. NY25 also appears to retain more gas into the higher temperature steps.

Figure 4. Degassing patterns for biotites PM1 and IV8. Both the incremental release and cumulative release patterns indicate IV8 outgasses at significantly lower temperatures than PM1, shows a consistent outgassing pattern until ~1100 ˚C where there is a pulse.

Figure 5. Degassing patterns and age vs. temperature plots comparing model attempts to predict age spectra shape using original degassing patterns. a. incremental degassing pattern determined from line-fitting the original cumulative release pattern for biotites IV8 and PM1. Discordance in fit of incremental release pattern for IV8 reflects the dependence of the release pattern on the heating schedule. b. relatively poor fit of predicted ages vs. measured mixed ages 1:1(IV8:PM1) based on incremental degassing pattern from plot a. c. measured incremental degassing patterns and model patterns based

on nearest neighbor line-fitting. d. comparison of model age vs. temperature based on patterns in c with that measured for 1:1(IV8:PM1). Shape of the spectra is better bit than b, however discordance occurs at the low and high temperature ends reflecting poor assumptions regarding degassing patterns inherent in the models.

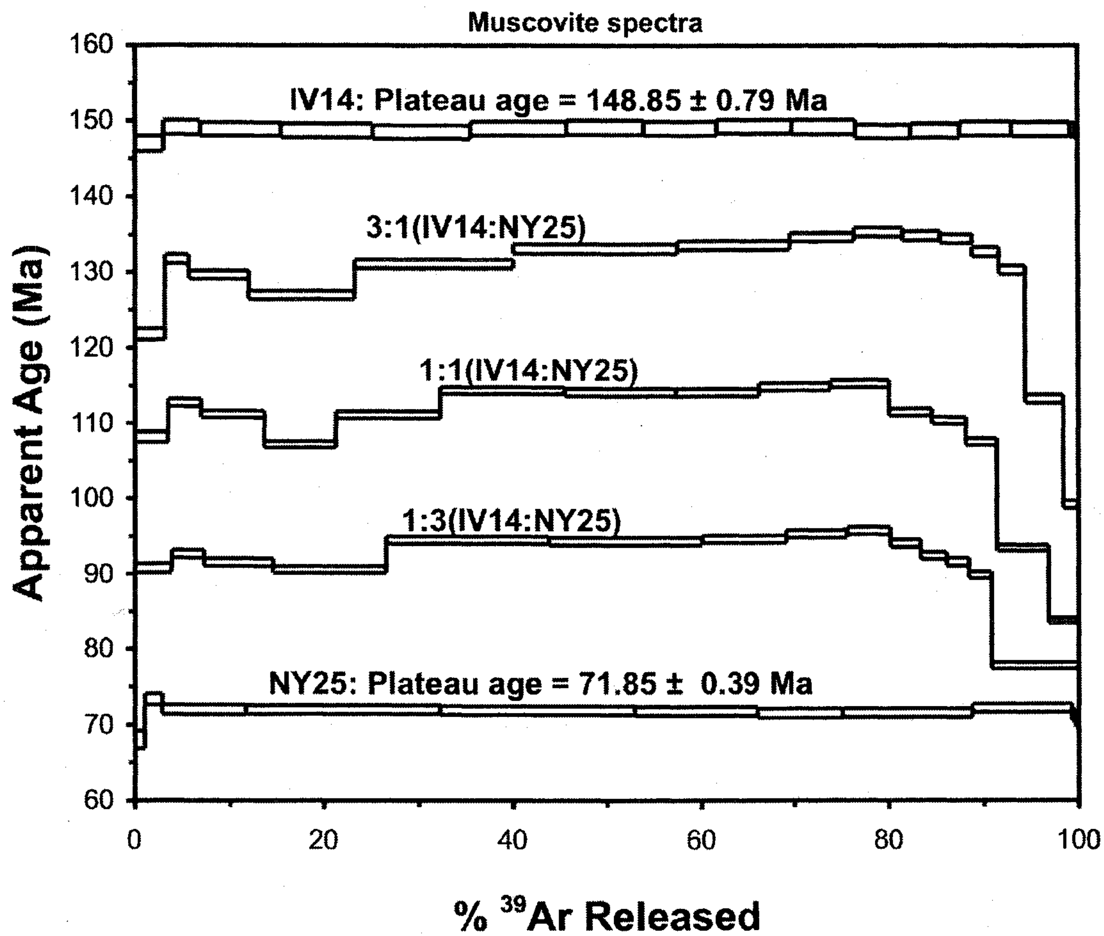
Muscovite spectra
IV14: Plateau age = 148.85 ± 0.79 Ma
3:1(IV14:NY25)
1:1(IV14:NY25)
1:3(IV14:NY25)
NY25: Plateau age = 71.85 ± 0.39 Ma
Apparent Age (Ma)
160
150
140
130
120
110
100
90
80
70
60
0
20
40
60
80
100
% 39Ar Released

Figure 1

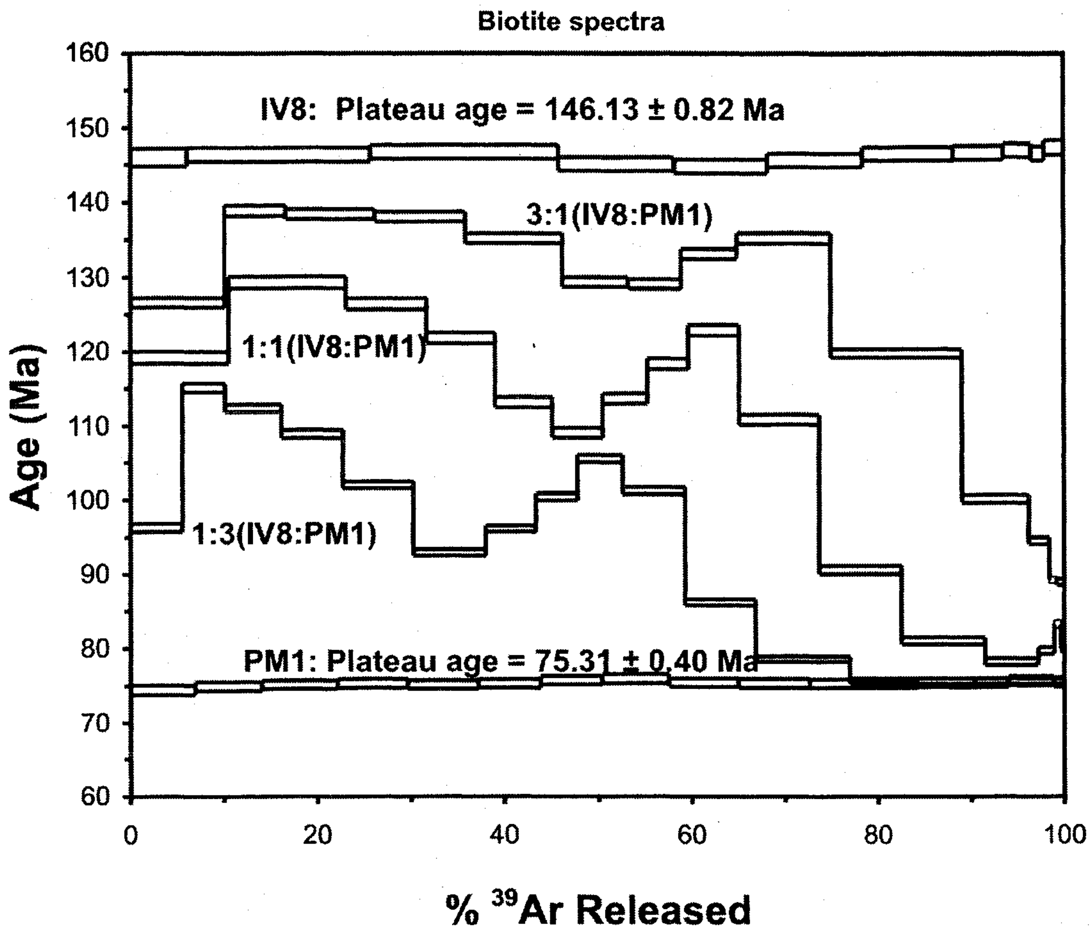

Biotite spectra
IV8: Plateau age = 146.13 ± 0.82 Ma
3:1(IV8:PM1)
1:1(IV8:PM1)
1:3(IV8:PM1)
PM1: Plateau age = 75.31 ± 0.40 Ma
Age (Ma)
160
150
140
130
120
110
100
90
80
70
60
0
20
40
60
80
100
% 39Ar Released

Figure 2

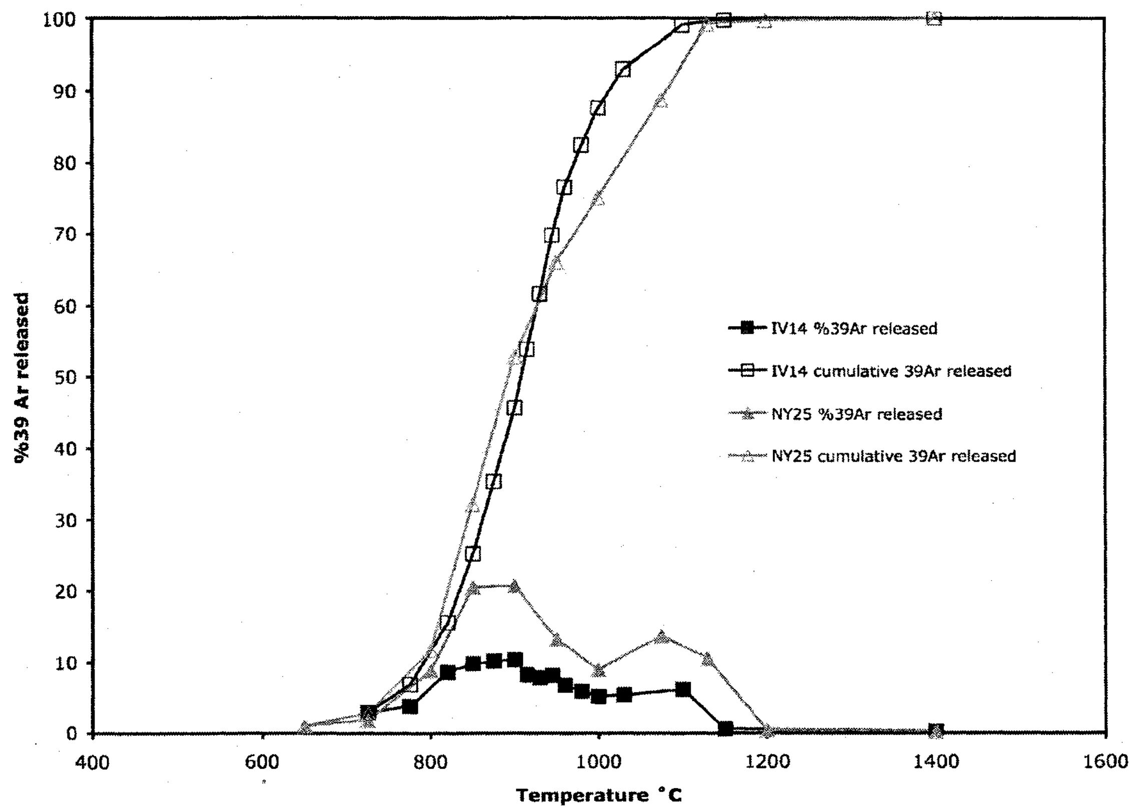
100
90
80
70
60
50
40
30
20
10
0
%39 Ar released
400
600
800
1000
1200
1400
1600
Temperature °C
IV14 %39Ar released
IV14 cumulative 39Ar released
NY25 %39Ar released
NY25 cumulative 39Ar released

Figure 3

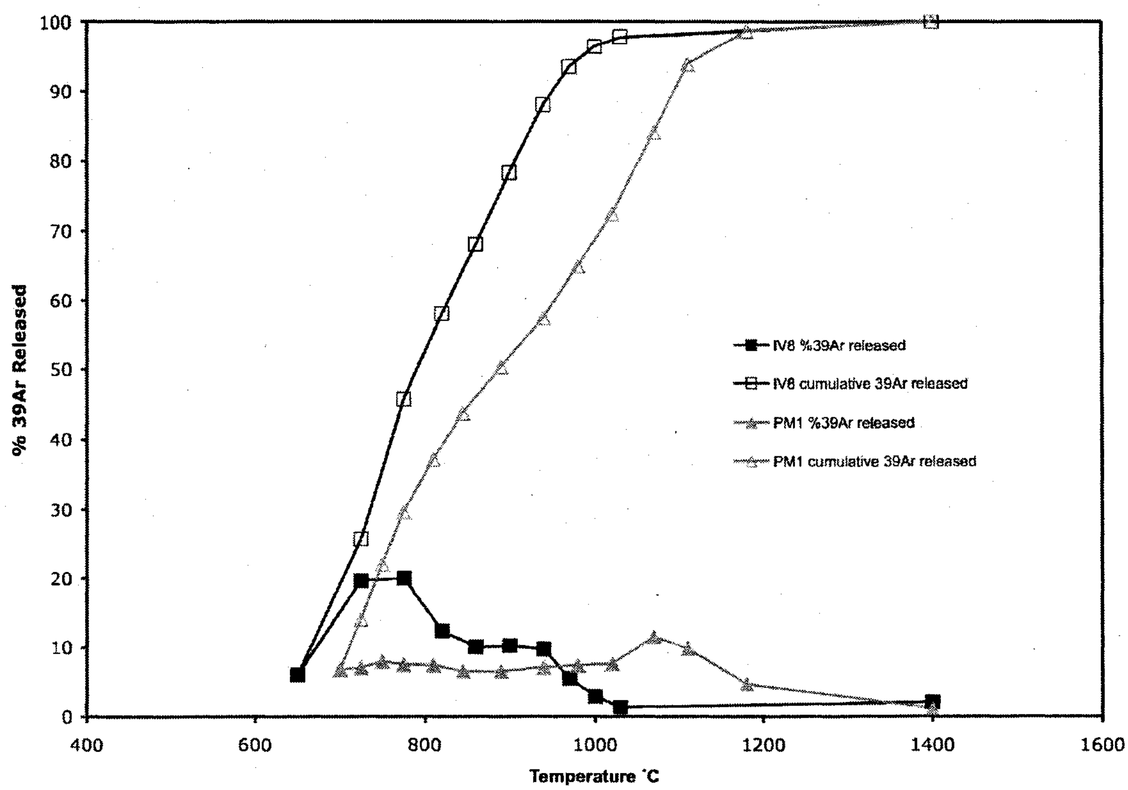

100
90
80
70
60
50
40
30
20
10
0
% 39Ar Released
400
600
800
1000
1200
1400
1600
Temperature ˚C
IV8 %39Ar released
IV8 cumulative 39Ar released
PM1 %39Ar released
PM1 cumulative 39Ar released

Figure 4

Table 1
Electron microprobe chemical composition of micas used in the experiment.

	Muscovite		Biotite	
	NY25	**IV14**	**IV8**	**PM1**
SiO_2	44.67	44.87	35.55	34.94
TiO_2	0.78	0.24	1.91	2.99
Al_2O_3	32.17	30.63	21.46	16.33
FeO	3.39	5.68	23.32	18.92
MnO	0.09	0.28	2.10	0.24
MgO	1.30	1.24	1.14	11.07
CaO	0.00	0.00	0.00	0.01
Na_2O	0.49	0.27	0.14	0.09
K2O	10.42	10.57	9.20	9.53
F	0.56	0.00	2.28	2.04
Cl	0.01	0.01	0.22	0.04
Total (Anhydrous)	93.87	93.79	97.29	96.19
Fe/(Fe+Mg)	0.593	0.719	0.920	0.489
Cl/K	0.001	0.001	0.031	0.005
F/(F+OH)	0.030	0.000	0.142	0.125
11 Oxygen				
Si	3.084	3.122	2.776	2.708
Ti	0.041	0.013	0.112	0.174
Al^{IV}	0.876	0.865	1.113	1.118
Sum	4.000	4.000	4.000	4.000
Al^{VI}	1.741	1.647	0.862	0.373
Fe	0.195	0.330	1.523	1.226
Mn	0.005	0.017	0.139	0.016
Mg	0.134	0.129	0.133	1.279
Sum	2.076	2.122	2.656	2.894
Ca	0.000	0.000	0.000	0.001
Na	0.065	0.036	0.021	0.013
K	0.918	0.938	0.916	0.942
Sum	0.983	0.974	0.937	0.956
F	0.121	0.000	0.563	0.499
Cl	0.001	0.001	0.029	0.005
OH	3.877	3.999	3.408	3.496

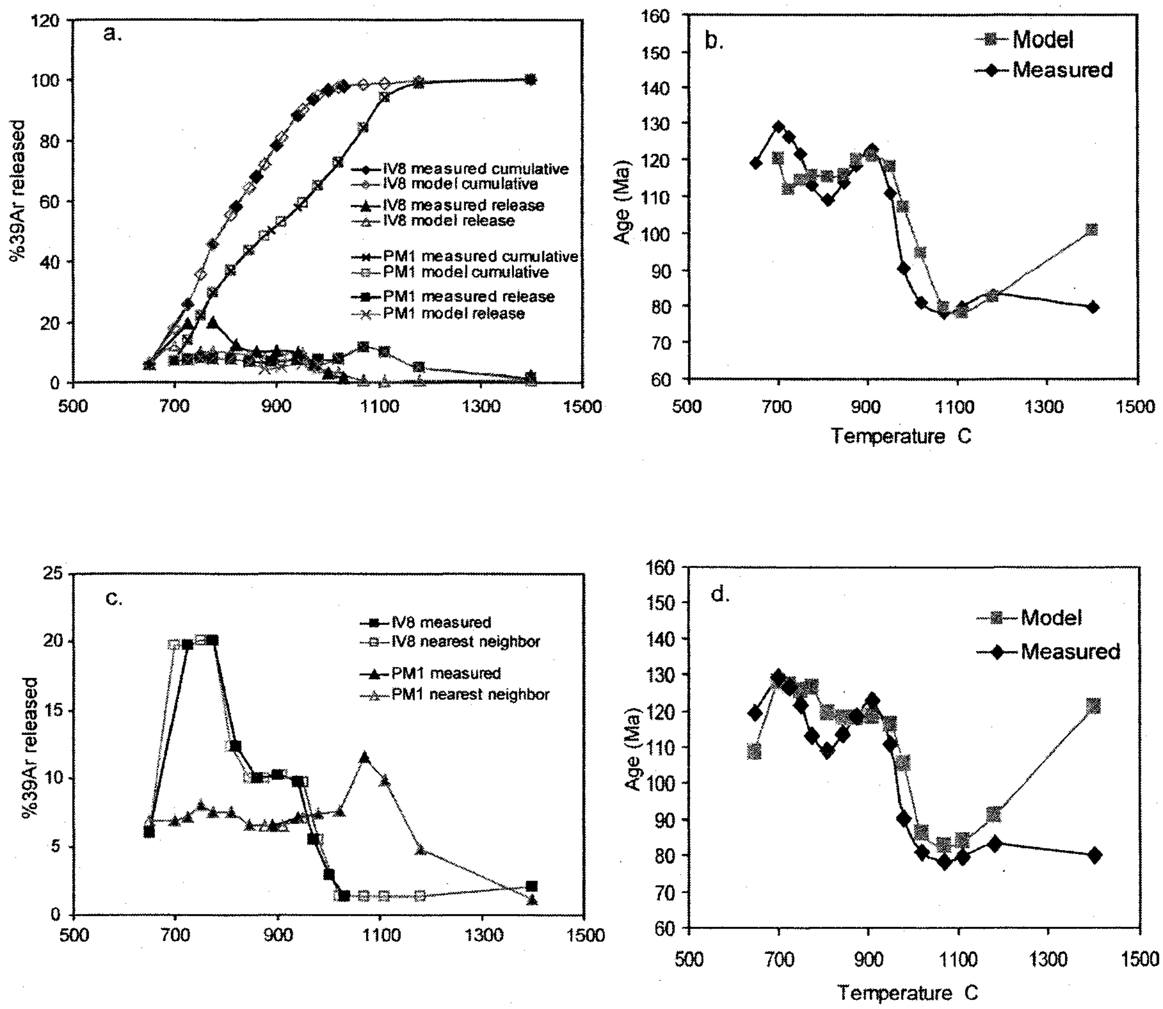
a.
%39Ar released
IV8 measured cumulative
IV8 model cumulative
IV8 measured release
IV8 model release
PM1 measured cumulative
PM1 model cumulative
PM1 measured release
PM1 model release
b.
Model
Measured
Age (Ma)
Temperature C
c.
%39Ar released
IV8 measured
IV8 nearest neighbor
PM1 measured
PM1 nearest neighbor
d.
Model
Measured
Age (Ma)
Temperature C

Figure 5

References

Chopin, C., and Maluski, H., 1980, ^{40}Ar-^{39}Ar dating of high pressure metamorphic micas from the Gran Paradiso Area (western Alps): Evidence against the blocking temperature concept: Contributions to Mineralogy and Petrology, v. 74, p. 109-122.

Dahl, P.S., 1996, The crystal-chemical basis for Ar retention in micas: inferences from interlayer partitioning and implications for geochronology: Contributions to Mineralogy and Petrology, v. 123, p. 22-39.

de Jong, K., Wijbrans, J.R., and Feraud, G., 1992, Repeated thermal resetting of phengites in the Mulhacen Complex (Betic Zone, southeastern Spain) shown by ^{40}Ar/^{39}Ar step heating and single grain laser probe dating: Earth and Planetary Science Letters, v. 110, p. 191.

Dunlap, W.J., 1998, The tectonic significance of a porphyroblastic blueschist facies overprint during Alpine orogenesis: Sifnos, Aegean Sea, Greece: Discussion: Journal of Structural Geology, v. 20, p. 819-821.

Forster, M.A., and Lister, G.S., 2004, The interpretation of ^{40}Ar/^{39}Ar apparent age spectra produced by mixing: application of the method of asymptotes and limits: Journal of Structural Geology, v. 26, p. 287-305.

Goodwin, L.B., and Renne, P.R., 1991, Effects of progressive mylonitization on Ar retention in biotites from the Santa Rosa mylonite zone, California, and thermochronologic implications: Contributions to Mineralogy and Petrology, v. 108, p. 283-297.

Grove, M., and Harrison, T.M., 1996, ^{40}Ar* diffusion in Fe-rich biotite: American

Mineralogist, v. 81, p. 940-951.

Hames, W.E., and Bowring, S.A., 1994, An empirical evaluation of the argon diffusion geometry in muscovite: Earth and Planetary Science Letters, v. 124, p. 161-167.

Hames, W.E., and Cheney, J.T., 1997, On the loss of $^{40}Ar^{*}$ from muscovite during polymetamorphism: Geochimica et Cosmochimica Acta, v. 61, p. 3863-3872.

Harrison, T.M., Duncan, I., and McDougall, I., 1985, Diffusion of ^{40}Ar in biotite: Temperature, pressure and compositional effects: Geochimica et Cosmochimica Acta, v. 49, p. 2461-2468.

Hames, W.E., and Hodges, K.V., 1993, Laser $^{40}Ar/^{39}Ar$ evaluation of slow cooling and episodic loss of 40Ar from a sample of polymetamorphic muscovite: Science, v. 261, p. 1721-1723.

Hodges, K.V., and Bowring, S.A., 1995, $^{40}Ar/^{39}Ar$ thermochronology of isotopically zoned micas: Insights from the southwestern USA Proterozoic orogen: Geochimica et Cosmochimica Acta, v. 59, p. 3205-3220.

Kirschner, D.L., Cosca, M.A., Masson, H., and Hunziker, J.C., 1996, Staircase $^{40}Ar/^{39}Ar$ spectra of fine-grained white mica: Timing and duration of deformation and empirical constraints on argon diffusion: Geology, v. 24, p. 747-750.

Kramar, N., Cosca, M.A., Hunziker, J.C., 2001, Heterogeneous $^{40}Ar^{*}$ distributions in naturally deformed muscovite: in situ UV-laser ablation evidence for microstructurally controlled intragrain diffusion: Earth and Planetary Science Letters, v. 192, p. 377-388.

Kula, J.L., Spell, T.L., and Wells, M.L., 2002, Syntectonic intrusion and exhumation of a

Mesozoic plutonic complex in the Late Cretaceous, Granite Mountains, southeastern California: Geological Society of America Abstracts with Programs, v. 34, p. 249.

Lanphere, M.A., and Albee, A.L., 1974, $^{40}Ar/^{39}Ar$ age measurements in the Worchester Mountains: Evidence of Ordovician and Devonian metamorphic events in northern Vermont: American Journal of Science, v. 274, p. 545-555.

Lee, J.K.W., Onstott, T.C., Cashman, K.V., Cumbest, R.J., and Johnson, D., 1991, Incremental heating of hornblende in vacuo: Implications for $^{40}Ar/^{39}Ar$ geochronology and the interpretation of thermal histories: Geology, v. 19, p. 872-876.

Lo, C.-H., Lee, J.K.W., and Onstott, T.C., 2000, Argon release mechanisms of biotite in vacuo and the role of short-circuit diffusion and recoil: Chemical Geology, v. 165, p. 135-166.

Lo, C.H., Onstott, T.C., 1989, ^{39}Ar recoil artifacts in chloritized biotite: Geochimica et Cosmochimica Acta, v. 53, p. 2697 – 2711.

Markley, M.J., Teyssier, C., and Cosca, M., 2002, The relation between grain size and $^{40}Ar/^{39}Ar$ date for Alpine white mica from the Siviez-Mischabel Nappe, Switzerland: Journal of Structural Geology, v. 24, p. 1937-1955.

McDougall, I. and Harrison, T.M., 1999, Geochronology and Thermochronology by the $^{40}Ar/^{39}Ar$ Method, 2nd edition, Oxford University Press, New York, NY, 269 p.

Putlitz, B., Cosca, M.A., Schumacher, J.C., 2005, Prograde mica $^{40}Ar/^{39}Ar$ growth ages recorded in high pressure rocks (Syros, Cyclades, Greece): Chemical Geology, v. 214, p. 79-98.

Reiners, P.W., Spell, T.L., Nicolescu, S., and Zanetti, K.A., 2004, Zircon (U-Th)/He thermochronometry: He diffusion and intercalibration with $^{40}Ar/^{39}Ar$ dating: Geochimica et Cosmochimica Acta, v. 68, p. 1857-1887.

Roberts, H.J., Kelley, S.P., and Dahl., P.S., 2001, Obaining geologically meaningful $^{40}Ar/^{39}Ar$ ages from altered biotite: Chemical Geology, v. 172, p. 277-290.

Scaillet, S., Feraud, G., Lagabrielle, Y., Ballevre, M., and Ruffaet, G., 1990, $^{40}Ar/^{39}Ar$ laser-probe dating by step heating and spot fusion of phengites from the Dora Maria nappe of the western Alps, Italy: Geology, v. 18, p. 741-744.

Scaillet, S., Feraud, G., Ballevre, M., and Amouric, M., 1992, Mg/Fe and [(Mg,Fe) Si-Al2] compositional control on argon behavior in high-pressure white micas: A $^{40}Ar/^{39}Ar$ continuous laser-probe study from the Dora-Maira nappe of the internal western Alps, Italy: Geochimica et Cosmochimica Acta, v. 56, p. 2851-2872.

Sletten, V.W., and Onstott, T.C., 1998, The effect of the instability of muscovite during in vacuo heating on $^{40}Ar/^{39}Ar$ step-heating spectra: Geochimica et Cosmochimica Acta, v. 62, p. 123-141.

Smith, S.R., Kelley, S.P., Tindle, A.G., and Breaks, F.W., 2005, Compositional controls on $^{40}Ar/^{39}Ar$ ages of zoned mica from a rare-element pegmatite: Contributions to Mineralogy and Petrology, v. 149, p. 613-626.

Staudacher, T., Jessberger, E.K., Dorflinger, D., and Kiko, J., 1978, A refined ultrahigh -vacuum furnace for rare gas analysis: Journal of Physical Engineering: Scientific Instrumentation, v. 11, p. 781-784.

Walker, J.D., Burchfiel, B.C., and Davis, G.A., 1995, New age controls on initiation and timing of foreland belt thrusting in the Clark Mountains, southern California: Geological Society of America Bulletin, v. 107, p. 742-750.

Wells, M.L., Beyene, M.A., Spell, T.L., Kula, J.L., Miller, D.M., Zanetti, K.A., 2005, The Pinto shear zone; A Laramide synconvergent extensional shear zone in the Mojave Desert region of the southwestern Cordilleran orogen, western United States: Journal of Structural Geology, v. 27, p. 1697-1720.

Wijbrans, J.R., and McDougall, I., 1986, $^{40}Ar/^{39}Ar$ dating of white micas from an Alpine high-pressure metamorphic belt on Naxos (Greece): the resetting of the argon isotopic system: Contributions to Mineralogy and Petrology, v. 93, p. 187-194.

Wijbrans, J.R., Schliestedt, M., and York, D., 1990, Single grain argon laser probe dating of phengites from the blueschist to greenschist transition on Sifnos (Cyclades, Greece): Contributions to Mineralogy and Petrology, v. 104, p. 582-593.

CHAPTER 4

THE TIMING OF MESOZOIC MAGMATISM AND TECTONISM IN THE CLARK MOUNTAINS REGION OF THE EAST MOJAVE DESERT, CALIFORNIA

Abstract

New U/Pb zircon and $^{40}Ar/^{39}Ar$ hornblende, biotite, and K-feldspar ages have been obtained from several plutons exposed throughout the Clark Mountains thrust complex of southeastern California. These plutons have crosscutting relationships with several thrust faults making their emplacement and cooling ages applicable to constraining the timing of crustal shortening. The new ages and field relations indicate the earliest episode of thrust faulting occurred prior to ~154 Ma when the Mescal diorite and Oro Wash/Ji granodiorites intruded into the Mesquite Pass allochthon. Deformation then stepped westward with development of the Winter Pass/Pachalka allochthon in the Early Cretaceous. The final episode of shortening along the Keaney/Mollusk Mine thrust can be correlated south into the Ivanpah Pluton along the ductile Morning Star Mine thrust. Portions of several plutons show evidence for argon loss due to reheating during emplacement of the Teutonia Batholith. The youngest Mesozoic magmatic event in the region is represented by the Kessler Spring adamellite, which intrudes the southern Ivanpah pluton and yields a thermal history that indicates cooling in the upper crust prior to Late Cretaceous extension.

Introduction

The Jurassic-Cretaceous history of the southwestern margin of North America includes alternating episodes of extension and convergence. Jurassic (~170 Ma) extension has been suggested within the magmatic arc based on graben fills consisting of craton-derived sands interfingered with volcanic rocks (Busby-Spera, 1988; Busby et al., 2002) and upper crustal emplacement of chemically heterogeneous plutons (Fox and Miller, 1990). Timing of this intra-arc extension overlaps with episodes of crustal shortening within the East Sierran thrust belt (~188-140 Ma), which displaced arc rocks eastward over rocks of the craton margin (Dunne and Walker, 2004). Transitions from extension to convergence are also seen in the western arc over this time frame. Extension led to development of the Josephine, Coast Range, and Smartville ophiolites (172-162 Ma), and was quickly followed by shortening (prior to 158 Ma) related to the Nevadan Orogeny (Saleeby and Busby-Spera, 1992). Walker et al. (2002) suggest an abrupt shift from extension to shortening took place at ca. 160 Ma, however this timing constraint may not apply to the entire continental/arc margin.

In the Late Jurassic-Early Cretaceous convergence continued as east-vergent thrust faults of the Sevier Orogen developed in the back-arc region (Liviccari, 1991; Burchfiel et al., 1992; Walker et al., 1995; DeCelles, 2004). This generally north-south trending deformational belt intersects the magmatic arc in southeast California in the Clark Mountains thrust complex (Fig. 1) (Burchfiel and Davis, 1971). The Clark Mountains area represents the eastern limits of the early and late foreland fold-thrust belt and the Cordilleran magmatic arc and thus contains a record of Jurassic and Cretaceous magmatism that interacts with folding and thrusting related to subduction along the western margin of North America (Burchfiel and Davis, 1988). North of the Clark Mountains area, the eastern fold-thrust belt exhibits thin-skinned decollement style thrusts (Sevier) separated from earlier ductile structures along the eastern margin of the magmatic arc (East Sierran thrust belt) by 10s of kilometers (Walker et al., 1995). The short <10 km cross-strike distance of the Clark Mountains thrust complex contains both early ductile and late brittle structures along with igneous bodies (Burchfiel and Davis, 1971, 1988; Walker et al., 1995). With shortening structures to the south typically involving Precambrian basement and Mesozoic plutonic rocks, the Clark Mountains thrust complex marks a transition in tectonic style along the Cordilleran trend (Walker et al., 1995; Howard et al., 1995).

The Clark Mountains area is considered to expose structures representing the earliest and latest thrusting events related to the Sevier Orogeny at this latitude, however the timing from initiation to culmination of tectonism and the rates of deformation are not well constrained. The thrust system consists of three plates from west to east, the Winters Pass/Pachalka allochthon, the Mesquite Pass allochthon, and the Keaney/Mollusk Mine allochthon (Fig. 1). Burchfiel and Davis (1971, 1988) suggested these three east-directed thrust plates accommodated a minimum of 65-80 km of movement during two distinct episodes; one in the latest Triassic and one in the Mid-to-Late Cretaceous. Walker et al. (1995) suggested the first thrusting event began during the Latest Jurassic along the Pachalka thrust (Fig. 2) based on U/Pb zircon ages from plutons interpreted to be pre-and post-kinematic, while dismissing a Cretaceous K/Ar age for a synkinematic diorite intrusion. Therefore, they concluded that initiation of the Clark Mountains thrust complex was either late in the history of the East Sierran thrust belt or early in the history of the Sevier thrust belt (~144 Ma). The second Cretaceous thrusting event has been constrained by U/Pb dating of the 100 Ma Delfonte volcanic suite, which sits folded in the footwall of the easternmost thrust in the Clark Mountain thrust complex, the Keaney/Mollusk Mine thrust (Fig. 2). The Keaney/Mollusk Mine thrust is in turn cut by plutons of the Teutonia batholith (~93 Ma) (Fleck et al., 1994; Miller et al., 1994; Walker et al., 1995). The best exposure of these crosscutting relationships is in the New York Mountains where the Sagamore Thrust (southern continuation of the Keaney/Mollusk Mine thrust) places Cambrian to Triassic rocks over 100 Ma metavolcanic Delfonte equivalents and is cut by the ~90 Ma Mid Hills monzogranite (U/Pb zircon by Smith et al., 2003).

While the timing of these two episodes of thrust faulting seem well-constrained, the presence of plutonic rocks with crosscutting relationships to thrust faults but lacking geochronological data affords an opportunity to better develop the sequence of deformation within the thrust complex as a whole. We report U/Pb zircon and $^{40}Ar/^{39}Ar$ amphibole, biotite, and K-feldspar ages from previously undated plutons within the Clark Mountains area with focus on the Ivanpah Mountains. These new timing constraints on magmatism, when coupled with field relationships, indicate thrust fault deformation did not evolve across the region from west to east as previously suggested (Burchfiel and Davis, 1988; Walker et al., 1995; Sheets, 1996). The proposed sequence of deformation is as follows: the earliest shortening within the region was emplacement of the Mesquite Pass allochthon prior to ~154 Ma. Deformation along the Pachalka Springs thrust to the west occurred next, but may be younger than ~144 Ma. The youngest deformation along the easternmost Keaney/Mollusk Mine thrust may be correlated to the south to the

Morning Star Mine thrust within the Ivanpah Pluton, representing a deeper crustal level of the deformation belt.

Samples and chronometry results

Clark Mountains

The Pachalka thrust on the western side of Clark Mountain (Fig. 2) represents the westernmost and structurally highest thrust fault in the Clark Mountains thrust complex (Burchfiel and Davis, 1988; Walker et al., 1995). It is interpreted to represent the earliest episode of thrust deformation at this latitude by Walker et al. (1995) who reported a Late Jurassic zircon age for a granitic pluton that is ductiley deformed above the Ediacaran-Cambrian Wood Canyon quartzite along the thrust fault. Sample GABE was collected from west of the trace of this east-vergent thrust from fractured, but undeformed granite (Fig. 2). Biotite was separated to obtain a cooling age for the hanging wall rocks, and yielded a discordant age spectrum with an initial increase in ages followed by a slight decrease then increase again over the final gas release. Ages range from 16-99 Ma, yielding a total gas age of 83.9 ± 0.5 Ma (Fig. 2). Omission of the first step because of its low age and high ^{36}Ar signal from the age calculation yields a total gas age of 87.5 Ma.

Sample Scott was collected from the Late Jurassic Pachalka pluton (Fig. 2) (Walker et al., 1995). This pluton is interpreted as post-kinematic with respect to the Pachalka thrust and therefore amphibole was separated from the sample to obtain thermal history information. Unfortunately, amphibole from sample Scott yielded unreliable ages due to excess argon (Fig. 2). The youngest age obtained in the analyses was 413

Ma, which is significantly older than the Late Jurassic zircon age for the intrusion reported by Walker et al. (1995).

Mohawk Hill

Sample JK05MH-2 was collected from a granitic stock in western Mohawk Hill (Fig. 3). This granite intrudes into the Cambrian Bonanza King limestone of the Mesquite Pass allochthon and exhibits an intermediate fine-to-coarse crystal size and sub-porphyritic texture indicating shallow crustal to hypabyssal emplacement. Since no previous geochronological data are available, biotite was separated from the sample to constrain the timing of emplacement of the stock and a minimum age for motion along the Mesquite Pass thrust. Biotite from the Mohawk Hill stock (JK05MH-2) gave a U-shaped age spectrum with a minimum age of 126.7 Ma and a total gas age of 135.4 ± .5 Ma (Fig. 3).

Mescal Range

Sample JK05MR-1 was collected from a diorite intrusion in the Mescal Range referred to as the "hornblende diorite 'breccia' pluton" (e.g. Sheets, 1996) that we refer to as the Mescal diorite (Fig. 4). This pluton intrudes into the Mesquite Pass thrust sheet and has been assigned an age of 200 Ma based on previous K/Ar geochronology and correlation of this intrusion with the Oro Wash granodiorite to the south (Sutter, 1968; Sheets, 1996). Porphyritic texture and the sharp nature and lack of skarn mineralization at the contact of the diorite roof with overlying limestone indicates shallow emplacement. Amphibole was separated for a constraint on the timing of emplacement/cooling. Amphibole from sample JK05MR-1 of the Mescal diorite pluton yielded a U-shaped age spectra with a minimum age of 157.4 Ma and a total gas age of 161.9 ± 0.7 Ma (Fig. 4).

Steps 9-13 yield an isochron with an age of 156 ± 3.8 Ma and a $^{40}Ar/^{36}Ar$ intercept of 460 ± 210.

Oro Wash and Ji granodiorites; eastern Ivanpah Mountains

The Oro Wash and Ji granodiorites are small stocks intruded within the Cambrian Bonanza King Formation to the east of the Ivanpah pluton (Fig. 5). These intrusions were sampled and analyzed to determine the timing of magmatism, constrain the timing of thrust faulting within the Bonanza King Formation, and test for significant offset along the planar eastern contact of the Ivanpah pluton and the southern portion of the Kokoweef syncline, as it remains uncertain whether this contact is intrusive or a fault. Ion probe U/Pb zircon analyses yield very similar results for the two intrusions indicating they were emplaced contemporaneously in the Late Jurassic (Fig. 6). The weighted mean ages of ~154 Ma are considered the best estimates of the emplacement age for these units as the Tera-Wasserburg intercept ages point to an upper intercept greater than the age of the Earth (Fig. 6).

Amphibole from both granodiorites yielded disturbed age spectra with total gas ages older than the U/Pb zircon ages indicating the presence of excess argon (Fig. 6). Biotite from both samples gave age spectra with initial low ages followed by a progressive increase into a plateau (Fig. 6). The Ji granodiorite (JK03IV-1) biotite yielded a plateau age of 150.0 ± 0.4 Ma and the Oro Wash (JK03IV-3) biotite yielded a plateau age of 154.1 ± 0.8 Ma (Fig. 6). K-feldspar from the Ji stock (JK03IV-1) yielded an age spectrum with ages ranging from ~40-159 Ma (Fig. 6).

Ivanpah pluton; Ivanpah Mountains

The majority of the central Ivanpah Mountains consists of the Ivanpah granite (Fig. 5). This pluton was originally interpreted to have intruded into an anticline paired with the Delfonte/Kokoweef syncline (Burchfiel and Davis, 1988). Walker et al. (1995) reported a Late Jurassic age for the granite and Fleck et al. (1994) determined the age of the Delfonte syncline to be younger than ~100 Ma. Therefore, the pluton intruded prior to faulting and folding related to the Keaney/Mollusk Mine thrust. The pluton is also cut by the ductile Morning Star Mine thrust (Fig. 5). This thrust fault is one in a system consisting of at least two other small strands of ductile deformation with poor exposures. These structures are described in Sheets (1996). The timing constraints on motion along the Morning Star Mine system are unclear aside from the structure being younger than the Ivanpah pluton. However, Sheets (1996) reported that the thrust truncates small diorite dikes near its southern extent in the Kewanee Hills region of the Ivanpah Mountains (Fig. 5). In this section $^{40}Ar/^{39}Ar$ age determinations are presented for several samples from the Ivanpah pluton and the diorite dike described by Sheets (1996).

Nine samples from the Ivanpah pluton (Figs 5, 7) were dated by the $^{40}Ar/^{39}Ar$ method. In the northeast region of the pluton samples JK03IV-8 and JK03IV-14 yielded biotite and muscovite ages of 146-149 Ma. K-feldspar from these samples yielded complex age spectra with ages ranging from ~80-145 Ma (Fig. 7). Both age spectra have a hump in the first 10% of the gas release with maximum ages of ~120 and ~129 Ma (JK03IV-14 and JK03IV-8, respectively). Following the hump, the ages steadily increase with final ages approaching those of the coexisting micas.

In the northwest part of the Ivanpah pluton, sample JK06IV-1 was collected from an amphibole-bearing phase near the contact with the Striped Hills pluton (Fig. 5). Amphibole yielded a moderately discordant age spectra with ages progressively decreasing throughout the analysis (Fig. 7). Ages range from 173-352 Ma, with a total gas age of 181.8 ± 0.8. Biotite gave a slightly U-shaped age spectrum with a minimum age of 132 Ma and a total gas age of 138.2 ± 0.4 Ma. K-feldspar yielded an age spectrum exhibiting highly discordant ages over the first 5% of the release due to excess argon followed by an increase in ages from ~80 Ma to ~120 Ma over the next 5%. The slope of the spectrum then decreases as the ages increase to ~140 Ma.

Three samples JK05IV-2, JK06IV-7, and JK06IV-11 were collected near the center of the (north-south) aerial extent of the Ivanpah pluton and west of the Morning Star Mine thrust (Fig. 5). Biotite from JK05IV-2 gave a slightly discordant age spectrum (Fig. 7) shaped similar to that reflecting the effects of recoil (e.g. Lo and Onsott, 1989). The total gas age for the sample is 122.1 ± 0.8 Ma with ages ranging from 111-129 Ma.

In the Kewanee Hills region of the southern Ivanpah Mountains (Fig. 5), dikes and lenses of diorite intrude into the Ivanpah granite. Biotite (JK05IV-4) yielded a slightly disturbed age spectrum with a total gase age of 103.4 ± 0.4 Ma (Figs. 5, 7).

Kessler Spring adamellite; southern Ivanpah Mountains

At the southern end of the Ivanpah Mountains near Cima Dome, the Ivanpah granite is intruded by the Kessler Spring Adamellite (Fig. 5). A sample from the Kessler Spring adamellite was collected and biotite and K-feldspar were analyzed to obtain thermal history information for this phase of the Teutonia batholith. Biotite yielded a plateau age of 79.8 ± 0.4 Ma with K-feldspar recording 78-80 Ma over the majority of the gas release (Fig. 8).

Timing constraints on magmatism and faulting

Clark Mountain, Mohawk Hill, the Mescal Range, and the Ivanpah Mountains all contain portions of the Clark Mountains thrust complex. The rocks making up these mountain ranges all consist of granitoid stocks and plutons that have crosscutting relationships with faults. Several of these intrusive rocks were sampled and dated by U/Pb zircon and/or $^{40}Ar/^{39}Ar$ chronometry to attempt to constrain the timing of magmatism and faulting. Below are brief descriptions of the geochronological and thermochronological data and discussions of the implications of these data and the field relationships of the rocks for constraining the timing of tectonism.

Clark Mountains

The shape of the biotite age spectrum obtained from sample Gabe is typically associated with recoil effects due to chloritization (e.g. Lo and Onstott, 1989). ^{36}Ar and ^{37}Ar release patterns indicate alteration and chloritization of the sample, which is also evident in thin-section. The high ^{37}Ar release in the fusion step may be an affect of sphene intergrowths within the biotite (Lo and Onstott, 1989). The 87.5 Ma age is considerably younger than the ~146 Ma crystallization age reported by Walker et al. (1995) and is consistent with biotite ages from the Halloran Hills to the west (DeWitt et al., 1984). Therefore, other than providing a minimum age for the timing of thrust deformation, the Late Cretaceous age likely reflects thermal resetting due to extensive ~90 Ma magmatism in the region.

Mohawk Hill

The hypabyssal nature of the Mohawk Hill intrusion indicates the biotite cooling age may approximate the timing of pluton emplacement, which results in a minimum age of ~126 Ma (when taking the minimum age in the age spectrum as a maximum age for the sample) for Mesquite Pass allochthon emplacement. However, field relations and data from the Mescal Range to the south of Mohawk Hill offer a better constraint (discussed below).

Mescal Range

The amphibole age from the Mescal diorite is similar to that of the Oro Wash and Ji granodiorites in the eastern Ivanpah Mountains (discussed below) and thus supports previous correlations between these units based on petrologic data. Additionally, this new age (~156 Ma) indicates the previously assigned age was overestimated by nearly 50 m.y. Therefore, the tectonic models (i.e. Burchfiel and Davis, 1988; Sheets, 1996) suggesting the Mesquite Pass thrust sheet was active prior to 190 Ma, can be revised with a new minimum age for emplacement of the Mesquite Pass allochthon of ~152 Ma (156 ± 3.8 Ma isochron age).

Oro Wash and Ji granodiorites, eastern Ivanpah Mountains

The Oro Wash and Ji granodiorites yielded similar chronometry results. However, considering the similarity in zircon age, intrusion size (aerial exposure) and stratigraphic level of intrusion, it is unexpected for the biotite ages of Ji and Oro Wash to be different by 4 m.y. Steps 11-15 define the plateau for JK03IV-3 (Oro Wash), however, steps 11-14 define an isochron with an age of 152.9 ± 2.3 Ma and a $^{40}Ar/^{36}Ar$ intercept of 511 ± 250 (MSWD = 0.60) indicating excess argon in the sample. This age coincides within uncertainty with the plateau age of sample JK03IV-1 (Ji). Additionally, the total gas ages for biotite from Ji and Oro Wash are in agreement at 149.1 ± 0.4 Ma and 150.7 ± 0.6 Ma, respectively. Therefore it is evident these two granodiorite stocks likely intruded at the same time and have the same subsequent thermal histories.

The high temperature steps of the Ji K-feldspar age spectrum consist of ages greater than the biotite ages, but within uncertainty of the U/Pb zircon ages. Isochron regressions of these steps to test for large domain excess argon (e.g. Foster et al., 1990) did not yield $^{40}Ar/^{36}Ar$ values greater than atmosphere, so these older ages (with respect to coexisting biotite) may reflect a high closure temperature for the large domains. MDD modeling (Lovera et al., 1989; 1991) was attempted, however satisfactory reproduction of the arrhenius data, domain distribution plot, and the shape of the sample age spectrum was not obtained. Regression of the low temperature linear array of the sample arrhenius data indicates an activation energy of E = 51.2 ± 1.5 kcal/mol, however a hump in the accompanying domain distribution plot indicates this value is likely an underestimate. Although acceptable model fits were not obtained for the complete data, satisfactory reproductions of the high temperature portion of the age spectrum yield thermal histories indicating large domain closure temperatures of 300-350° C. This result is not compatible with age discrepancy between the K-feldspar and the biotite mentioned above. Additionaly, the poor model reproductions of the initial steps of the age spectrum may be a result of the sample violating the monotonic cooling assumption inherent in the MDD model. It is possible the increase in ages over the first ~10% of the gas release is a result of reheating due to emplacement of other younger magma bodies (i.e. Teutonia batholith, discussed below) rather than monotonic cooling following emplacement.

The ages determined for the Ji and Oro Wash granodiorites also place timing constraints on faulting in the eastern Ivanpah Mountains. Mapping around the Oro Wash granodiorite indicates the intrusion cuts thrust faults within the Cambrian Bonanza King Formation, and therefore this deformation is older than ~154 Ma and may correlate to deformation associated to emplacement of the Mesquite Pass thrust sheet in the Mescal Range (discussed above). Along the western edge of the Ji granodiorite a deep brown gouge with slickenlines locally separates the intrusion from the Bonanza King Formation, indicating the presence of a fault. The contact between these units, however, is dominated by a calc-silicate interval typical of skarn development along an intrusive contact, but the presence of gouge and slickenlines indicates some shearing along this contact after intrusion (post ~154 Ma).

Ivanpah pluton, Ivanpah Mountains

The muscovite and biotite ages from the northeastern Ivanpah pluton are consistent with the 147 ± 7 Ma U/Pb zircon age presented by Walker et al. (1995). The similarity between biotite and muscovite ages for these two samples is consistent with rapid cooling of this portion of the pluton through ~300°C upon intrusion into overlying Paleozoic platform sediments (Burchfiel and Davis, 1988; Walker et al., 1995). The coexisting K-feldspar age gradients may indicate relatively slow cooling following rapid cooling through mica closure upon intrusion.

All the amphibole ages from JK06IV-1 in the northwest Ivanpah pluton are older than the U/Pb zircon age (147 ± 7 Ma) reported by Walker et al. (1995), indicating either the effects of excess argon in the sample resulting in erroneous ages, or this sample represents a small older intrusion of which, the amphibole was not thermally disturbed by emplacement of the Ivanpah granite. The biotite and K-feldspar results are consistent with the 142 ± 11 Ma U/Pb zircon age reported by Walker et al. (1995) for the Striped Mountain pluton. Together these data may indicate the Striped Mountain pluton is slightly younger than the eastern Ivanpah pluton and the ages recorded from sample JK06IV-1 record Early Jurassic emplacement (amphibole age) followed by Early Cretaceous reheating and subsequent cooling (biotite, K-feldspar) at ~138 Ma.

The JK05IV-2 biotite age (~122 Ma) from the central Ivanpah pluton is consistent with the oldest ages recorded in the high-temperature steps of K-feldspar from JK06IV-7 and JK06IV-11 (Fig. 7). This age is approximately 20 m.y. younger than the timing of initial closure recorded in Ivanpah micas and K-feldspar to the north (discussed above).

Since these samples are all within 2-3 km map distance from a pluton margin, it seems unlikely the discrepancy in ages can be satisfactorily explained by slow cooling. An alternative explanation may be that these samples represent a previously unrecognized Early Cretaceous magmatic event that contributed mass to the western portion of the composite Ivanpah pluton. Emplacement of this portion of the pluton may have occurred at ~122 Ma (approximated by JK05IV-2 biotite), which corresponds with the age of the humps in the eastern Ivanpah K-feldspar age spectra (JK03IV-14, 8; Fig. 7). Hump-shaped age spectra from K-feldspars are typically attributed to thermal disturbances that dominantly only affect smaller diffusion domains (Warnock and van de Kamp, 1999; Harrison et al., 2004), therefore the similarity between western Ivanpah biotite/K-feldspar ages and eastern Ivanpah K-feldspar humps may indicate the presence of multiple intrusions making up the Ivanpah pluton.

The ~122 Ma biotite and K-feldspar ages may also indicate the timing of initial motion along the Morning Star thrust. This interpretation may explain the 5 m.y. discrepancy between oldest ages recorded by the three western Ivanpah samples just discussed and sample JK06IV-12 from the southeastern Ivanpah pluton (Figs 5, 7). Walker et al. (1995) report and dismiss 120 and 126 Ma hornblende ages from a diorite intrusion along the Pachalka thrust as thermally disturbed, while neglecting to explain a 130 Ma minimum age for the unit. It is possible the similarity in these ages and their spatial relationships to thrust faults is geologically significant. Alternatively, sample JK06IV-12 may represent yet another small intrusion making up the Ivanpah pluton. Mapping along the eastern contact of the Ivanpah pluton indicates several northwest striking sheet-like units may be distinguished based on abundance of mafic minerals, color of feldspar crystals, and overall crystal size, however more detailed and aerially extensive mapping is required to confirm this postulation.

Biotite from the Kewanee Hills diorite (sample JK05IV-4) yielded a slightly discordant age spectrum similar to those reflecting recoil effects (Lo and Onstott, 1989) and a total gas age of 103.4 ± 0.4 Ma (Figs. 5, 7). This age is slightly older than that reported by Fleck et al. (1994) for the Delfonte volcanic suite to the north in the eastern Mescal Range (Fig. 5).

Rhyolite dikes interpreted to be feeders to the Delfonte suite outcrop discontinuously along the eastern margin of the Ivanpah pluton and therefore, the small diorite intrusions in the Kewanee Hills may be related to the magmatism leading to eruption the Delfonte sequence. Small diorite stocks have also been observed to the west in the Ivanpah pluton (southwest of samples JK06IV-7, 11 in figure 5) and are likely related to the same magmatic event.

The 103 Ma biotite age from the diorite may also have implications for timing of motion along the Morning Star Mine thrust. Sheets (1996) demonstrated the Morning Star Mine thrust truncated a diorite unit referred to as the Morning Star dike. If all dioritic intrusions in the vicinity of the Kewanee Hills are coeval and can be approximated by the biotite cooling age, then deformation along the Morning Star thrust post-dates 103 Ma. The similarity of this age with the Delfonte volcanic sequence indicates possible correlation of the near surface Keaney-Mollusk Mine thrust in the Mescal Range (Fig. 4) to the deeper seated Morning Star thrust as the two structures were likely active contemporaneously.

In the southwest Ivanpah Mountains sample JK06IV-20 yielded discordant biotite and K-feldspar ages (Figs. 5, 7). K-feldspar ages are greater than those from biotite indicating either higher retentivity than the coexisting mica or excess argon. The disturbed form of the age spectra indicates excess argon is the more likely explanation. The slightly disturbed age spectrum from the biotite gave a ~91 Ma total gas age. This age is consistent with ages reported for the widespread Teutonia Batholith (Beckerman et al., 1982; Anderson et al., 1992; Barth et al., 2004; Wells et al., 2005) and thus likely reflects thermal resetting due to this major magmatic event.

<u>Kessler Spring adamellite, southern Ivanpah Mountains</u>

Barth et al. (2004) report a U/Pb zircon age of 82.3 ± 1.6 Ma for the Kessler Spring Adamellite and shallow emplacement into the crust has been inferred by Beckerman et al. (1982) and Anderson et al. (1992). The ages reported here indicate that cooling through biotite and K-feldspar closure occurred very shortly after emplacement, which is consistent with rapid cooling due to emplacement into the upper crust. MDD modeling of the K-feldspar age spectrum and gas release indicates the Kessler Spring Adamellite had cooled through ~200°C by 75 Ma followed by a transition to very slow cooling at ~72 Ma. Therefore, the Ivanpah Mountains area was in the upper crust prior to the onset of widespread extension through the east Mojave Desert region in the Late Cretaceous (e.g., Wells et al., 2005).

Discussion

The new U/Pb and $^{40}Ar/^{39}Ar$ chronometry data presented above may be used to constrain the temporal evolution of magmatism and deformation within the Clark Mountains thrust complex. The Mescal diorite, Oro Wash granodiorite, and Ji granodiorite appear to have all been emplaced contemporaneously at ~154 Ma. The Mescal diorite intruded into the Mesquite Pass allochthon, and the Oro Wash and Ji stocks intrude internally thrusted Cambrian Bonanza King Formation dolostones indicating this deformation is all older than the ~154 Ma emplacement age. This early deformation may be related to thrust fault deformation documented to the south in the Clipper Mountains at ~160 Ma (Howard et al., 1995), however it can also be older. A minimum age of ~154 Ma for imbrication of Cambrian rocks within the Mesquite Pass allochthon makes this the oldest event in the Clark Mountains complex.

To the west of the Mesquite Pass thrust, is the Mescal thrust (Fig. 4), which places a thick sequence of Cambrian to Neoproterozoic rocks above the imbricated Cambrian sequence (Burchfiel and Davis, 1988). The Mescal thrust carries the Striped Mountain syncline, which Burchfiel and Davis (1988) attribute to deformation along the Winters Pass/Pachalka thrust further to the west. Therefore, imbrication involving the Mesquite Pass thrust occurred by ~154 Ma, after which deformation jumped westward developing the Winters Pass/Pachalka thrust at ~144 Ma (Walker et al., 1995) and producing the Striped Mountain syncline. Then the Mesquite Pass allochthon was evidently partially reactivated along the Mescal thrust. As mentioned above, the Pachalka thrust may be younger (~120 Ma), which would require several thrust faults cut by the Pachalka pluton to be related to an older deformation event (i.e. initial Mesquite Pass?), however this is highly speculative.

To the south of the Clark Mountains area in the Ivanpah Mountains, the Ivanpah pluton was emplaced at ~147 Ma (Walker et al., 1995) and rapidly cooled through muscovite and biotite closure at its eastern contact. Ivanpah muscovite ages reported here (JK03IV-14) indicate a minimum age of ~149 Ma for emplacement, thus requiring a revision to the Walker et al. (1995) emplacement age. Even so, intrusion of the Ivanpah pluton appears to have followed emplacement of the Oro Wash and Ji granodiorites by a few million years. Sheets (1996) determined an emplacement pressure of ~0.2 GPa for the Oro Wash granodiorite, and ~0.6 GPa for the Ivanpah pluton indicating that if the two were emplaced relatively contemporaneous, a vertical throw equivalent to ~13 km (~0.4 GPa) is required to be accommodated along a structure between these units. Gouge formation and slickenlines along the eastern contact of the pluton indicate some thrust deformation occurred following emplacement, however the limited presence of fault rock and prevalent calc-silicate skarn outcrops indicates a significant amount of offset was unlikely accomplished.

The Morning Star Mine thrust cuts the Ivanpah pluton and may have a speculative Early Cretaceous initiation, based on K-feldspar $^{40}Ar/^{39}Ar$ ages. However, it is likely the thrust was active after 100 Ma during formation of the Delfonte and Kokoweef synclines below the Keaney/Mollusk Mine thrust. This interpretation is based on the ~103 Ma biotite age from diorite that is truncated by the thrust in the Kewanee Hills. Therefore, the Morning Star thrust may be a deeper-seated correlative to the Keaney/Mollusk Mine thrust. Although the depth of the Morning Star thrust is constrained to the mid-to-upper crust by the ages recorded in surrounding Ivanpah K-feldspar (Fig. 7) the magmatism represented by the prekinematic diorites in the Kewanee Hills may have provided the heat to accommodate the >450°C deformation temperatures inferred by Sheets (1996).

The sequence of deformation and magmatism presented here indicates that the Clark Mountains thrust complex contains a record of episodic deformation spanning the Middle Jurassic to the late Early Cretaceous. The youngest magmatism yet recorded in the area is the emplacement of the Kessler Spring adamellite. The thermal history recorded for this intrusion indicates the Ivanpah Mountains area was cooled to upper-crustal temperatures prior to the onset of Late Cretaceous extension throughout the east Mojave Desert region (Wells et al., 2005).

Figure captions

Figure 1. Simplified map of major thrust sheets in the Clark Mountain area. (from Walker et al., 1995). KRD = Kingston Range detachment, SM = Spring Mountains, MM = Mesquite Mountains, CM = Clark Mountain, IM = Ivanpah Mountains.

Figure 2. a. Simplified map of the western Clark Mountain showing the Pachalka thrust and the Pachalka pluton (from Burchfiel and Davis, 1988; Walker et al., 1995; Miller et al., 2003). Dots indicate thermochronology sample locations. b. Age spectra obtained for biotite and amphibole from the Pachalka thrust hanging wall and Pachalka pluton, respectively.

Figure 3. a. Simplified map of Mohawk Hill showing the Mesquite Pass thrust, Keaney thrust, and granite stock intruding into the Mesquite Pass sheet (from Burchfiel and Davis, 1988; Miller et al., 2003). Dot indicates thermochronology sample location. b. Age spectrum obtained from biotite separated from the Mohawk Hill granite.

Figure 4. a. Simplified map of the Mescal Range (from Walker et al., 1995; Miller et al., 2003) showing the Mesquite Pass thrust and a small diorite pluton that intrudes into the thrust sheet. Also shown is the Keaney-Mollusk Mine thrust cutting the Delfonte volcanic rocks (north) and also cutting a small outcrop of Ivanpah granite (south). Dot indicates thermochronology sample location. b. Age spectrum and isochron obtained from amphibole from the Mescal diorite that intrudes into the Mesquite Pass thrust sheet.

Figure 5. Simplified map of the Ivanpah Mountains (from Burchfiel and Davis, 1988; Miller et al., 2003). The majority of the range consists of the Jurassic Ivanpah granite, which is cut by the Morning Star Mine thrust. East of the Ivanpah pluton, two

granodiorite stocks- Oro Wash and Ji- intrude into lower Paleozoic rocks. Labelled dots indicate thermochronology sample locations.

Figure 6. U/Pb zircon and $^{40}Ar/^{39}Ar$ chronometry results for sample a. JK03IV-1 collected from the Ji granodiorite and b. JK03IV-3 from the Oro Wash granodiorite in the eastern Ivanpah Mountains.

Figure 7. $^{40}Ar/^{39}Ar$ age spectra for samples from the Ivanpah Pluton of the Ivanpah Mountains. Spectra are spatially organized consistent with the sample locations depicted in figure 5.

Figure 8. a. $^{40}Ar/^{39}Ar$ spectra for biotite and K-feldspar from the Kessler Spring Adamellite sample JK06KS-1. b. Isochron plot for biotite.

Figure 9. K-feldspar MDD model results for sample JK06KS-1. a. Arrhenius plot. b. Domain distribution plot. c. Age spectra diagram. d. Thermal histories.

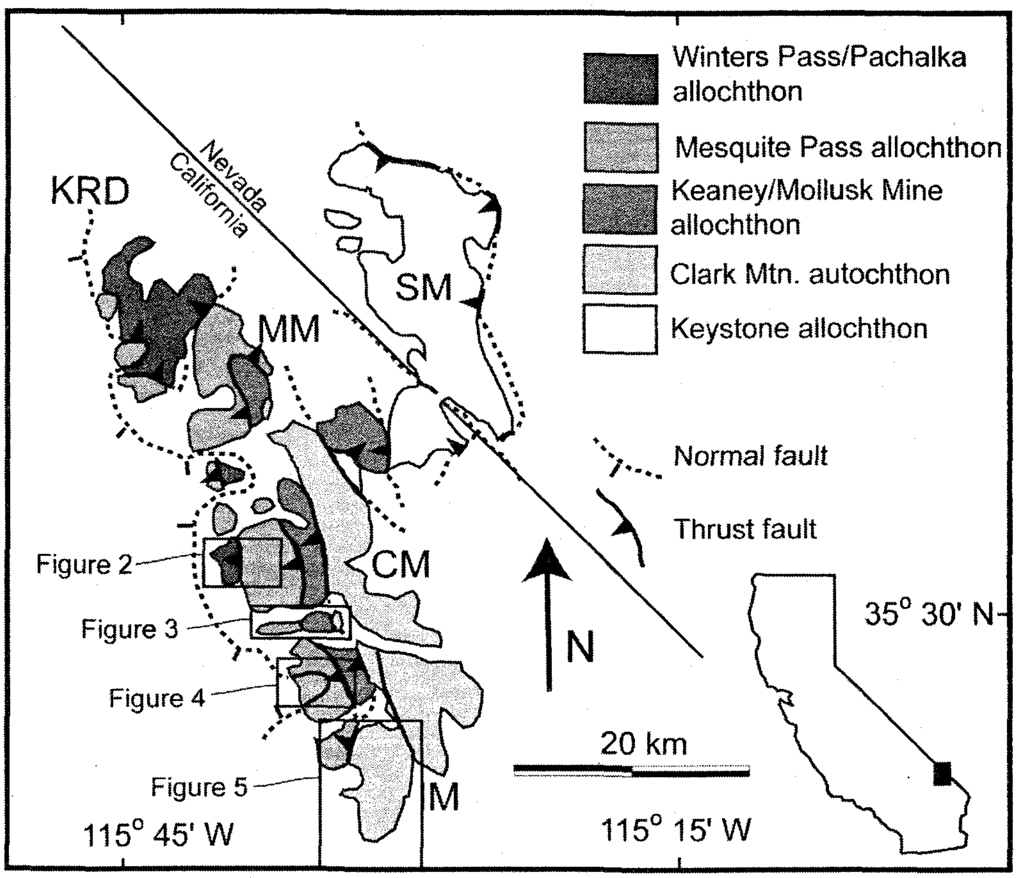
Winters Pass/Pachalka allochthon
Mesquite Pass allochthon
Keaney/Mollusk Mine allochthon
Clark Mtn. autochthon
Keystone allochthon
Nevada
California
KRD
MM
SM
CM
M
Figure 2
Figure 3
Figure 4
Figure 5
Normal fault
Thrust fault
N
20 km
35° 30' N
115° 45' W
115° 15' W

Figure 1

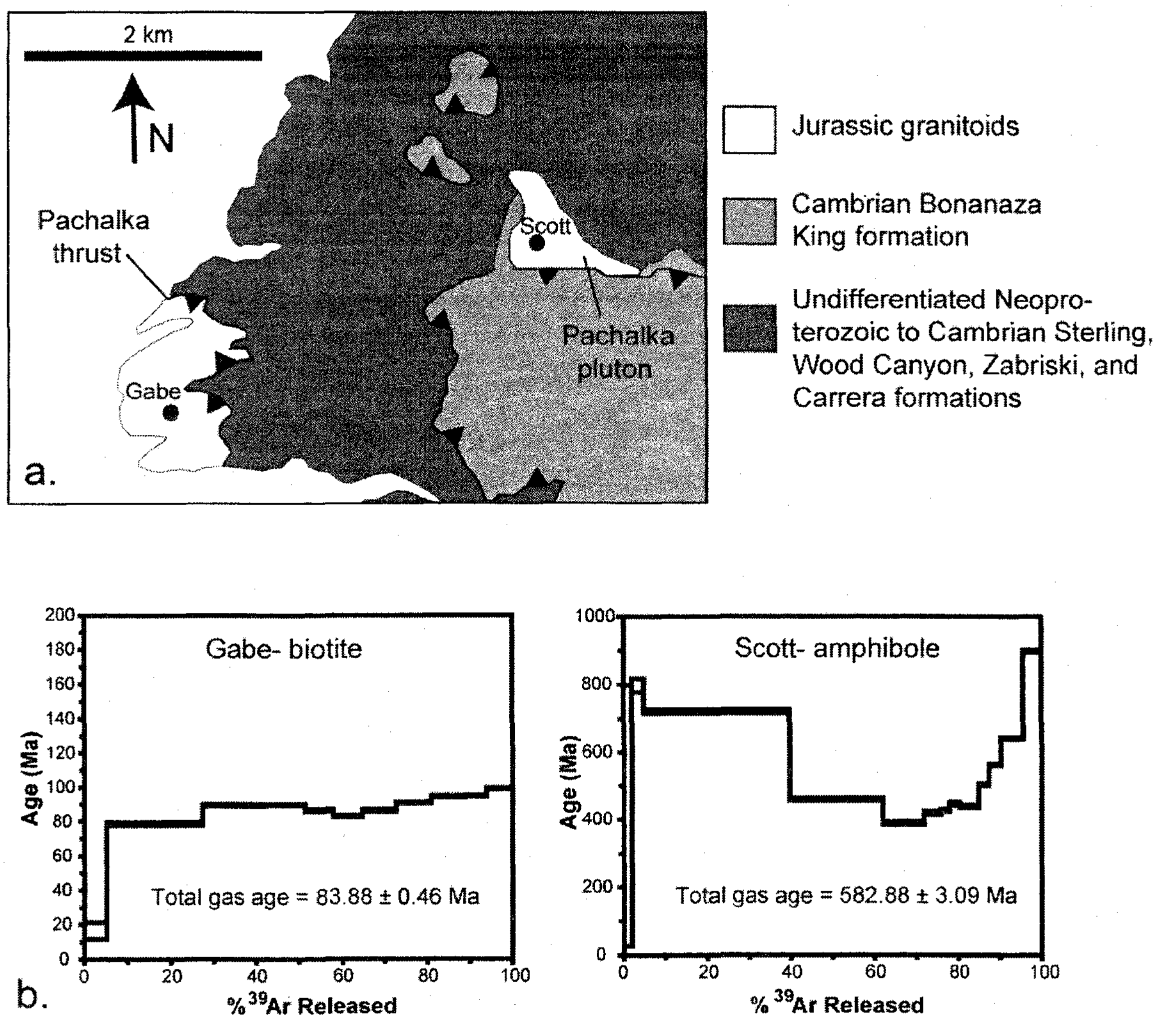
2 km
N
Pachalka thrust
Scott
Gabe
Pachalka pluton
a.
Jurassic granitoids
Cambrian Bonanaza King formation
Undifferentiated Neoproterozoic to Cambrian Sterling, Wood Canyon, Zabriski, and Carrera formations
Gabe- biotite
Total gas age = 83.88 ± 0.46 Ma
Age (Ma)
% ^{39}Ar Released
Scott- amphibole
Total gas age = 582.88 ± 3.09 Ma
b.

Figure 2

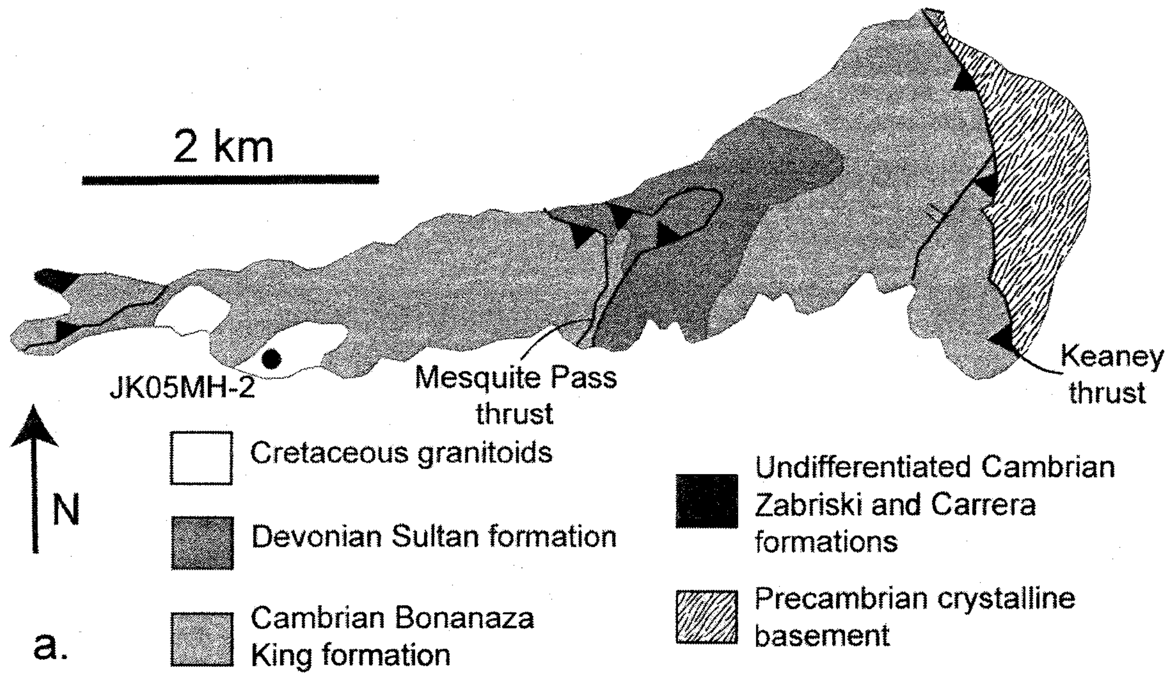
2 km
JK05MH-2
Mesquite Pass thrust
Keaney thrust
N
Cretaceous granitoids
Devonian Sultan formation
Cambrian Bonanaza King formation
Undifferentiated Cambrian Zabriski and Carrera formations
Precambrian crystalline basement

a.

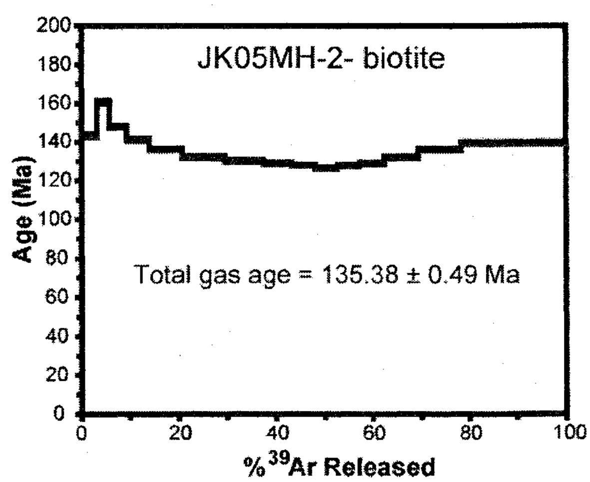
JK05MH-2- biotite
Total gas age = 135.38 ± 0.49 Ma
Age (Ma)
0
20
40
60
80
100
120
140
160
180
200
0
20
40
60
80
100
%39Ar Released

b.

Figure 3

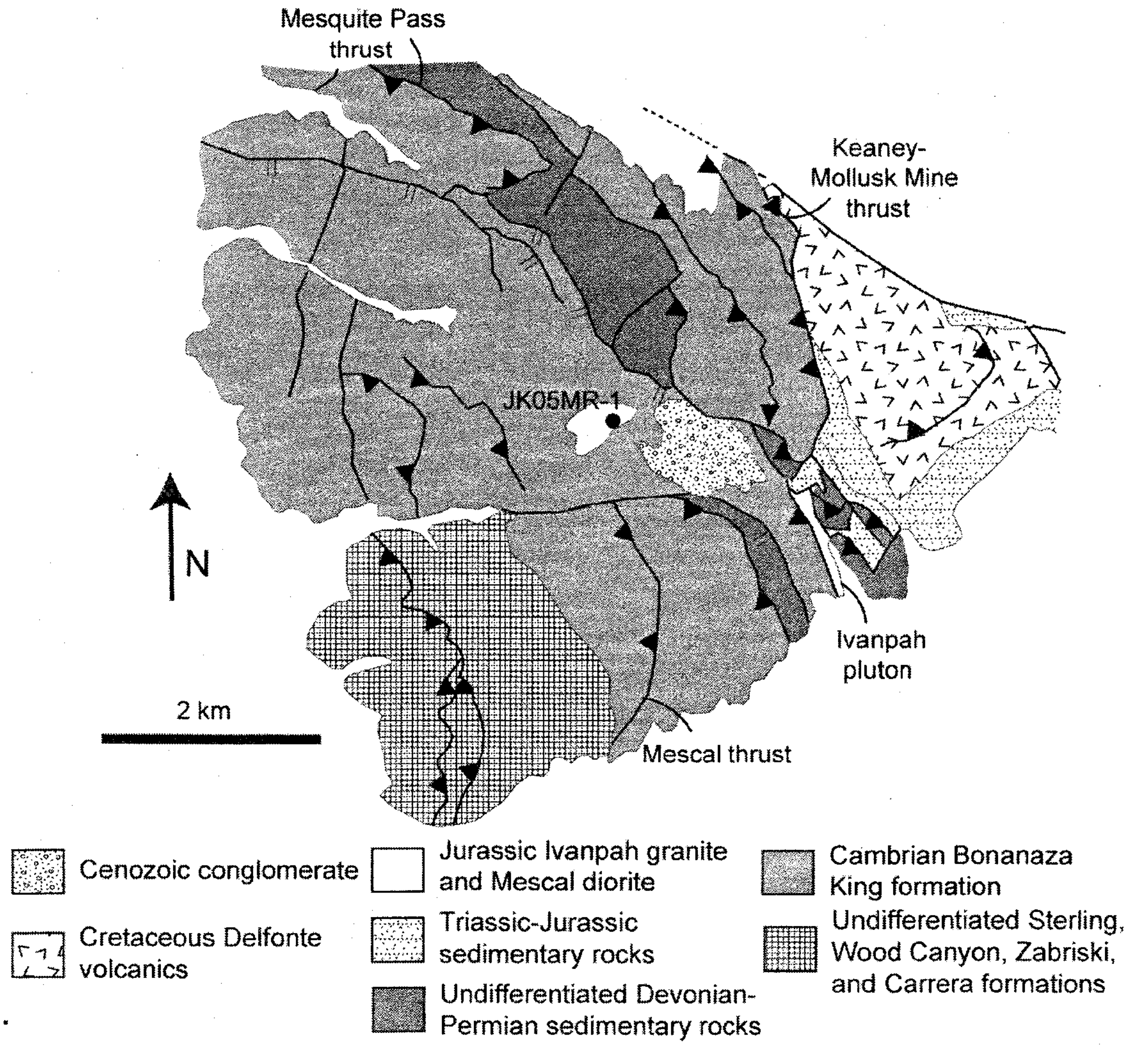
Mesquite Pass thrust
Keaney-Mollusk Mine thrust
JK05MR-1
N
2 km
Ivanpah pluton
Mescal thrust
Cenozoic conglomerate
Cretaceous Delfonte volcanics
Jurassic Ivanpah granite and Mescal diorite
Triassic-Jurassic sedimentary rocks
Undifferentiated Devonian-Permian sedimentary rocks
Cambrian Bonanaza King formation
Undifferentiated Sterling, Wood Canyon, Zabriski, and Carrera formations

a.

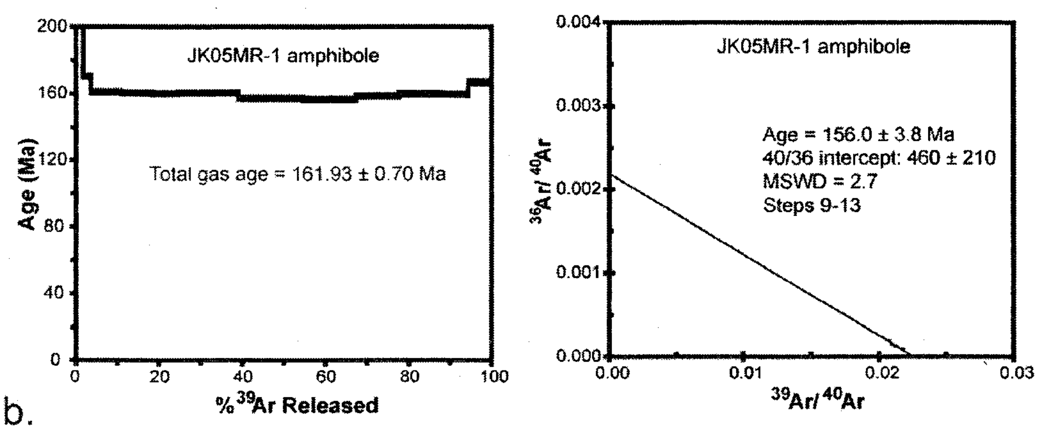
JK05MR-1 amphibole
Total gas age = 161.93 ± 0.70 Ma
Age (Ma)
% 39Ar Released
JK05MR-1 amphibole
Age = 156.0 ± 3.8 Ma
40/36 intercept: 460 ± 210
MSWD = 2.7
Steps 9-13
36Ar/ 40Ar
39Ar/ 40Ar

b.

Figure 4

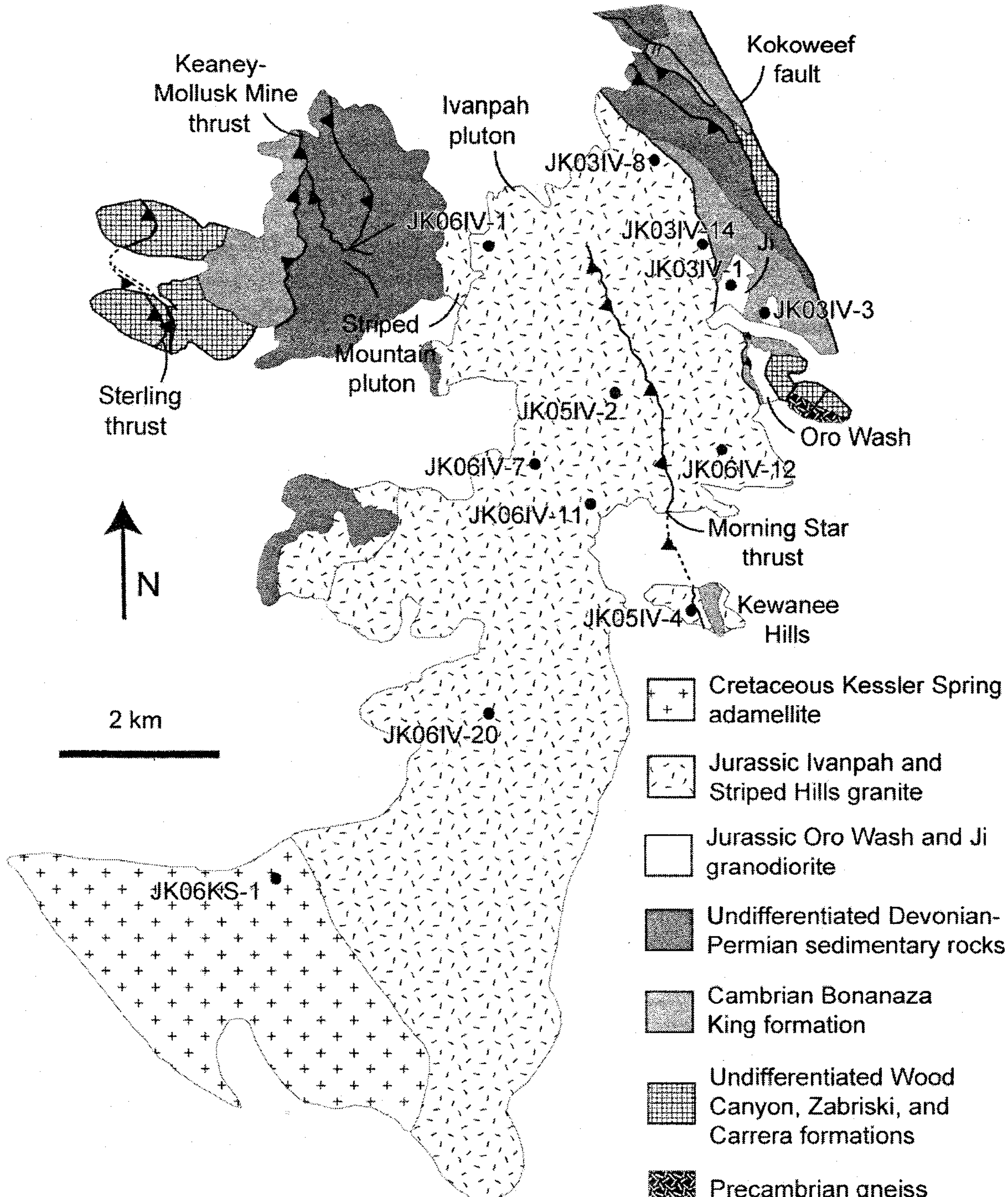
Kokoweef
fault
Keaney-
Mollusk Mine
thrust
Ivanpah
pluton
JK03IV-8
JK06IV-1
JK03IV-14
Ji
JK03IV-1
JK03IV-3
Striped
Mountain
pluton
Sterling
thrust
JK05IV-2
Oro Wash
JK06IV-7
JK06IV-12
JK06IV-11
Morning Star
thrust
N
Kewanee
Hills
JK05IV-4
2 km
JK06IV-20
JK06KS-1
Cretaceous Kessler Spring
adamellite
Jurassic Ivanpah and
Striped Hills granite
Jurassic Oro Wash and Ji
granodiorite
Undifferentiated Devonian-
Permian sedimentary rocks
Cambrian Bonanaza
King formation
Undifferentiated Wood
Canyon, Zabriski, and
Carrera formations
Precambrian gneiss

Figure 5

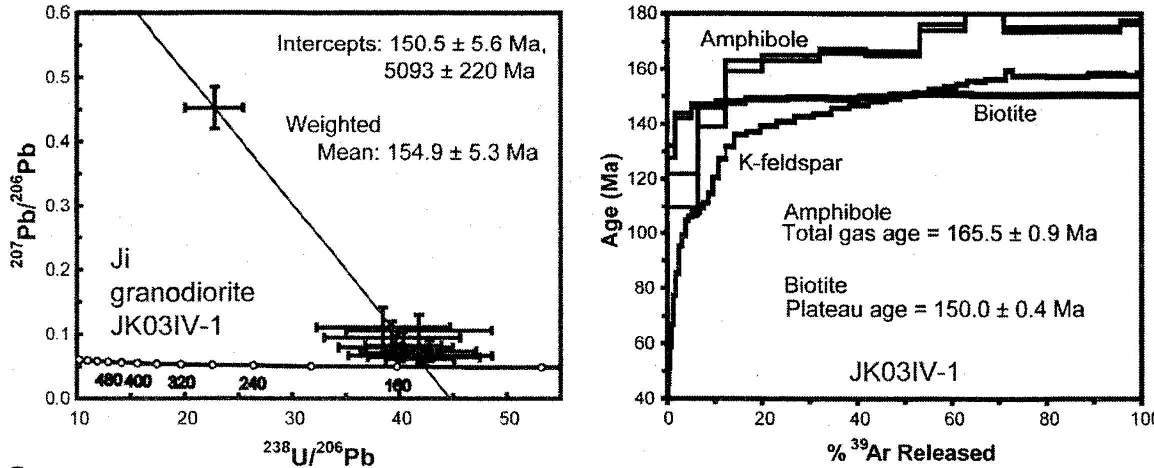
Intercepts: 150.5 ± 5.6 Ma,
5093 ± 220 Ma
Weighted
Mean: 154.9 ± 5.3 Ma
Ji
granodiorite
JK03IV-1
207Pb/206Pb
238U/206Pb
480 400 320 240 160
Amphibole
Biotite
K-feldspar
Amphibole
Total gas age = 165.5 ± 0.9 Ma
Biotite
Plateau age = 150.0 ± 0.4 Ma
JK03IV-1
Age (Ma)
% 39Ar Released

a.

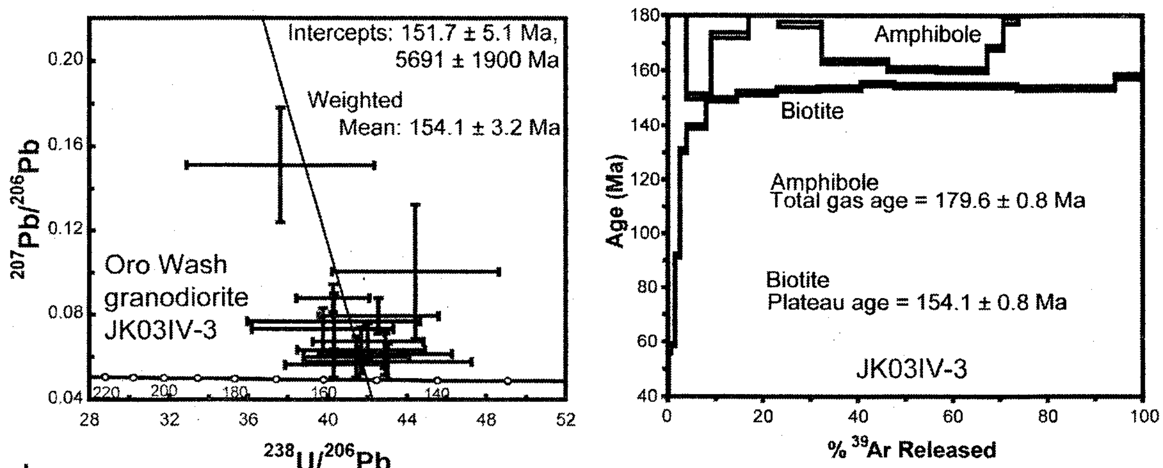
Intercepts: 151.7 ± 5.1 Ma,
5691 ± 1900 Ma
Weighted
Mean: 154.1 ± 3.2 Ma
Oro Wash
granodiorite
JK03IV-3
207Pb/206Pb
238U/206Pb
220 200 180 160 140
Amphibole
Biotite
Amphibole
Total gas age = 179.6 ± 0.8 Ma
Biotite
Plateau age = 154.1 ± 0.8 Ma
JK03IV-3
Age (Ma)
% 39Ar Released

b.

Figure 6

Figure 7

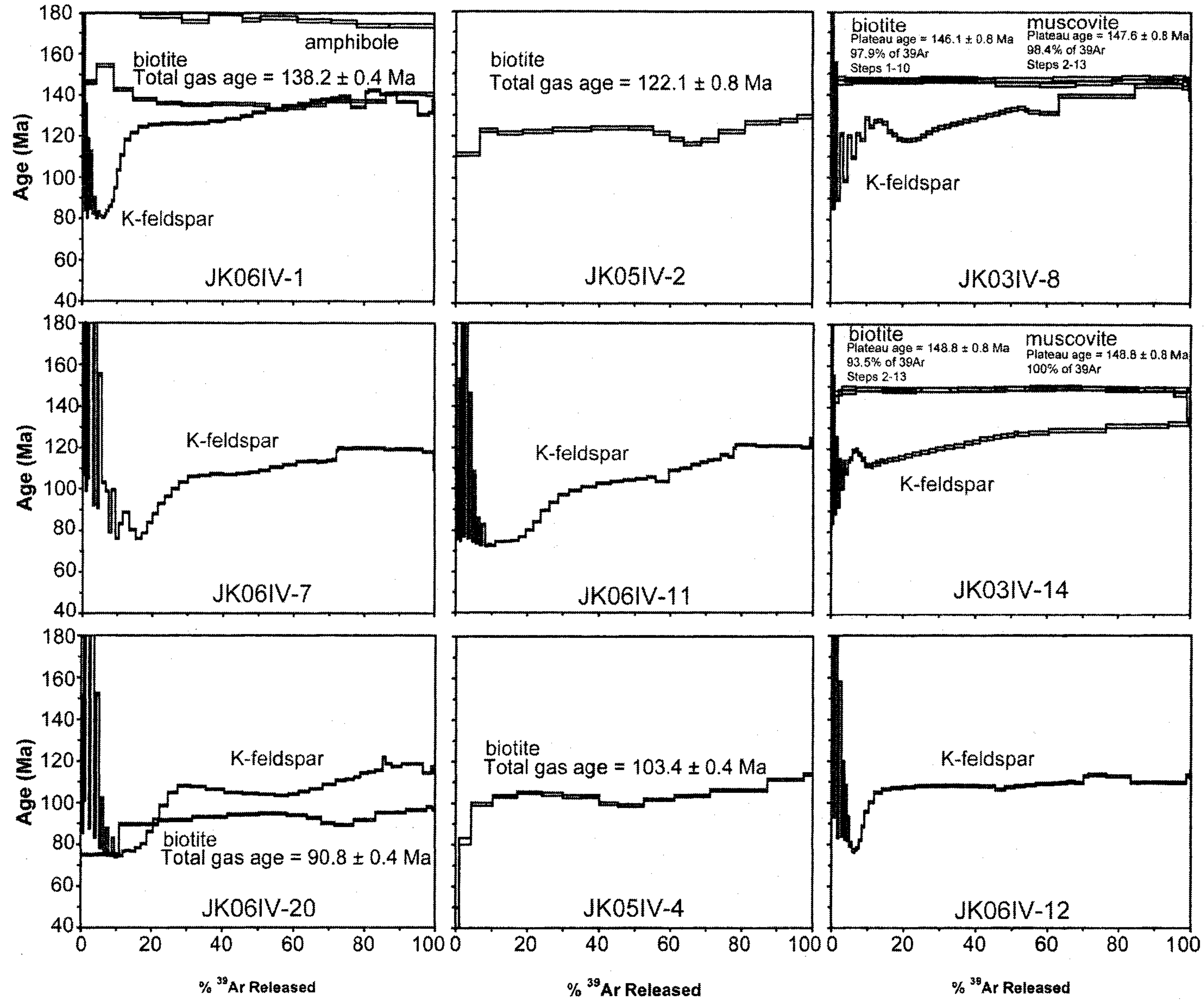
amphibole
biotite
Total gas age = 138.2 ± 0.4 Ma
K-feldspar
JK06IV-1
biotite
Total gas age = 122.1 ± 0.8 Ma
JK05IV-2
biotite
Plateau age = 146.1 ± 0.8 Ma
97.9% of 39Ar
Steps 1-10
muscovite
Plateau age = 147.6 ± 0.8 Ma
98.4% of 39Ar
Steps 2-13
K-feldspar
JK03IV-8
K-feldspar
JK06IV-7
K-feldspar
JK06IV-11
biotite
Plateau age = 148.8 ± 0.8 Ma
93.5% of 39Ar
Steps 2-13
muscovite
Plateau age = 148.8 ± 0.8 Ma
100% of 39Ar
K-feldspar
JK03IV-14
K-feldspar
biotite
Total gas age = 90.8 ± 0.4 Ma
JK06IV-20
biotite
Total gas age = 103.4 ± 0.4 Ma
JK05IV-4
K-feldspar
JK06IV-12
Age (Ma)
% 39Ar Released

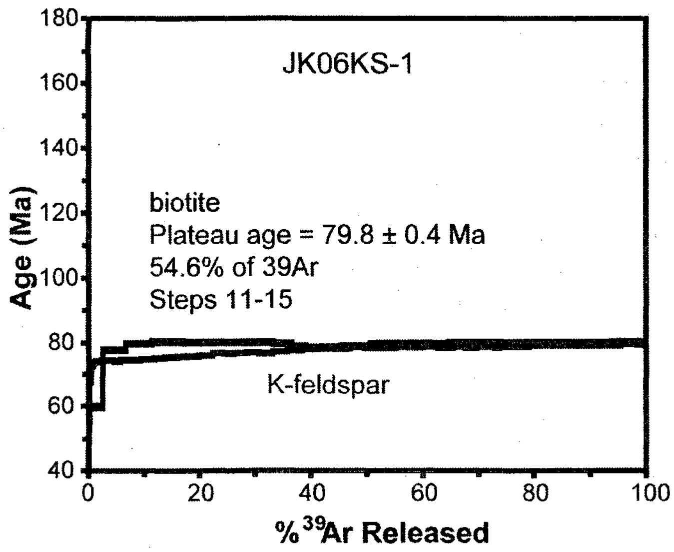
JK06KS-1
biotite
Plateau age = 79.8 ± 0.4 Ma
54.6% of 39Ar
Steps 11-15
K-feldspar
Age (Ma)
% 39Ar Released

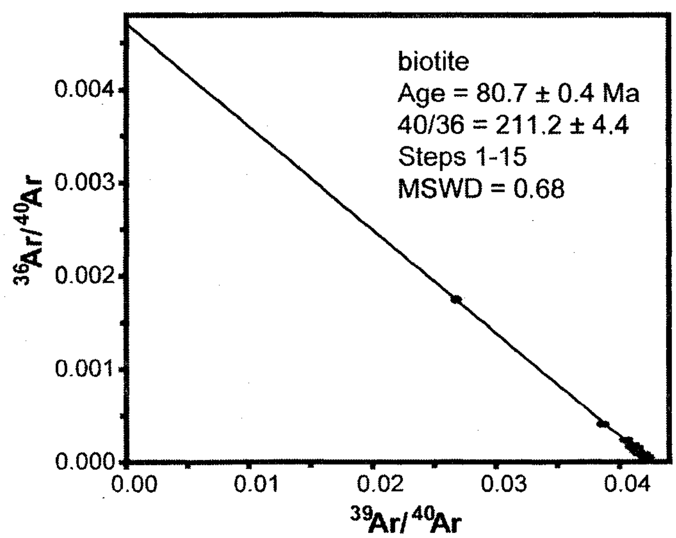
biotite
Age = 80.7 ± 0.4 Ma
40/36 = 211.2 ± 4.4
Steps 1-15
MSWD = 0.68
36Ar/40Ar
39Ar/40Ar

Figure 8

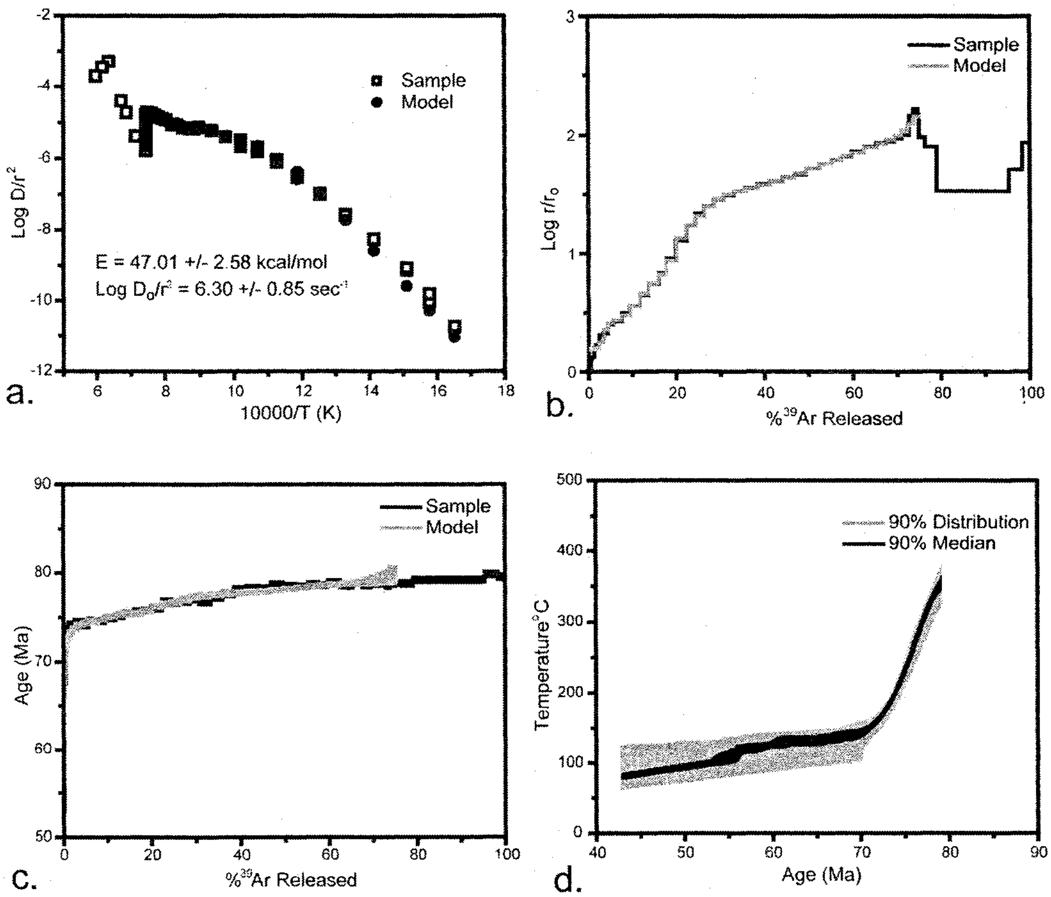
Sample
Model
E = 47.01 +/- 2.58 kcal/mol
Log D_o/r^2 = 6.30 +/- 0.85 sec^{-1}
Log D/r^2
10000/T (K)
a.
Sample
Model
Log r/r_o
%^{39}Ar Released
b.
Sample
Model
Age (Ma)
%^{39}Ar Released
c.
90% Distribution
90% Median
Temperature°C
Age (Ma)
d.

Figure 9

References

Anderson, J.L., Barth, A.P., Young, E.D., Davis, M.J., Farber, D., Hayes, E.M., and Johnson, K.A., 1992, Plutonism across the Tujunga-North American terrane boundary: A middle to upper crustal view of two juxtaposed arcs, in Bartholomew, M. J., Hyndman, D. W., Mogk, D. W., and Mason, R., editors, Characterization and Comparison of Ancient and Mesozoic Continental Margins - Proceedings of the 8th International Conference on Basement Tectonics, Kluwer Academic Publishers, Dordrecht, Netherlands, p. 205-230.

Barth, A.P., Wooden, J.L., Jacobson, C.E., and Probst, K., 2004, U-Pb geochronology and geochemistry of the McCoy Mountains Formation, southeastern California: A Cretaceous retroarc foreland basin: Geological Society of America Bulletin, v. 116, p. 142-153.

Beckerman, G.M., Robinson, J.P., and Anderson, J.L., 1982, The Teutonia batholith; A large intrusive complex of Jurassic and Cretaceous age in the eastern Mojave Desert, California. *in* Frost, E.G., and Martin, D.M., eds., Mesozoic-Cenozoic Tectonic Evolution of the Colorado River Region, California, Arizona, and Nevada: San Diego, California, Cordilleran Publishers, p. 205-220.

Burchfiel, B.C., and Davis, G.A., 1971, Clark Mountain thrust complex in the Cordillera of southeastern California: Geologic summary and field trip guide, *in* Elders, W.A., ed., Geological excursions in southern California: Riverside, California, University of California-Riverside, p. 1-28.

Burchfiel, B.C., and Davis, G.A., 1988, Mesozoic thrust faults and Cenozoic low-angle normal faults, eastern Spring Mountains, Nevada, and Clark Mountains thrust complex, California, in Weide, D.L., and Faber, M.L., eds., This extended land: Geological Journeys in the Southern Basin and Range: Las Vegas, University of Nevada, Las Vegas Department of Geoscience, p. 87-106.

Burchfiel, B.C., Cowan, D.S., and Davis, G.A., 1992, Tectonic Overview of the Cordilleran Orogen in the Western United States, *in* Burchfiel, B.C., Lipman, P.W., and Zoback, M.L., eds., The Cordilleran Orogen: Conterminous U.S.: Boulder, Colorado, Geological Society of America, The Geology of North America, v. G-3, p. 407-479.

Busby, C.J., Schermer, E.R., and Mattinson, J.M., 2002, Extensional arc setting and ages of Middle Jurassic eolianites, Cowhole Mountains (eastern Mojave Desert block, California), *in* Glazner, A.F., Walker, J.D., and Bartley, J.M., eds., Geologic Evolution of the Mojave Desert and Southwestern Basin and Range: Boulder, Colorado, Geological Society of America Memoir 195, p. 79-91.

Busby-Spera, C.J., 1988, Speculative tectonic model for the early Mesozoic arc of the southwest Cordilleran United States: Geology, v. 16, p. 1121-1125.

DeCelles, P.G., 2004, Late Jurassic to Eocene evolution of the Cordilleran thrust belt and foreland basin system, western U.S.A.: American Journal of Science, v. 304, p. 105-168.

Dunne, G.C., and Walker, J.D., 2004, Structure and evolution of the East Sierran thrust system, east central California: Tectonics, v. 23, doi: 10.1029/2002TC001478.

Fleck, R.J., Mattinson, J.M., Busby, C.J., Carr, M.D., Davis, G.A., and Burchfiel, B.C., 1994, Isotopic complexities and the age of the Delfonte volcanic rocks, eastern Mescal Range, southeastern California: Stratigraphic and tectonic implications: Geological Society of America Bulletin, v. 106, p. 1242-1253.

Foster, D.A., Harrison, T.M., Copeland, P., and Heizler, M.T., 1990, Effects of excess argon within large diffusion domains on K-feldspar age spectra: Geochimica et Cosmochimica Acta, v. 54, p. 1699-1708.

Fox, L. K., and Miller, D. M., 1990, Jurassic granitoids and related rocks of the southern Bristol Mountains, southern Providence Mountains, and Colton Hills, Mojave Desert, California. *in* Anderson, J.L., ed., The Nature and Origin of Cordilleran Magmatism. Geological Society of America Memoir 174: p. 111-132.

Harrison, T.M., Grove, M., Lovera, O.M., Zeitler, P.K., 2005, Continuous thermal histories from closure profiles, *in* Reiners, P.W., and Ehlers, T.A., eds., Low-temperature thermochronology: techniques, interpretations, and applications, Reviews in Mineralogy and Petrology, v. 58, p. 389-409.

Howard, K.A., McCaffrey, K.J.W., Wooden, J.L., Foster, D.A., and Shaw, S.E., 1995, Jurassic thrusting of Precambrian basement over Paleozoic cover in the Clipper Mountains, southeastern California, *in* Miller, D.M., and Busby, C., Jurassic Magmatism and Tectonics of the North American Cordillera: Boulder, Colorado, Geological society of America Special Paper 299, p. 375-392.

Livaccari, R.F., 1991, Role of crustal thickening and extensional collapse in the tectonic evolution of the Sevier-Laramide orogeny, western United States, Geology, v. 19, p. 1104-1107.

Lo, C.-H., Onstott, T.C., 1989, ^{39}Ar recoil artifacts in chloritized biotite: Geochimica et

Cosmochimica Acta, v. 53, p. 2697-2711.

Lovera, O.M., Richter, F.M., and Harrison, T.M., 1989, The $^{40}Ar/^{39}Ar$ thermochronometry for slowly cooled samples having a distribution of diffusion domain sizes: Journal of Geophysical Research, v. 94, p. 17,917-17,935.

Lovera, O.M., Richter, F.M., and Harrison, T.M., 1991, Diffusion domains determined by ^{39}Ar released during step heating: Journal of Geophysical Research, v. 96, p. 2057-2069.

Miller, D.M., Miller, R.J., Nielsen, J.E., Wilshire, H.G., Howard, K.A., and Stone, P., 2003, Geologic map of the East Mojave National Scenic Area, California: U.S. Geological Survey Miscellaneous Field Studies, MF-2414.

Miller, D.M., Walker, J.D., DeWitt, E., Nakata, J.K., 1994, Mesozoic episodes of horizontal crustal extension, U.S. Cordillera: Geological Society of America Abstracts with Programs, v. 26, p. 74.

Saleeby, J.B., and Busby-Spera, C., 1992, Early Mesozoic tectonic evolution of the western U.S. Cordillera, *in* Burchfiel, B.C., et al., eds., The Cordilleran Orogen: Conterminous U.S.: Boulder, Colorado, Geological Society of America, Geology of North America, p. 107-168.

Sheets, R.W., 1996, Geology and mineralization in the vicinity of the Morning Star precious-metal deposit of the Ivanpah Mountains, San Bernardino County, California: [PhD Dissertation], Virginia Polytechnic Institute and State University, Blacksburg, VA, 293 p.

Smith, A.G., Wells, M.L., and Foster, D.A., 2003 Timing and development of an orogenparallel lineation and of frontal thrusting in the southern Cordilleran fold-thrust belt, New York Mountains, California: Geological Society of America Abstracts with Programs, v. 35, p. 513.

Sutter, J.F., 1968, Geochronology of major thrusts, southern Great Basin, California, [M.S. Thesis]: Rice University, Houston, Texas, 32 p.

Walker, J.D., Burchfiel, B.C., and Davis, G.A., 1995, New age controls on initiation and timing of foreland belt thrusting in the Clark Mountains, southern California: Geological Society of America Bulletin, v. 107, p. 742-750.

Walker, J.D., Martin, M.W., and Glazner, A.F., 2002, Late Paleozoic to Mesozoic development of the Mojave Desert and environs, California, *in* Glazner, A.F., Walker, J.D., and Bartley, J.M., eds., Geologic Evolution of the Mojave Desert and Southwestern Basin and Range: Boulder, Colorado, Geological Society of America Memoir 195, p. 1-18.

Warnock, A.C., and van de Kamp, P.C., 1999, Hump-shaped $^{40}Ar/^{39}Ar$ age spectra in K-feldspar and evidence for Cretaceous authigenesis in the Fountain Formation near Eldorado Springs, Colorado: Earth and Planetary Science Letters, v. 174, p. 99-111.

Wells, M.L., Beyene, M.A., Spell, T.L., Kula, J.L., Miller, D.M., Zanetti, K.A., 2005, The Pinto shear zone; A Laramide synconvergent extensional shear zone in the Mojave Desert region of the southwestern Cordilleran orogen, western United States: Journal of Structural Geology, v. 27, p. 1697-1720.

APPENDIX A

CHAPTER 1 APPENDICES

Appendix Table DR1 - $^{40}Ar/^{39}Ar$ data tables

P76106 muscovite, 5.36 mg, J = 0.00173333 ± 0.0762% **Collection location: 47.17296 °S, 167.75776 °E (NZGD49)**
4 amu discrimination = 1.02740 ± 0.35%, 40/39K = .010817 ± 99.4%, 36/37Ca = 0.000284 ± 5.75%, 39/37Ca = 0.000685 ± 2.37%

step	T (C)	t (min.)	36Ar	37Ar	38Ar	39Ar	40Ar	%40Ar*	% 39Ar rlsd	Ca/K	40Ar*/39ArK	Age (Ma)	1s.d.
1	725	12	10.318	0.046	2.666	48.361	4276.340	30.7	4.17	0.006468	27.1850	83.07	1.01
2	775	12	1.555	0.031	1.300	70.695	2598.320	83.2	6.09	0.002982	30.5944	93.22	0.46
3	820	12	1.341	0.015	3.144	222.307	7240.190	94.8	19.16	0.000459	31.0060	94.44	0.42
4	850	12	0.540	0.021	2.561	184.824	5837.680	97.5	15.93	0.000773	30.9167	94.18	0.41
5	875	12	0.364	0.023	1.475	106.795	3370.740	97.3	9.20	0.001464	30.7530	93.69	0.41
6	900	12	0.318	0.012	0.964	68.037	2165.260	96.5	5.86	0.001199	30.6496	93.38	0.41
7	915	12	0.263	0.022	0.618	43.290	1395.950	95.7	3.73	0.003456	30.6674	93.44	0.42
8	930	12	0.230	0.017	0.479	34.125	1105.450	95.5	2.94	0.003388	30.6227	93.30	0.42
9	945	12	0.205	0.020	0.437	30.168	979.180	95.6	2.60	0.004508	30.6701	93.45	0.43
10	960	12	0.194	0.016	0.434	30.873	998.032	96.0	2.66	0.003524	30.6866	93.49	0.41
11	980	12	0.215	0.015	0.511	37.999	1219.670	96.3	3.27	0.002684	30.6378	93.35	0.42
12	1000	12	0.215	0.017	0.634	47.953	1528.370	97.0	4.13	0.002411	30.7516	93.69	0.41
13	1030	12	0.199	0.018	0.927	68.853	2175.980	98.1	5.93	0.001778	30.9433	94.26	0.41
14	1100	12	0.174	0.052	1.698	129.055	4041.650	99.3	11.12	0.002740	31.1081	94.75	0.41
15	1150	12	0.096	0.072	0.346	25.134	802.421	99.4	2.17	0.019480	31.0239	94.50	0.40
16	1400	12	0.163	0.104	0.190	11.846	407.273	95.9	1.02	0.059700	30.5641	93.13	0.47
						Cumulative %39Ar rlsd =			100.0		Total gas age =	93.54	0.51
											Plateau age =	93.77	0.23
											(steps 2-16)		

note: isotope beams in mV, rlsd = released, age uncertainty includes J uncertainty, all uncertainties 1 sigma
(36Ar through 40Ar are measured beam intensities, corrected for decay in the age calculations)

P76106 biotite, 9.63 mg, J = 0.00174095 ± 0.0615% **Collection location: 47.17296 °S, 167.75776 °E (NZGD49)**
4 amu discrimination = 1.02617 ± 0.16%, 40/39K = 0.010817 ± 99.4%, 36/37Ca = 0.000284 ± 5.75%, 39/37Ca = 0.000685 ± 2.37%

step	T (C)	t (min.)	36Ar	37Ar	38Ar	39Ar	40Ar	%40Ar*	% 39Ar rlsd	Ca/K	40Ar*/39ArK	Age (Ma)	1s.d.
1	650	12	93.586	0.058	21.144	75.347	28824.010	6.5	4.75	0.006607	24.95033932	76.71	2.01
2	690	12	86.531	0.087	23.007	151.995	29374.930	15.2	9.59	0.004939	29.45613977	90.22	0.99
3	720	12	44.283	0.066	16.859	198.030	18527.770	31.2	12.49	0.002876	29.31724823	89.81	0.50
4	750	12	28.693	0.054	16.756	260.734	15917.960	48.1	16.44	0.001787	29.51806558	90.41	0.40
5	780	12	10.807	0.024	7.411	121.372	6681.200	53.5	7.65	0.001706	29.56560213	90.55	0.35
6	820	12	12.004	0.030	5.770	73.709	5602.280	38.3	4.65	0.003512	29.26236977	89.64	0.45

7	860	12	13.296	0.040	5.358	59.225	5549.820	31.0	3.74	0.005827	29.21050752	89.49	0.49
8	900	12	13.337	0.037	5.404	62.699	5663.770	32.2	3.95	0.005092	29.23794377	89.57	0.48
9	940	12	12.388	0.032	6.159	86.480	6048.780	41.1	5.45	0.003193	28.85194348	88.42	0.39
10	970	12	10.817	0.023	7.044	117.282	6525.270	52.3	7.40	0.001692	29.23894756	89.57	0.32
11	1000	12	13.401	0.022	8.723	145.584	8120.720	52.5	9.18	0.001304	29.43404886	90.16	0.32
12	1030	12	12.559	0.028	6.903	107.105	6758.820	46.5	6.75	0.002256	29.49965454	90.35	0.36
13	1070	12	10.190	0.032	4.954	71.041	5051.180	42.0	4.48	0.003887	29.9627789	91.74	0.44
14	1400	12	7.791	0.405	3.822	54.988	3761.990	40.8	3.47	0.06355	27.80556755	85.28	0.62
							Cumulative %39Ar rlsd =		100.00		Total gas age =	89.26	0.50
											Plateau age = (steps 2-8)	90.02	0.35
											Isochron age =	90.6	0.62

note: isotope beams in mV, rlsd = released, age uncertainty includes J uncertainty, all uncertainties 1 sigma
(36Ar through 40Ar are measured beam intensities, corrected for decay in the age calculations)

P76106 K-feldspar, 18.32 mg, J = 0.00164713 ± 0.2107% **Collection location: 47.17296 °S, 167.75776 °E (NZGD49)**
4 amu discrimination = 1.03120 ± 0.11%, 40/39K = 0.01868 ± 52.3%, 36/37Ca = 0.0002586 ± 10.31%, 39/37Ca = 0.0008080 ± 27.74%

step	T (C)	t (min.)	36Ar	37Ar	38Ar	39Ar	40Ar	%40Ar*	% 39Ar rlsd	Ca/K	40Ar*/39ArK	Age (Ma)	1s.d.
1	448	18	1.336	0.015	0.336	2.951	415.278	8.2	0.06	0.027121	11.27674409	33.20	2.02
2	473	18	0.419	0.017	0.143	4.275	166.268	30.1	0.09	0.021218	11.03342141	32.49	0.48
3	473	43	0.412	0.018	0.184	7.705	206.080	49.1	0.15	0.012465	11.65562698	34.31	0.24
4	514	18	0.291	0.029	0.257	14.851	266.242	71.7	0.30	0.010419	12.43091642	36.57	0.15
5	514	43	0.356	0.032	0.430	27.684	481.857	83.2	0.56	0.006167	13.84740385	40.69	0.14
6	555	18	0.240	0.057	0.633	45.115	761.055	92.2	0.91	0.006741	15.45207051	45.34	0.13
7	555	43	0.293	0.072	0.959	71.460	1316.340	95.4	1.44	0.005376	17.36888346	50.89	0.14
8	596	18	0.193	0.098	1.123	85.502	1713.050	97.5	1.72	0.006115	19.512815	57.07	0.15
9	596	43	0.257	0.128	1.539	116.841	2568.250	98.1	2.35	0.005845	21.49300042	62.76	0.16
10	638	18	0.166	0.149	1.443	113.690	2712.830	98.7	2.29	0.006993	23.59620031	68.79	0.18
11	638	43	0.258	0.200	1.802	139.470	3571.340	98.6	2.80	0.007651	25.24463653	73.50	0.19
12	679	19	0.159	0.173	1.382	105.112	2830.520	98.8	2.11	0.008782	26.67039543	77.56	0.20
13	679	44	0.255	0.207	1.649	124.420	3477.340	98.6	2.50	0.008877	27.54646024	80.05	0.20
14	720	19	0.176	0.191	1.231	94.058	2675.680	98.6	1.89	0.010835	28.088806	81.59	0.21
15	720	44	0.247	0.202	1.415	109.561	3175.220	98.6	2.20	0.009837	28.52907647	82.84	0.21
16	761	19	0.169	0.151	1.013	73.727	2155.700	98.3	1.48	0.010928	28.77435131	83.54	0.22
17	761	44	0.232	0.151	1.175	89.146	2625.560	98.5	1.79	0.009038	28.90513275	83.91	0.21
18	802	19	0.151	0.130	0.807	63.174	1866.710	98.7	1.27	0.01098	29.05075127	84.32	0.21
19	843	19	0.211	0.167	1.160	89.044	2635.130	98.4	1.79	0.010007	29.10223698	84.47	0.22

20	884	19	0.270	0.192	1.468	109.889	3279.360	98.2	2.21	0.009322	29.32762415	85.11	0.22
21	910	19	0.299	0.158	1.398	103.248	3116.530	97.8	2.08	0.008165	29.54568018	85.73	0.22
22	935	19	0.388	0.145	1.440	105.346	3227.000	97.1	2.12	0.007344	29.76910628	86.36	0.22
23	961	19	0.497	0.138	1.516	112.367	3470.470	96.7	2.26	0.006553	29.81535434	86.49	0.22
24	976	19	0.541	0.123	1.400	104.324	3261.120	96.1	2.10	0.006291	29.97248159	86.94	0.23
25	1002	19	0.709	0.149	1.651	119.478	3772.340	95.4	2.40	0.006654	30.07207442	87.22	0.22
26	1018	19	0.719	0.152	1.624	112.500	3583.360	95.0	2.26	0.007209	30.2211396	87.64	0.23
27	1033	19	0.780	0.159	1.595	111.366	3572.550	94.5	2.24	0.007618	30.27307333	87.79	0.23
28	1048	19	0.821	0.167	1.600	110.807	3583.360	94.2	2.23	0.008041	30.41723812	88.20	0.23
29	1064	19	0.866	0.183	1.598	112.080	3637.080	93.9	2.25	0.008712	30.43844157	88.26	0.23
30	1074	19	0.869	0.173	1.536	103.834	3400.750	93.5	2.09	0.00889	30.55648702	88.59	0.23
31	1084	19	0.883	0.160	1.448	99.405	3283.060	93.1	2.00	0.008588	30.68586731	88.96	0.23
32	1089	24	1.018	0.173	1.633	108.911	3615.670	92.8	2.19	0.008475	30.72475723	89.07	0.23
33	1089	29	1.018	0.144	1.558	104.937	3495.550	92.6	2.11	0.007322	30.73748535	89.10	0.24
34	1089	29	0.893	0.107	1.321	87.636	2935.960	92.4	1.76	0.006515	30.78981475	89.25	0.23
35	1089	39	1.052	0.097	1.459	97.243	3276.670	92.0	1.96	0.005322	30.80501937	89.29	0.23
36	1089	59	1.400	0.122	1.818	118.960	4036.540	91.2	2.39	0.005472	30.77072109	89.20	0.24
37	1089	74	1.527	0.109	1.822	117.292	4032.550	90.4	2.36	0.004958	30.84038034	89.39	0.23
38	1089	74	1.371	0.090	1.517	97.377	3380.060	89.9	1.96	0.004931	30.86513419	89.46	0.24
39	1089	74	1.232	0.071	1.259	81.577	2869.570	89.5	1.64	0.004644	31.03631567	89.95	0.23
40	1089	74	1.131	0.056	1.162	70.207	2475.830	89.0	1.41	0.004256	30.83224715	89.37	0.23
41	1089	89	1.242	0.060	1.167	71.324	2551.200	88.4	1.43	0.004488	30.96911085	89.76	0.24
42	1089	119	1.557	0.061	1.358	80.162	2909.840	87.2	1.61	0.00406	30.9330354	89.65	0.24
43	1089	149	1.816	0.057	1.416	81.105	3009.730	85.6	1.63	0.00375	30.9004985	89.56	0.24
44	1141	19	0.598	0.035	0.718	44.579	1550.640	91.8	0.90	0.004189	31.13253698	90.22	0.23
45	1200	20	1.913	0.093	2.421	150.738	5239.130	90.3	3.03	0.003292	31.32006873	90.75	0.24
46	1230	20	2.339	0.127	3.455	221.922	7519.700	91.6	4.46	0.003053	31.06355332	90.02	0.23
47	1300	20	3.870	0.247	7.521	514.602	16978.108	93.9	10.35	0.002561	31.03773058	89.95	0.23
48	1350	20	1.394	0.147	3.080	218.409	7094.910	95.5	4.39	0.003591	30.85311078	89.43	0.23
49	1400	20	0.443	0.030	0.311	17.448	674.072	93.9	0.35	0.009174	31.53208131	91.35	0.25
50	1500	20	0.568	0.019	0.199	6.284	360.512	73.4	0.13	0.016132	31.5876622	91.50	0.49
							Cumulative %39Ar rlsd =		100.0		Total gas age =	84.22	0.17

note: isotope beams in mV, rlsd = released, age uncertainty includes J uncertainty, all uncertainties 1 sigma
(36Ar through 40Ar are measured beam intensities, corrected for decay in the age calculations)

P67866, K-feldspar, 19.96 mg, J = 0.0015535 ± 0.5% **Collection location: 47.23197 °S, 167.57142 °E (NZGD49)**
4 amu discrimination = 1.01907 ± 0.39%, 40/39K = 0.0002 ± 0.03%, 36/37Ca = 0.000272 ± 23.61%, 39/37Ca = 0.000701 ± 1.75%

step	T (C)	t (min.)	36Ar	37Ar	38Ar	39Ar	40Ar	%40Ar*	% 39Ar rlsd	Ca/K	40Ar*/39ArK	Age (Ma)	1s.d.
1	473	43	0.950	0.024	0.189	1.846	326.897	16.9	0.04	0.04058	28.4596253	78.05	2.10
2	514	18	0.663	0.028	0.176	2.970	270.652	30.1	0.07	0.029426	27.1166914	74.44	1.11
3	514	43	0.803	0.033	0.215	5.458	377.090	40.2	0.12	0.018872	26.70370656	73.33	1.11
4	555	18	0.573	0.052	0.201	7.016	360.613	55.0	0.16	0.023134	28.09124231	77.06	0.70
5	555	43	0.804	0.061	0.333	13.554	620.511	64.3	0.30	0.014047	28.7667033	78.87	0.67
6	596	18	0.598	0.083	0.371	18.913	739.629	77.2	0.42	0.013698	30.16037641	82.61	0.64
7	596	43	0.723	0.138	0.534	30.206	1122.790	82.6	0.67	0.01426	30.3878916	83.22	0.62
8	636	18	0.561	0.206	0.595	37.413	1312.850	88.0	0.83	0.017186	30.91307604	84.62	0.62
9	638	43	0.533	0.241	0.693	45.087	1552.050	91.1	1.00	0.016684	31.13785281	85.22	0.61
10	679	19	0.355	0.261	0.557	39.465	1330.800	92.7	0.88	0.020642	31.28263224	85.61	0.61
11	679	44	0.387	0.368	0.820	56.687	1876.560	94.9	1.26	0.020262	31.2665441	85.57	0.60
12	720	19	0.251	0.363	0.672	49.200	1604.890	95.8	1.09	0.023029	31.30395897	85.67	0.60
13	720	44	0.279	0.461	1.049	75.773	2446.690	97.4	1.68	0.01899	31.36233029	85.82	0.60
14	761	19	0.166	0.399	0.825	63.678	2038.270	97.9	1.41	0.019557	31.40910583	85.95	0.60
15	761	44	0.230	0.662	1.679	126.519	4025.960	98.8	2.81	0.016332	31.43081078	86.01	0.60
16	802	19	0.116	0.486	1.198	89.533	2839.020	99.0	1.99	0.016943	31.48283066	86.15	0.60
17	843	19	0.116	0.726	1.718	129.054	4082.530	99.6	2.86	0.017559	31.5109006	86.22	0.60
18	884	19	0.121	0.956	2.395	183.537	5820.540	99.5	4.07	0.016258	31.65763184	86.61	0.60
19	910	19	0.100	0.851	2.269	172.735	5488.570	99.6	3.83	0.015377	31.74261578	86.84	0.60
20	935	19	0.105	0.748	2.234	170.654	5463.310	99.5	3.79	0.013681	31.97253781	87.45	0.60
21	961	19	0.115	0.594	2.160	166.165	5338.200	99.5	3.69	0.011158	32.06243089	87.69	0.60
22	976	19	0.115	0.401	1.941	147.311	4763.190	99.4	3.27	0.008496	32.24599974	88.18	0.60
23	1002	19	0.130	0.344	2.125	163.329	5294.260	99.4	3.62	0.006574	32.32581154	88.40	0.62
24	1018	19	0.142	0.273	2.113	162.534	5286.320	99.4	3.61	0.005243	32.41800027	88.64	0.61
25	1033	19	0.149	0.229	2.035	160.010	5222.960	99.3	3.55	0.004467	32.5191975	88.91	0.61
26	1048	19	0.159	0.209	2.150	162.714	5327.190	99.3	3.61	0.004009	32.60391497	89.14	0.61
27	1064	19	0.181	0.201	2.091	160.749	5277.660	99.2	3.57	0.003903	32.65340089	89.27	0.61
28	1074	19	0.184	0.193	1.942	145.889	4813.460	99.1	3.24	0.004129	32.77825644	89.60	0.62
29	1084	19	0.204	0.187	1.762	132.861	4397.710	98.9	2.95	0.004393	32.80600524	89.68	0.62
30	1089	24	0.224	0.195	1.794	137.322	4564.560	98.8	3.05	0.004432	32.92113745	89.98	0.62
31	1089	29	0.252	0.201	1.708	125.714	4211.120	98.6	2.79	0.00499	33.07605306	90.40	0.62
32	1089	39	0.306	0.217	1.658	124.390	4191.530	98.3	2.76	0.005445	33.12632386	90.53	0.63

33	1089	59	0.389	0.247	1.857	137.904	4667.070	98.2	3.06	0.00559	33.17922478	90.67	0.63
34	1089	74	0.405	0.231	1.716	125.134	4266.460	98.0	2.78	0.005762	33.29967419	90.99	0.63
35	1089	74	0.337	0.182	1.256	95.253	3231.220	98.0	2.11	0.005964	33.39011915	91.23	0.63
36	1089	74	0.290	0.147	1.019	73.138	2525.420	98.0	1.62	0.006273	33.52111688	91.58	0.64
37	1089	74	0.268	0.121	0.838	61.071	2110.870	97.9	1.36	0.006184	33.43891191	91.36	0.63
38	1089	89	0.269	0.105	0.770	55.813	1940.410	98.2	1.24	0.005872	33.53275401	91.61	0.64
39	1089	119	0.256	0.079	0.561	39.312	1379.280	98.8	0.87	0.006272	33.35746751	91.15	0.64
40	1089	149	0.289	0.069	0.544	39.789	1404.610	99.2	0.88	0.005413	33.34283107	91.11	0.63
41	1141	19	0.080	0.046	0.167	12.118	424.403	97.9	0.27	0.011848	33.22575098	90.80	0.65
42	1200	15	0.122	0.098	0.310	23.510	825.469	97.1	0.52	0.013011	33.71972623	92.11	0.64
43	1230	15	0.173	0.152	0.494	36.746	1289.900	97.0	0.82	0.012911	33.86167937	92.49	0.65
44	1255	15	0.250	0.172	0.695	50.500	1762.270	96.5	1.12	0.010631	33.58831466	91.76	0.64
45	1300	15	0.649	0.257	1.776	127.267	4447.900	96.0	2.82	0.006303	33.60595988	91.81	0.64
46	1350	15	0.518	0.120	1.876	135.595	4614.520	97.2	3.01	0.002762	33.056546	90.35	0.63
47	1400	15	0.524	0.095	2.144	162.030	5468.280	97.6	3.60	0.00183	32.94364115	90.04	0.63
48	1500	15	0.712	0.126	3.007	223.340	7633.890	97.6	4.96	0.001761	33.39237105	91.24	0.63
							Cumulative %39Ar rlsd =		100.0		Total gas age =	88.81	0.46

note: isotope beams in mV, rlsd = released, age uncertainty includes J uncertainty, all uncertainties 1 sigma
(36Ar through 40Ar are measured beam intensities, corrected for decay in the age calculations)

P62424, K-feldspar, 14.82 mg, J = 0.00165007 ± 0.1479% **Collection location: 47.37 °S, 167.88433 °E (NZGD49)**
4 amu discrimination = 1.02934 ± 0.62%, 40/39K = 0.01868 ± 52.3%, 36/37Ca = 0.0002586 ± 10.31%, 39/37Ca = 0.0008080 ± 27.74%

step	T (C)	t (min.)	36Ar	37Ar	38Ar	39Ar	40Ar	%40Ar*	% 39Ar rlsd	Ca/K	40Ar*/39ArK	Age (Ma)	1s.d.
1	448	18	1.849	0.024	0.371	0.636	547.803	3.0	0.02	0.186696	25.70650598	74.95	15.04
2	473	18	0.506	0.013	0.118	1.229	162.465	11.0	0.03	0.052331	13.56578148	39.94	2.28
3	473	43	0.509	0.025	0.116	2.018	174.707	18.5	0.06	0.061289	13.61317865	40.08	2.41
4	514	18	0.241	0.032	0.102	3.565	127.290	49.9	0.10	0.044407	16.22251031	47.66	0.64
5	514	43	0.368	0.047	0.145	6.021	215.492	57.6	0.17	0.038618	18.14044073	53.21	0.64
6	555	18	0.233	0.051	0.166	8.642	252.700	76.9	0.24	0.029196	21.55871148	63.06	0.62
7	555	43	0.400	0.088	0.256	13.058	428.356	77.8	0.37	0.03334	24.05793929	70.23	0.70
8	596	18	0.274	0.100	0.251	15.360	499.975	86.6	0.43	0.032208	27.49632604	80.05	0.69
9	596	43	0.397	0.110	0.366	22.465	793.340	88.8	0.63	0.024224	30.33058976	88.10	0.75
10	638	18	0.319	0.139	0.379	23.869	861.938	90.8	0.67	0.02881	32.41160821	93.99	0.78
11	638	43	0.400	0.151	0.522	33.585	1265.440	93.0	0.95	0.022243	34.40925604	99.63	0.81
12	679	19	0.314	0.146	0.445	30.003	1159.850	93.3	0.84	0.024074	35.82691055	103.62	0.83

13	679	44	0.383	0.159	0.626	41.322	1616.720	94.8	1.16	0.019036	36.64074828	105.90	0.84
14	720	19	0.328	0.134	0.507	35.152	1402.490	94.2	0.99	0.018859	37.41067694	108.06	0.87
15	720	44	0.348	0.173	0.650	46.252	1828.390	96.0	1.30	0.018504	37.55942213	108.48	0.86
16	761	19	0.362	0.153	0.526	34.272	1398.490	93.5	0.97	0.022086	37.96766707	109.63	0.88
17	761	44	0.320	0.177	0.610	42.319	1685.910	96.1	1.19	0.020692	37.85380351	109.31	0.86
18	802	19	0.367	0.152	0.481	32.521	1335.250	93.7	0.92	0.023123	38.05441677	109.87	0.88
19	843	19	0.658	0.233	0.763	48.223	2023.200	91.7	1.36	0.023904	38.27509213	110.49	0.90
20	884	19	1.096	0.296	1.044	60.180	2621.040	88.7	1.69	0.024333	38.56372671	111.29	0.92
21	910	19	1.091	0.253	1.002	55.788	2451.960	88.0	1.57	0.022436	38.57587506	111.33	0.93
22	935	19	1.638	0.246	1.229	64.667	2965.470	84.8	1.82	0.01882	38.82532412	112.03	0.96
23	961	19	2.433	0.282	1.641	82.770	3898.400	82.8	2.33	0.016855	38.89074006	112.21	0.98
24	976	19	2.650	0.277	1.835	89.010	4224.320	82.6	2.51	0.015396	39.14460243	112.92	0.98
25	1002	19	4.297	0.413	2.803	135.054	6505.420	81.4	3.80	0.015129	39.27121339	113.27	1.00
26	1018	19	4.437	0.461	3.087	149.156	7087.750	82.4	4.20	0.01529	39.21577333	113.12	0.99
27	1033	19	4.953	0.562	3.576	172.763	8189.850	82.9	4.87	0.016093	39.41323321	113.67	0.99
28	1048	19	6.591	0.838	4.803	241.505	11391.480	83.6	6.80	0.017166	39.57496637	114.12	0.98
29	1064	19	6.664	0.929	5.189	255.519	11912.360	84.1	7.20	0.017987	39.373164	113.56	0.98
30	1074	19	5.823	0.895	4.499	242.656	11176.140	85.3	6.83	0.018247	39.40858219	113.66	0.97
31	1084	19	3.677	0.590	3.116	168.223	7686.270	86.6	4.74	0.017351	39.65656395	114.35	0.96
32	1089	24	3.479	0.570	3.104	168.461	7653.480	87.3	4.74	0.016739	39.74354116	114.59	0.96
33	1089	29	2.660	0.434	2.475	139.565	6265.000	88.3	3.93	0.015384	39.65584814	114.35	0.95
34	1089	29	1.887	0.300	1.802	102.448	4566.850	88.9	2.89	0.014487	39.52379419	113.98	0.94
35	1089	39	1.898	0.279	1.829	104.397	4677.060	89.2	2.94	0.013221	39.8459244	114.88	0.95
36	1089	59	2.144	0.270	2.033	114.412	5168.130	89.0	3.22	0.011675	40.02352264	115.38	0.95
37	1089	74	2.072	0.233	1.845	102.497	4671.110	88.5	2.89	0.011246	39.99559064	115.30	0.96
38	1089	74	1.785	0.173	1.499	80.735	3726.880	87.8	2.27	0.010601	40.03498226	115.41	0.97
39	1089	74	1.540	0.120	1.177	62.068	2913.840	86.7	1.75	0.009565	40.03498226	115.41	0.97
40	1089	74	1.322	0.093	0.929	48.937	2325.380	86.1	1.38	0.009402	39.96443716	115.21	0.98
41	1089	89	1.212	0.079	0.914	48.414	2275.640	87.7	1.36	0.008073	40.07043677	115.51	0.97
42	1089	119	1.605	0.079	0.977	47.748	2370.800	83.9	1.34	0.008185	40.24021563	115.98	1.01
43	1089	149	1.855	0.063	1.000	45.454	2353.610	81.2	1.28	0.006857	40.2839212	116.10	1.03
44	1141	19	0.818	0.039	0.692	37.894	1757.990	89.2	1.07	0.005092	40.40609754	116.44	0.96
45	1200	20	2.116	0.140	2.066	116.784	5280.710	89.3	3.29	0.005931	40.25239557	116.01	0.96
46	1230	20	1.401	0.093	1.473	85.458	3825.430	90.7	2.41	0.005384	40.28929504	116.12	0.95
47	1300	20	0.921	0.075	0.885	50.711	2281.760	92.4	1.43	0.007317	40.05217208	115.46	0.93

48	1350	20	0.505	0.024	0.293	13.464	682.789	92.3	0.38	0.008819	40.28069692	116.09	1.01
49	1400	20	0.463	0.030	0.202	8.073	461.889	91.0	0.23	0.018384	41.15040268	118.52	1.02
50	1500	20	0.834	0.033	0.377	15.723	874.684	82.0	0.44	0.010383	40.72830951	117.34	1.03
								Cumulative %39Ar rlsd =	100.0		Total gas age =	112.58	0.29
											Plateau age =	114.84	0.42
											(steps 24-48)		

note: isotope beams in mV, rlsd = released, age uncertainty includes J uncertainty, all uncertainties 1 sigma
(36Ar through 40Ar are measured beam intensities, corrected for decay in the age calculations)

Appendix DR2 - Textural Documentation

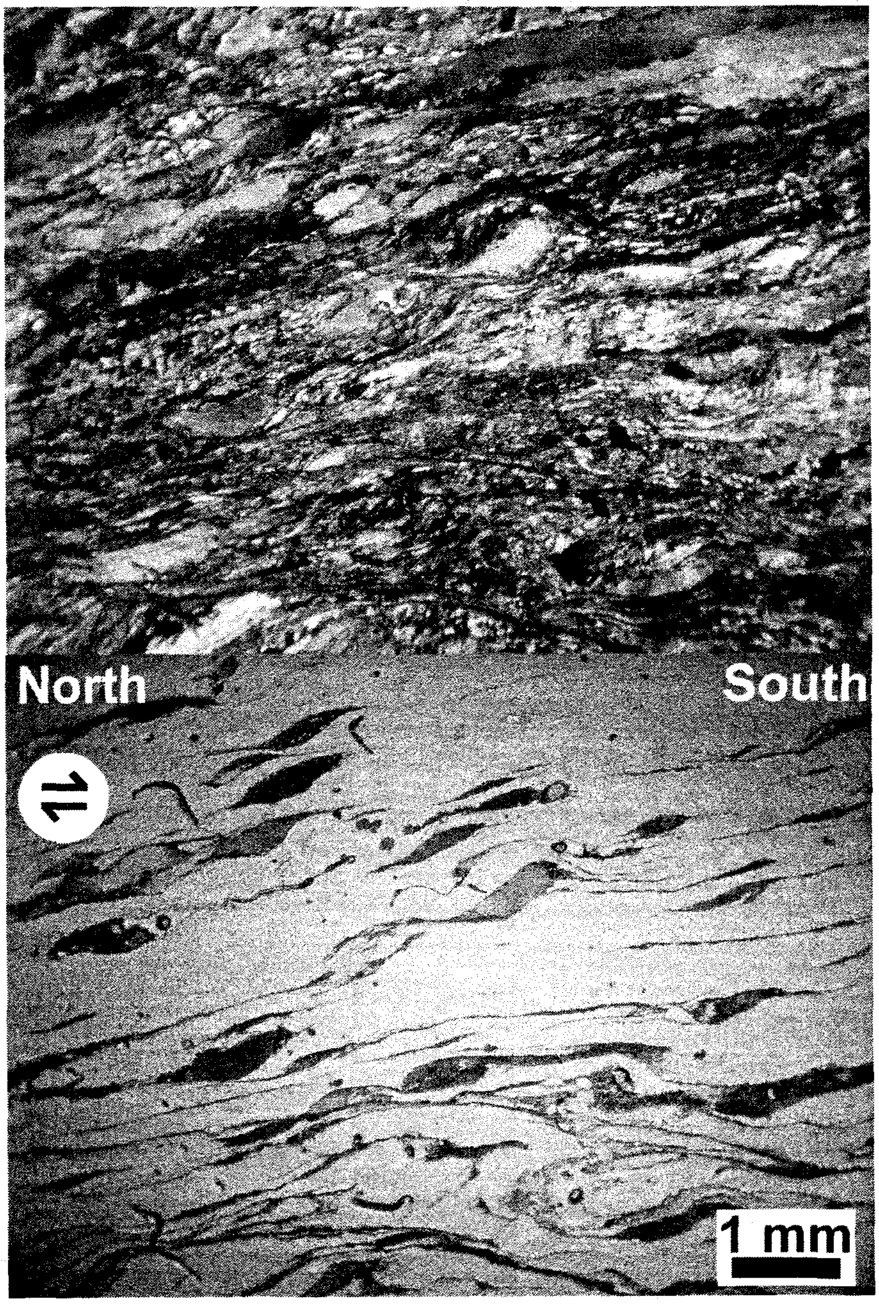

Figure DR1. Crossed polarized (top) and plane polarized light (bottom) photomicrographs of granitic mylonite sample collected from the Port Pegasus region of the northern segment of the Sisters Shear Zone. Biotite mica fish and quartz grain-shape fabric indicate top-to-south sense of shear.

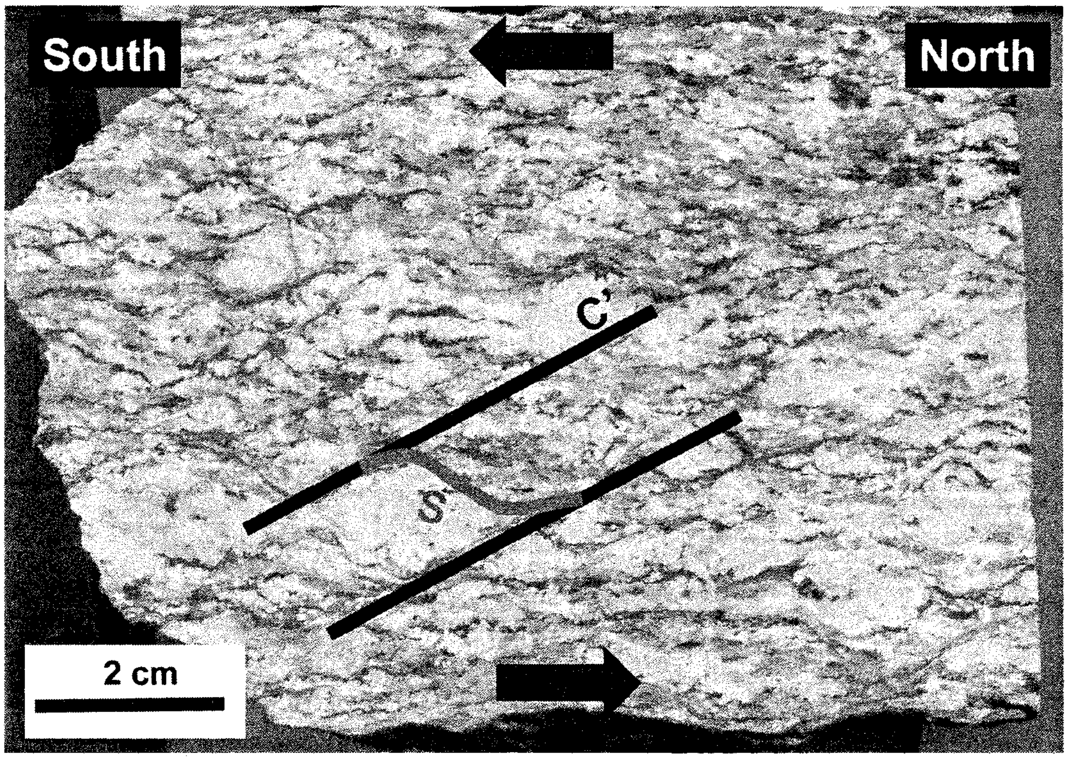

Figure DR2. Polished slab of coarse Knob Pluton sample (P75092- PETLAB database) from the northern segment of the Sisters Shear Zone. Shear bands indicate top-to-south kinematics.

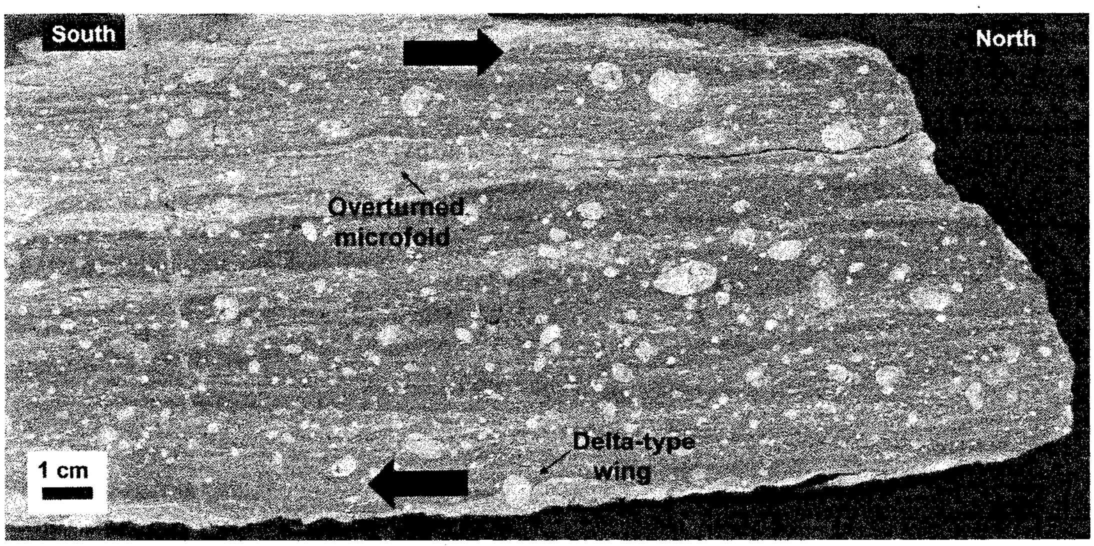

Figure DR3. Polished slab of ultramylonite sample (P75074 PETLAB database) collected from the southern segment of the Sisters Shear Zone. Overturned microfold and delta-type clast are pointed out as indicators of top-to-north shear sense.

Appendix DR3 - Analytical Procedures for $^{40}Ar/^{39}Ar$ analyses

$^{40}Ar/^{39}Ar$ analyses were done at the Nevada Isotope Geochronology Laboratory at the University of Nevada, Las Vegas using a MAP 215-50 mass spectrometer. Atmospheric argon ($^{40}Ar/^{36}Ar$ ratio) and corresponding mass discrimination (4 AMU) factors are measured weekly and are recorded in the data tables for individual samples. Prior to analysis, samples were wrapped in Al foil and stacked in 6 mm inside diameter Pyrex tubes. Individual packets averaged 3 mm thick and neutron fluence monitors (FC-2, Fish Canyon Tuff sanidine) were placed every 5-10 mm along the tube. Synthetic K-glass and optical grade CaF_2 were included in the irradiation packages to monitor neutron induced argon interferences from K and Ca. Loaded tubes were packed in an Al container for irradiation. Sample P67866 was irradiated at McMaster Nuclear Reactor at McMaster University, Ontario, Canada. The sample package was in-core for 7 hours in the 5C position where they are surrounded by fuel rods on all four sides. Samples Sest-2 and P62424 were irradiated at the Nuclear Science Center at Texas A&M University were in-core for 14 hours in the D3 position on the core edge (fuel rods on three sides, moderator on the fourth side) of the 1MW TRIGA type reactor. Irradiations were performed in a dry tube device, shielded against thermal neutrons by a 5 mm thick jacket of B_4C powder, which rotates about its axis at a rate of 0.7 revolutions per minute to mitigate horizontal fluence gradients. Correction factors for interfering neutron reactions on K and Ca for both irradiation facilities were determined by repeated analysis of K-glass and CaF_2 fragments. J-factors were calculated using single crystal laser fusion of 3 to 5 Fish Canyon Tuff sanidines from each level throughout the irradiation package.

Samples analyzed by the furnace step heating method utilized a double vacuum resistance furnace similar to the Staudacher et al. (1978) design. Reactive gases were removed by three GP-50 SAES getters prior to being admitted to a MAP 215-50 mass spectrometer by expansion. The relative volumes of the extraction line and mass spectrometer allow 76% of the gas to be admitted to the mass spectrometer for furnace heating analyses. Peak intensities were measured using a Balzers electron multiplier by peak hopping through 7 cycles; initial peak heights were determined by linear regression to the time of gas admission. Sample ages were calculated using an age of 27.9 Ma (Steven et al., 1967; Cebula et al., 1986) for the Fish Canyon Tuff sanidine. Plateaus are defined as three or more consecutive steps totaling at least 50% of the ^{39}Ar released with ages that overlap at 2σ analytical uncertainties (excluding J uncertainty). Isochrons are defined by greater than three consecutive steps corresponding to at least 50% of the ^{39}Ar released, and follow the MSWD criterion of Wendt and Carl (1991).

References

Cebula, G.T., M.J. Kunk, H.H. Mehnert, C.W. Naeser, J.D. Obradovich, and J.F. Sutter, The Fish Canyon Tuff, a potential standard for the ^{40}Ar-^{39}Ar and fission-track dating methods (abstract), *Terra Cognita (6th Int. Conf. on Geochronology, Cosmochronology and Isotope Geology), 6*, 139, 1986.

Staudacher, T.H., Jessberger, E.K., Dorflinger, D., and Kiko, J., A refined ultrahigh-vacuum furnace for rare gas analysis, *J. Phys. E: Sci. Instrum.*, *11*, 781-784, 1978.

Steven, T.A., H.H. Mehnert, and J.D. Obradovich, Age of volcanic activity in the San Juan Mountains, Colorado, *U.S. Geol. Surv. Prof. Pap., 575-D*, 47-55, 1967.

Wendt, I., and Carl, C., 1991, The statistical distribution of the mean squared weighted deviation, *Chemical Geology*, v. 86, p. 275-285.

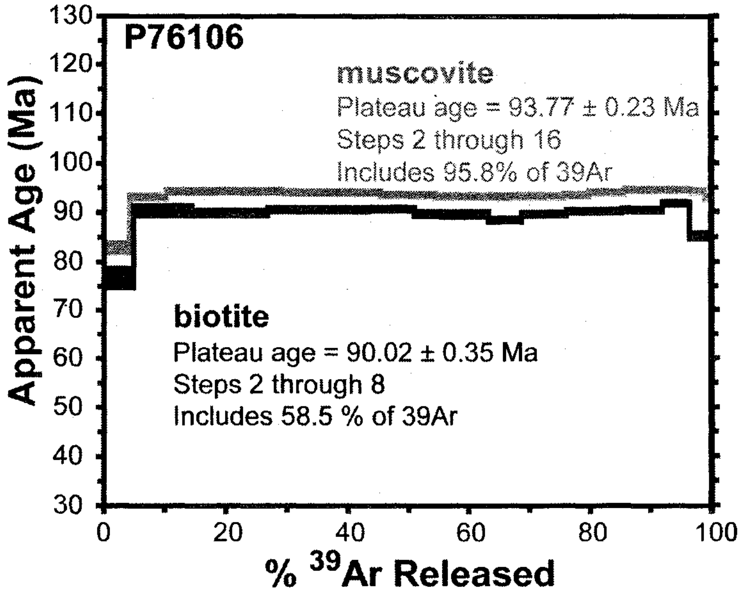

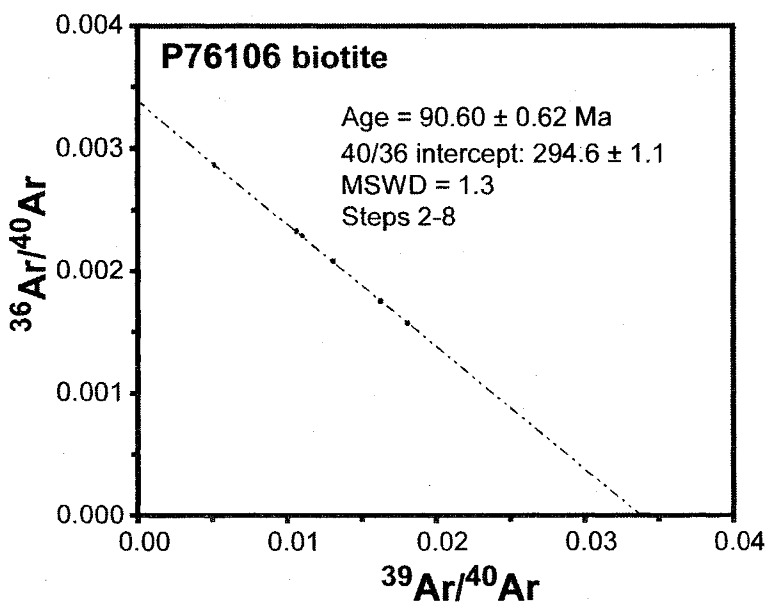

Figure DR4. Summary of sample P76106 mica ages

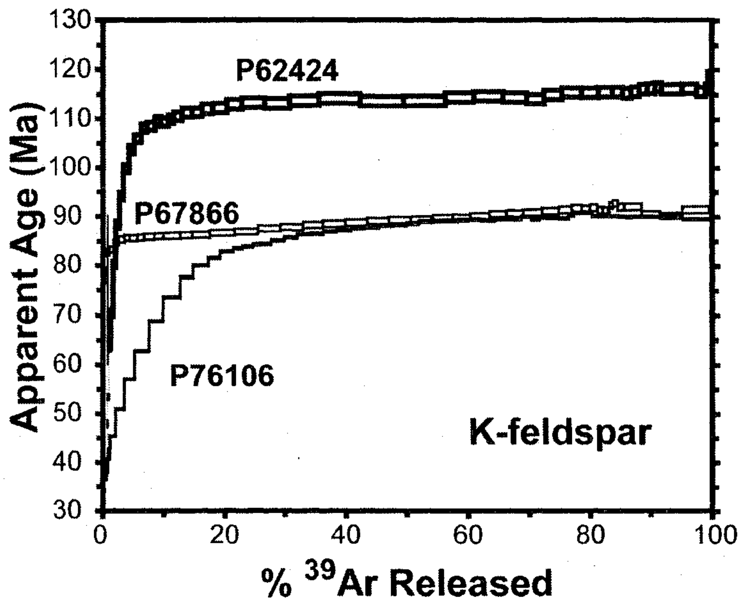

Figure DR5. Summary diagram of K-feldspar age spectra

Summary of MDD modeling of K-feldspar procedures

K-feldspars were analyzed using detailed furnace step-heating including isothermal duplicates to obtain diffusion properties (E, D_o/r_2) for application of the multiple diffusion domain (MDD) modeling approach of Lovera et al. (1989, 1991). Activation energy (E) and frequency factor (D_o) for each sample was determined using a least squares linear regression of low-temperature steps of the experiment plotted on an Arrhenius diagram (Lovera et al., 1989). Ten E, D_o pairs were then randomly selected from a Gaussian distribution around the values obtained from the Arrhenius diagram based on the uncertainties. For each pair, E was assumed to be representative of all domains used in the modeling. The number of domains along with their size and volume concentration was modeled using a variational iterative technique to determine the best fit between the experimental and modeled results on a domain size distribution plot [log (r/r_o) vs. $\%^{39}Ar$ released] (Richter et al., 1991). Five cooling histories were then determined for each E, D_o pair by fitting modeled age spectra to the experimental age spectrum using these parameters and domain distributions. The distribution of the 50 calculated cooling histories for each sample reflects the uncertainty in the obtained activation energies. The cooling histories were then used to calculate 90% confidence intervals for the total distribution and the median of the distribution (Lovera et al., 1997).

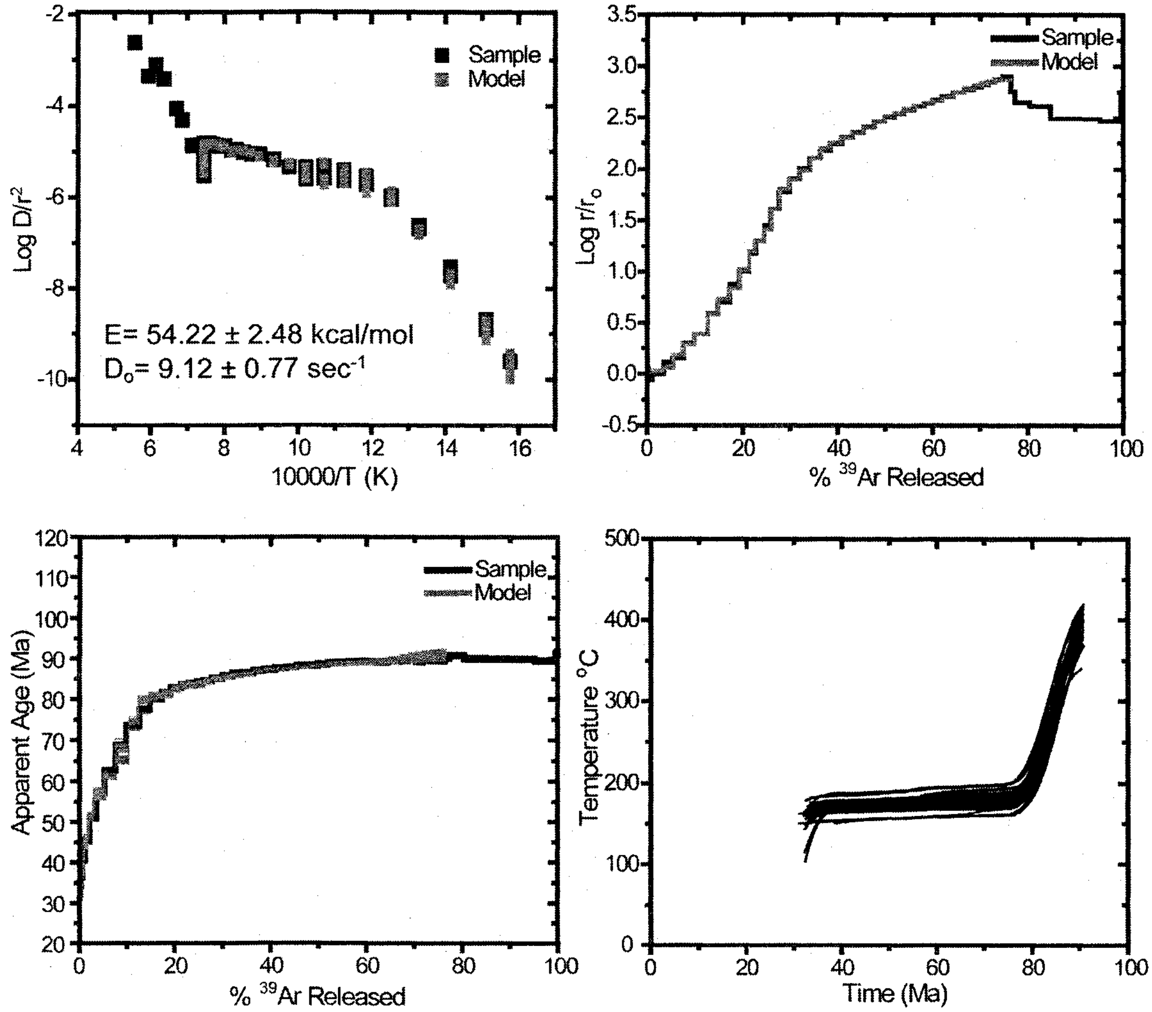

Figure DR6. P76106 summary of K-feldspar MDD modeling

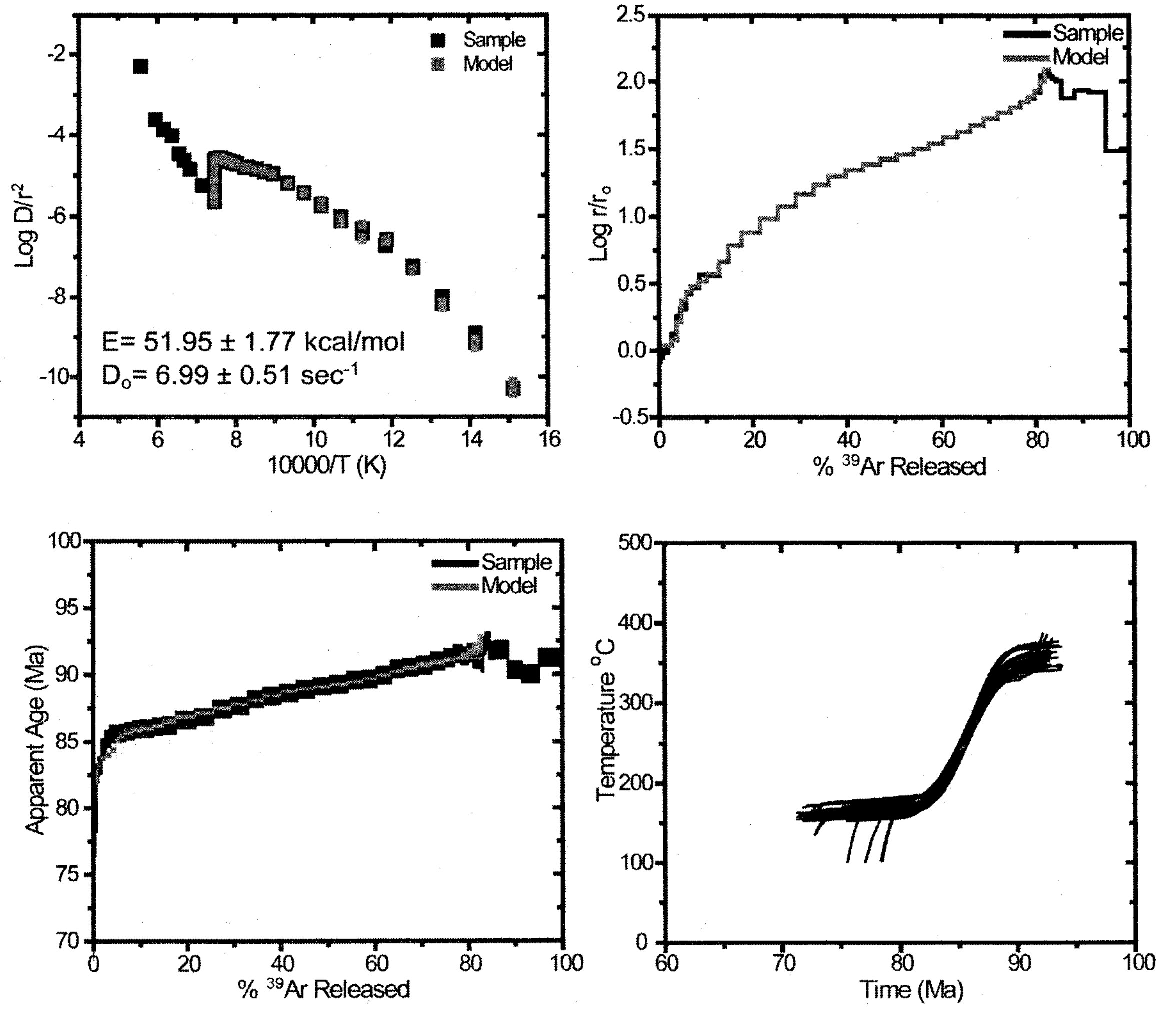

Figure DR7. P67866 summary of K-feldspar MDD modeling

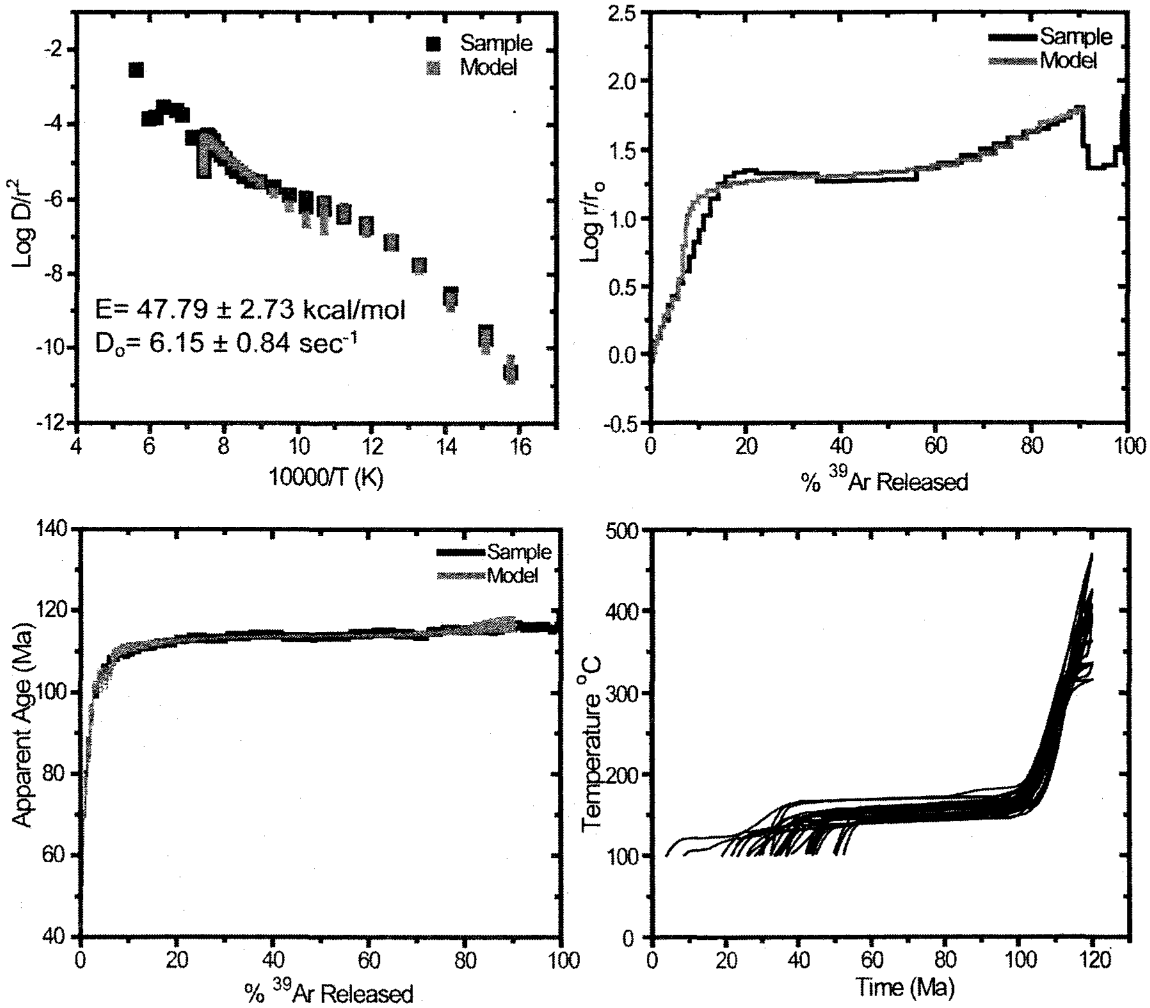

Figure DR8. P62424 summary of K-feldspar MDD modeling

References

Lovera, O.M., Richter, F.M., and Harrison, T.M., 1989, The $^{40}Ar/^{39}Ar$ Thermochronometry for Slowly Cooled Samples Having a Distribution of Diffusion Domain Sizes: Journal of Geophysical Research, v. 94, p. 17,917-17,935.

Lovera, O.M., Richter, F.M., and Harrison, T.M., 1991, Diffusion domains determined by ^{39}Ar released during step heating: Journal of Geophysical Research, v. 96, p. 2057-2069.

Lovera, O.M., Grove, M., Harrison, T.M., and Mahon, K.I., 1997, Systematic analysis of K-feldspar $^{40}Ar/^{39}Ar$ step heating results: I. Significance of activation energy determinations: Geochimica et Cosmochimica Acta, v. 61, p. 3171-3192.

Richter, F.M., Lovera, O.M., Harrison, T.M., and Copeland, P., 1991, Tibetan tectonics from $^{40}Ar/^{39}Ar$ analysis of a single K-feldspar sample: Earth and Planetary Science Letters, v. 105, p. 266-278.

APPENDIX B

CHAPTER 2 APPENDICES

Appendix B. $^{40}Ar/^{39}Ar$ data tables

P75086, biotite, 7.88 mg — J= 0.00198 ± 0.3667 %

4 amu discrim. = 1.0425 ± 0.42 % — 36/37Ca = 0.00025 ± 4.51 %

40/39K = 0.0071 ± 0.56 % — 39/37Ca = 0.00068 ± 2.07 %

step	T (C)	t (min.)	36Ar	37Ar	38Ar	39Ar	40Ar	% 39Ar rlsd	%40Ar*	Ca/K	40Ar*/39ArK	Age (Ma)	1s.d.
1	650	12	3.85	0.02	2.63	92.63	3404.88	4.4	66.7	0.0028	24.6311	85.78	0.61
2	680	12	0.78	0.02	2.17	100.53	2876.45	4.8	92.3	0.0029	26.5533	92.30	0.53
3	710	12	0.56	0.03	2.88	141.67	3920.44	6.8	96.1	0.0059	26.7392	92.93	0.52
4	735	12	0.44	0.03	3.51	170.64	4668.66	8.2	97.6	0.0060	26.8478	93.30	0.52
5	770	12	0.42	0.02	4.38	219.69	5964.86	10.5	98.2	0.0035	26.8292	93.24	0.51
6	810	12	0.39	0.03	3.86	192.71	5238.91	9.2	98.1	0.0057	26.8317	93.25	0.51
7	845	12	0.36	0.03	2.26	110.58	3053.97	5.3	97.0	0.0073	26.9098	93.51	0.52
8	875	12	0.27	0.02	1.43	69.39	1921.64	3.3	96.6	0.0106	26.7784	93.07	0.52
9	910	12	0.26	0.05	1.23	57.51	1599.79	2.7	96.3	0.0206	26.7405	92.94	0.52
10	950	12	0.34	0.03	1.46	70.83	1974.34	3.4	95.8	0.0077	26.7076	92.83	0.52
11	980	12	0.34	0.02	1.81	85.74	2370.84	4.1	96.5	0.0045	26.7158	92.86	0.52
12	1020	12	0.35	0.02	2.56	124.85	3426.58	6.0	97.5	0.0033	26.8680	93.37	0.51
13	1070	12	0.39	0.05	3.66	182.14	4955.46	8.7	98.0	0.0067	26.8161	93.19	0.52
14	1100	12	0.31	0.05	3.05	153.70	4177.91	7.3	98.3	0.0107	26.8461	93.30	0.51
15	1400	12	0.62	1.15	6.50	319.45	8718.93	15.3	98.3	0.1155	26.9731	93.73	0.51
										Total gas age =	92.90	0.40	
										Plateau age =	93.14	0.40	

note: 36Ar through 40Ar are measured beam intensities in mV, corrected for decay in age calculations, age uncertainty includes J uncertainty, rlsd = released, all uncertainties 1 sigma

P75086, K-feldspar, 9.95 mg — J= 0.00202 ± 0.186 %

4 amu discrim. = 1.0351 ± 0.39 % — 36/37Ca = 0.00026 ± 1.61 %

40/39K = 0.0024 ± 76.1 % — 39/37Ca = 0.00070 ± 10.1 %

step	T (C)	t (min.)	36Ar	37Ar	38Ar	39Ar	40Ar	% 39Ar rlsd	%40Ar*	Ca/K	40Ar*/39ArK	Age (Ma)	1s.d.
1	450	18	1.01	0.03	0.23	3.63	421.76	0.1	30.3	0.0274	34.3994	121.26	2.11
2	475	18	0.20	0.04	0.07	2.72	124.17	0.1	59.2	0.0487	24.8854	88.53	0.66
3	475	43	0.17	0.03	0.07	2.82	115.89	0.1	78.9	0.0235	24.0909	85.77	0.50
4	500	18	0.08	0.03	0.05	2.39	80.73	0.1	81.9	0.0242	24.2185	86.21	0.56
5	500	43	0.12	0.03	0.07	3.54	113.34	0.1	95.4	0.0328	22.5210	80.30	0.36
6	540	18	0.07	0.04	0.08	4.75	132.46	0.1	93.9	0.0331	24.3074	86.52	0.52

7	540	43	0.09	0.04	0.10	7.01	193.41	0.2	99.6	0.0284	23.3413	83.16	0.35
8	580	18	0.07	0.04	0.13	9.82	256.12	0.3	96.5	0.0160	24.3338	86.61	0.39
9	580	43	0.08	0.07	0.20	14.96	379.91	0.4	100.0	0.0249	23.5520	83.89	0.36
10	620	18	0.07	0.08	0.24	19.23	477.48	0.5	98.4	0.0246	24.0852	85.75	0.37
11	620	43	0.09	0.10	0.37	28.78	713.47	0.8	100.0	0.0216	23.9128	85.15	0.36
12	660	19	0.06	0.11	0.40	33.24	812.68	0.9	99.4	0.0229	24.1851	86.10	0.37
13	660	43	0.10	0.16	0.61	48.79	1189.78	1.4	100.0	0.0238	23.9515	85.28	0.36
14	700	19	0.06	0.19	0.63	50.91	1235.82	1.4	99.5	0.0270	24.1474	85.96	0.37
15	700	43	0.11	0.35	0.96	75.07	1819.21	2.1	100.0	0.0362	24.0194	85.52	0.37
16	740	19	0.07	0.29	0.85	69.23	1679.83	2.0	99.4	0.0327	24.1733	86.05	0.37
17	740	43	0.10	0.28	1.12	87.10	2116.71	2.5	100.0	0.0246	24.1450	85.96	0.36
18	780	19	0.05	0.26	0.92	73.16	1776.44	2.1	99.8	0.0272	24.2819	86.43	0.37
19	780	43	0.10	0.34	1.15	90.99	2225.09	2.6	100.0	0.0288	24.3137	86.54	0.37
20	820	18	0.07	0.32	0.86	67.51	1652.99	1.9	99.5	0.0370	24.4145	86.89	0.37
21	860	18	0.08	0.50	1.28	101.70	2486.02	2.9	99.5	0.0392	24.4245	86.93	0.37
22	900	18	0.10	0.58	1.53	122.72	3013.71	3.5	99.4	0.0377	24.5276	87.29	0.37
23	925	18	0.09	0.49	1.36	108.44	2672.73	3.1	99.4	0.0360	24.6123	87.58	0.37
24	950	18	0.09	0.42	1.20	97.32	2404.81	2.8	99.4	0.0342	24.6477	87.70	0.37
25	975	18	0.10	0.40	1.20	97.81	2420.76	2.8	99.6	0.0332	24.6735	87.79	0.37
26	990	18	0.10	0.33	1.10	86.94	2159.61	2.5	99.6	0.0307	24.7365	88.01	0.37
27	1015	18	0.10	0.33	1.15	93.14	2328.82	2.6	99.6	0.0285	24.8992	88.58	0.38
28	1030	18	0.12	0.29	1.12	88.35	2215.23	2.5	99.3	0.0265	24.8969	88.57	0.38
29	1045	18	0.13	0.25	1.05	85.02	2144.22	2.4	99.2	0.0235	25.0052	88.94	0.38
30	1060	18	0.14	0.20	1.00	78.10	1968.50	2.2	99.0	0.0206	24.9177	88.64	0.38
31	1075	18	0.15	0.18	0.99	77.32	1952.49	2.2	98.7	0.0180	24.8992	88.58	0.38
32	1085	18	0.16	0.16	0.94	72.87	1858.22	2.1	98.6	0.0172	25.0851	89.22	0.38
33	1095	18	0.17	0.16	0.93	70.24	1796.78	2.0	98.3	0.0182	25.0858	89.22	0.39
34	1100	24	0.19	0.15	0.98	76.24	1953.03	2.2	98.3	0.0155	25.1009	89.28	0.38
35	1100	29	0.20	0.14	0.93	71.62	1842.89	2.0	98.1	0.0148	25.0917	89.24	0.38
36	1100	29	0.20	0.12	0.73	57.09	1478.22	1.6	97.7	0.0160	25.0517	89.11	0.39
37	1100	39	0.25	0.14	0.84	63.27	1651.57	1.8	97.6	0.0165	25.1572	89.47	0.39
38	1100	59	0.33	0.16	1.01	73.54	1935.80	2.1	97.6	0.0168	25.2214	89.69	0.39
39	1100	74	0.40	0.16	0.96	71.35	1890.07	2.0	97.0	0.0168	25.0583	89.13	0.39
40	1100	74	0.38	0.12	0.78	57.56	1539.25	1.6	96.9	0.0163	25.0614	89.14	0.39
41	1100	74	0.33	0.05	0.57	42.39	1157.60	1.2	97.0	0.0076	25.2698	89.86	0.39

42	1100	74	0.26	0.04	0.22	13.86	418.60	0.4	96.5	0.0179	24.9945	88.91	0.39
43	1100	89	0.30	0.04	0.22	13.22	415.00	0.4	96.9	0.0194	25.1523	89.45	0.40
44	1100	119	0.37	0.03	0.25	14.48	464.76	0.4	98.1	0.0120	25.0334	89.04	0.38
45	1100	149	0.44	0.04	0.28	16.15	529.15	0.5	99.1	0.0149	25.1591	89.48	0.40
46	1150	20	0.07	0.02	0.09	5.48	159.55	0.2	99.8	0.0182	25.1778	89.54	0.39
47	1200	20	0.12	0.04	0.23	16.55	450.11	0.5	99.9	0.0140	25.1469	89.44	0.39
48	1230	20	0.16	0.06	0.34	25.67	689.84	0.7	99.3	0.0168	25.4701	90.56	0.38
49	1300	20	0.42	0.18	1.77	137.95	3581.52	3.9	99.0	0.0100	25.2956	89.95	0.38
50	1350	20	0.80	0.32	4.25	332.52	8548.52	9.4	98.3	0.0077	25.2147	89.67	0.38
51	1400	20	1.23	0.42	6.14	483.74	12435.14	13.7	97.8	0.0071	25.1699	89.52	0.39
52	1500	20	0.70	0.31	1.20	86.95	2380.02	2.5	95.0	0.0283	25.2708	89.87	0.40
											Total gas age =	88.42	0.37

note: 36Ar through 40Ar are measured beam intensities in mV, corrected for decay in age calculations, age uncertainty includes J uncertainty, rlsd = released, all uncertainties 1 sigma

P75079, biotite, 8.07 mg

4 amu discrim. = 1.0344 ± 0.26 %
40/39K = 0.0071 ± 0.56 %

J= 0.00205 ± 0.2993 %
36/37Ca = 0.00025 ± 4.51 %
39/37Ca = 0.00068 ± 2.07 %

step	T (C)	t (min.)	36Ar	37Ar	38Ar	39Ar	40Ar	% 39Ar rlsd	%40Ar*	Ca/K	40Ar*/39ArK	Age (Ma)	1s.d.
1	650	12	7.50	0.13	8.24	415.83	10930.28	18.7	79.8	0.0091	21.0962	76.44	0.48
2	680	12	0.81	0.03	3.85	248.95	6742.76	11.2	96.7	0.0019	26.3244	94.90	0.37
3	710	12	0.55	0.02	4.46	298.62	8079.14	13.4	98.2	0.0018	26.6957	96.20	0.38
4	735	12	0.41	0.04	4.29	284.10	7657.08	12.8	98.7	0.0037	26.7151	96.27	0.37
5	770	12	0.35	0.03	3.51	238.45	6390.78	10.7	98.6	0.0039	26.5504	95.69	0.37
6	810	12	0.35	0.02	1.84	121.95	3282.22	5.5	97.3	0.0050	26.2380	94.59	0.38
7	845	12	0.40	0.01	1.07	65.99	1800.27	3.0	94.4	0.0050	25.6618	92.57	0.37
8	875	12	0.36	0.02	0.81	49.47	1343.52	2.2	93.3	0.0141	25.1832	90.89	0.37
9	910	12	0.34	0.01	0.83	52.13	1399.62	2.3	94.4	0.0003	25.1125	90.64	0.36
10	950	12	0.40	0.03	1.12	71.64	1911.61	3.2	95.0	0.0068	25.2215	91.02	0.36
11	980	12	0.30	0.02	1.06	67.44	1786.33	3.0	96.3	0.0022	25.3590	91.50	0.36
12	1020	12	0.25	0.03	1.05	69.24	1829.17	3.1	97.2	0.0101	25.5536	92.19	0.36
13	1070	12	0.20	0.03	1.24	81.34	2142.81	3.7	98.3	0.0074	25.8062	93.08	0.37
14	1400	12	0.33	0.91	2.34	158.80	4220.09	7.1	98.6	0.1734	26.1759	94.38	0.37
											Total gas age =	91.19	0.31

note: 36Ar through 40Ar are measured beam intensities in mV, corrected for decay in age calculations, age uncertainty includes J uncertainty, rlsd = released, all uncertainties 1 sigma

P77056, biotite, 5.60 mg								J=	0.001649 ± 0.1771 %				
4 amu discrim. =			1.0279 ± 0.5 %					36/37Ca =	0.000259 ± 10.31 %				
40/39K =			0.0187 ± 52.3 %					39/37Ca =	0.000808 ± 27.74 %				
step	T (C)	t (min.)	36Ar	37Ar	38Ar	39Ar	40Ar	% 39Ar rlsd	%40Ar*	Ca/K	40Ar*/39ArK	Age (Ma)	1s.d.
1	650	12	54.91	0.07	13.53	80.73	17649.25	8.3	8.1	0.0035	17.2210	50.51	3.18
2	690	12	30.74	0.06	10.04	108.45	11849.38	11.2	23.4	0.0021	25.4359	74.12	1.58
3	720	12	15.06	0.03	5.97	84.62	6868.94	8.7	35.3	0.0016	28.6078	83.15	1.17
4	750	12	10.66	0.04	5.04	85.58	5672.92	8.8	44.6	0.0017	29.5523	85.83	0.95
5	780	12	6.85	0.04	3.84	74.49	4254.99	7.7	52.7	0.0022	30.0526	87.25	0.82
6	820	12	4.52	0.04	3.06	65.06	3294.34	6.7	59.8	0.0023	30.2070	87.69	0.75
7	860	12	2.94	0.04	2.18	49.09	2333.97	5.1	63.3	0.0034	29.9444	86.94	0.70
8	900	12	2.63	0.04	1.81	40.42	1966.29	4.2	61.5	0.0021	29.5802	85.91	0.70
9	940	12	3.10	0.04	1.90	39.69	2068.89	4.1	56.6	0.0028	29.1910	84.81	0.75
10	970	12	3.32	0.06	2.01	40.30	2145.73	4.2	55.1	0.0051	29.0414	84.38	0.77
11	1000	12	3.51	0.03	2.24	44.87	2351.11	4.6	56.7	0.0012	29.4542	85.55	0.76
12	1030	12	3.35	0.03	2.36	49.79	2458.98	5.1	60.5	0.0006	29.6235	86.03	0.71
13	1070	12	3.64	0.01	2.80	62.90	2956.31	6.5	64.3	0.0001	30.0583	87.27	0.68
14	1400	12	7.09	0.04	6.13	142.20	6453.48	14.7	68.5	0.0011	30.8187	89.42	0.66
											Total gas age =	82.15	0.42

note: 36Ar through 40Ar are measured beam intensities in mV, corrected for decay in age calculations, age uncertainty includes J uncertainty, rlsd = released, all uncertainties 1 sigma

P75084, biotite, 5.97 mg								J=	0.002011 ± 0.3241 %				
4 amu discrim. =			1.0425 ± 0.42 %					36/37Ca =	0.000254 ± 4.51 %				
40/39K =			0.0071 ± 0.56 %					39/37Ca =	0.000685 ± 2.07 %				
step	T (C)	t (min.)	36Ar	37Ar	38Ar	39Ar	40Ar	% 39Ar rlsd	%40Ar*	Ca/K	40Ar*/39ArK	Age (Ma)	1s.d.
1	650	12	6.86	0.05	5.07	247.10	7190.81	16.5	71.9	0.0044	21.0556	74.82	0.49
2	680	12	0.62	0.02	2.63	167.09	4536.69	11.1	96.2	0.0017	26.2907	92.96	0.49
3	710	12	0.35	0.02	3.07	202.18	5462.24	13.5	98.4	0.0028	26.7475	94.53	0.50
4	735	12	0.25	0.03	2.96	199.04	5360.86	13.3	98.9	0.0042	26.8101	94.74	0.49
5	770	12	0.22	0.03	2.74	184.24	4949.90	12.3	99.0	0.0046	26.7595	94.57	0.49
6	810	12	0.24	0.01	1.50	99.08	2675.00	6.6	97.8	0.0025	26.5068	93.70	0.49
7	845	12	0.33	0.01	0.84	52.69	1453.08	3.5	94.3	0.0077	25.9822	91.89	0.49

8	875	12	0.27	0.03	0.59	35.94	991.61	2.4	93.3	0.0217	25.5801	90.51	0.49
9	910	12	0.24	0.01	0.56	35.29	962.21	2.3	94.2	0.0009	25.4526	90.07	0.48
10	950	12	0.26	0.03	0.76	48.88	1307.51	3.3	95.5	0.0128	25.4338	90.00	0.48
11	980	12	0.20	0.02	0.80	49.90	1323.64	3.3	96.9	0.0075	25.5782	90.50	0.48
12	1020	12	0.15	0.03	0.76	49.81	1324.31	3.3	98.0	0.0107	25.9498	91.78	0.48
13	1070	12	0.12	0.03	0.85	57.41	1520.14	3.8	98.8	0.0087	26.0838	92.24	0.48
14	1100	12	0.08	0.02	0.53	34.24	913.49	2.3	99.6	0.0219	26.2635	92.86	0.49
15	1400	12	0.19	0.67	0.61	38.72	1059.04	2.6	97.7	0.5378	26.1565	92.49	0.49
											Total gas age =	90.25	0.20

note: 36Ar through 40Ar are measured beam intensities in mV, corrected for decay in age calculations, age uncertainty includes J uncertainty, rlsd = released, all uncertainties 1 sigma

P75084, K-feldspar, 11.12 mg

4 amu discrim. = 1.0351 ± 0.39 %

40/39K = 0.0024 ± 76.1 %

J= 0.001981 ± 0.1847 %

36/37Ca = 0.000258 ± 1.61 %

39/37Ca = 0.000704 ± 10.06 %

step	T (C)	t (min.)	36Ar	37Ar	38Ar	39Ar	40Ar	% 39Ar rlsd	%40Ar*	Ca/K	40Ar*/39ArK	Age (Ma)	1s.d.
1	450	18	1.75	0.03	0.39	4.70	685.04	0.1	25.2	0.0129	36.1999	124.96	2.64
2	475	18	0.35	0.03	0.11	3.45	187.04	0.1	47.9	0.0225	24.6822	86.13	1.01
3	475	43	0.30	0.03	0.09	4.32	186.04	0.1	64.5	0.0160	23.3637	81.64	0.51
4	500	18	0.13	0.03	0.07	3.71	121.17	0.1	76.2	0.0116	22.9245	80.13	0.58
5	500	43	0.17	0.02	0.11	5.96	185.92	0.1	88.4	0.0029	23.2341	81.19	0.38
6	540	18	0.12	0.04	0.13	9.02	249.78	0.2	90.5	0.0143	24.2010	84.49	0.43
7	540	43	0.12	0.03	0.17	12.49	325.65	0.3	99.1	0.0069	23.6163	82.50	0.36
8	580	18	0.14	0.04	0.22	16.31	426.99	0.4	93.2	0.0100	23.9815	83.75	0.39
9	580	43	0.10	0.04	0.29	23.43	583.86	0.6	99.9	0.0088	23.7974	83.12	0.35
10	620	18	0.11	0.05	0.37	27.47	690.26	0.6	96.8	0.0107	24.1472	84.31	0.38
11	620	43	0.09	0.08	0.48	37.69	929.43	0.9	100.0	0.0126	24.0348	83.93	0.35
12	660	19	0.09	0.08	0.51	40.83	1011.98	1.0	98.7	0.0118	24.3995	85.17	0.37
13	660	43	0.10	0.10	0.70	54.55	1344.46	1.3	100.0	0.0119	24.2800	84.76	0.36
14	700	19	0.09	0.11	0.72	56.27	1394.56	1.3	98.9	0.0132	24.5254	85.60	0.37
15	700	43	0.10	0.12	0.84	67.49	1663.45	1.6	100.0	0.0129	24.3887	85.13	0.36
16	740	19	0.07	0.10	0.67	53.26	1317.12	1.3	99.4	0.0128	24.5867	85.81	0.37
17	740	43	0.09	0.12	0.85	69.50	1721.14	1.6	100.0	0.0123	24.5184	85.58	0.36
18	780	19	0.06	0.08	0.66	52.33	1301.77	1.2	99.6	0.0106	24.7744	86.45	0.37
19	780	43	0.09	0.10	0.89	69.97	1733.44	1.7	100.0	0.0100	24.5311	85.62	0.36

20	820	18	0.06	0.07	0.62	49.53	1228.68	1.2	99.6	0.0092	24.6856	86.15	0.37
21	860	18	0.06	0.09	0.96	76.55	1897.93	1.8	99.6	0.0082	24.7635	86.41	0.37
22	900	18	0.07	0.11	1.14	92.62	2308.07	2.2	99.7	0.0081	24.9217	86.95	0.37
23	925	18	0.08	0.09	1.02	82.47	2075.28	1.9	99.5	0.0073	25.1052	87.58	0.37
24	950	18	0.07	0.09	0.96	78.07	1967.19	1.8	99.5	0.0072	25.1476	87.72	0.37
25	975	18	0.12	0.08	0.97	78.30	1987.21	1.8	99.3	0.0080	25.1735	87.81	0.38
26	990	18	0.11	0.07	0.82	65.82	1673.58	1.6	99.4	0.0077	25.1901	87.86	0.38
27	1015	18	0.11	0.07	0.93	75.45	1926.05	1.8	99.5	0.0069	25.3480	88.40	0.38
28	1030	18	0.11	0.07	0.94	72.86	1868.52	1.7	99.3	0.0069	25.4220	88.65	0.38
29	1045	18	0.13	0.07	0.94	72.75	1866.91	1.7	99.0	0.0065	25.3690	88.47	0.38
30	1060	18	0.15	0.08	1.03	81.18	2085.57	1.9	98.8	0.0073	25.3728	88.49	0.38
31	1075	18	0.19	0.09	1.14	90.05	2317.81	2.1	98.5	0.0080	25.3447	88.39	0.38
32	1085	18	0.19	0.09	1.06	80.94	2088.76	1.9	98.3	0.0081	25.3481	88.40	0.38
33	1095	18	0.20	0.09	1.08	84.34	2190.14	2.0	98.2	0.0082	25.4938	88.90	0.38
34	1100	24	0.25	0.10	1.25	99.43	2579.86	2.3	98.1	0.0080	25.4266	88.67	0.38
35	1100	29	0.24	0.08	1.16	90.69	2358.10	2.1	98.1	0.0064	25.4253	88.66	0.38
36	1100	29	0.23	0.07	0.92	71.99	1870.39	1.7	97.8	0.0077	25.2515	88.07	0.39
37	1100	39	0.27	0.07	1.00	76.84	2014.07	1.8	97.8	0.0070	25.3953	88.56	0.38
38	1100	59	0.35	0.07	1.17	90.06	2381.82	2.1	97.8	0.0060	25.5186	88.98	0.39
39	1100	74	0.42	0.09	1.21	91.09	2433.81	2.1	97.5	0.0075	25.5982	89.25	0.38
40	1100	74	0.31	0.06	0.65	48.73	1321.84	1.1	98.0	0.0081	25.5196	88.99	0.38
41	1100	74	0.27	0.04	0.39	26.87	754.31	0.6	98.0	0.0096	25.4301	88.68	0.38
42	1100	74	0.24	0.04	0.30	20.86	594.39	0.5	99.0	0.0141	25.4449	88.73	0.38
43	1100	89	0.25	0.03	0.31	20.91	599.96	0.5	99.9	0.0087	25.4437	88.73	0.38
44	1100	119	0.32	0.04	0.37	24.54	712.52	0.6	100.0	0.0098	25.4486	88.74	0.38
45	1100	149	0.39	0.03	0.41	27.12	798.88	0.6	100.0	0.0057	25.3760	88.50	0.38
46	1150	20	0.08	0.04	0.12	9.61	265.20	0.2	99.9	0.0252	25.4255	88.67	0.41
47	1200	20	0.15	0.03	0.37	27.98	751.99	0.7	99.8	0.0074	25.7156	89.65	0.38
48	1230	20	0.22	0.05	0.60	47.43	1264.92	1.1	98.2	0.0073	25.6230	89.34	0.38
49	1300	20	0.90	0.15	3.02	232.38	6149.89	5.5	97.1	0.0050	25.5509	89.09	0.39
50	1350	20	2.09	0.35	8.20	636.44	16700.96	15.0	96.8	0.0046	25.4834	88.86	0.38
51	1400	20	2.56	0.35	9.77	752.78	19826.79	17.8	96.6	0.0039	25.5448	89.07	0.39
52	1500	20	0.94	0.12	2.03	148.67	4065.23	3.5	95.3	0.0061	25.7202	89.67	0.39
											Total gas age =	88.18	0.37

note: 36Ar through 40Ar are measured beam intensities in mV, corrected for decay in age calculations, age uncertainty includes J uncertainty, rlsd = released, all uncertainties 1 sigma

P77057, muscovite, 7.53 mg — J= 0.00175 ± 0.0599 %

4 amu discrim. = 1.0274 ± 0.34 % — 36/37Ca = 0.00028 ± 5.75 %

40/39K = 0.0108 ± 99.4 % — 39/37Ca = 0.00069 ± 2.37 %

step	T (C)	t (min.)	36Ar	37Ar	38Ar	39Ar	40Ar	% 39Ar rlsd	%40Ar*	Ca/K	40Ar*/39ArK	Age (Ma)	1s.d.
1	725	12	11.30	0.22	2.81	51.55	4553.30	3.2	26.7	0.0301	23.5222	72.92	0.93
2	775	12	2.39	0.16	1.50	82.77	3150.59	5.2	77.9	0.0135	29.6760	91.52	0.39
3	820	12	1.53	0.12	2.81	198.82	6446.04	12.4	93.2	0.0040	30.3176	93.45	0.34
4	850	12	0.66	0.10	3.28	244.07	7567.92	15.2	97.6	0.0027	30.3857	93.66	0.32
5	875	12	0.38	0.08	2.12	160.43	4933.63	10.0	98.0	0.0032	30.2195	93.16	0.32
6	900	12	0.33	0.07	1.49	113.17	3486.94	7.1	97.7	0.0036	30.1228	92.87	0.34
7	915	12	0.27	0.07	1.06	79.70	2465.38	5.0	97.4	0.0050	30.0984	92.79	0.32
8	930	12	0.24	0.06	0.88	65.61	2038.03	4.1	97.4	0.0050	30.1689	93.00	0.32
9	945	12	0.21	0.06	0.81	59.18	1838.97	3.7	97.5	0.0060	30.1949	93.08	0.33
10	960	12	0.21	0.06	0.77	56.95	1767.62	3.6	97.5	0.0061	30.1296	92.89	0.33
11	980	12	0.22	0.05	0.86	63.81	1989.04	4.0	97.6	0.0041	30.3304	93.49	0.33
12	1000	12	0.23	0.07	1.04	77.23	2394.87	4.8	97.9	0.0052	30.3199	93.46	0.33
13	1030	12	0.22	0.08	1.46	111.75	3435.57	7.0	98.6	0.0045	30.3364	93.51	0.32
14	1100	12	0.19	0.23	2.03	156.49	4812.56	9.8	99.3	0.0104	30.5778	94.23	0.32
15	1150	12	0.12	0.31	0.57	43.87	1380.29	2.7	99.2	0.0496	30.8754	95.13	0.34
16	1400	12	0.27	0.80	0.52	37.04	1227.17	2.3	96.1	0.1543	31.2009	96.10	0.35
											Total gas age =	92.76	0.18
											Plateau age =	93.21	0.20

note: 36Ar through 40Ar are measured beam intensities in mV, corrected for decay in age calculations, age uncertainty includes J uncertainty, rlsd = released, all uncertainties 1 sigma

P77057, biotite, 7.27 mg — J= 0.001748 ± 0.0618 %

4 amu discrim. = 1.0274 ± 0.35 % — 36/37Ca = 0.000284 ± 5.75 %

40/39K = 0.0108 ± 99.4 % — 39/37Ca = 0.000685 ± 2.37 %

step	T (C)	t (min.)	36Ar	37Ar	38Ar	39Ar	40Ar	% 39Ar rlsd	%40Ar*	Ca/K	40Ar*/39ArK	Age (Ma)	1s.d.
1	650	12	50.28	0.08	11.97	79.30	16057.13	6.1	7.5	0.0061	14.7617	45.95	2.20
2	690	12	25.84	0.09	10.35	181.13	12158.05	13.8	37.2	0.0034	25.0070	77.17	0.77
3	720	12	10.54	0.07	8.28	211.42	9003.18	16.1	65.5	0.0021	27.9745	86.12	0.46
4	750	12	4.73	0.05	5.86	169.13	6244.26	12.9	77.8	0.0019	28.8107	88.63	0.39
5	780	12	3.16	0.05	3.70	105.75	3988.80	8.1	76.9	0.0027	29.0411	89.32	0.41

6	820	12	2.82	0.06	2.47	65.85	2732.28	5.0	69.9	0.0054	28.9869	89.16	0.44
7	860	12	2.13	0.10	1.67	45.42	1927.43	3.5	67.8	0.0136	28.6966	88.28	0.45
8	900	12	1.61	0.09	1.40	38.16	1575.71	2.9	70.7	0.0143	29.0038	89.21	0.45
9	940	12	1.58	0.05	1.61	46.05	1791.11	3.5	74.7	0.0066	28.9055	88.91	0.41
10	970	12	1.76	0.05	2.31	65.89	2417.21	5.0	79.0	0.0044	28.9386	89.01	0.39
11	1000	12	2.61	0.06	3.33	97.53	3579.70	7.4	78.9	0.0036	28.9546	89.06	0.39
12	1030	12	2.84	0.07	3.04	86.70	3342.16	6.6	75.3	0.0053	29.0268	89.28	0.41
13	1400	12	4.04	0.79	4.09	117.74	4621.22	9.0	74.7	0.0475	29.2563	89.96	0.42
											Total gas age =	84.37	0.25
											Plateau age =	89.08	0.27
											Isochron age =	89.60	0.85

note: 36Ar through 40Ar are measured beam intensities in mV, corrected for decay in age calculations, age uncertainty includes J uncertainty, rlsd = released, all uncertainties 1 sigma

P75092, muscovite, 5.25 mg

4 amu discrim. = 1.0425 ± 0.42 %

40/39K = 0.0071 ± 0.56 %

J= 0.00200 ± 0.339 %

36/37Ca = 0.00025 ± 4.51 %

39/37Ca = 0.00068 ± 2.07 %

step	T (C)	t (min.)	36Ar	37Ar	38Ar	39Ar	40Ar	% 39Ar rlsd	%40Ar*	Ca/K	40Ar*/39ArK	Age (Ma)	1s.d.
1	725	12	2.27	0.03	1.57	69.08	2358.53	4.6	72.0	0.0150	24.6206	86.84	0.57
2	775	12	0.48	0.03	0.88	62.80	1796.42	4.1	92.8	0.0160	26.5699	93.54	0.52
3	820	12	0.55	0.03	1.21	92.77	2581.35	6.1	94.2	0.0092	26.3060	92.64	0.51
4	850	12	0.54	0.01	1.62	123.79	3396.71	8.2	95.7	0.0033	26.3885	92.92	0.50
5	875	12	0.45	6.02	1.90	146.63	3976.43	9.7	97.2	1.2935	26.5504	93.48	0.50
6	900	12	0.25	0.01	1.71	137.22	3661.11	9.1	98.5	-0.0002	26.3785	92.89	0.49
7	915	12	0.18	0.00	1.05	83.36	2224.62	5.5	98.4	-0.0026	26.2765	92.54	0.49
8	930	12	0.15	0.00	0.82	62.29	1673.77	4.1	98.4	-0.0050	26.3895	92.92	0.50
9	945	12	0.13	0.01	0.68	52.06	1402.42	3.4	98.5	0.0024	26.4371	93.09	0.49
10	960	12	0.15	0.00	0.59	46.81	1266.55	3.1	97.8	-0.0054	26.3305	92.72	0.49
11	980	12	0.15	0.02	0.65	49.93	1343.86	3.3	98.0	0.0057	26.2704	92.51	0.50
12	1000	12	0.15	0.02	0.67	52.88	1419.45	3.5	98.1	0.0030	26.2445	92.43	0.49
13	1030	12	0.20	0.03	0.89	69.98	1875.04	4.6	97.8	0.0067	26.1899	92.24	0.49
14	1100	12	0.46	0.02	2.56	200.98	5400.02	13.3	97.8	0.0033	26.4331	93.07	0.50
15	1150	12	0.21	0.01	2.65	217.24	5772.58	14.4	99.3	0.0016	26.5339	93.42	0.50
16	1400	12	0.50	0.03	0.64	45.97	1354.54	3.0	91.3	0.0178	26.4951	93.29	0.52
											Total gas age =	92.72	0.37
											Plateau age =	92.90	0.37
											Isochron age =	92.75	0.69

note: 36Ar through 40Ar are measured beam intensities in mV, corrected for decay in age calculations, age uncertainty includes J uncertainty, rlsd = released, all uncertainties 1 sigma

P75092, biotite, 6.99 mg

4 amu discrim. = 1.0344 ± 0.26 % | J= 0.002069 ± 0.3848 %

40/39K = 0.0071 ± 0.56 % | 36/37Ca = 0.000254 ± 4.51 % | 39/37Ca = 0.000685 ± 2.07 %

step	T (C)	t (min.)	36Ar	37Ar	38Ar	39Ar	40Ar	% 39Ar rlsd	%40Ar*	Ca/K	40Ar*/39ArK	Age (Ma)	1s.d.
1	650	12	6.35	0.03	4.33	188.41	5850.56	10.2	68.1	0.0027	21.2311	77.55	0.42
2	680	12	1.04	0.00	2.89	183.99	4738.41	10.0	93.8	-0.0016	24.2733	88.39	0.41
3	710	12	0.68	0.00	3.36	220.97	5615.27	12.0	96.7	0.0000	24.6770	89.82	0.41
4	735	12	0.46	0.02	3.16	210.17	5322.06	11.4	97.7	0.0027	24.8422	90.41	0.41
5	770	12	0.40	0.01	2.93	192.84	4863.07	10.5	97.9	0.0011	24.7770	90.18	0.42
6	810	12	0.33	0.03	2.00	128.25	3251.43	7.0	97.6	0.0077	24.7671	90.14	0.41
7	845	12	0.31	0.02	1.11	70.56	1807.25	3.8	95.9	0.0077	24.4899	89.16	0.41
8	875	12	0.31	0.03	0.80	48.68	1259.59	2.6	94.0	0.0160	24.1516	87.96	0.42
9	910	12	0.34	0.05	0.82	53.14	1366.82	2.9	94.2	0.0249	23.9994	87.42	0.41
10	950	12	0.44	0.04	1.28	81.32	2070.54	4.4	94.7	0.0092	24.0291	87.52	0.41
11	980	12	0.37	0.01	1.38	92.54	2345.44	5.0	96.3	0.0000	24.3450	88.64	0.41
12	1020	12	0.33	0.03	1.85	122.51	3088.17	6.7	97.6	0.0042	24.5952	89.53	0.41
13	1070	12	0.27	0.04	1.67	110.92	2806.63	6.0	98.0	0.0081	24.7777	90.18	0.41
14	1400	12	0.38	0.42	2.01	134.27	3414.67	7.3	97.9	0.0942	24.8109	90.30	0.41
											Total gas age =	89.50	0.36

note: 36Ar through 40Ar are measured beam intensities in mV, corrected for decay in age calculations, age uncertainty includes J uncertainty, rlsd = released, all uncertainties 1 sigma

P75092, K-feldspar, 6.19 mg

4 amu discrim. = 1.0351 ± 0.39 % | J= 0.00155 ± 0.472 %

40/39K = 0.0002 ± 150 % | 36/37Ca = 0.00031 ± 7.09 % | 39/37Ca = 0.00074 ± 9.92 %

step	T (C)	t (min.)	36Ar	37Ar	38Ar	39Ar	40Ar	% 39Ar rlsd	%40Ar*	Ca/K	40Ar*/39ArK	Age (Ma)	1s.d.
1	450	18	0.30	0.03	0.08	0.76	97.75	0.0	12.3	0.2639	13.8941	38.51	1.59
2	475	18	0.11	0.02	0.07	3.55	106.96	0.2	79.5	0.0324	21.7565	59.94	0.42
3	475	43	0.13	0.03	0.16	9.90	273.32	0.6	97.1	0.0174	23.9924	65.99	0.41
4	500	18	0.08	0.02	0.15	11.67	347.69	0.7	96.8	-0.0074	28.1823	77.27	0.50
5	500	43	0.12	0.02	0.26	18.58	553.58	1.1	99.4	0.0015	28.1938	77.31	0.47
6	540	18	0.09	0.02	0.34	25.14	774.30	1.5	98.1	0.0011	30.0561	82.30	0.50
7	540	43	0.13	0.03	0.48	35.46	1110.80	2.1	99.5	0.0097	30.5554	83.63	0.51
8	580	18	0.09	0.03	0.56	40.08	1272.14	2.3	98.7	0.0043	31.3278	85.70	0.52

9	580	43	0.14	0.03	0.68	49.62	1591.29	2.9	99.5	0.0070	31.5440	86.27	0.52
10	620	18	0.08	0.03	0.59	43.16	1390.31	2.5	99.2	0.0053	31.9625	87.39	0.53
11	620	43	0.12	0.03	0.68	49.56	1607.83	2.9	99.7	0.0041	31.9906	87.47	0.53
12	660	19	0.08	0.04	0.48	35.62	1164.52	2.1	98.9	0.0162	32.2915	88.27	0.54
13	660	43	0.13	0.02	0.54	39.07	1276.11	2.3	99.6	0.0000	32.0142	87.53	0.53
14	700	19	0.08	0.03	0.39	26.88	875.34	1.6	98.7	0.0150	32.0145	87.53	0.53
15	700	43	0.13	0.03	0.48	34.21	1119.55	2.0	99.5	0.0101	31.9403	87.33	0.52
16	740	19	0.10	0.03	0.33	25.20	864.28	1.5	97.9	0.0149	33.4084	91.25	0.55
17	740	43	0.13	0.04	0.46	33.80	1232.98	2.0	99.6	0.0153	35.7032	97.35	0.59
18	780	19	0.09	0.03	0.33	24.80	993.28	1.5	98.4	0.0093	39.3088	106.89	0.65
19	780	43	0.15	0.04	0.47	32.48	1321.38	1.9	99.1	0.0204	39.7131	107.96	0.65
20	820	18	0.10	0.04	0.31	23.32	937.92	1.4	98.2	0.0272	39.3505	107.00	0.64
21	860	18	0.13	0.03	0.54	39.48	1674.52	2.3	98.4	0.0095	41.8078	113.48	0.68
22	900	18	0.17	0.05	0.65	46.81	2060.83	2.7	98.2	0.0172	43.3546	117.54	0.71
23	925	18	0.18	0.02	0.56	42.15	1777.51	2.5	97.7	0.0014	41.2921	112.12	0.67
24	950	18	0.22	0.05	0.59	42.36	1656.60	2.5	96.8	0.0184	37.9017	103.17	0.63
25	975	18	0.24	0.04	0.63	44.10	1672.36	2.6	97.0	0.0170	36.6658	99.90	0.60
26	990	18	0.23	0.03	0.56	38.07	1436.56	2.2	96.8	0.0114	36.3271	99.00	0.60
27	1015	18	0.30	0.04	0.62	44.09	1677.92	2.6	95.9	0.0190	36.3669	99.11	0.61
28	1030	18	0.31	0.04	0.61	41.70	1589.76	2.4	95.4	0.0228	36.2331	98.75	0.60
29	1045	18	0.34	0.02	0.63	43.25	1671.11	2.5	95.1	0.0047	36.6274	99.80	0.61
30	1060	18	0.37	0.03	0.61	41.87	1647.01	2.5	94.6	0.0110	37.0652	100.96	0.63
31	1075	18	0.39	0.03	0.66	42.86	1681.22	2.5	94.3	0.0114	36.8689	100.44	0.61
32	1085	18	0.42	0.03	0.59	39.92	1585.96	2.3	93.4	0.0166	36.9683	100.70	0.62
33	1095	18	0.38	0.02	0.56	38.47	1544.09	2.3	94.0	0.0105	37.5826	102.33	0.63
34	1100	24	0.44	0.03	0.61	42.10	1729.96	2.5	93.7	0.0109	38.3067	104.25	0.64
35	1100	29	0.50	0.04	0.65	40.67	1683.71	2.4	92.8	0.0177	38.0906	103.67	0.65
36	1100	29	0.41	0.04	0.47	30.33	1238.90	1.8	92.2	0.0275	37.1204	101.11	0.62
37	1100	39	0.48	0.04	0.53	32.75	1329.56	1.9	91.8	0.0229	36.5685	99.64	0.62
38	1100	59	0.65	0.03	0.62	38.23	1569.28	2.2	90.9	0.0136	36.3714	99.12	0.62
39	1100	74	0.71	0.03	0.62	37.60	1525.79	2.2	90.2	0.0153	35.3536	96.42	0.61
40	1100	74	0.64	0.03	0.51	29.57	1230.02	1.7	89.4	0.0234	35.5517	96.95	0.61
41	1100	74	0.58	0.03	0.41	23.52	996.88	1.4	88.6	0.0208	35.4733	96.74	0.61
42	1100	74	0.52	0.03	0.34	19.13	815.24	1.1	88.1	0.0361	34.9547	95.36	0.61
43	1100	89	0.53	0.02	0.19	6.95	391.18	0.4	74.4	0.0497	34.1451	93.21	0.64

44	1100	119	0.67	0.02	0.20	6.79	421.29	0.4	70.3	0.0339	33.6503	91.89	0.66
45	1100	149	0.79	0.03	0.24	6.91	455.21	0.4	67.8	0.0792	32.8421	89.74	0.68
46	1150	20	0.16	0.03	0.07	2.46	121.04	0.1	94.7	0.1891	32.7713	89.55	0.56
47	1200	20	0.25	0.02	0.16	8.23	339.09	0.5	89.6	0.0386	33.2024	90.70	0.57
48	1230	20	0.34	0.03	0.26	14.49	571.04	0.8	88.7	0.0338	32.9540	90.04	0.58
49	1300	20	0.81	0.03	1.02	66.76	2419.76	3.9	93.6	0.0099	32.9878	90.13	0.56
50	1350	20	0.97	0.04	1.30	87.05	3129.70	5.1	93.6	0.0096	32.9830	90.11	0.55
51	1400	20	0.97	0.04	1.10	71.83	2643.62	4.2	92.3	0.0125	33.1352	90.52	0.56
52	1500	20	1.43	0.03	0.68	32.35	1463.36	1.9	75.8	0.0170	32.5367	88.92	0.61
											Total gas age =	95.86	0.34

note: 36Ar through 40Ar are measured beam intensities in mV, corrected for decay in age calculations, age uncertainty includes J uncertainty, rlsd = released, all uncertainties 1 sigma

APPENDIX C

CHAPTER 3 APPENDICES

Appendix A. $^{40}Ar/^{39}Ar$ data tables for original micas.

NY25 muscovite, 3.65 mg, J = 0.0011893 ± 0.5%

4 amu discrimination = 1.01641 ± 0.48%, 40/39K = 0.0505 ± 94.4%, 36/37Ca = 0.0002771 ± 1.6%, 39/37Ca = 0.0007433 ± 8.5%

step	T (C)	t (min.)	36Ar	37Ar	38Ar	39Ar	40Ar	%40Ar*	% 39Ar rlsd	Ca/K	40Ar*/39ArK	Age (Ma)	1s.d.
1	650	12	2.10	0.17	0.51	7.89	864.94	30.6	1.03	0.110053	32.34087	68.09	1.16
2	725	12	1.28	0.15	0.42	14.35	872.74	59.6	1.86	0.054389	34.91955	73.41	0.74
3	800	12	2.47	0.22	1.30	67.64	3028.70	77.1	8.79	0.017224	34.23633	72.00	0.63
4	850	12	1.40	0.18	2.31	157.66	5796.65	93.4	20.49	0.005873	34.25719	72.04	0.58
5	900	12	0.88	0.15	2.22	159.16	5681.04	96.0	20.69	0.004804	34.16745	71.86	0.57
6	950	12	0.80	0.11	1.45	101.73	3699.17	94.6	13.22	0.005420	34.14902	71.82	0.57
7	1000	12	0.81	0.10	1.04	69.08	2581.89	92.1	8.98	0.007680	34.01905	71.55	0.58
8	1075	12	0.76	0.09	1.49	105.39	3800.65	95.0	13.70	0.004294	34.04136	71.60	0.57
9	1130	12	0.28	0.08	1.10	80.76	2845.86	98.6	10.50	0.004959	34.33625	72.21	0.57
10	1200	12	0.21	0.08	0.08	3.15	166.34	85.4	0.41	0.130616	33.88862	71.28	0.69
11	1400	12	0.27	0.08	0.08	2.54	162.42	74.9	0.33	0.155821	33.48676	70.46	0.79

note: isotope beams in mV, rlsd = released, age uncertainty includes J uncertainty, all uncertainties 1 sigma
(36Ar through 40Ar are measured beam intensities, corrected for decay in the age calculations)

	Age (Ma)	1s.d.
Total gas age =	71.86	0.47
Plateau age =	71.85	0.39
Isochron age =	72.18	0.89

IV14, muscovite, 5.82 mg, J = 0.001657 ± 0.5%

4 amu discrimination = 1.02357 ± 0.31%, 40/39K = 0.0002 ± 0.03%, 36/37Ca = 0.00027 ± 2.46%, 39/37Ca = 0.00063 ± 0.98%

step	T (C)	t (min.)	36Ar	37Ar	38Ar	39Ar	40Ar	%40Ar*	% 39Ar rlsd	Ca/K	40Ar*/39ArK	Age (Ma)	1s.d.
1	725	12	3.17	0.12	1.10	38.73	2885.66	68.4	2.99	0.014919	51.20875	146.93	1.03
2	775	12	1.34	0.06	0.88	49.92	2967.91	87.1	3.86	0.005883	52.00727	149.13	0.95
3	820	12	0.83	0.06	1.61	111.44	5994.34	96.0	8.62	0.002592	51.91462	148.88	0.92
4	850	12	0.42	0.06	1.69	125.69	6600.99	98.2	9.72	0.002183	51.85032	148.70	0.92
5	875	12	0.33	0.06	1.76	131.34	6858.29	98.7	10.16	0.002163	51.78167	148.51	0.91
6	900	12	0.33	0.06	1.78	133.20	6975.42	98.7	10.30	0.002241	51.94877	148.97	0.92
7	915	12	0.28	0.04	1.41	106.17	5573.04	98.6	8.21	0.001632	52.00654	149.13	0.92
8	930	12	0.28	0.03	1.34	100.77	5287.03	98.5	7.79	0.001624	51.96076	149.00	0.92
9	945	12	0.27	0.03	1.44	104.80	5501.10	98.7	8.10	0.001332	52.04143	149.23	0.92
10	960	12	0.24	0.02	1.16	87.33	4587.47	98.6	6.75	0.001213	52.03270	149.20	0.92
11	980	12	0.16	0.03	1.04	76.48	3985.43	98.9	5.91	0.001700	51.81218	148.59	0.92
12	1000	12	0.09	0.03	0.88	66.72	3465.76	99.4	5.16	0.002237	51.85722	148.72	0.91
13	1030	12	0.05	0.04	0.92	69.86	3623.94	99.7	5.40	0.002412	51.95459	148.99	0.92
14	1100	12	0.03	0.06	1.03	79.31	4105.45	99.8	6.13	0.003339	51.93061	148.92	0.92
15	1150	12	0.01	0.03	0.11	7.75	402.86	100.0	0.60	0.016771	51.89682	148.83	0.95

16	1400	12	0.02	0.02	0.04	3.60	189.67	99.9	0.28	0.032062	51.81836	148.61	1.04

note: isotope beams in mV, rlsd = released, age uncertainty includes J uncertainty, all uncertainties 1 sigma — Total gas age = 148.85 0.79

(36Ar through 40Ar are measured beam intensities, corrected for decay in the age calculations) — Plateau age = 148.83 0.79 (steps 1-16)

PM1, biotite, 10.21 mg, J = 0.001733302 ± 0.3814%

4 amu discrimination = 1.03795 ± 0.55%, 40/39K = 0.00960 ± 66.73%, 36/37Ca = 0.000276 ± 3.81%, 39/37Ca = 0.000702 ± 1.71%

step	T (C)	t (min.)	36Ar	37Ar	38Ar	39Ar	40Ar	%40Ar*	% 39Ar rlsd	Ca/K	40Ar*/39ArK	Age (Ma)	1s.d.
1	700	12	2.74	0.20	2.38	126.15	3829.24	79.8	6.87	0.028129	24.28778	74.39	0.66
2	725	12	0.99	0.15	2.10	131.75	3482.98	92.2	7.18	0.019600	24.44910	74.88	0.61
3	750	12	0.71	0.16	2.28	148.11	3812.40	95.0	8.07	0.018503	24.52977	75.12	0.60
4	775	12	0.60	0.16	2.16	138.76	3561.85	95.5	7.56	0.020762	24.58945	75.30	0.60
5	810	12	0.62	0.17	2.11	138.52	3553.67	95.4	7.55	0.021559	24.53110	75.12	0.60
6	845	12	0.51	0.16	1.81	121.01	3100.66	95.7	6.59	0.023661	24.58345	75.28	0.60
7	890	12	0.62	0.25	1.88	120.34	3133.02	94.8	6.56	0.035909	24.72350	75.70	0.60
8	940	12	0.68	0.38	2.02	131.14	3427.65	94.7	7.15	0.051437	24.79688	75.92	0.61
9	980	12	0.34	0.33	2.00	135.82	3422.61	97.5	7.40	0.042941	24.62246	75.40	0.59
10	1020	12	0.26	0.37	2.04	140.45	3508.79	98.2	7.65	0.046779	24.59545	75.32	0.59
11	1070	12	0.31	0.50	3.00	211.94	5267.74	98.5	11.55	0.041277	24.58578	75.29	0.59
12	1110	12	0.24	0.86	2.57	181.70	4510.51	98.9	9.90	0.083340	24.61646	75.38	0.59
13	1180	12	0.14	3.10	1.29	88.27	2203.94	99.1	4.81	0.617207	24.70950	75.66	0.59
14	1400	12	0.13	0.64	0.33	21.33	561.81	97.5	1.16	0.528005	24.63480	75.43	0.60

note: isotope beams in mV, rlsd = released, age uncertainty includes J uncertainty, all uncertainties 1 sigma — Total gas age = 75.28 0.40

(36Ar through 40Ar are measured beam intensities, corrected for decay in the age calculations) — Plateau age = 75.31 0.40 (steps 1-14)

Isochron age = 75.71 0.64

IV8, biotite, 3.96 mg, J = 0.0016435 ± 0.5%

4 amu discrimination = 1.02357 ± 0.31%, 40/39K = 0.0002 ± 0.03%, 36/37Ca = 0.00027 ± 2.46%, 39/37Ca = 0.00063 ± 0.98%

step	T (C)	t (min.)	36Ar	37Ar	38Ar	39Ar	40Ar	%40Ar*	% 39Ar rlsd	Ca/K	40Ar*/39ArK	Age (Ma)	1s.d.
1	650	12	8.28	0.13	2.20	45.30	4701.20	49.2	6.05	0.013837	50.86880	146.00	1.19
2	725	12	2.75	0.15	2.47	147.30	8328.82	90.5	19.66	0.004954	51.01282	146.39	0.92
3	775	12	1.64	0.12	2.28	150.02	8166.79	94.2	20.03	0.003982	51.13618	146.73	0.91
4	820	12	1.37	0.12	1.46	92.46	5083.08	92.3	12.34	0.006196	50.54026	145.09	0.91
5	860	12	1.40	0.12	1.24	75.12	4204.93	90.4	10.03	0.008083	50.44130	144.82	0.91
6	900	12	1.37	0.10	1.26	76.64	4294.25	90.9	10.23	0.006645	50.73062	145.61	0.92
7	940	12	1.14	0.12	1.17	72.88	4059.43	92.0	9.73	0.008198	51.04619	146.48	0.92
8	970	12	0.56	0.09	0.64	41.29	2278.86	93.0	5.51	0.011148	51.10606	146.65	0.92

9	1000	12	0.30	0.08	0.35	21.96	1214.11	93.2	2.93	0.018731	51.22617	146.98	0.92
10	1030	12	0.14	0.06	0.15	10.36	572.10	93.2	1.38	0.026475	51.05526	146.51	0.93
11	1400	12	0.30	0.19	0.26	15.77	897.89	90.9	2.11	0.059000	51.36664	147.37	0.98

note: isotope beams in mV, rlsd = released, age uncertainty includes J uncertainty, all uncertainties 1 sigma
(36Ar through 40Ar are measured beam intensities, corrected for decay in the age calculations)

Total gas age =	146.10	0.81
Plateau age = (steps 1-10)	146.13	0.82

Appendix B. Analytical Procedures for Electron Microprobe Chemistry Determinations

Muscovite and biotite grains were mounted in epoxy, stepwise polished down to 1.0 μm corundum paste, and analyzed for major element chemistry using a JEOL 8900 Electron Probe Microanalyzer at the Electron Microanalysis and Imaging Laboratory (EMIL) at the University of Nevada, Las Vegas. A 5 μm diameter beam spotsize was used with a 15 μA beam current and 15 keV accelerating voltage. Eight spot analyses were collected for each sample and a representative analysis for each is presented in Table 1.

Appendix C. $^{40}Ar/^{39}Ar$ data tables for mixed mica samples.

3:1(IV14:NY25), muscovite, 9.20 mg, J = 0.00205557 ± 0.3113%

4 amu discrimination = 1.03441 ± 0.26%, 40/39K = 0.0071 ± 56%, 36/37Ca = 0.00025397 ± 4.51%, 39/37Ca = 0.00068493 ± 2.07%

step	T (C)	t (min.)	36Ar	37Ar	38Ar	39Ar	40Ar	%40Ar*	% 39Ar rlsd	Ca/K	40Ar*/39ArK	Age (Ma)	1s.d.
1	725	12	10.59	0.12	3.57	92.06	6137.52	50.9	3.2	0.036	33.99	121.86	0.75
2	775	12	1.39	0.02	1.23	74.49	3128.33	88.1	2.6	0.009	36.87	131.81	0.61
3	820	12	1.53	0.04	2.74	185.53	7118.49	94.3	6.4	0.006	36.26	129.69	0.58
4	850	12	1.14	0.03	4.43	327.39	11860.89	97.5	11.2	0.003	35.48	127.00	0.57
5	875	12	1.09	0.05	6.64	487.57	18061.60	98.4	16.7	0.003	36.67	131.10	0.58
6	900	12	0.97	0.04	7.04	510.07	19149.24	98.7	17.5	0.002	37.26	133.15	0.59
7	915	12	0.90	0.01	4.92	352.36	13343.97	98.3	12.1	0.001	37.40	133.61	0.59
8	930	12	0.58	0.02	2.72	199.97	7657.46	98.2	6.8	0.003	37.71	134.69	0.60
9	945	12	0.43	0.03	2.09	151.96	5846.33	98.4	5.2	0.005	37.90	135.33	0.60
10	960	12	0.33	0.02	1.60	114.81	4403.71	98.5	3.9	0.004	37.76	134.86	0.60
11	980	12	0.28	0.02	1.36	97.70	3737.85	98.6	3.3	0.007	37.64	134.46	0.59
12	1000	12	0.22	0.02	1.12	80.47	3036.68	98.9	2.8	0.005	37.16	132.79	0.59
13	1030	12	0.21	0.04	1.15	82.50	3050.96	99.1	2.8	0.012	36.45	130.36	0.57
14	1100	12	0.25	0.02	1.55	115.69	3694.66	99.1	4.0	0.005	31.54	113.33	0.50
15	1400	12	0.52	0.02	0.70	47.30	1440.18	92.6	1.6	0.010	27.49	99.17	0.50

note: isotope beams in mV, rlsd = released, age uncertainty includes J uncertainty, all uncertainties 1 sigma — Total gas age = 130.47 0.45

(36Ar through 40Ar are measured beam intensities, corrected for decay in the age calculations)

1:1(IV14:NY25), muscovite, 9.70 mg, J = 0.00203765 ± 0.2866%

4 amu discrimination = 1.03441 ± 0.26%, 40/39K = 0.0071 ± 56%, 36/37Ca = 0.00025397 ± 4.51%, 39/37Ca = 0.00068493 ± 2.07%

step	T (C)	t (min.)	36Ar	37Ar	38Ar	39Ar	40Ar	%40Ar*	% 39Ar rlsd	Ca/K	40Ar*/39ArK	Age (Ma)	1s.d.
1	725	12	10.81	0.14	3.95	104.06	6223.25	50.5	3.5	0.036	30.33	108.19	0.66
2	775	12	1.44	0.04	1.56	101.34	3596.88	89.0	3.4	0.010	31.66	112.79	0.50
3	820	12	1.94	0.07	2.88	199.84	6747.15	92.0	6.8	0.009	31.21	111.24	0.49
4	840	12	0.82	0.04	2.98	222.71	6878.87	96.8	7.5	0.004	30.05	107.21	0.46
5	860	12	0.83	0.06	4.37	326.00	10333.14	97.8	11.0	0.005	31.19	111.16	0.48
6	880	12	0.79	0.05	5.26	390.95	12696.05	98.3	13.2	0.003	32.13	114.40	0.49
7	895	12	0.75	0.05	4.69	349.40	11334.81	98.2	11.8	0.004	32.06	114.17	0.49
8	915	12	0.66	0.01	3.56	264.72	8611.95	98.1	8.9	0.001	32.06	114.17	0.49
9	935	12	0.63	0.02	3.06	224.23	7364.71	97.8	7.6	0.002	32.28	114.92	0.49
10	955	12	0.58	0.01	2.49	185.88	6145.37	97.7	6.3	0.001	32.42	115.39	0.49
11	975	12	0.44	0.01	1.79	133.25	4264.68	97.6	4.5	0.003	31.30	111.55	0.48

12	1000	12	0.33	0.01	1.41	105.04	3322.40	97.8	3.6	0.002	30.97	110.41	0.46
13	1030	12	0.29	0.01	1.27	94.90	2923.93	97.9	3.2	0.004	30.17	107.64	0.46
14	1100	12	0.31	0.02	2.08	161.59	4276.64	98.4	5.5	0.004	26.09	93.46	0.40
15	1400	12	0.67	0.02	1.28	94.02	2371.22	93.3	3.2	0.006	23.34	83.81	0.37

note: isotope beams in mV, rlsd = released, age uncertainty includes J uncertainty, all uncertainties 1 sigma — Total gas age = 110.46 0.36
(36Ar through 40Ar are measured beam intensities, corrected for decay in the age calculations)

1:3(IV14:NY25), muscovite, 9.3 mg, J = 0.00207412 ± 0.4310%
4 amu discrimination = 1.03441 ± 0.26%, 40/39K = 0.0071 ± 56%, 36/37Ca = 0.00025397 ± 4.51%, 39/37Ca = 0.00068493 ± 2.07%

step	T (C)	t (min.)	36Ar	37Ar	38Ar	39Ar	40Ar	%40Ar*	% 39Ar rlsd	Ca/K	40Ar*/39ArK	Age (Ma)	1s.d.
1	725	12	10.00	0.19	3.82	109.82	5575.05	49.0	3.8	0.047	24.88	90.79	0.63
2	775	12	1.78	0.07	1.59	98.11	2988.19	83.8	3.4	0.020	25.41	92.66	0.52
3	820	12	2.55	0.07	3.15	212.02	6018.54	88.3	7.4	0.009	25.10	91.57	0.50
4	850	12	1.33	0.06	4.55	340.72	8783.32	96.0	11.9	0.004	24.83	90.59	0.49
5	875	12	1.28	0.08	6.51	493.39	13065.36	97.4	17.2	0.004	25.92	94.46	0.51
6	900	12	1.16	0.05	6.32	468.74	12375.78	97.6	16.4	0.003	25.88	94.32	0.51
7	915	12	0.81	0.02	3.44	258.02	6884.24	97.1	9.0	0.002	25.96	94.63	0.51
8	930	12	0.62	0.02	2.47	185.93	5007.06	97.2	6.5	0.003	26.16	95.32	0.51
9	945	12	0.49	0.02	1.77	132.22	3591.60	97.1	4.6	0.004	26.29	95.79	0.51
10	960	12	0.36	0.01	1.25	91.03	2434.70	97.3	3.2	0.003	25.80	94.06	0.51
11	980	12	0.33	0.03	1.07	78.93	2079.94	97.2	2.8	0.010	25.33	92.38	0.50
12	1000	12	0.29	0.01	0.89	65.17	1706.67	97.3	2.3	0.002	25.11	91.61	0.50
13	1030	12	0.28	0.03	0.91	68.28	1749.13	97.5	2.4	0.010	24.62	89.85	0.48
14	1400	12	1.21	0.05	3.51	263.94	5915.05	94.9	9.2	0.005	21.24	77.79	0.42

note: isotope beams in mV, rlsd = released, age uncertainty includes J uncertainty, all uncertainties 1 sigma — Total gas age = 91.91 0.43
(36Ar through 40Ar are measured beam intensities, corrected for decay in the age calculations) — Pseudo plateau age = 94.68 0.51
49.1% of release

3:1(IV8:PM1), biotite, 9.80 mg, J = 0.00197456 ± 0.3682%
4 amu discrimination = 1.03441 ± 0.26%, 40/39K = 0.0071 ± 56%, 36/37Ca = 0.00025397 ± 4.51%, 39/37Ca = 0.00068493 ± 2.07%

step	T (C)	t (min.)	36Ar	37Ar	38Ar	39Ar	40Ar	%40Ar*	% 39Ar rlsd	Ca/K	40Ar*/39ArK	Age (Ma)	1s.d.
1	650	12	10.47	0.41	9.15	262.58	12587.02	76.3	10.1	0.045	36.81	126.59	0.67
2	680	12	4.26	0.09	5.07	171.67	8121.70	85.1	6.6	0.014	40.52	138.86	0.70
3	710	12	2.52	0.09	6.60	249.33	10714.18	93.4	9.5	0.010	40.37	138.38	0.68
4	735	12	2.55	0.09	6.74	251.74	10789.96	93.4	9.6	0.011	40.26	138.00	0.68
5	770	12	1.51	0.13	6.96	270.56	11009.15	96.2	10.4	0.014	39.39	135.12	0.65
6	810	12	0.94	0.07	4.46	182.74	7096.50	96.4	7.0	0.011	37.64	129.32	0.63

7	845	12	0.86	0.07	3.57	147.72	5755.43	96.0	5.7	0.014	37.57	129.11	0.63
8	875	12	0.88	0.05	3.86	157.16	6302.58	96.3	6.0	0.010	38.79	133.14	0.64
9	910	12	1.40	0.19	6.44	261.64	10629.92	96.4	10.0	0.021	39.40	135.16	0.65
10	950	12	1.30	0.28	8.14	370.62	13161.78	97.3	14.2	0.022	34.77	119.81	0.58
11	980	12	0.42	0.46	3.39	187.80	5508.43	98.2	7.2	0.070	28.91	100.14	0.49
12	1020	12	0.15	0.81	0.97	56.16	1560.60	98.7	2.1	0.412	27.25	94.55	0.46
13	1070	12	0.10	0.26	0.33	20.93	560.38	99.1	0.8	0.354	25.67	89.22	0.49
14	1400	12	0.26	0.19	0.40	21.43	619.77	93.4	0.8	0.251	25.59	88.92	0.48

note: isotope beams in mV, rlsd = released, age uncertainty includes J uncertainty, all uncertainties 1 sigma — Total gas age = 127.93 0.48

(36Ar through 40Ar are measured beam intensities, corrected for decay in the age calculations)

1:1(IV8:PM1), biotite, 8.9 mg, J = 0.00208115 ± 0.5040%

4 amu discrimination = 1.03441 ± 0.26%, 40/39K = 0.0071 ± 56%, 36/37Ca = 0.00025397 ± 4.51%, 39/37Ca = 0.00068493 ± 2.07%

step	T (C)	t (min.)	36Ar	37Ar	38Ar	39Ar	40Ar	%40Ar*	% 39Ar rlsd	Ca/K	40Ar*/39ArK	Age (Ma)	1s.d.
1	650	12	12.00	0.48	8.59	245.05	11417.11	70.1	10.5	0.052	32.82	119.21	0.78
2	700	12	4.43	0.19	7.90	293.49	11676.12	89.4	12.6	0.017	35.71	129.33	0.77
3	725	12	2.03	0.08	5.15	201.44	7561.66	92.7	8.6	0.011	34.88	126.44	0.75
4	750	12	0.76	0.07	4.00	171.37	5930.21	96.8	7.3	0.011	33.56	121.79	0.72
5	775	12	0.60	0.05	3.08	141.21	4535.84	96.9	6.0	0.010	31.11	113.17	0.67
6	810	12	0.64	0.07	2.60	125.37	3913.04	96.1	5.4	0.014	29.93	109.01	0.65
7	845	12	0.58	0.06	2.43	110.20	3588.72	96.2	4.7	0.015	31.24	113.65	0.68
8	875	12	0.56	0.06	2.33	102.86	3489.68	96.3	4.4	0.016	32.58	118.35	0.70
9	910	12	0.73	0.11	3.02	127.72	4502.20	96.2	5.5	0.024	33.86	122.86	0.72
10	950	12	0.80	0.21	4.10	200.05	6277.21	96.9	8.6	0.028	30.45	110.85	0.66
11	980	12	0.46	0.21	3.40	207.56	5228.17	98.2	8.9	0.027	24.73	90.56	0.54
12	1020	12	0.35	0.33	3.04	210.06	4704.01	98.6	9.0	0.041	22.08	81.04	0.48
13	1070	12	0.27	0.67	1.85	131.74	2863.69	98.5	5.6	0.135	21.30	78.24	0.47
14	1110	12	0.21	0.91	0.59	41.28	951.89	97.5	1.8	0.588	21.71	79.74	0.48
15	1180	12	0.29	0.96	0.32	17.27	472.89	89.6	0.7	1.473	22.69	83.23	0.54
16	1400	12	0.65	0.33	0.22	7.87	356.15	54.9	0.3	1.118	21.77	79.94	0.60

note: isotope beams in mV, rlsd = released, age uncertainty includes J uncertainty, all uncertainties 1 sigma — Total gas age = 110.175043 0.53

(36Ar through 40Ar are measured beam intensities, corrected for decay in the age calculations)

1:3(IV8:PM1), biotite, 10.50 mg, J = 0.00199605 ± 0.3487%

4 amu discrimination = 1.03441 ± 0.26%, 40/39K = 0.0071 ± 56%, 36/37Ca = 0.00025397 ± 4.51%, 39/37Ca = 0.00068493 ± 2.07%

step	T (C)	t (min.)	36Ar	37Ar	38Ar	39Ar	40Ar	%40Ar*	% 39Ar rlsd	Ca/K	40Ar*/39ArK	Age (Ma)	1s.d.

1	650	12	8.33	0.50	5.54	145.58	6347.89	62.6	5.6	0.098	27.46	96.28	0.55
2	680	12	5.36	0.12	3.50	118.42	5409.45	71.9	4.5	0.029	33.01	115.11	0.62
3	710	12	2.39	0.13	3.63	156.87	5697.01	88.3	6.0	0.024	32.19	112.35	0.55
4	735	12	1.16	0.10	3.57	171.30	5634.78	94.4	6.6	0.017	31.18	108.92	0.52
5	770	12	0.72	0.09	3.73	196.41	5887.36	96.8	7.5	0.012	29.13	101.97	0.48
6	810	12	0.88	0.13	3.57	201.95	5561.05	95.8	7.8	0.019	26.47	92.90	0.44
7	845	12	0.62	0.10	2.48	136.92	3905.28	95.9	5.3	0.021	27.42	96.12	0.46
8	875	12	0.50	0.09	2.19	115.65	3437.56	96.3	4.4	0.021	28.68	100.42	0.48
9	910	12	0.58	0.16	2.49	126.55	3960.60	96.3	4.9	0.036	30.20	105.60	0.50
10	950	12	0.73	0.29	3.24	173.05	5174.40	96.4	6.6	0.048	28.90	101.19	0.48
11	980	12	0.45	0.29	2.98	197.42	4933.76	97.8	7.6	0.042	24.51	86.18	0.41
12	1020	12	0.33	0.35	3.66	264.46	5950.01	98.8	10.2	0.037	22.30	78.55	0.37
13	1070	12	0.34	0.56	4.67	348.15	7516.17	99	13.4	0.046	21.46	75.66	0.36
14	1400	12	0.72	4.60	3.52	252.19	5569.67	97	9.7	0.515	21.45	75.63	0.36
											Total gas age =	92.74	0.36

note: isotope beams in mV, rlsd = released, age uncertainty includes J uncertainty, all uncertainties 1 sigma
(36Ar through 40Ar are measured beam intensities, corrected for decay in the age calculations)

APPENDIX D

CHAPTER 4 APPENDICES

Appendix A

$^{40}Ar/^{39}Ar$ data for samples from the Clark Mountains, Mohawk Hill, and Mescal Range

Clark Mountains

Gabe, biotite, 7.14 mg — J = 0.00175643 ± 0.0564 %

4 amu discrimination = 1.0274 ± 0.35 % — 36/37Ca = 0.000284 ± 5.75 %

40/39K = 0.010817 ± 99.4 % — 39/37Ca = 0.000685 ± 2.37 %

step	T (C)	t (min.)	36Ar	37Ar	38Ar	39Ar	40Ar	% 39Ar rlsd	%40Ar*	Ca/K	40Ar*/39ArK	Age (Ma)	1s.d.
1	650	12	80.61	0.52	17.85	55.65	24165.44	5.1	1.4	0.066	5.248	16.55	4.84
2	725	12	48.08	0.96	20.43	244.56	20419.17	22.3	30.4	0.028	25.410	78.77	0.90
3	775	12	9.15	0.37	9.17	160.50	7329.68	14.7	63.2	0.016	28.951	89.48	0.49
4	820	12	4.38	0.49	5.41	101.67	4227.73	9.3	69.6	0.033	28.999	89.63	0.45
5	860	12	4.63	0.86	4.04	70.95	3339.25	6.5	59.3	0.085	27.929	86.40	0.50
6	900	12	8.59	1.66	4.91	74.30	4523.64	6.8	44.1	0.158	26.820	83.04	0.66
7	940	12	7.73	1.71	5.45	88.13	4734.37	8.0	51.9	0.137	27.918	86.36	0.58
8	970	12	4.88	0.86	5.07	89.49	4057.12	8.2	64.8	0.067	29.377	90.76	0.50
9	1000	12	3.97	0.79	4.94	88.48	3868.73	8.1	70.0	0.063	30.631	94.54	0.47
10	1030	12	2.39	1.68	2.95	52.94	2323.65	4.8	70.2	0.225	30.745	94.88	0.47
11	1400	12	2.27	28.50	3.71	68.13	2831.58	6.2	77.4	2.976	32.142	99.08	0.44
											Total gas age =	83.88	0.46

Scott, amphibole, 10.96 mg — J = 0.0017289 ± 0.0954 %

4 amu discrimination = 1.03795 ± 0.55 % — 36/37Ca = 0.000284 ± 5.75 %

40/39K = 0.010817 ± 99.4 % — 39/37Ca = 0.000685 ± 2.37 %

step	T (C)	t (min.)	36Ar	37Ar	38Ar	39Ar	40Ar	% 39Ar rlsd	%40Ar*	Ca/K	40Ar*/39ArK	Age (Ma)	1s.d.
1	750	12	122.61	12.75	23.82	1.88	36612.30	1.9	1.0	29.516	148.845	413.13	386.18
2	850	12	13.39	24.54	3.56	2.91	4866.54	3.0	18.8	36.118	321.510	797.45	19.54
3	950	12	17.93	278.23	25.79	34.13	14644.74	34.9	64.2	35.369	284.076	720.80	5.11
4	990	12	10.57	117.98	16.13	21.61	6638.80	22.1	53.3	23.459	167.595	459.05	4.35
5	1020	12	6.04	50.32	7.08	9.66	3093.48	9.9	42.7	22.230	139.358	389.44	4.51
6	1050	12	3.07	20.89	2.64	3.91	1485.52	4.0	39.4	22.761	151.561	419.85	6.00
7	1070	12	1.01	10.98	1.19	2.08	610.52	2.1	52.7	22.485	154.652	427.48	4.06
8	1095	12	1.36	13.57	1.39	2.29	763.78	2.3	48.5	25.258	162.740	447.27	4.52

9	1130	12	1.49	24.07	2.77	4.41	1115.96	4.5	62.1	23.338	159.046	438.26	3.46
10	1155	12	0.45	13.00	1.61	2.46	573.57	2.5	80.0	22.616	185.842	502.65	3.17
11	1200	12	0.46	16.10	1.88	2.82	710.87	2.9	83.6	24.443	211.431	562.06	3.19
12	1250	12	0.48	32.59	3.75	5.23	1391.29	5.4	91.6	26.697	247.549	642.73	3.60
13	1400	12	0.49	40.27	3.28	4.37	1711.54	4.5	93.1	39.718	373.522	898.82	4.22
											Total gas age =	582.88	3.09

Mohawk Hill

JK05MH-2, biotite, 7.26 mg J = 0.00204576 ± 0.2889 %

4 amu discrimination = 1.04252 ± 0.42 % 36/37Ca = 0.0002539 ± 4.51 %

40/39K = 0.0071 ± 0.56 % 39/37Ca = 0.00068493 ± 2.07 %

step	T (C)	t (min.)	36Ar	37Ar	38Ar	39Ar	40Ar	% 39Ar rlsd	%40Ar*	Ca/K	40Ar*/39ArK	Age (Ma)	1s.d.
1	650	12	3.76	0.27	2.46	57.55	3422.58	3.2	67.7	0.138	40.472	143.51	0.95
2	680	12	0.58	0.07	1.58	46.02	2250.82	2.5	92.8	0.039	45.609	160.93	0.85
3	710	12	0.44	0.06	2.18	66.44	2877.91	3.6	96.0	0.029	41.757	147.88	0.75
4	735	12	0.38	0.07	2.68	83.04	3390.21	4.6	97.1	0.025	39.833	141.33	0.71
5	770	12	0.39	0.06	3.90	122.53	4773.52	6.7	97.9	0.014	38.366	136.31	0.68
6	810	12	0.53	0.07	5.09	159.38	6021.32	8.8	97.7	0.014	37.147	132.14	0.66
7	845	12	0.49	0.10	4.61	143.61	5365.49	7.9	97.6	0.022	36.687	130.56	0.65
8	875	12	0.44	0.12	3.39	107.27	3988.27	5.9	97.1	0.033	36.315	129.28	0.65
9	910	12	0.48	0.20	2.71	87.34	3254.48	4.8	96.1	0.066	35.960	128.06	0.65
10	950	12	0.47	0.23	2.62	86.16	3173.04	4.7	96.2	0.078	35.558	126.68	0.65
11	980	12	0.36	0.17	2.50	81.97	3023.15	4.5	97.0	0.058	35.916	127.91	0.65
12	1020	12	0.33	0.24	2.96	95.05	3513.11	5.2	97.7	0.073	36.279	129.16	0.66
13	1070	12	0.37	0.45	3.96	125.55	4724.44	6.9	98.1	0.108	37.114	132.03	0.66
14	1100	12	0.31	0.68	5.27	162.33	6255.17	8.9	98.9	0.129	38.340	136.23	0.68
15	1400	12	0.61	4.35	12.99	396.21	15602.35	21.8	99.1	0.342	39.319	139.57	0.69
											Total gas age =	135.38	0.49

Mescal Range

JK05MR-1, amphibole, 8.10 mg J = 0.00202566 ± 0.3446 %

4 amu discrimination = 1.03181 ± 0.39 % 36/37Ca = 0.00027178 ± 4.66 %

40/39K = 0.0051 ± 63 % 39/37Ca = 0.00067376 ± 0.992 %

step	T (C)	t (min.)	36Ar	37Ar	38Ar	39Ar	40Ar	% 39Ar rlsd	%40Ar*	Ca/K	40Ar*/39ArK	Age (Ma)	1s.d.
1	750	12	2.63	1.37	0.53	1.90	936.41	0.2	17.9	5.787	86.484	291.23	6.06
2	850	12	0.43	3.90	0.16	5.09	488.76	0.7	77.9	6.188	73.021	248.87	1.42
3	950	12	0.28	3.07	0.20	6.83	521.82	0.9	88.8	3.624	64.942	222.96	1.17
4	990	12	0.16	9.00	0.44	14.35	740.72	1.8	97.4	5.082	49.104	171.08	0.89
5	1020	12	0.25	37.25	1.64	57.31	2679.20	7.4	98.6	5.275	46.285	161.68	0.81
6	1050	12	0.27	37.75	1.63	57.79	2696.11	7.5	98.4	5.304	46.105	161.08	0.81
7	1070	12	0.21	30.88	1.33	47.05	2189.78	6.1	98.8	5.329	46.060	160.93	0.81
8	1095	12	0.38	73.92	3.15	112.91	5232.85	14.6	98.8	5.326	46.196	161.38	0.82
9	1110	12	0.45	77.86	3.34	120.47	5475.07	15.5	98.6	5.261	45.175	157.97	0.79
10	1130	12	0.47	63.41	2.77	98.94	4510.89	12.8	98.1	5.218	45.013	157.43	0.79
11	1150	12	0.49	51.65	2.26	79.73	3711.82	10.3	97.5	5.273	45.589	159.35	0.80
12	1180	12	0.55	52.69	2.22	78.23	3690.61	10.1	97.0	5.485	45.972	160.63	0.82
13	1220	12	0.53	36.01	1.48	51.53	2474.43	6.6	95.6	5.692	45.876	160.31	0.82
14	1400	12	0.61	37.16	1.28	43.52	2221.71	5.6	94.7	6.960	48.069	167.63	0.86
											Total gas age =	161.93	0.70
											Isochron age =	160.70	5.50

Appendix B

$^{40}Ar/^{39}Ar$ data for samples from the Oro Wash and Ji intrusions, New Trail Canyon, eastern Ivanpah Mountains

JK03IV-1, amphibole, 11.33 mg J= 0.00173734 ± 0.0656 %
4 amu discrimination = 1.0274 ± 0.34 % 36/37Ca = 0.000284 ± 5.75 %
40/39K = 0.010817 ± 99.4 % 39/37Ca = 0.000685 ± 2.37 %

step	T (C)	t (min.)	36Ar	37Ar	38Ar	39Ar	40Ar	% 39Ar rlsd	%40Ar*	Ca/K	40Ar*/39ArK	Age (Ma)	1s.d.
1	750	12	111.30	1.63	20.97	2.44	32204.12	1.5	-2.1	4.716	-310.710	-1400.17	479.25
2	850	12	59.39	2.37	11.45	6.05	17499.16	3.8	-0.3	2.765	-14.851	-47.16	33.46
3	950	12	18.25	10.88	4.44	10.18	5781.86	6.4	6.8	7.523	38.128	115.71	6.11
4	990	12	9.07	22.44	4.11	9.08	3097.47	5.7	13.7	17.464	47.291	142.45	3.43
5	1020	12	5.53	35.42	5.61	12.51	2280.40	7.9	29.0	20.057	53.784	161.16	1.90
6	1050	12	3.24	45.19	8.05	19.12	1968.10	12.1	52.4	16.757	54.806	164.09	1.01
7	1070	12	1.64	31.33	5.89	15.23	1306.07	9.6	64.3	14.560	55.676	166.57	0.88
8	1095	12	1.72	36.46	6.35	18.09	1476.35	11.4	67.1	14.277	55.365	165.68	0.81
9	1130	12	1.99	34.18	5.60	15.37	1458.01	9.7	61.3	15.763	58.697	175.19	1.05
10	1155	12	1.18	29.96	5.19	12.82	1099.54	8.1	70.5	16.562	60.765	181.06	0.84
11	1200	12	1.37	50.85	9.03	22.18	1655.23	14.0	77.5	16.304	58.475	174.55	0.75
12	1250	12	1.02	45.72	7.70	16.94	1251.00	10.7	78.3	19.205	58.477	174.56	0.75
13	1400	12	0.504	22.296	3.471	6.984	543.212	4.4	78.3	22.706	59.295	176.89	0.83
											Total gas age =	142.19	0.86

JK03IV-1, biotite, 8.47 mg J = 0.00175123 ± 0.0617 %
4 amu discrimination = 1.0274 ± 0.34 % 36/37Ca = 0.000284 ± 5.75 %
40/39K = 0.010817 ± 99.4 % 39/37Ca = 0.000685 ± 2.37 %

step	T (C)	t (min.)	36Ar	37Ar	38Ar	39Ar	40Ar	% 39Ar rlsd	%40Ar*	Ca/K	40Ar*/39ArK	Age (Ma)	1s.d.
1	650	12	81.14	0.60	16.33	15.79	23953.31	1.1	-0.1	0.271	-4.993	-15.85	16.75
2	690	12	13.30	0.30	4.23	22.75	4905.30	1.7	19.9	0.093	42.666	130.00	2.18
3	720	12	7.56	0.32	4.95	47.16	4447.78	3.4	49.9	0.047	47.105	143.00	0.96
4	750	12	3.34	0.27	5.72	69.08	4309.60	5.0	77.4	0.027	48.361	146.66	0.76
5	780	12	3.16	0.26	7.19	87.23	5164.34	6.3	82.1	0.020	48.769	147.85	0.61
6	820	12	2.95	0.32	9.76	122.76	6876.26	8.9	87.5	0.018	49.197	149.10	0.58
7	860	12	2.16	0.32	8.95	113.28	6191.10	8.2	89.9	0.020	49.314	149.44	0.57
8	900	12	3.11	0.40	7.66	92.73	5459.04	6.7	83.4	0.031	49.232	149.20	0.59
9	940	12	4.86	0.57	7.51	87.20	5723.73	6.3	75.1	0.047	49.424	149.76	0.66
10	970	12	3.97	0.55	6.60	76.39	4949.30	5.5	76.6	0.051	49.703	150.57	0.65

11	1000	12	3.43	0.55	6.79	80.11	4983.79	5.8	80.0	0.049	49.852	151.00	0.62
12	1030	12	3.05	0.61	7.00	85.09	5114.92	6.2	82.7	0.051	49.799	150.85	0.64
13	1400	12	5.03	7.78	38.71	493.84	25880.24	35.8	94.4	0.117	49.701	150.56	0.55
											Total gas age =	149.09	0.39
											plateau age =	150.03	0.43

JK03IV-1, K-feldspar, 13.15 mg
4 amu discrimination = 1.0312 ± 0.11 %
40/39K = 0.01868 ± 52.3 %

J = 0.00164495 ± 0.1842 %
36/37Ca = 0.00025867 ± 10.31 %
39/37Ca = 0.00080803 ± 27.74 %

step	T (C)	t (min.)	36Ar	37Ar	38Ar	39Ar	40Ar	% 39Ar rlsd	%40Ar*	Ca/K	40Ar*/39ArK	Age (Ma)	1s.d.
1	448	18	0.93	0.01	0.20	0.34	289.40	0.0	5.2	0.000	41.363	118.75	24.82
2	473	18	0.22	0.04	0.05	0.44	69.62	0.0	12.2	0.385	16.262	47.63	4.32
3	473	43	0.26	0.18	0.07	0.83	87.07	0.0	18.4	1.187	13.745	40.33	0.33
4	514	18	0.14	0.50	0.07	1.52	62.94	0.0	41.9	1.849	14.456	42.40	0.14
5	514	43	0.22	0.48	0.11	2.69	99.39	0.1	50.0	1.008	14.004	41.09	0.12
6	555	18	0.14	0.39	0.11	4.51	109.90	0.1	70.3	0.492	15.522	45.49	0.12
7	555	43	0.20	0.23	0.16	7.69	191.31	0.2	80.0	0.167	17.454	51.07	0.15
8	596	18	0.14	0.16	0.19	10.70	254.74	0.3	88.8	0.079	20.109	58.71	0.15
9	596	43	0.20	0.15	0.28	16.01	421.04	0.4	92.8	0.050	22.938	66.82	0.15
10	638	18	0.15	0.15	0.29	17.89	517.33	0.5	94.1	0.044	26.645	77.39	0.17
11	638	43	0.21	0.18	0.37	24.25	770.14	0.7	95.8	0.041	29.517	85.53	0.19
12	679	19	0.16	0.16	0.36	22.33	777.68	0.6	95.6	0.038	32.910	95.11	0.20
13	679	44	0.20	0.15	0.41	27.83	1005.80	0.8	97.1	0.030	34.353	99.17	0.23
14	720	19	0.16	0.14	0.33	21.72	831.20	0.6	96.0	0.035	36.349	104.77	0.31
15	720	44	0.20	0.15	0.40	26.04	1010.82	0.7	97.0	0.032	36.845	106.16	0.23
16	761	19	0.13	0.13	0.28	18.61	736.36	0.5	96.6	0.038	37.745	108.67	0.23
17	761	44	0.21	0.17	0.33	23.36	918.43	0.7	96.5	0.039	37.028	106.67	0.23
18	802	19	0.16	0.13	0.25	17.16	683.04	0.5	96.1	0.042	37.367	107.62	0.24
19	843	19	0.30	0.20	0.47	26.80	1100.27	0.8	93.8	0.041	38.039	109.50	0.30
20	884	19	0.41	0.24	0.60	35.35	1478.72	1.0	93.2	0.038	38.696	111.33	0.25
21	910	19	0.48	0.21	0.60	35.38	1545.23	1.0	92.1	0.033	39.941	114.80	0.28
22	935	19	0.75	0.23	0.79	41.33	1944.19	1.2	89.6	0.031	41.967	120.43	0.26
23	961	19	1.15	0.29	1.08	54.48	2747.68	1.5	88.7	0.030	44.497	127.44	0.29
24	976	19	1.29	0.29	1.24	61.56	3196.70	1.7	89.0	0.027	46.066	131.77	0.28
25	1002	19	2.08	0.46	2.05	95.74	5145.17	2.7	88.6	0.028	47.647	136.13	0.29
26	1018	19	1.99	0.47	2.19	106.45	5667.55	3.0	90.1	0.026	48.037	137.20	0.29

27	1033	19	1.98	0.56	2.42	122.17	6504.69	3.4	91.4	0.026	48.772	139.22	0.30
28	1048	19	1.89	0.57	2.60	133.08	7082.81	3.7	92.5	0.025	49.351	140.81	0.30
29	1064	19	1.82	0.60	2.79	143.37	7659.75	4.0	93.4	0.024	50.014	142.63	0.30
30	1074	19	1.47	0.52	2.51	132.32	7060.92	3.7	94.3	0.023	50.423	143.75	0.31
31	1084	19	1.34	0.47	2.50	133.68	7188.93	3.7	94.9	0.020	51.155	145.76	0.32
32	1089	24	1.31	0.47	2.72	145.39	7828.86	4.1	95.5	0.019	51.542	146.82	0.31
33	1089	29	1.16	0.35	2.45	133.94	7270.58	3.8	95.8	0.015	52.084	148.30	0.32
34	1089	29	0.90	0.24	1.86	104.14	5681.41	2.9	96.0	0.013	52.379	149.11	0.32
35	1089	39	0.88	0.21	1.81	99.45	5471.61	2.8	96.0	0.012	52.786	150.22	0.32
36	1089	59	1.13	0.22	2.17	117.49	6538.74	3.3	95.7	0.010	53.201	151.35	0.32
37	1089	74	1.25	0.20	2.13	115.61	6531.68	3.2	95.3	0.010	53.670	152.63	0.33
38	1089	74	1.11	0.16	1.78	94.62	5402.58	2.7	95.0	0.009	54.011	153.56	0.33
39	1089	74	1.03	0.13	1.49	79.70	4602.81	2.2	94.7	0.009	54.305	154.36	0.33
40	1089	74	0.94	0.10	1.33	69.41	4051.25	1.9	94.6	0.008	54.748	155.57	0.33
41	1089	89	1.05	0.10	1.34	69.59	4092.06	1.9	94.1	0.008	54.725	155.50	0.34
42	1089	119	1.28	0.11	1.48	75.36	4491.36	2.1	93.4	0.008	54.978	156.19	0.33
43	1089	149	1.51	0.09	1.55	76.65	4629.94	2.1	92.5	0.007	55.013	156.29	0.33
44	1141	19	0.62	0.07	1.04	52.84	3133.91	1.5	95.7	0.007	56.243	159.63	0.34
45	1200	20	2.62	0.33	4.78	253.59	14745.97	7.1	95.1	0.008	55.465	157.52	0.34
46	1230	20	2.71	0.33	5.70	317.46	18262.44	8.9	95.9	0.006	55.374	157.27	0.33
47	1300	20	2.11	0.27	4.73	271.04	15612.47	7.6	96.6	0.006	55.682	158.11	0.63
48	1350	20	0.53	0.06	0.95	53.80	3121.10	1.5	98.0	0.007	55.557	157.77	0.33
49	1400	20	0.53	0.05	0.77	44.44	2604.20	1.2	97.5	0.006	55.492	157.59	0.34
50	1500	20	0.61	0.04	0.60	30.45	1867.43	0.9	95.1	0.007	55.846	158.55	0.34
											Total gas age =	144.63	0.20

JK03IV-3, amphibole, 6.67 mg
4 amu discrimination = 1.04252 ± 0.42 %
40/39K = 0.0071 ± 56 %

J = 0.00198425 ± 0.3618 %
36/37Ca = 0.00025397 ± 4.51 %
39/37Ca = 0.00068493 ± 2.07 %

step	T (C)	t (min.)	36Ar	37Ar	38Ar	39Ar	40Ar	% 39Ar rlsd	%40Ar*	Ca/K	40Ar*/39ArK	Age (Ma)	1s.d.
1	750	12	2.43	0.60	0.74	5.03	1095.64	3.9	35.0	3.771	75.668	252.37	2.98
2	850	12	0.33	0.41	0.36	6.76	391.03	5.2	77.9	1.914	43.836	150.47	0.96
3	950	12	0.37	1.68	0.69	10.20	615.81	7.9	85.1	5.202	50.680	172.87	1.01
4	990	12	0.31	4.00	1.16	8.32	553.55	6.4	87.2	15.340	57.729	195.65	1.12
5	1020	12	0.28	5.95	2.04	11.68	664.66	9.0	91.0	16.268	51.907	176.85	1.00
6	1050	12	0.27	8.75	3.45	18.04	908.29	13.9	94.0	15.504	47.772	163.39	0.89

7	1070	12	0.17	5.79	2.35	13.33	651.66	10.3	95.9	13.874	46.911	160.57	0.87
8	1095	12	0.17	5.75	2.33	13.96	680.99	10.8	95.9	13.154	46.823	160.28	0.86
9	1110	12	0.10	1.61	0.64	4.51	241.78	3.5	97.4	11.458	49.312	168.41	0.91
10	1130	12	0.13	1.82	0.68	4.11	244.58	3.2	92.8	14.202	52.314	178.18	1.02
11	1150	12	0.16	2.63	0.96	4.31	284.51	3.3	91.4	19.585	58.221	197.23	1.13
12	1180	12	0.15	2.58	0.90	3.98	281.66	3.1	91.5	20.813	62.441	210.72	1.17
13	1220	12	0.18	2.88	0.95	4.41	299.93	3.4	89.2	21.015	58.832	199.19	1.11
14	1400	12	0.70	23.07	4.45	21.15	1360.22	16.3	88.5	35.233	58.396	197.79	1.12
											Total gas age =	179.61	0.77

JK03IV-3, biotite, 4.7 mg
4 amu discrimination = 1.03181 ± 0.39 %
40/39K = 0.0051 ± 63 %

J = 0.00204263 ± 0.4019 %
36/37Ca = 0.00027178 ± 4.66 %
39/37Ca = 0.00067376 ± 0.992 %

step	T (C)	t (min.)	36Ar	37Ar	38Ar	39Ar	40Ar	% 39Ar rlsd	%40Ar*	Ca/K	40Ar*/39ArK	Age (Ma)	1s.d.
1	650	12	1.78	0.23	0.41	1.84	540.77	0.2	2.9	0.959	7.879	28.80	8.23
2	700	12	0.66	0.31	0.29	3.76	249.34	0.4	25.3	0.624	15.622	56.67	1.00
3	725	12	0.44	0.73	0.39	7.38	245.29	0.8	52.1	0.775	16.180	58.66	0.54
4	750	12	0.56	0.60	0.48	9.20	395.69	1.1	61.7	0.514	25.552	91.79	0.67
5	775	12	0.56	0.48	0.60	11.96	599.93	1.4	75.0	0.314	36.769	130.65	0.83
6	810	12	0.65	0.89	1.60	35.96	1594.82	4.1	89.1	0.195	39.365	139.53	0.80
7	845	12	0.32	1.44	2.37	56.47	2462.20	6.5	97.0	0.202	42.302	149.52	0.82
8	875	12	0.28	1.44	3.17	74.04	3236.19	8.5	98.1	0.155	42.977	151.80	0.82
9	910	12	0.24	1.07	3.27	76.10	3351.22	8.7	98.7	0.112	43.407	153.26	0.83
10	950	12	0.29	1.20	3.37	77.91	3449.59	8.9	98.3	0.122	43.483	153.52	0.83
11	980	12	0.27	1.33	2.73	61.90	2783.11	7.1	98.1	0.170	43.984	155.21	0.85
12	1020	12	0.31	2.31	3.28	73.96	3303.94	8.5	98.1	0.249	43.778	154.52	0.84
13	1100	12	0.41	4.75	6.65	152.32	6739.14	17.4	98.8	0.250	43.787	154.55	0.84
14	1180	12	0.38	8.23	7.86	179.75	7873.89	20.6	99.1	0.367	43.526	153.66	0.83
15	1400	12	0.27	3.79	2.26	50.93	2341.83	5.8	98.3	0.595	44.786	157.92	0.86
											Total gas age =	150.74	0.62
											Plateau age =	154.11	0.77

Appendix C
$^{40}Ar/^{39}Ar$ data for samples from the Ivanpah Pluton

JK06IV-1, amphibole, 6.94 mg
4 amu discrimination = 1.03432 ± 0.45 %
40/39K = 0.0024333 ± 76.1 %
J = 0.00188779 ± 0.2151 %
36/37Ca = 0.0002575 ± 1.61 %
39/37Ca = 0.00070416 ± 10.06 %

step	T (C)	t (min.)	36Ar	37Ar	38Ar	39Ar	40Ar	% 39Ar rlsd	%40Ar*	Ca/K	40Ar*/39ArK	Age (Ma)	1s.d.
1	750	12	1.34	2.51	0.39	2.22	645.25	1.6	39.2	6.189	114.354	352.63	4.39
2	850	12	0.22	1.78	0.12	1.10	133.95	0.8	55.6	8.952	66.027	211.92	1.93
3	950	12	0.20	9.86	0.34	2.83	209.52	2.0	76.6	19.243	56.853	183.92	1.11
4	990	12	0.20	21.73	1.21	5.42	391.68	3.9	88.3	22.120	64.832	208.30	1.10
5	1020	12	0.25	37.60	2.79	10.88	685.98	7.8	91.6	19.066	58.969	190.42	0.98
6	1050	12	0.28	52.69	3.88	16.84	971.49	12.0	93.3	17.271	55.030	178.31	0.89
7	1070	12	0.23	32.28	2.16	10.58	614.95	7.5	91.5	16.827	54.128	175.52	0.89
8	1095	12	0.24	39.27	2.47	13.37	784.08	9.5	92.8	16.209	55.480	179.70	0.93
9	1110	12	0.19	22.16	1.39	7.23	433.36	5.2	90.1	16.915	54.420	176.42	0.91
10	1130	12	0.27	46.16	2.97	14.72	853.00	10.5	92.7	17.330	54.758	177.47	0.89
11	1150	12	0.25	41.92	2.03	13.41	773.10	9.6	92.5	17.277	54.292	176.03	0.98
12	1180	12	0.23	32.02	1.97	10.46	613.66	7.5	91.0	16.916	54.137	175.55	0.91
13	1220	12	0.26	38.33	2.45	12.98	743.62	9.3	92.5	16.354	53.484	173.53	0.89
14	1400	12	0.44	56.30	3.78	18.23	1064.80	13.0	90.1	17.120	53.463	173.47	0.89
											Total gas age =	181.78	0.82

JK06IV-1, biotite, 4.05 mg
4 amu discrimination = 1.03432 ± 0.45 %
40/39K = 0.0024333 ± 76.1 %
J = 0.00204588 ± 0.1789 %
36/37Ca = 0.0002575 ± 1.61 %
39/37Ca = 0.00070416 ± 10.06 %

step	T (C)	t (min.)	36Ar	37Ar	38Ar	39Ar	40Ar	% 39Ar rlsd	%40Ar*	Ca/K	40Ar*/39ArK	Age (Ma)	1s.d.
1	650	12	3.18	2.51	2.84	46.75	2854.79	4.0	67.3	0.301	41.290	146.30	0.99
2	700	12	0.58	0.47	2.81	58.55	2701.61	5.0	94.2	0.043	43.620	154.22	0.75
3	725	12	0.29	0.30	2.90	64.00	2636.53	5.5	97.3	0.024	40.241	142.73	0.68
4	750	12	0.23	0.28	3.43	77.47	3047.93	6.6	98.2	0.019	38.816	137.86	0.66
5	775	12	0.20	0.29	3.72	84.48	3261.14	7.2	98.7	0.018	38.263	135.97	0.64
6	810	12	0.22	0.36	4.35	99.12	3800.50	8.5	98.7	0.019	38.045	135.23	0.64
7	845	12	0.19	0.35	3.63	82.55	3178.96	7.1	98.7	0.022	38.194	135.74	0.64
8	875	12	0.17	0.39	2.46	56.77	2193.82	4.9	98.4	0.036	38.139	135.55	0.66
9	910	12	0.19	0.60	2.09	48.67	1887.89	4.2	98.1	0.067	38.003	135.08	0.64

10	950	12	0.25	0.87	2.55	58.53	2239.39	5.0	97.6	0.082	37.364	132.89	0.66
11	980	12	0.22	0.93	2.65	60.97	2334.41	5.2	98.2	0.084	37.612	133.74	0.64
12	1020	12	0.21	2.09	2.98	67.13	2586.95	5.8	98.9	0.174	38.005	135.09	0.68
13	1100	12	0.36	9.37	8.93	200.29	7764.27	17.2	99.1	0.265	38.586	137.08	0.65
14	1180	12	0.24	9.73	6.14	133.88	5330.25	11.5	99.3	0.411	39.668	140.77	0.66
15	1400	12	0.89	1.50	1.39	26.69	1310.62	2.3	82.9	0.316	39.579	140.47	0.78
											Total gas age =	138.18	0.41

JK06IV-1, K-feldspar, 7.91 mg
4 amu discrimination = 1.02661 ± 0.27 %
40/39K = 0.0002 ± 150 %

J = 0.00154423 ± 0.1995 %
36/37Ca = 0.00031335 ± 7.09 %
39/37Ca = 0.00073573 ± 9.92 %

step	T (C)	t (min.)	36Ar	37Ar	38Ar	39Ar	40Ar	% 39Ar rlsd	%40Ar*	Ca/K	40Ar*/39ArK	Age (Ma)	1s.d.
1	450	18	2.20	0.02	0.42	0.36	674.03	0.0	3.6	8.251	63.879	169.72	50.79
2	475	18	0.83	0.01	0.17	1.53	864.39	0.1	72.4	0.548	405.628	877.43	5.24
3	475	43	0.31	0.01	0.08	1.40	144.11	0.1	48.1	0.600	39.254	106.17	0.75
4	500	18	0.65	0.02	0.16	3.20	982.34	0.2	81.2	0.329	248.159	585.26	3.09
5	500	43	0.21	0.02	0.07	2.71	150.25	0.1	75.9	0.698	33.758	91.68	0.48
6	540	18	0.67	0.02	0.22	6.34	1061.42	0.3	82.0	0.365	136.743	345.63	1.73
7	540	43	0.21	0.02	0.10	4.63	202.70	0.2	82.7	0.409	30.952	84.23	0.34
8	580	18	0.25	0.02	0.13	5.68	357.01	0.3	81.8	0.334	50.350	135.08	0.51
9	580	43	0.18	0.01	0.11	6.00	226.41	0.3	89.9	0.141	29.565	80.54	0.29
10	620	18	0.27	0.02	0.14	7.42	403.24	0.4	82.3	0.228	43.940	118.44	0.46
11	620	43	0.16	0.02	0.14	8.25	300.89	0.4	94.7	0.231	31.231	84.97	0.30
12	660	19	0.25	0.02	0.19	10.10	492.38	0.5	86.7	0.126	41.693	112.57	0.42
13	660	43	0.14	0.02	0.17	10.89	366.19	0.5	97.6	0.194	30.289	82.47	0.28
14	700	19	0.16	0.02	0.16	10.32	388.09	0.5	89.9	0.144	33.188	90.17	0.33
15	700	43	0.12	0.02	0.17	11.62	374.34	0.6	98.9	0.182	29.455	80.25	0.27
16	740	19	0.11	0.01	0.15	10.01	337.57	0.5	92.5	0.064	30.520	83.08	0.29
17	740	43	0.12	0.02	0.16	11.19	365.84	0.6	99.1	0.133	29.879	81.38	0.27
18	780	19	0.09	0.01	0.12	8.18	266.03	0.4	93.5	0.078	29.504	80.38	0.28
19	780	43	0.12	0.02	0.16	10.85	352.12	0.5	99.3	0.117	29.600	80.63	0.27
20	820	18	0.10	0.02	0.14	8.68	288.43	0.4	93.6	0.319	30.208	82.25	0.29
21	860	18	0.16	0.02	0.19	13.23	449.72	0.7	92.0	0.129	30.771	83.75	0.30
22	900	18	0.21	0.01	0.26	16.90	591.83	0.8	91.2	0.038	31.578	85.89	0.30
23	925	18	0.20	0.02	0.23	14.35	521.60	0.7	90.9	0.089	32.600	88.61	0.32

24	950	18	0.30	0.02	0.26	16.08	643.97	0.8	88.1	0.106	34.930	94.78	0.35
25	975	18	0.43	0.02	0.35	20.39	903.63	1.0	87.0	0.146	38.227	103.47	0.37
26	990	18	0.51	0.02	0.39	22.49	1066.79	1.1	86.9	0.047	40.958	110.64	0.41
27	1015	18	0.88	0.03	0.66	35.75	1818.29	1.8	86.3	0.096	43.828	118.15	0.43
28	1030	18	0.92	0.02	0.74	43.65	2230.54	2.2	88.3	0.059	45.129	121.54	0.43
29	1045	18	1.15	0.02	1.00	58.54	3034.72	2.9	89.1	0.044	46.242	124.44	0.44
30	1060	18	1.28	0.03	1.22	75.55	3885.08	3.7	90.5	0.048	46.633	125.45	0.44
31	1075	18	1.38	0.02	1.47	91.93	4690.43	4.5	91.6	0.028	46.823	125.94	0.45
32	1085	18	1.15	0.02	1.41	90.85	4568.71	4.5	92.8	0.019	46.788	125.85	0.43
33	1095	18	0.99	0.02	1.33	88.73	4434.98	4.4	93.6	0.022	46.910	126.17	0.43
34	1100	24	0.92	0.02	1.45	94.94	4737.97	4.7	94.6	0.027	47.303	127.19	0.43
35	1100	29	0.72	0.02	1.27	86.02	4300.23	4.2	95.5	0.032	47.749	128.35	0.43
36	1100	29	0.56	0.02	0.99	68.42	3447.42	3.4	95.8	0.031	48.232	129.60	0.44
37	1100	39	0.61	0.02	1.10	76.05	3880.51	3.8	96.1	0.028	48.919	131.38	0.44
38	1100	59	0.74	0.02	1.33	92.58	4780.51	4.6	96.4	0.012	49.523	132.95	0.45
39	1100	74	0.77	0.02	1.32	91.83	4815.41	4.5	96.5	0.019	50.212	134.73	0.45
40	1100	74	0.67	0.02	1.09	73.92	3920.68	3.7	96.4	0.038	50.634	135.82	0.45
41	1100	74	0.58	0.02	0.90	61.52	3307.08	3.0	96.6	0.028	51.252	137.42	0.46
42	1100	74	0.55	0.02	0.77	52.25	2833.89	2.6	96.3	0.037	51.417	137.84	0.46
43	1100	89	0.60	0.02	0.83	54.22	2961.26	2.7	96.5	0.036	51.675	138.51	0.47
44	1100	119	0.73	0.02	0.93	60.79	3358.51	3.0	96.5	0.018	52.024	139.41	0.46
45	1100	149	1.09	0.02	1.34	86.41	4617.40	4.3	95.6	0.018	49.984	134.14	0.45
46	1150	20	0.21	0.02	0.27	18.33	1026.61	0.9	95.5	0.083	52.892	141.64	0.50
47	1200	20	0.63	0.02	0.98	66.55	3709.76	3.3	95.4	0.020	53.202	142.44	0.48
48	1230	20	0.84	0.02	1.41	96.39	5277.31	4.8	95.6	0.016	52.452	140.51	0.48
49	1300	20	0.83	0.02	1.71	119.82	6316.20	5.9	96.6	-0.002	50.961	136.66	0.45
50	1350	20	0.62	0.02	0.94	63.74	3261.08	3.1	95.3	-0.010	48.563	130.46	0.44
51	1400	20	0.37	0.02	0.34	21.75	1164.26	1.1	93.2	-0.010	48.913	131.37	0.45
52	1500	20	0.42	0.02	0.22	10.84	674.09	0.5	85.4	0.020	51.232	137.36	0.50
											Total gas age =	129.44	0.23

JK06IV-7, K-feldspar, 12.38 mg J = 0.00185927 ± 0.2845 %
4 amu discrimination = 1.02954 ± 0.26 % 36/37Ca = 0.0002575 ± 1.61 %
40/39K = 0.0024333 ± 76.1 % 39/37Ca = 0.00070416 ± 10.06 %

step	T (C)	t (min.)	36Ar	37Ar	38Ar	39Ar	40Ar	% 39Ar rlsd	%40Ar*	Ca/K	40Ar*/39ArK	Age (Ma)	1s.d.
1	450	18	1.54	0.02	0.66	8.85	3320.63	0.2	86.8	-0.012	326.476	855.81	2.86

2	475	18	0.56	0.02	0.31	10.60	1164.90	0.2	87.1	0.000	95.081	293.67	1.16
3	475	43	0.32	0.02	0.19	8.77	443.51	0.2	88.5	0.006	40.807	131.93	0.53
4	500	18	0.30	0.02	0.22	6.83	928.35	0.2	92.3	-0.015	124.388	375.33	1.48
5	500	43	0.18	0.02	0.09	4.43	182.77	0.1	95.0	-0.012	30.365	99.08	0.38
6	540	18	0.35	0.02	0.30	11.67	1375.10	0.3	93.7	0.000	110.003	335.71	1.26
7	540	43	0.18	0.02	0.13	6.57	246.32	0.1	97.1	-0.032	30.404	99.20	0.41
8	580	18	0.72	0.02	0.54	18.45	2336.81	0.4	91.7	-0.011	116.123	352.68	1.51
9	580	43	0.19	0.01	0.18	10.29	379.83	0.2	97.8	-0.040	32.338	105.33	0.40
10	620	18	1.58	0.02	1.26	42.56	5188.20	1.0	91.3	0.012	111.659	340.32	1.27
11	620	43	0.21	0.02	0.31	20.66	637.45	0.5	97.6	0.025	28.195	92.18	0.36
12	660	19	0.64	0.02	0.69	33.12	2242.24	0.7	92.4	0.019	62.449	198.18	0.76
13	660	43	0.20	0.02	0.36	24.60	736.30	0.6	98.3	0.030	27.816	90.97	0.35
14	700	19	0.66	0.02	0.70	40.44	2131.28	0.9	91.7	0.015	48.225	154.91	0.61
15	700	43	0.37	0.03	0.64	45.21	1524.56	1.0	95.9	0.019	31.589	102.96	0.39
16	740	19	0.25	0.02	0.54	35.97	1155.47	0.8	95.0	0.017	30.275	98.80	0.38
17	740	43	0.23	0.03	0.51	37.84	974.25	0.9	97.7	0.023	24.168	79.30	0.31
18	780	19	0.33	0.01	0.65	45.54	1475.09	1.0	94.5	0.002	30.462	99.39	0.39
19	780	43	0.23	0.02	0.64	48.50	1184.39	1.1	98.2	0.010	23.222	76.26	0.29
20	820	18	0.22	0.02	0.60	44.92	1200.77	1.0	96.2	0.013	25.425	83.33	0.33
21	860	18	0.43	0.03	1.12	82.75	2358.96	1.9	95.4	0.012	27.117	88.74	0.35
22	900	18	0.31	0.04	1.18	90.30	2293.30	2.0	96.9	0.016	24.532	80.47	0.31
23	925	18	0.27	0.03	0.94	69.38	1681.75	1.6	96.4	0.016	23.224	76.27	0.30
24	950	18	0.36	0.03	0.87	65.27	1667.42	1.5	94.8	0.017	24.046	78.90	0.31
25	975	18	0.47	0.03	0.99	69.73	1910.26	1.6	94.3	0.015	25.607	83.91	0.33
26	990	18	0.48	0.03	0.95	66.99	1932.61	1.5	94.1	0.017	26.914	88.09	0.34
27	1015	18	0.63	0.04	1.19	83.69	2546.45	1.9	93.8	0.016	28.416	92.88	0.36
28	1030	18	0.65	0.03	1.26	86.80	2735.17	2.0	94.0	0.014	29.509	96.36	0.38
29	1045	18	0.75	0.03	1.41	95.85	3139.61	2.2	93.8	0.012	30.638	99.95	0.39
30	1060	18	0.85	0.03	1.64	111.66	3765.09	2.5	94.0	0.011	31.670	103.22	0.40
31	1075	18	1.01	0.04	1.97	132.99	4595.65	3.0	94.1	0.010	32.524	105.92	0.41
32	1085	18	1.02	0.04	2.08	144.23	4987.19	3.3	94.5	0.010	32.690	106.45	0.41
33	1095	18	1.02	0.04	2.27	155.04	5371.05	3.5	94.9	0.010	32.915	107.16	0.41
34	1100	24	1.10	0.05	2.46	173.24	5978.88	3.9	95.1	0.011	32.841	106.93	0.41
35	1100	29	1.03	0.04	2.28	159.93	5546.67	3.6	95.2	0.010	32.994	107.41	0.41
36	1100	29	0.82	0.03	1.77	122.01	4261.52	2.8	95.3	0.008	33.178	107.99	0.41
37	1100	39	0.93	0.03	1.97	131.71	4651.90	3.0	95.2	0.009	33.453	108.86	0.42

38	1100	59	1.22	0.03	2.45	164.53	5908.72	3.7	95.1	0.006	33.960	110.46	0.43
39	1100	74	1.38	0.03	2.55	171.29	6249.42	3.9	94.9	0.006	34.336	111.65	0.43
40	1100	74	1.28	0.03	2.26	150.80	5597.07	3.4	94.8	0.006	34.844	113.25	0.44
41	1100	74	1.14	0.02	1.68	108.57	4099.87	2.5	93.9	0.004	34.916	113.47	0.44
42	1100	74	0.89	0.02	1.05	65.44	2522.54	1.5	92.9	0.011	34.774	113.03	0.44
43	1100	89	0.96	0.02	0.97	57.61	2271.43	1.3	92.0	0.005	34.797	113.10	0.44
44	1100	119	1.15	0.02	1.02	58.59	2369.50	1.3	91.2	0.008	34.972	113.65	0.45
45	1100	149	1.29	0.02	1.03	57.99	2392.82	1.3	91.0	0.006	35.072	113.96	0.46
46	1150	20	0.26	0.01	0.36	22.55	893.80	0.5	95.8	0.000	36.554	118.62	0.45
47	1200	20	0.52	0.02	1.05	68.25	2655.15	1.5	95.7	0.006	36.910	119.74	0.46
48	1230	20	0.74	0.02	1.60	107.71	4162.81	2.4	95.7	0.004	36.872	119.62	0.46
49	1300	20	2.29	0.06	5.98	409.71	15714.04	9.3	96.2	0.006	36.922	119.78	0.46
50	1350	20	2.67	0.05	6.86	476.54	18186.53	10.8	96.1	0.004	36.728	119.17	0.45
51	1400	20	1.61	0.01	2.24	141.79	5599.99	3.2	92.9	0.001	36.358	118.01	0.46
52	1500	20	1.89	0.02	0.45	8.37	841.84	0.2	37.2	0.074	33.836	110.07	0.84
											Total gas age =	114.57	0.50

JK06IV-20, biotite, 7.22 mg
4 amu discrimination = 1.03432 ± 0.45 %
40/39K = 0.0024333 ± 76.1 %

J = 0.00203494 ± 0.1828 %
36/37Ca = 0.0002575 ± 1.61 %
39/37Ca = 0.00070416 ± 10.06 %

step	T (C)	t (min.)	36Ar	37Ar	38Ar	39Ar	40Ar	% 39Ar rlsd	%40Ar*	Ca/K	40Ar*/39ArK	Age (Ma)	1s.d.
1	650	12	7.88	1.01	8.51	242.36	7354.93	11.0	68.4	0.023	20.883	75.08	0.51
2	700	12	1.34	0.65	7.25	239.32	6333.21	10.9	94.0	0.015	25.020	89.59	0.46
3	725	12	0.78	0.43	6.54	213.73	5642.94	9.7	96.2	0.011	25.550	91.44	0.47
4	750	12	0.60	0.40	6.79	217.61	5782.31	9.9	97.2	0.010	25.984	92.95	0.49
5	775	12	0.41	0.35	6.09	193.04	5160.73	8.8	98.0	0.009	26.342	94.20	0.46
6	810	12	0.38	0.42	5.50	172.30	4629.69	7.8	97.9	0.013	26.456	94.60	0.46
7	845	12	0.41	0.61	4.00	125.50	3386.48	5.7	96.8	0.026	26.252	93.89	0.46
8	875	12	0.41	0.87	2.78	88.63	2391.24	4.0	95.6	0.053	25.867	92.55	0.50
9	910	12	0.48	1.16	2.57	81.92	2178.41	3.7	94.5	0.077	25.122	89.95	0.45
10	950	12	0.65	0.99	3.55	118.75	3120.66	5.4	94.5	0.045	24.902	89.18	0.45
11	980	12	0.51	0.73	4.27	137.78	3640.67	6.3	96.4	0.029	25.568	91.50	0.45
12	1020	12	0.43	1.09	6.06	189.48	5119.27	8.6	98.1	0.032	26.587	95.06	0.46
13	1100	12	0.34	6.55	4.15	128.24	3522.16	5.8	98.1	0.283	26.967	96.38	0.47
14	1180	12	0.21	8.37	1.20	36.58	1047.41	1.7	97.2	1.270	27.376	97.80	0.48
15	1400	12	0.28	0.99	0.57	16.54	525.92	0.8	92.4	0.329	27.043	96.64	0.50

Total gas age = 90.83 0.41

JK06IV-20, K-feldspar, 9.26 mg
4 amu discrimination = 1.02661 ± 0.27 %
40/39K = 0.0024333 ± 76.1 %

J = 0.00192789 ± 0.1764 %
36/37Ca = 0.0002575 ± 1.61 %
39/37Ca = 0.00070416 ± 10.06 %

step	T (C)	t (min.)	36Ar	37Ar	38Ar	39Ar	40Ar	% 39Ar rlsd	%40Ar*	Ca/K	40Ar*/39ArK	Age (Ma)	1s.d.
1	450	18	0.92	0.02	0.48	8.54	2462.50	0.3	89.3	0.084	257.813	727.92	2.24
2	475	18	0.18	0.01	0.15	7.83	406.21	0.2	88.5	0.030	45.126	150.50	0.57
3	475	43	0.15	0.02	0.16	9.65	284.16	0.3	95.5	0.068	25.257	85.77	0.30
4	500	18	0.25	0.02	0.25	10.55	927.57	0.3	93.0	0.045	81.366	262.88	1.01
5	500	43	0.13	0.02	0.13	8.12	277.47	0.3	97.9	0.103	29.959	101.30	0.36
6	540	18	0.60	0.02	0.79	30.17	2789.74	1.0	94.0	0.026	87.070	279.95	0.92
7	540	43	0.11	0.02	0.18	13.07	366.64	0.4	99.9	0.064	25.861	87.78	0.30
8	580	18	0.63	0.02	0.67	34.02	2543.57	1.1	93.0	0.018	69.640	227.28	0.77
9	580	43	0.10	0.02	0.23	17.19	450.27	0.5	99.9	0.049	24.542	83.40	0.30
10	620	18	0.22	0.03	0.45	27.18	1298.49	0.9	95.6	0.035	45.614	152.06	0.52
11	620	43	0.10	0.03	0.26	19.51	476.73	0.6	99.9	0.046	22.993	78.25	0.25
12	660	19	0.12	0.02	0.29	21.50	680.20	0.7	96.2	0.034	30.199	102.09	0.34
13	660	43	0.08	0.02	0.27	21.56	507.69	0.7	99.9	0.028	22.244	75.75	0.25
14	700	19	0.09	0.03	0.31	22.86	611.95	0.7	97.3	0.045	25.799	87.57	0.29
15	700	43	0.09	0.03	0.34	26.73	616.06	0.8	99.6	0.050	21.934	74.72	0.24
16	740	19	0.08	0.03	0.32	24.39	617.27	0.8	97.5	0.044	24.447	83.09	0.27
17	740	43	0.09	0.03	0.35	27.03	618.29	0.9	99.3	0.040	21.717	73.99	0.24
18	780	19	0.06	0.03	0.29	21.61	494.41	0.7	98.1	0.050	22.160	75.47	0.24
19	780	43	0.09	0.03	0.37	27.94	640.87	0.9	99.4	0.037	21.846	74.42	0.24
20	820	18	0.06	0.03	0.30	23.11	533.99	0.7	98.8	0.057	22.542	76.75	0.25
21	860	18	0.08	0.04	0.49	38.59	889.35	1.2	98.8	0.041	22.635	77.06	0.26
22	900	18	0.09	0.05	0.65	50.62	1160.22	1.6	98.8	0.043	22.577	76.86	0.25
23	925	18	0.09	0.04	0.62	48.71	1139.88	1.5	98.8	0.031	23.051	78.44	0.25
24	950	18	0.11	0.04	0.66	50.81	1225.65	1.6	98.2	0.031	23.626	80.36	0.26
25	975	18	0.15	0.04	0.75	56.69	1474.31	1.8	97.7	0.028	25.350	86.08	0.28
26	990	18	0.19	0.03	0.77	56.42	1581.54	1.8	97.1	0.026	27.170	92.11	0.30
27	1015	18	0.31	0.04	1.08	75.68	2285.39	2.4	96.6	0.022	29.162	98.68	0.54
28	1030	18	0.34	0.04	1.20	87.10	2786.62	2.8	96.8	0.024	31.008	104.75	0.34
29	1045	18	0.38	0.04	1.52	110.69	3635.56	3.5	97.2	0.017	32.006	108.02	0.35
30	1060	18	0.41	0.05	1.91	137.75	4493.57	4.4	97.5	0.016	31.904	107.68	0.34

31	1075	18	0.44	0.04	2.20	165.15	5305.55	5.2	97.8	0.013	31.509	106.39	0.34
32	1085	18	0.35	0.05	2.10	156.45	4934.02	5.0	98.1	0.015	31.036	104.84	0.33
33	1095	18	0.32	0.05	1.97	145.98	4575.90	4.6	98.2	0.017	30.855	104.24	0.33
34	1100	24	0.31	0.05	1.90	141.75	4425.94	4.5	98.3	0.016	30.754	103.91	0.33
35	1100	29	0.25	0.04	1.64	119.36	3706.24	3.8	98.6	0.014	30.600	103.41	0.33
36	1100	29	0.20	0.04	1.22	91.99	2879.41	2.9	98.6	0.017	30.821	104.13	0.34
37	1100	39	0.22	0.03	1.35	98.39	3115.97	3.1	98.9	0.012	31.181	105.31	0.33
38	1100	59	0.30	0.03	1.58	115.67	3718.27	3.7	98.9	0.012	31.558	106.55	0.34
39	1100	74	0.33	0.03	1.54	112.41	3691.25	3.6	99.0	0.010	32.159	108.52	0.35
40	1100	74	0.30	0.03	1.31	91.70	3076.77	2.9	99.1	0.012	32.780	110.55	0.35
41	1100	74	0.28	0.03	1.03	74.42	2519.80	2.4	99.1	0.014	32.951	111.11	0.35
42	1100	74	0.25	0.02	0.82	58.87	2023.26	1.9	99.2	0.014	33.280	112.19	0.36
43	1100	89	0.29	0.03	0.91	61.75	2164.03	2.0	99.4	0.019	33.870	114.12	0.36
44	1100	119	0.36	0.02	0.96	66.21	2344.77	2.1	99.7	0.012	34.035	114.66	0.36
45	1100	149	0.42	0.02	0.96	65.78	2366.69	2.1	100.0	0.011	34.301	115.52	0.36
46	1150	20	0.13	0.02	0.39	27.17	1016.31	0.9	98.0	0.018	36.209	121.73	0.39
47	1200	20	0.19	0.03	0.80	57.93	2086.91	1.8	98.2	0.018	35.264	118.66	0.38
48	1230	20	0.22	0.02	1.20	86.12	3047.38	2.7	98.4	0.009	34.804	117.16	0.38
49	1300	20	0.39	0.03	2.64	191.19	6811.23	6.1	98.8	0.003	35.207	118.48	0.38
50	1350	20	0.27	0.02	1.02	74.17	2578.13	2.4	98.2	0.003	33.882	114.16	0.37
51	1400	20	0.18	0.02	0.25	16.53	623.25	0.5	96.7	-0.011	34.794	117.13	0.40
52	1500	20	0.28	0.03	0.28	17.09	658.95	0.5	92.0	0.018	33.960	114.41	0.40
											Total gas age =	109.48	0.39

JK05IV-2, biotite, 6.16 mg J = 0.00209126 ± 0.635 %
4 amu discrimination = 1.03441 ± 0.26 % 36/37Ca = 0.00025397 ± 4.51 %
40/39K = 0.0071 ± 56 % 39/37Ca = 0.00068493 ± 2.07 %

step	T (C)	t (min.)	36Ar	37Ar	38Ar	39Ar	40Ar	% 39Ar rlsd	%40Ar*	Ca/K	40Ar*/39ArK	Age (Ma)	1s.d.
1	650	12	5.44	0.17	3.37	104.79	4771.08	6.7	66.5	0.046	30.386	111.14	0.81
2	680	12	0.77	0.05	1.85	77.86	2823.89	4.9	92.4	0.014	33.618	122.57	0.82
3	710	12	0.60	0.03	2.52	110.17	3817.52	7.0	95.8	0.008	33.282	121.39	0.81
4	735	12	0.46	0.05	3.09	131.85	4517.85	8.4	97.4	0.011	33.476	122.07	0.81
5	770	12	0.42	0.04	3.93	170.51	5837.78	10.8	98.2	0.006	33.751	123.04	0.82
6	810	12	0.37	0.04	3.72	163.62	5626.92	10.4	98.4	0.008	33.973	123.83	0.82
7	845	12	0.30	0.04	2.56	108.95	3759.53	6.9	98.1	0.011	33.937	123.70	0.82
8	875	12	0.30	0.06	1.66	71.87	2461.75	4.6	97.2	0.025	33.279	121.38	0.81

9	910	12	0.36	0.07	1.45	64.13	2170.67	4.1	96.2	0.028	32.469	118.52	0.79
10	950	12	0.42	0.07	1.77	77.23	2561.99	4.9	96.0	0.022	31.814	116.20	0.78
11	980	12	0.36	0.08	1.76	77.45	2588.37	4.9	96.8	0.025	32.305	117.94	0.79
12	1020	12	0.38	0.10	2.68	117.37	4010.17	7.5	97.8	0.023	33.483	122.10	0.81
13	1070	12	0.42	0.23	3.63	155.91	5488.97	9.9	98.2	0.042	34.689	126.34	0.84
14	1100	12	0.21	0.20	1.70	73.51	2614.19	4.7	98.4	0.081	35.009	127.47	0.85
15	1400	12	0.36	0.25	1.64	69.22	2542.11	4.4	97.3	0.108	35.538	129.33	0.86
											Total gas age =	122.05	0.79

JK06IV-11, K-feldspar, 15.99 mg J = 0.00186885 ± 0.2579 %
4 amu discrimination = 1.02954 ± 0.26 % 36/37Ca = 0.0002575 ± 1.61 %
40/39K = 0.0024333 ± 76.1 % 39/37Ca = 0.00070416 ± 10.06 %

step	T (C)	t (min.)	36Ar	37Ar	38Ar	39Ar	40Ar	% 39Ar rlsd	%40Ar*	Ca/K	40Ar*/39ArK	Age (Ma)	1s.d.
1	450	18	1.62	0.03	0.52	12.82	2275.76	0.2	79.4	0.077	141.170	422.41	1.62
2	475	18	0.43	0.02	0.31	17.23	721.65	0.3	83.8	0.029	34.773	113.59	0.45
3	475	43	0.33	0.02	0.30	19.50	539.73	0.4	87.0	0.028	22.995	75.91	0.31
4	500	18	0.22	0.02	0.24	13.83	714.28	0.3	92.3	0.036	47.212	152.54	0.64
5	500	43	0.20	0.02	0.23	16.02	417.98	0.3	92.4	0.034	22.688	74.92	0.28
6	540	18	0.44	0.03	0.52	30.69	2137.64	0.6	94.4	0.034	65.817	209.28	0.75
7	540	43	0.19	0.04	0.35	24.16	616.12	0.5	95.4	0.073	23.409	77.25	0.29
8	580	18	0.47	0.04	0.66	38.81	2606.06	0.7	95.1	0.047	63.966	203.72	0.74
9	580	43	0.15	0.06	0.34	25.55	626.59	0.5	97.7	0.106	23.062	76.13	0.28
10	620	18	0.33	0.07	0.54	34.10	1623.53	0.7	94.7	0.099	45.060	145.86	0.53
11	620	43	0.14	0.08	0.36	25.72	615.71	0.5	98.1	0.159	22.590	74.60	0.28
12	660	19	0.20	0.14	0.42	28.71	1001.41	0.5	95.3	0.246	33.089	108.25	0.40
13	660	43	0.13	0.23	0.39	30.61	714.03	0.6	98.8	0.399	22.322	73.73	0.27
14	700	19	0.12	0.27	0.41	31.55	850.74	0.6	97.3	0.453	26.082	85.86	0.31
15	700	43	0.13	0.30	0.49	38.52	879.34	0.7	99.0	0.413	22.055	72.87	0.26
16	740	19	0.13	0.08	0.51	39.37	1022.46	0.8	97.3	0.097	25.167	82.92	0.31
17	740	43	0.12	0.03	0.60	48.62	1091.62	0.9	99.4	0.025	21.909	72.39	0.26
18	780	19	0.08	0.03	0.53	42.62	961.15	0.8	98.7	0.025	22.151	73.18	0.26
19	780	43	0.13	0.04	0.73	58.51	1313.48	1.1	99.2	0.024	21.955	72.55	0.26
20	820	18	0.09	0.03	0.61	48.54	1113.61	0.9	98.8	0.027	22.559	74.50	0.27
21	860	18	0.12	0.05	1.02	79.36	1813.26	1.5	98.8	0.026	22.561	74.50	0.27
22	900	18	0.15	0.07	1.33	106.76	2438.60	2.0	98.8	0.033	22.594	74.61	0.28
23	925	18	0.16	0.06	1.32	105.33	2424.42	2.0	98.6	0.027	22.725	75.04	0.27

24	950	18	0.21	0.07	1.35	105.81	2512.97	2.0	98.1	0.033	23.327	76.98	0.28
25	975	18	0.30	0.07	1.46	111.17	2776.89	2.1	97.5	0.031	24.340	80.25	0.29
26	990	18	0.33	0.06	1.36	102.83	2704.34	2.0	97.1	0.027	25.518	84.05	0.31
27	1015	18	0.50	0.08	1.71	129.54	3648.81	2.5	96.5	0.029	27.208	89.48	0.34
28	1030	18	0.51	0.07	1.76	133.82	3926.89	2.6	96.6	0.023	28.387	93.26	0.34
29	1045	18	0.61	0.07	2.03	152.91	4666.19	2.9	96.5	0.023	29.526	96.90	0.35
30	1060	18	0.65	0.08	2.37	177.62	5520.97	3.4	96.8	0.021	30.184	99.00	0.36
31	1075	18	0.73	0.07	2.80	213.25	6738.16	4.1	97.1	0.017	30.782	100.91	0.37
32	1085	18	0.67	0.07	2.78	208.40	6688.09	4.0	97.3	0.017	31.337	102.68	0.37
33	1095	18	0.58	0.06	2.47	186.15	6013.92	3.6	97.5	0.016	31.587	103.47	0.37
34	1100	24	0.88	0.06	2.52	186.03	6141.92	3.6	96.1	0.016	31.812	104.19	0.38
35	1100	29	0.55	0.06	2.14	162.79	5338.06	3.1	97.4	0.016	31.985	104.74	0.39
36	1100	29	0.44	0.04	1.70	126.36	4185.06	2.4	97.4	0.013	32.284	105.69	0.39
37	1100	39	0.64	0.06	2.61	193.84	6273.21	3.7	97.5	0.014	31.597	103.50	0.38
38	1100	59	0.67	0.05	2.27	167.17	5731.81	3.2	97.3	0.014	33.305	108.93	0.39
39	1100	74	0.73	0.04	2.25	163.87	5691.70	3.1	97.2	0.009	33.636	109.98	0.40
40	1100	74	0.64	0.03	1.82	130.82	4627.37	2.5	97.1	0.009	34.152	111.62	0.41
41	1100	74	0.57	0.03	1.50	109.35	3920.04	2.1	97.1	0.010	34.556	112.90	0.41
42	1100	74	0.54	0.03	1.33	93.71	3402.47	1.8	96.9	0.010	34.862	113.87	0.41
43	1100	89	0.61	0.02	1.41	100.40	3669.95	1.9	96.8	0.008	34.981	114.24	0.42
44	1100	119	0.74	0.02	1.59	112.65	4215.71	2.2	96.8	0.007	35.719	116.58	0.42
45	1100	149	0.77	0.02	1.19	80.49	3052.95	1.5	95.9	0.010	35.391	115.54	0.44
46	1150	20	0.18	0.02	0.42	28.44	1090.10	0.5	97.8	0.000	36.731	119.77	0.43
47	1200	20	0.53	0.03	1.55	109.75	4221.11	2.1	97.0	0.003	37.271	121.48	0.44
48	1230	20	0.77	0.04	2.58	185.21	7085.78	3.5	97.2	0.005	37.266	121.46	0.44
49	1300	20	2.25	0.08	9.06	667.17	25249.55	12.8	97.6	0.006	37.075	120.86	0.43
50	1350	20	0.66	0.02	1.71	122.66	4685.78	2.3	97.2	0.005	36.853	120.16	0.44
51	1400	20	0.40	0.02	0.33	20.18	883.18	0.4	93.5	0.040	38.243	124.54	0.46
52	1500	20	0.64	0.02	0.46	26.06	1146.15	0.5	88.5	0.031	37.006	120.64	0.53
											Total gas age =	105.23	0.36

KULA-UNLV, JK05IV-4, biotite, 7.59 mg
4 amu discrimination = 1.03869 ± 0.43 %
40/39K = 0.01868 ± 52.3 %

J = 0.00164612 ± 0.2053 %
36/37Ca = 0.00025867 ± 10.31 %
39/37Ca = 0.00080803 ± 27.74 %

step	T (C)	t (min.)	36Ar	37Ar	38Ar	39Ar	40Ar	% 39Ar rlsd	%40Ar*	Ca/K	40Ar*/39ArK	Age (Ma)	1s.d.
1	650	12	13.52	0.69	3.12	7.10	4005.84	1.0	0.3	0.962	-0.026	-0.08	7.77

2	700	12	7.78	0.38	2.20	23.29	2954.17	3.3	22.3	0.162	28.102	81.58	1.57
3	725	12	2.69	0.27	1.79	43.00	2263.85	6.1	65.2	0.062	34.439	99.48	0.67
4	750	12	1.61	0.15	1.78	50.07	2249.74	7.1	79.2	0.029	35.760	103.19	0.58
5	775	12	1.12	0.14	1.67	48.75	2089.71	6.9	84.5	0.028	36.396	104.97	0.56
6	810	12	2.14	0.17	1.70	42.63	2159.79	6.0	71.0	0.039	36.122	104.21	0.66
7	845	12	2.37	0.22	1.61	37.78	2036.32	5.3	66.0	0.055	35.699	103.02	0.72
8	875	12	1.33	0.25	1.30	34.15	1603.26	4.8	75.9	0.071	35.768	103.21	0.61
9	910	12	2.36	0.42	1.59	37.16	1972.81	5.2	65.0	0.112	34.566	99.84	0.68
10	950	12	2.82	0.57	2.15	52.13	2606.25	7.4	68.2	0.110	34.226	98.88	0.64
11	980	12	1.59	0.84	2.20	61.39	2617.04	8.7	82.3	0.138	35.222	101.68	0.56
12	1020	12	1.35	1.61	2.47	71.27	2932.05	10.1	86.7	0.227	35.833	103.39	0.54
13	1100	12	1.55	2.02	3.79	116.43	4707.80	16.4	90.6	0.175	36.815	106.15	0.53
14	1180	12	0.61	4.92	2.39	71.80	2924.53	10.1	94.4	0.690	38.613	111.17	0.54
15	1400	12	0.34	1.66	0.68	18.50	817.20	2.6	91.2	0.908	39.544	113.77	0.60
											Total gas age =	103.40	0.37

JK03IV-8, muscovite, 9.07 mg J = 0.001633 ± 0.5%
4 amu discrimination = 1.02357 ± 0.31% 36/37Ca = 0.00027 ± 2.46%
40/39K = 0.0002 ± 0.03% 39/37Ca = 0.00063 ± 0.98%

step	T (C)	t (min.)	36Ar	37Ar	38Ar	39Ar	40Ar	% 39Ar rlsd	%40Ar*	Ca/K	40Ar*/39ArK	Age (Ma)	1s.d.
1	650	12	5.24	0.09	1.26	19.76	2472.62	0.9	38.9	0.022	48.889	138.57	1.31
2	700	12	1.86	0.07	0.68	23.32	1738.35	1.1	69.3	0.015	51.834	146.59	1.02
3	750	12	2.06	0.07	1.01	47.16	3046.89	2.1	80.6	0.007	52.297	147.84	0.97
4	795	12	1.89	0.09	1.52	89.86	5194.76	4.1	89.6	0.005	52.042	147.15	0.93
5	830	12	1.49	0.08	2.03	134.44	7383.66	6.1	94.2	0.003	52.021	147.09	0.92
6	865	12	1.73	0.18	3.48	244.72	13157.20	11.1	96.2	0.004	52.007	147.06	0.91
7	900	12	1.71	0.14	4.68	339.76	18145.60	15.3	97.3	0.002	52.246	147.71	0.91
8	930	12	1.66	0.15	6.33	466.67	24644.10	21.1	98.1	0.002	52.070	147.23	0.91
9	960	12	1.07	0.09	5.65	431.97	22765.10	19.5	98.7	0.001	52.268	147.77	0.91
10	990	12	0.36	0.04	2.21	166.17	8772.99	7.5	98.9	0.001	52.463	148.29	0.91
11	1025	12	0.18	0.04	1.95	148.53	7786.91	6.7	99.4	0.001	52.373	148.05	0.91
12	1060	12	0.07	0.05	0.94	71.39	3748.51	3.2	99.6	0.004	52.535	148.49	0.91
13	1095	12	0.04	0.05	0.21	15.75	828.11	0.7	99.1	0.015	52.223	147.64	0.92
14	1150	12	0.04	0.10	0.10	7.16	377.09	0.3	98.1	0.068	51.570	145.87	0.92
15	1400	12	0.07	0.03	0.12	7.60	387.45	0.3	96.2	0.022	48.811	138.36	0.92
											Total gas age =	147.45	0.79

note: isotope beams in mV, rlsd = released, error in age includes 0.5% J error, all errors 1 sigma — Plateau age = 147.62 0.80
(Not corrected for decay) — (steps 2-13)

JK03IV-8, biotite, 3.96 mg — J = 0.0016435 ± 0.5%
4 amu discrimination = 1.02357 ± 0.31% — 36/37Ca = 0.00027 ± 2.46%
40/39K = 0.0002 ± 0.03% — 39/37Ca = 0.00063 ± 0.98%

step	T (C)	t (min.)	36Ar	37Ar	38Ar	39Ar	40Ar	% 39Ar rlsd	%40Ar*	Ca/K	40Ar*/39ArK	Age (Ma)	1s.d.
1	650	12	8.28	0.13	2.20	45.30	4701.20	6.0	49.2	0.014	50.869	146.00	1.19
2	725	12	2.75	0.15	2.47	147.30	8328.82	19.7	90.5	0.005	51.013	146.39	0.92
3	775	12	1.64	0.12	2.28	150.02	8166.79	20.0	94.2	0.004	51.136	146.73	0.91
4	820	12	1.37	0.12	1.46	92.46	5083.08	12.3	92.3	0.006	50.540	145.09	0.91
5	860	12	1.40	0.12	1.24	75.12	4204.93	10.0	90.4	0.008	50.441	144.82	0.91
6	900	12	1.37	0.10	1.26	76.64	4294.25	10.2	90.9	0.007	50.731	145.61	0.92
7	940	12	1.14	0.12	1.17	72.88	4059.43	9.7	92.0	0.008	51.046	146.48	0.92
8	970	12	0.56	0.09	0.64	41.29	2278.86	5.5	93.0	0.011	51.106	146.65	0.92
9	1000	12	0.30	0.08	0.35	21.96	1214.11	2.9	93.2	0.019	51.226	146.98	0.92
10	1030	12	0.14	0.06	0.15	10.36	572.10	1.4	93.2	0.026	51.055	146.51	0.93
11	1400	12	0.30	0.19	0.26	15.77	897.89	2.1	90.9	0.059	51.367	147.37	0.98
								Cumulative %	100		Total gas age =	146.10	0.81

note: isotope beams in mV, rlsd = released, error in age includes 0.5% J error, all errors 1 sigma — Plateau age = 146.13 0.82
(Not corrected for decay) — (steps 1-10)

JK03IV-8, K-feldspar, 13.61 mg — J = 0.001561 ± 0.5%
4 amu discrimination = 1.01743 ± 0.33% — 36/37Ca = 0.000272 ± 23.61%
40/39K = 0.0002 ± 150.0% — 39/37Ca = 0.000701 ± 1.75%

step	T (C)	t (min.)	36Ar	37Ar	38Ar	39Ar	40Ar	% 39Ar rlsd	%40Ar*	Ca/K	40Ar*/39ArK	Age (Ma)	1s.d.
1	422	18	4.49	0.02	0.85	0.33	1338.86	0.0	2.8	0.265	120.786	311.62	24.70
2	448	18	1.91	0.03	0.36	0.47	576.51	0.0	4.2	0.268	53.211	143.95	7.83
3	448	43	1.67	0.02	0.33	0.79	519.26	0.0	7.3	0.117	47.851	129.96	4.43
4	473	18	0.72	0.02	0.15	0.68	230.39	0.0	10.7	0.148	36.927	101.11	5.19
5	473	43	0.96	0.03	0.19	1.28	317.57	0.0	13.6	0.093	32.478	89.22	2.15
6	514	18	1.27	0.03	0.28	2.85	718.34	0.1	49.3	0.043	125.019	321.62	2.36
7	514	43	1.11	0.04	0.28	4.66	472.42	0.2	33.3	0.039	32.692	89.79	0.90
8	555	18	2.45	0.04	0.59	10.75	2187.68	0.4	67.6	0.016	138.199	352.42	2.11
9	555	43	0.88	0.05	0.33	13.57	673.30	0.5	64.2	0.016	31.087	85.49	0.55
10	596	18	1.48	0.05	0.52	18.40	1483.62	0.6	71.1	0.013	57.423	154.87	0.94

11	596	43	0.72	0.07	0.46	24.67	1012.45	0.8	80.6	0.013	32.570	89.47	0.55
12	636	18	1.19	0.09	0.56	27.61	1566.44	0.9	78.0	0.014	44.350	120.76	0.71
13	638	43	0.53	0.10	0.55	34.70	1396.54	1.2	90.1	0.012	35.914	98.41	0.58
14	679	19	0.74	0.11	0.55	33.03	1660.80	1.1	87.3	0.014	43.948	119.70	0.69
15	679	44	0.38	0.12	0.60	39.87	1704.66	1.3	94.5	0.014	40.120	109.59	0.63
16	720	19	0.45	0.10	0.49	32.43	1566.91	1.1	91.7	0.013	44.391	120.87	0.68
17	720	44	0.26	0.11	0.57	40.81	1840.48	1.4	96.7	0.012	43.349	118.12	0.67
18	761	19	0.35	0.10	0.47	32.22	1619.23	1.1	93.9	0.014	47.267	128.43	0.73
19	761	44	0.24	0.13	0.58	41.00	1938.12	1.4	97.3	0.014	45.722	124.37	0.70
20	802	19	0.19	0.11	0.41	28.09	1360.60	0.9	96.4	0.018	46.725	127.01	0.71
21	843	19	0.24	0.20	0.56	40.34	1950.28	1.3	96.7	0.022	46.854	127.35	0.72
22	884	19	0.41	0.26	0.68	45.69	2231.08	1.5	94.9	0.025	46.416	126.20	0.73
23	910	19	0.26	0.24	0.57	40.03	1863.25	1.3	96.2	0.026	44.868	122.13	0.68
24	935	19	0.28	0.23	0.55	38.00	1756.77	1.3	95.7	0.026	44.307	120.65	0.69
25	961	19	0.37	0.22	0.61	39.43	1817.33	1.3	94.4	0.024	43.523	118.59	0.67
26	976	19	0.37	0.17	0.53	35.68	1648.11	1.2	93.8	0.021	43.330	118.08	0.67
27	1002	19	0.53	0.18	0.64	42.08	1968.14	1.4	92.4	0.019	43.267	117.91	0.67
28	1018	19	0.55	0.15	0.64	40.73	1920.23	1.4	91.9	0.016	43.390	118.23	0.67
29	1033	19	0.61	0.16	0.65	41.91	1992.44	1.4	91.4	0.017	43.494	118.51	0.67
30	1048	19	0.66	0.16	0.71	44.49	2145.18	1.5	91.3	0.015	44.054	119.98	0.69
31	1064	19	0.72	0.17	0.77	48.17	2350.74	1.6	91.3	0.015	44.638	121.52	0.69
32	1074	19	0.70	0.16	0.76	48.11	2370.50	1.6	91.6	0.015	45.204	123.01	0.70
33	1084	19	0.69	0.17	0.74	48.82	2416.88	1.6	92.0	0.015	45.604	124.06	0.71
34	1089	24	0.77	0.19	0.86	56.23	2791.25	1.9	92.3	0.015	45.849	124.71	0.71
35	1089	29	0.70	0.19	0.84	55.87	2774.50	1.9	93.1	0.015	46.213	125.66	0.71
36	1089	29	0.57	0.16	0.72	47.41	2360.42	1.6	93.5	0.015	46.485	126.38	0.71
37	1089	39	0.61	0.18	0.84	53.84	2688.04	1.8	94.0	0.014	46.818	127.25	0.72
38	1089	59	0.75	0.22	1.01	67.71	3395.24	2.3	94.4	0.014	47.112	128.02	0.72
39	1089	74	0.78	0.21	1.07	69.88	3534.98	2.3	94.6	0.013	47.532	129.13	0.73
40	1089	74	0.67	0.18	0.93	58.88	3002.97	2.0	94.7	0.013	47.945	130.21	0.75
41	1089	74	0.60	0.16	0.77	51.43	2641.92	1.7	94.7	0.013	48.121	130.67	0.76
42	1089	74	0.55	0.15	0.68	45.68	2367.03	1.5	94.7	0.014	48.470	131.58	0.76
43	1089	89	0.61	0.15	0.76	49.01	2560.13	1.6	94.8	0.013	48.794	132.43	0.76
44	1089	119	0.75	0.16	0.90	57.90	3041.26	1.9	94.9	0.012	48.983	132.92	0.77
45	1089	149	0.84	0.16	0.95	63.29	3348.85	2.1	95.1	0.011	49.240	133.60	0.79
46	1141	19	0.46	0.09	0.43	27.05	1449.35	0.9	91.5	0.014	48.870	132.63	0.76

47	1200	20	1.80	0.26	1.50	90.17	4879.34	3.0	89.5	0.013	48.524	131.72	0.75
48	1230	20	3.19	0.38	2.68	159.45	8595.51	5.3	89.4	0.010	48.301	131.14	0.74
49	1300	20	9.89	0.56	10.16	644.59	35944.50	21.5	92.1	0.004	51.517	139.54	0.78
50	1350	20	5.91	0.19	6.24	392.31	22578.30	13.1	92.5	0.002	53.405	144.46	0.81
51	1400	20	1.22	0.09	0.92	52.80	3138.66	1.8	89.2	0.007	53.088	143.63	0.81
52	1500	20	0.39	0.04	0.26	13.25	808.84	0.4	87.9	0.012	53.405	144.46	0.83
											Total gas age =	131.96	0.63

JK03IV-14, muscovite, 5.82 mg — J = 0.001657 ± 0.5%
4 amu discrimination = 1.02357 ± 0.31% — 36/37Ca = 0.00027 ± 2.46%
40/39K = 0.0002 ± 0.03% — 39/37Ca = 0.00063 ± 0.98%

step	T (C)	t (min.)	36Ar	37Ar	38Ar	39Ar	40Ar	% 39Ar rlsd	%40Ar*	Ca/K	40Ar*/39ArK	Age (Ma)	1s.d.
1	725	12	3.17	0.12	1.10	38.73	2885.66	3.0	68.4	0.015	51.209	146.93	1.03
2	775	12	1.34	0.06	0.88	49.92	2967.91	3.9	87.1	0.006	52.007	149.13	0.95
3	820	12	0.83	0.06	1.61	111.44	5994.34	8.6	96.0	0.003	51.915	148.88	0.92
4	850	12	0.42	0.06	1.69	125.69	6600.99	9.7	98.2	0.002	51.850	148.70	0.92
5	875	12	0.33	0.06	1.76	131.34	6858.29	10.2	98.7	0.002	51.782	148.51	0.91
6	900	12	0.33	0.06	1.78	133.20	6975.42	10.3	98.7	0.002	51.949	148.97	0.92
7	915	12	0.28	0.04	1.41	106.17	5573.04	8.2	98.6	0.002	52.007	149.13	0.92
8	930	12	0.28	0.03	1.34	100.77	5287.03	7.8	98.5	0.002	51.961	149.00	0.92
9	945	12	0.27	0.03	1.44	104.80	5501.10	8.1	98.7	0.001	52.041	149.23	0.92
10	960	12	0.24	0.02	1.16	87.33	4587.47	6.8	98.6	0.001	52.033	149.20	0.92
11	980	12	0.16	0.03	1.04	76.48	3985.43	5.9	98.9	0.002	51.812	148.59	0.92
12	1000	12	0.09	0.03	0.88	66.72	3465.76	5.2	99.4	0.002	51.857	148.72	0.91
13	1030	12	0.05	0.04	0.92	69.86	3623.94	5.4	99.7	0.002	51.955	148.99	0.92
14	1100	12	0.03	0.06	1.03	79.31	4105.45	6.1	99.8	0.003	51.931	148.92	0.92
15	1150	12	0.01	0.03	0.11	7.75	402.86	0.6	100.0	0.017	51.897	148.83	0.95
16	1400	12	0.02	0.02	0.04	3.60	189.67	0.3	99.9	0.032	51.818	148.61	1.04
								Cumulative %	100		Total gas age =	148.85	0.79
											Plateau age =	148.83	0.79
											(steps 1-16)		

note: isotope beams in mV, rlsd = released, error in age includes 0.5% J error, all errors 1 sigma
(Not corrected for decay)

JK03IV-14, biotite, 5.17 mg — J = 0.001656 ± 0.5%
4 amu discrimination = 1.02357 ± 0.31% — 36/37Ca = 0.00027 ± 2.46%
40/39K = 0.0002 ± 0.03% — 39/37Ca = 0.00063 ± 0.98%

step	T (C)	t (min.)	36Ar	37Ar	38Ar	39Ar	40Ar	% 39Ar rlsd	%40Ar*	Ca/K	40Ar*/39ArK	Age (Ma)	1s.d.

1	650	12	6.89	0.41	1.58	18.59	2917.36	2.1	31.9	0.121	50.187	144.11	1.57
2	700	12	1.73	0.23	0.93	45.09	2806.65	5.0	82.3	0.028	51.419	147.51	0.97
3	725	12	0.93	0.18	1.04	65.91	3666.92	7.3	92.8	0.015	51.838	148.66	0.93
4	750	12	0.71	0.19	1.24	84.84	4562.16	9.4	95.6	0.012	51.602	148.02	0.92
5	775	12	0.66	0.23	1.22	83.91	4512.60	9.3	95.9	0.015	51.771	148.48	0.93
6	810	12	0.76	0.30	1.16	75.73	4126.59	8.4	94.7	0.022	51.842	148.68	0.92
7	845	12	0.73	0.36	1.03	64.79	3551.37	7.2	94.2	0.031	51.816	148.61	0.92
8	875	12	0.55	0.39	0.90	60.68	3301.77	6.7	95.3	0.035	52.040	149.22	0.93
9	910	12	0.62	0.63	0.96	61.80	3386.67	6.8	94.8	0.056	52.186	149.62	0.93
10	950	12	0.61	0.95	1.00	65.97	3603.12	7.3	95.2	0.079	52.206	149.68	0.93
11	980	12	0.40	0.88	0.98	69.42	3714.06	7.7	96.9	0.070	52.078	149.33	0.92
12	1020	12	0.37	1.61	1.10	78.36	4167.65	8.7	97.5	0.113	52.075	149.32	0.92
13	1100	12	0.31	3.98	1.24	89.18	4689.64	9.9	98.2	0.247	51.845	148.68	0.92
14	1180	12	0.10	1.58	0.44	30.52	1578.52	3.4	98.3	0.286	51.020	146.41	0.90
15	1400	12	0.08	0.63	0.13	8.73	424.49	1.0	96.2	0.399	46.622	134.25	0.85
											Total gas age =	148.50	0.79
											Plateau age =	148.84	0.81
											(steps 2-13)		

note: isotope beams in mV, rlsd = released, error in age includes 0.5% J error, all errors 1 sigma
(Not corrected for decay)

JK03IV-14, K-feldspar, 11.29 mg J = 0.001568 ± 0.5%
4 amu discrimination = 1.01274 ± 0.34% 36/37Ca = 0.000272 ± 23.61%
40/39K = 0.0002 ± 150.0% 39/37Ca = 0.000701 ± 1.75%

step	T (C)	t (min.)	36Ar	37Ar	38Ar	39Ar	40Ar	% 39Ar rlsd	%40Ar*	Ca/K	40Ar*/39ArK	Age (Ma)	1s.d.
1	422	18	3.70	0.02	0.74	0.23	1110.10	0.0	2.9	0.355	142.561	363.96	39.65
2	448	18	1.51	0.02	0.29	0.32	450.10	0.0	2.3	0.337	33.526	92.43	15.87
3	448	43	1.19	0.02	0.22	0.51	366.80	0.0	5.3	0.224	38.135	104.78	7.87
4	473	18	0.50	0.02	0.10	0.42	162.23	0.0	10.2	0.219	39.417	108.19	4.53
5	473	43	0.59	0.02	0.12	0.71	196.11	0.0	13.9	0.144	35.897	98.79	3.11
6	514	18	1.41	0.02	0.31	3.31	1058.59	0.1	61.2	0.031	196.595	484.75	3.48
7	514	43	0.58	0.02	0.16	2.41	244.87	0.1	33.1	0.045	31.839	87.89	1.19
8	555	18	1.37	0.04	0.36	6.78	1241.47	0.2	67.9	0.029	124.538	321.81	2.24
9	555	43	0.53	0.04	0.18	6.13	341.40	0.2	57.3	0.036	30.663	84.72	0.78
10	596	18	0.82	0.05	0.27	9.57	781.56	0.3	69.8	0.027	56.978	154.38	1.11
11	596	43	0.45	0.05	0.23	11.61	504.67	0.4	76.3	0.023	32.308	89.15	0.65
12	638	18	0.69	0.07	0.30	13.80	831.02	0.5	76.2	0.025	45.842	125.23	0.89
13	638	43	0.33	0.07	0.25	14.89	592.75	0.5	86.0	0.023	33.519	92.41	0.64

14	679	19	0.41	0.08	0.28	15.86	779.74	0.5	85.1	0.026	41.811	114.56	0.78
15	679	44	0.23	0.09	0.28	18.24	734.08	0.6	92.8	0.025	36.727	101.01	0.68
16	720	19	0.31	0.09	0.28	16.91	790.46	0.6	88.8	0.029	41.497	113.73	0.76
17	720	44	0.16	0.09	0.29	20.05	833.91	0.7	96.2	0.023	39.449	108.28	0.71
18	761	19	0.20	0.09	0.25	16.26	735.06	0.5	92.3	0.028	41.669	114.18	0.75
19	761	44	0.15	0.10	0.28	20.27	893.50	0.7	96.7	0.026	42.086	115.29	0.75
20	802	19	0.19	0.08	0.23	15.01	704.79	0.5	92.8	0.027	43.454	118.92	0.78
21	802	44	0.13	0.10	0.28	18.49	839.35	0.6	97.4	0.028	43.563	119.20	0.77
22	843	19	0.26	0.09	0.22	13.33	653.69	0.4	89.4	0.035	43.738	119.67	0.81
23	843	44	0.18	0.11	0.23	17.29	790.80	0.6	95.6	0.034	42.993	117.70	0.77
24	884	19	0.35	0.10	0.24	13.06	657.51	0.4	85.3	0.039	42.820	117.24	0.79
25	884	44	0.30	0.13	0.29	18.01	837.14	0.6	91.6	0.036	41.947	114.92	0.81
26	910	19	0.27	0.08	0.19	10.28	507.01	0.3	85.5	0.038	41.977	115.00	0.86
27	910	44	0.45	0.10	0.31	17.23	829.03	0.6	86.2	0.030	40.826	111.94	0.76
28	935	19	0.45	0.08	0.24	11.26	589.83	0.4	78.4	0.036	40.915	112.18	0.80
29	935	44	0.54	0.10	0.35	19.56	951.74	0.7	85.1	0.026	40.861	112.04	0.76
30	961	19	0.53	0.08	0.26	13.62	705.89	0.5	78.8	0.029	40.690	111.58	0.82
31	961	44	0.71	0.11	0.47	24.60	1213.89	0.8	84.1	0.023	41.063	112.57	0.77
32	976	19	0.44	0.06	0.27	13.68	692.50	0.5	82.2	0.021	41.456	113.62	0.80
33	1002	19	0.83	0.09	0.47	23.33	1198.23	0.8	80.2	0.020	41.145	112.79	0.79
34	1018	19	0.82	0.09	0.51	27.77	1393.24	0.9	83.2	0.017	41.744	114.38	0.78
35	1033	19	0.91	0.12	0.60	33.96	1672.93	1.1	84.4	0.018	41.589	113.97	0.77
36	1048	19	1.02	0.12	0.74	41.36	2025.80	1.4	85.5	0.015	41.910	114.82	0.77
37	1064	19	1.13	0.17	0.87	50.55	2447.60	1.7	86.7	0.017	42.041	115.17	0.78
38	1074	19	1.05	0.17	0.90	54.37	2600.78	1.8	88.5	0.016	42.358	116.01	0.77
39	1084	19	1.00	0.18	0.94	58.58	2784.03	2.0	89.7	0.016	42.682	116.87	0.78
40	1089	24	1.06	0.22	1.10	69.00	3267.04	2.3	90.8	0.016	43.017	117.76	0.78
41	1089	29	0.91	0.22	1.05	69.40	3260.01	2.3	92.2	0.016	43.321	118.56	0.78
42	1089	29	0.68	0.18	0.89	58.78	2748.76	2.0	93.2	0.016	43.577	119.24	0.78
43	1089	39	0.68	0.20	1.00	66.50	3113.23	2.2	94.0	0.016	43.959	120.25	0.78
44	1089	59	0.77	0.23	1.23	81.96	3842.57	2.8	94.7	0.015	44.272	121.08	0.79
45	1089	74	0.75	0.24	1.22	83.15	3909.43	2.8	95.1	0.015	44.524	121.75	0.79
46	1089	74	0.55	0.18	0.97	68.35	3228.06	2.3	95.9	0.013	44.995	122.99	0.80
47	1089	74	0.47	0.15	0.84	58.40	2770.31	2.0	96.1	0.013	45.222	123.59	0.82
48	1089	89	0.48	0.14	0.86	60.45	2895.32	2.0	96.4	0.012	45.748	124.98	0.81
49	1089	89	0.42	0.13	0.77	52.74	2531.57	1.8	96.6	0.012	45.833	125.20	0.81

50	1089	119	0.49	0.13	0.87	61.05	2949.07	2.1	96.8	0.011	46.086	125.87	0.82
51	1089	119	0.44	0.11	0.76	53.18	2581.58	1.8	96.9	0.011	46.268	126.35	0.83
52	1089	149	0.50	0.12	0.85	58.07	2832.88	2.0	97.0	0.011	46.413	126.74	0.82
53	1141	19	0.32	0.09	0.41	27.30	1367.51	0.9	93.7	0.016	46.792	127.73	0.83
54	1200	20	1.21	0.25	1.50	97.43	4878.95	3.3	92.9	0.013	46.588	127.20	0.83
55	1230	20	1.61	0.34	2.33	157.97	7848.82	5.3	94.1	0.011	46.859	127.91	0.83
56	1270	20	3.85	0.57	6.78	479.05	23705.80	16.1	95.3	0.006	47.280	129.02	0.84
57	1300	20	3.64	0.32	7.49	523.49	26177.30	17.6	96.0	0.003	48.110	131.21	0.85
58	1350	20	1.63	0.08	2.41	165.35	8477.68	5.6	94.5	0.002	48.523	132.29	0.86
59	1400	20	0.17	0.03	0.13	6.83	382.97	0.2	90.3	0.021	48.918	133.33	0.89
60	1500	20	0.13	0.02	0.06	3.34	214.09	0.1	87.3	0.035	53.076	144.22	1.02
											Total gas age =	125.09	0.61

JK06IV-12, K-feldspar, 12.13 mg
4 amu discrimination = 1.02736 ± 0.29 %
40/39K = 0.0002 ± 150 %

J = 0.00155525 ± 0.4199 %
36/37Ca = 0.00031335 ± 7.09 %
39/37Ca = 0.00073573 ± 9.92 %

step	T (C)	t (min.)	36Ar	37Ar	38Ar	39Ar	40Ar	% 39Ar rlsd	%40Ar*	Ca/K	40Ar*/39ArK	Age (Ma)	1s.d.
1	450	18	2.72	0.02	0.52	0.24	796.28	0.0	-0.8	0.538	-34.885	-100.63	104.49
2	475	18	0.62	0.02	0.12	0.23	188.51	0.0	3.4	1.113	25.968	71.43	7.46
3	475	43	0.56	0.02	0.12	0.39	167.92	0.0	3.1	0.651	11.367	31.61	4.90
4	500	18	0.26	0.02	0.05	0.46	94.93	0.0	22.3	0.000	44.316	120.24	2.92
5	500	43	0.37	0.02	0.09	0.97	133.94	0.0	21.3	0.397	26.579	73.08	1.05
6	540	18	1.85	0.03	0.62	19.33	3253.88	0.6	83.4	0.040	140.905	357.47	1.78
7	540	43	0.23	0.02	0.12	5.92	266.42	0.2	79.4	0.022	34.203	93.50	0.58
8	580	18	0.82	0.03	0.46	21.47	2094.05	0.7	88.7	0.048	86.834	228.53	1.16
9	580	43	0.17	0.02	0.17	10.80	375.62	0.4	90.1	0.036	30.418	83.39	0.45
10	620	18	0.47	0.02	0.37	21.98	1421.41	0.7	90.5	0.006	58.622	157.41	0.84
11	620	43	0.13	0.02	0.18	11.80	398.28	0.4	93.8	-0.033	30.722	84.20	0.44
12	660	19	0.24	0.03	0.24	14.56	706.66	0.5	90.9	0.088	44.031	119.50	0.63
13	660	43	0.10	0.03	0.15	9.85	324.97	0.3	94.9	0.104	30.105	82.55	0.42
14	700	19	0.18	0.02	0.19	11.91	524.32	0.4	90.7	0.032	39.707	108.10	0.57
15	700	43	0.09	0.02	0.14	10.00	324.25	0.3	95.8	-0.051	29.870	81.92	0.42
16	740	19	0.14	0.02	0.17	10.84	406.66	0.4	91.5	-0.012	34.076	93.16	0.48
17	740	43	0.09	0.03	0.18	11.96	370.09	0.4	96.5	0.064	28.884	79.28	0.41
18	780	19	0.09	0.03	0.15	10.69	338.08	0.4	94.2	0.072	29.512	80.96	0.42
19	780	43	0.09	0.02	0.19	12.92	385.04	0.4	97.0	0.010	27.995	76.89	0.40

20	820	18	0.06	0.02	0.14	9.89	290.05	0.3	96.7	0.168	27.832	76.45	0.40
21	860	18	0.10	0.03	0.24	16.75	497.72	0.5	95.7	0.122	28.203	77.44	0.40
22	900	18	0.13	0.03	0.31	21.84	655.88	0.7	95.5	0.111	28.510	78.27	0.40
23	925	18	0.14	0.02	0.31	21.66	683.34	0.7	95.2	0.077	29.902	82.01	0.42
24	950	18	0.20	0.02	0.38	25.19	867.94	0.8	94.1	0.061	32.326	88.49	0.45
25	975	18	0.32	0.02	0.50	34.76	1303.92	1.1	93.7	0.015	35.046	95.75	0.49
26	990	18	0.44	0.02	0.65	43.77	1726.23	1.4	93.3	0.003	36.762	100.31	0.51
27	1015	18	0.64	0.03	1.00	66.99	2745.24	2.2	93.7	0.027	38.431	104.73	0.53
28	1030	18	0.70	0.03	1.14	76.85	3187.12	2.5	94.0	0.012	39.039	106.34	0.54
29	1045	18	0.74	0.03	1.37	95.00	3929.29	3.1	94.8	0.018	39.314	107.07	0.54
30	1060	18	0.81	0.03	1.59	107.72	4456.58	3.5	95.0	0.014	39.405	107.31	0.54
31	1075	18	0.84	0.04	1.89	132.70	5474.33	4.4	95.7	0.014	39.624	107.89	0.54
32	1085	18	0.71	0.04	1.83	129.61	5323.60	4.3	96.3	0.018	39.693	108.07	0.54
33	1095	18	0.68	0.04	1.87	131.93	5410.79	4.3	96.6	0.016	39.730	108.17	0.54
34	1100	24	0.66	0.03	2.00	144.40	5894.05	4.7	96.9	0.012	39.691	108.06	0.54
35	1100	29	0.60	0.04	1.89	136.62	5551.98	4.5	97.1	0.019	39.574	107.75	0.54
36	1100	29	0.37	0.03	1.16	83.19	3330.25	2.7	97.2	0.015	38.965	106.14	0.53
37	1100	39	0.37	0.03	1.16	81.99	3320.87	2.7	97.3	0.016	39.419	107.34	0.54
38	1100	59	0.42	0.03	1.26	90.86	3703.26	3.0	97.4	0.008	39.643	107.94	0.54
39	1100	74	0.45	0.02	1.27	90.83	3724.36	3.0	97.3	0.006	39.784	108.31	0.54
40	1100	74	0.42	0.02	1.11	79.70	3296.60	2.6	97.2	0.005	40.041	108.99	0.55
41	1100	74	0.37	0.02	0.94	65.62	2720.15	2.2	97.2	0.004	40.052	109.02	0.56
42	1100	74	0.34	0.03	0.83	57.12	2378.03	1.9	97.1	0.020	40.146	109.26	0.55
43	1100	89	0.37	0.02	0.85	59.79	2500.04	2.0	97.2	0.000	40.266	109.58	0.55
44	1100	119	0.46	0.02	0.99	68.86	2897.21	2.3	97.0	0.000	40.373	109.86	0.55
45	1100	149	0.55	0.02	1.07	73.47	3098.77	2.4	96.6	0.007	40.195	109.39	0.56
46	1150	20	0.24	0.02	0.60	41.53	1776.78	1.4	97.5	0.009	41.429	112.65	0.57
47	1200	20	0.73	0.03	2.18	155.01	6643.55	5.1	97.2	0.008	41.723	113.42	0.57
48	1230	20	0.84	0.03	2.91	210.17	8915.36	6.9	97.5	0.004	41.476	112.77	0.56
49	1300	20	1.46	0.10	6.43	464.81	19054.59	15.3	98.0	0.025	40.307	109.69	0.55
50	1350	20	0.20	0.03	0.40	29.61	1272.32	1.0	99.5	0.066	41.654	113.24	0.56
51	1400	20	0.18	0.02	0.14	8.21	378.07	0.3	99.9	0.169	41.338	112.41	0.56
52	1500	20	0.30	0.02	0.11	4.20	251.95	0.1	81.0	0.469	42.406	115.22	0.62
											Total gas age =	109.90	0.49

Appendix D

$^{40}Ar/^{39}Ar$ data for samples from the Kessler Spring Adamellite, southern Ivanpah Mountains

JK06KS-1, biotite, 6.60 mg — J = 0.00194597 ± 0.1768 %
4 amu discrimination = 1.03432 ± 0.45 % — 36/37Ca = 0.0002575 ± 1.61 %
40/39K = 0.0024333 ± 76.1 % — 39/37Ca = 0.00070416 ± 10.06 %

step	T (C)	t (min.)	36Ar	37Ar	38Ar	39Ar	40Ar	% 39Ar rlsd	%40Ar*	Ca/K	40Ar*/39ArK	Age (Ma)	1s.d.
1	650	12	3.77	0.44	1.56	55.80	2077.51	2.6	46.5	0.044	17.346	59.89	0.59
2	700	12	1.03	0.32	1.57	89.83	2316.15	4.1	87.5	0.019	22.623	77.72	0.41
3	725	12	0.47	0.23	1.58	101.37	2470.69	4.7	95.0	0.012	23.219	79.73	0.39
4	750	12	0.33	0.20	1.87	120.56	2892.18	5.6	97.2	0.009	23.405	80.35	0.39
5	775	12	0.29	0.20	1.87	124.12	2953.89	5.7	97.6	0.008	23.332	80.11	0.39
6	810	12	0.36	0.19	1.97	127.60	3057.67	5.9	97.0	0.008	23.352	80.17	0.39
7	845	12	0.35	0.17	1.55	100.62	2430.02	4.6	96.3	0.009	23.335	80.12	0.39
8	875	12	0.32	0.18	1.15	71.77	1744.63	3.3	95.4	0.012	23.226	79.75	0.39
9	910	12	0.32	0.19	0.92	57.21	1397.97	2.6	94.6	0.017	23.014	79.04	0.39
10	950	12	0.43	0.27	0.98	61.05	1509.75	2.8	92.9	0.023	22.878	78.58	0.40
11	980	12	0.51	0.30	1.17	73.99	1830.37	3.4	92.8	0.022	22.919	78.72	0.40
12	1020	12	0.53	0.41	1.74	111.30	2693.24	5.1	95.4	0.020	23.029	79.09	0.40
13	1100	12	0.71	2.20	4.68	306.22	7265.55	14.1	97.6	0.041	23.247	79.82	0.39
14	1180	12	0.87	18.11	9.57	630.97	14841.67	29.1	98.5	0.166	23.321	80.07	0.38
15	1400	12	0.36	2.55	2.10	134.18	3217.97	6.2	98.2	0.109	23.398	80.33	0.39
											Total gas age =	79.27	0.24
											Plateau age =	79.84	0.39
											Isochron age =	80.71	0.35

note: isotope beams in mV, rlsd = released, error in age includes J error, all errors 1 sigma

KAS-Big, K-feldspar, 10.42 mg — J = 0.0015522 ± 0.145 %
4 amu discrimination = 1.02661 ± 0.27 % — 36/37Ca = 0.00031335 ± 7.09 %
40/39K = 0.0002 ± 150 % — 39/37Ca = 0.00073573 ± 9.92 %

step	T (C)	t (min.)	36Ar	37Ar	38Ar	39Ar	40Ar	% 39Ar rlsd	%40Ar*	Ca/K	40Ar*/39ArK	Age (Ma)	1s.d.
1	450	18	4.94	0.02	0.91	0.43	1421.51	0.0	-2.7	5.281	-95.369	-289.02	88.40
2	475	18	0.82	0.02	0.16	0.65	255.12	0.0	5.1	3.497	18.550	51.21	10.61
3	475	43	0.73	0.02	0.16	1.16	232.02	0.0	9.1	1.773	15.621	43.22	1.66
4	500	18	0.35	0.02	0.09	1.26	126.90	0.0	20.9	1.986	19.482	53.75	0.84
5	500	43	0.48	0.02	0.13	2.25	183.66	0.1	29.5	1.016	20.203	55.70	0.54
6	540	18	0.34	0.02	0.12	3.66	190.84	0.1	49.7	0.687	24.798	68.14	0.45

7	540	43	0.43	0.02	0.15	5.49	260.16	0.2	58.8	0.375	24.705	67.89	0.34
8	580	18	0.28	0.02	0.16	7.55	282.11	0.3	72.9	0.364	26.489	72.69	0.29
9	580	43	0.32	0.02	0.21	11.36	397.20	0.4	82.9	0.121	26.886	73.76	0.32
10	620	18	0.20	0.02	0.22	13.75	428.16	0.5	88.2	0.133	27.028	74.14	0.27
11	620	43	0.24	0.02	0.31	20.76	624.24	0.8	93.8	0.144	26.955	73.95	0.25
12	660	19	0.13	0.02	0.31	22.51	645.66	0.8	95.5	0.132	27.158	74.49	0.23
13	660	43	0.18	0.03	0.49	34.58	983.70	1.2	98.0	0.106	27.155	74.48	0.24
14	700	19	0.11	0.03	0.49	34.82	967.50	1.3	97.6	0.112	27.018	74.11	0.23
15	700	43	0.15	0.02	0.69	52.61	1467.60	1.9	99.1	0.048	27.224	74.67	0.23
16	740	19	0.10	0.03	0.64	47.96	1327.40	1.7	98.4	0.077	27.185	74.56	0.23
17	740	43	0.14	0.02	0.91	67.40	1869.76	2.4	99.5	0.031	27.298	74.87	0.23
18	780	19	0.08	0.02	0.67	51.48	1428.18	1.9	98.9	0.063	27.397	75.13	0.23
19	780	43	0.13	0.02	0.85	65.33	1822.10	2.4	99.8	0.039	27.501	75.41	0.23
20	820	18	0.10	0.02	0.62	46.44	1301.05	1.7	98.7	0.070	27.595	75.66	0.23
21	860	18	0.13	0.02	0.84	61.61	1730.28	2.2	98.4	0.049	27.626	75.75	0.23
22	900	18	0.21	0.03	0.90	66.56	1896.13	2.4	97.3	0.056	27.728	76.02	0.23
23	925	18	0.25	0.02	0.79	56.18	1639.08	2.0	96.1	0.029	28.016	76.79	0.24
24	950	18	0.38	0.02	0.77	54.24	1619.40	2.0	93.7	0.043	27.952	76.62	0.24
25	975	18	0.54	0.02	0.90	60.57	1845.75	2.2	92.0	0.046	27.997	76.74	0.25
26	990	18	0.53	0.02	0.84	58.13	1782.64	2.1	91.8	0.048	28.097	77.01	0.26
27	1015	18	0.71	0.02	1.05	71.12	2187.91	2.6	91.0	0.046	27.971	76.67	0.26
28	1030	18	0.66	0.02	1.05	71.26	2192.27	2.6	91.6	0.046	28.169	77.20	0.25
29	1045	18	0.67	0.02	1.07	73.46	2267.37	2.7	91.8	0.028	28.324	77.62	0.25
30	1060	18	0.65	0.02	1.09	75.58	2336.67	2.7	92.2	0.018	28.514	78.13	0.25
31	1075	18	0.68	0.02	1.17	80.69	2491.92	2.9	92.4	0.040	28.546	78.22	0.25
32	1085	18	0.61	0.03	1.13	76.50	2350.61	2.8	92.9	0.046	28.532	78.18	0.25
33	1095	18	0.59	0.02	1.08	75.01	2315.59	2.7	93.0	0.034	28.705	78.64	0.25
34	1100	24	0.57	0.02	1.14	80.51	2461.52	2.9	93.8	0.035	28.632	78.45	0.26
35	1100	29	0.52	0.02	1.09	75.03	2290.13	2.7	94.2	0.019	28.631	78.44	0.25
36	1100	29	0.43	0.02	0.87	61.11	1874.16	2.2	94.3	0.046	28.739	78.73	0.25
37	1100	39	0.46	0.02	0.98	66.70	2040.23	2.4	94.7	0.042	28.689	78.60	0.25
38	1100	59	0.57	0.02	1.11	78.84	2426.00	2.8	95.0	0.030	28.811	78.93	0.25
39	1100	74	0.61	0.03	1.09	76.38	2356.86	2.8	94.8	0.046	28.665	78.53	0.25
40	1100	74	0.53	0.02	0.90	61.51	1918.12	2.2	94.7	0.030	28.786	78.86	0.25
41	1100	74	0.50	0.02	0.80	54.32	1696.15	2.0	94.6	0.047	28.676	78.57	0.25
42	1100	74	0.45	0.02	0.66	45.21	1425.13	1.6	94.6	0.052	28.753	78.77	0.25

43	1100	89	0.50	0.02	0.69	44.71	1424.69	1.6	94.5	0.063	28.764	78.80	0.26
44	1100	119	0.40	0.02	0.42	27.61	903.49	1.0	97.7	0.043	28.678	78.57	0.28
45	1100	149	0.43	0.02	0.43	26.02	871.80	0.9	99.4	0.081	28.780	78.84	0.25
46	1150	20	0.11	0.02	0.13	8.73	281.77	0.3	94.5	0.217	28.743	78.75	0.26
47	1200	20	0.38	0.03	0.56	37.37	1182.73	1.3	91.8	0.095	28.778	78.84	0.26
48	1230	20	0.64	0.01	1.06	72.87	2273.70	2.6	92.5	0.013	28.760	78.79	0.26
49	1300	20	2.72	0.05	6.40	451.49	13793.99	16.3	94.4	0.018	28.910	79.19	0.25
50	1350	20	0.74	0.02	1.24	82.46	2611.46	3.0	92.7	0.000	29.144	79.82	0.26
51	1400	20	0.29	0.02	0.31	19.83	659.98	0.7	91.3	-0.036	29.027	79.51	0.26
52	1500	20	0.44	0.02	0.39	25.20	864.00	0.9	88.4	-0.028	29.297	80.23	0.27
											Total gas age =	77.56	0.29

VITA

Graduate College
University of Nevada, Las Vegas

Joseph Kula

Home Address:
1022 Prince St
Houston, TX 77008

Degrees:
Bachelor of Science, Geoscience, 2000
Montclair State University; Upper Montclair, NJ

Master of Science, Geoscience, 2002
University of Nevada, Las Vegas; Las Vegas, NV

Special Honors and Awards:
UNLV Summer GREAT Assistantship: 2002, 2005, 2006, 2007
AGU 2006 Fall Meeting Outstanding Student Paper Award; Tectonophysics Section
3rd Place UNLV GPSA Research Forum Science & Engineering Platform Speaker: Spring 2006
UNLV Department of Geoscience Bernada E. French Scholarship: 2001-2004, 2006
Geological Society of Nevada Scholarship: 2006
UNLV Department of Geoscience Edwards & Olswang Fund scholarship: 2005
UNLV Summer Sessions Scholarship: 2003, 2004
UNLV Phi Kappa Phi Honor Society: 2001-2002
Montclair State University College of Science and Mathematics Outstanding Baccalaureate Award 2000; Geoscience: 2000

Publications:

Kula, J., Tulloch, A., Spell, T.L., Wells, M.L., 2007, Two-stage rifting of Zealandia-Australia- Antarctica: evidence from $^{40}Ar/^{39}Ar$ thermochronometry of the Sisters Shear Zone; Stewart Island, New Zealand: Geology, v. 35, p. 411-414.

Kula, J.L., Tulloch, A.J., Spell, T.L., Wells, M.L., 2006, $^{40}Ar/^{39}Ar$ thermochronometry

of the Sisters Shear Zone, Stewart Island, New Zealand; implications for driving mechanisms and multi-stage breakup of the Pacific margin of Gondwana: Eos Trans. AGU, 87(52), Fall Meet. Suppl., Abstract T53A-1588.

McLaurin, B.T., Kula, J.L., Hirsch, A.C., Watson, J.T., Ochoa, S., 2006, Hills to river: artifact resource procurement at La Playa, Mexico: Geological Society of America Abstracts with Programs

Tulloch, A.J., Beggs, M., Kula, J.L., Spell, T.L., Mortimer, N., 2006, Cordillera Zealandia, the Sisters Shear Zone and their influence on the early development of the Great South Basin: New Zealand Petroleum Conference Proceedings.

Kula, J.L., Tulloch, A.J., Spell, T.L., Wells, M.L., 2005, Timing of continental extension leading to separation of eastern New Zealand from west Antarctica; $^{40}Ar/^{39}Ar$ thermochronometry from Stewart Island, NZ: Geological Society of America Abstracts with Programs v. 37, p. 73.

Wells, M.L., Beyene, M.A., Spell, T.L., Kula, J.L., Miller, D.M., Zanetti, K.A., 2005, The Pinto shear zone; A Laramide synconvergent extensional shear zone in the Mojave Desert region of the southwestern Cordilleran orogen, western United States: Journal of Structural Geology, v. 27, p. 1697-1720.

Wells, M.L., Hoisch, T.D., Kula, J.L., Burgett, D., 2004 Removal of mantle lithosphere, synconvergent extension, and crustal anatexis in the Late Cretaceous Cordilleran interior: Geological Society of America Abstracts with Programs, v. 36, p. 119-120.

Kula, J.L., Spell, T.L., and Wells, M.L., 2002, Syntectonic intrusion and exhumation of a Mesozoic plutonic complex in the Late Cretaceous, Granite Mountains, southeastern California: Geological Society of America Abstracts with Programs, v. 34 p. 249

Taylor, W.J., Criscione, J.J., Gilbert, J.J., Justet, L., Kula, J.L., Schiefelbein, I., Sheely, J.C., Stickny, E., 2001, Geometry and neotectonics of the north California Wash Fault, Nevada: Geological Society of America Abstracts with Programs v.33 p. 58

Kula, J.L. and Gorring, M.L., 2000, Tectonic setting and protolith for middle Proterozoic amphibolites within the Losee gneiss of the New Jersey Highlands: Geological Society of America Abstracts with Programs, v. 32 p. 455

Dissertation Title: Thermochronological constraints on Mesozoic tectonism in southwest U.S. and New Zealand; and $^{40}Ar/^{39}Ar$ age spectra from artificially mixed micas

Thesis Examining Committee:
Chairperson, Dr. Terry L. Spell, Ph.D.
Chairperson, Dr. Michael L. Wells, Ph.D.

Committee Member, Dr. Rodney V. Metcalf, Ph.D.
Committee Member, Dr. Wanda J. Taylor, Ph.D.
Graduate Faculty Representative, Dr. Barbara Luke, Ph.D.